Wayne State University Dissertations

1-1-2017

Synthesis Of Low-Coordinate Transition Metal Bis(alkoxide) Complexes And Their Reactivity Toward Small Molecules

Maryam Yousif
Wayne State University,

Follow this and additional works at: https://digitalcommons.wayne.edu/oa_dissertations

Part of the Inorganic Chemistry Commons

SYNTHESIS OF LOW-COORDINATE TRANSITION METAL BIS(ALKOXIDE) COMPLEXES AND THEIR REACTIVIY TOWARD SMALL MOLECULES

by

MARYAM YOUSIF

DISSERTATION

Submitted to the Graduate School

of Wayne State University,

Detroit, Michigan

in partial fulfillment of the requirements

for the degree of

DOCTOR OF PHILOSOPHY

2017

MAJOR: INORGANIC CHEMISTRY

Approved by:

_____

Advisor   Date

_____

_____

_____

well as for the Rumble Research Fellowship, Knoller Fellowship, and Summer Dissertation Fellowship.

I would like to thank my undergraduate professor, Dr. Donahue, for always pushing me to do better and inspiring me to pursue a higher education in chemistry.

My thanks also go to my English high school teacher, Ani Kasparian, for being a great friend and supporter of my career path until this day. Much more than teaching me English, she taught me that I can achieve more than I was told I was capable of. Thank you for your willingness to help me in every possible way and showing interest in all aspects of my life.

Finally, I would like to thank God for his grace and my wonderful family and friends for always being there for me. I am blessed to have such a loving family and my Ph.D. journey would have been impossible without my parents, sister, and brother. Their support, encouragement, and love made it possible to continue my educational path. Lastly, I must give a very special thanks to my best friend and amazing mother for going above and beyond to support me in all that I do and it is my pleasure to dedicate all my Ph.D. work to her.

TABLE OF CONTENTS

LIST OF TABLES

LIST OF FIGURES

CHAPTER 1 INTRODUCTION

Parts of the text in this chapter were reprinted or adapted with permission from: Yousif, M.;

Tjapkes, D. J.; Lord, R. L.; Groysman, S. *Organometallics* **2015**, *34*, 5119-5128.

1.1. Organic Azides as Nitrogen Sources: N-C and N-N Bond Formation Reactions

      The catalytic bond formation and activation reactions involving azide precursors (RN_3) are

receiving great attention due to the many advantages offered by organic azides.[1-4] A variety of

azides are commercially available or can be easily synthesized using simple synthetic procedures.

Organoazides undergo a multitude of reactions, including reductive coupling to form nitrogen-rich

compounds and cycloaddition.[2] One of the most synthetically useful reactions of organoazides is

their decomposition to form reactive nitrene intermediates [NR]. Nitrenes have been shown to

participate in numerous catalytic N-C and N-N bond formation reactions, including C-H bond

activation, C=C bond aziridination, and nitrene coupling with various substrates. Also, [NR] group

transfer from an azide provides the advantage that the only side product is the environmentally

friendly dinitrogen.[3,4]

      To enable selective reactivity of organoazides under mild conditions, transition-metal

catalysis is often necessary to promote N-N bond cleavage. Transition metal-catalyzed

transformation of azides generally proceeds via the initial binding of an organoazide to the

electrophilic metal center, which is followed by a two-electron reductive splitting to form nitrene

intermediates (M=NR) along with N_2 release (**Figure 1.1**).[2,4]
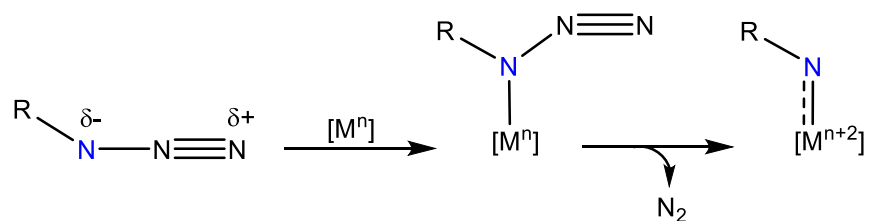
Figure 1.1. Transformation of azides to form metal imido (nitrene) complexes.

When coordinated to middle and late transition metals, nitrenes adopt a reactive electrophilic nature (akin to Fischer carbenes), making them capable of coupling with nucleophilic reagents: alkenes, isocyanides (CNR), carbon monoxide, or C-H bonds. This electrophilic behavior can be rationalized by filled d-orbitals on the metal center preventing additional π-bonding from the nitrene fragment. In contrast, earlier transition metal-imido compounds form multiple bonds (usually triple M≡NR bonds) due to empty d-orbitals on the metal center and therefore have a nucleophilic nitrene fragment (akin to Schrock carbenes). **Figure 1.2** describes the electrophilic and nucleophilic behavior of the early and late transition metal-imido complexes.[3a,c,d]

Late transition metal:
electrophilic "nitrene"

Early transition metal:
nucleophilic "imido"

Figure 1.2. Binding of late (left) and early (right) transition metal-imido complexes.

Among the most attractive chemical applications of organoazides is the synthesis of carbodiimides and azoarene compounds via the reactive M=NR intermediates. Carbodiimides, RN=C=NR', are widely used organic compounds that accept water, hydrolyze readily and thus serve as excellent dehydration agents. Large-scale applications of carbodiimides include acting as stabilizers and antihydrolysis agents in polymers production, as coupling agents in peptide synthesis, and in various organic transformations.[5] Carbodiimides are synthesized by numerous

transition-metal-catalyzed routes,[6] including oxidative coupling of amines with isocyanides[7] and coupling of two isocyanates (R′NCO) with the loss of one equivalent of CO_2,[8] as well as by transition-metal-free stoichiometric routes such as the reaction of isocyanates with phosphinimines (aza-Wittig)[9] and by tin-mediated addition of silylamines to isocyanates.[10] Coupling of an [NR] group (originating in organoazides) with an isocyanide is among the most useful methods to synthesize carbodiimides. Most of the nitrene-isocyanide coupling reactions take place at late-transition-metal centers stabilized by nitrogen, carbon, or phosphorus ligands where the M=NR functionality is suggested to operate as the reactive intermediate (**Figure 1.3**). The combination of soft electron-rich late transition metals with hard π-donating imido functionalities makes the imido functionality reactive and thus susceptible to transfer.[11-20] Warren and Holland groups demonstrated that bulky β-diketiminate-supporting nickel(I) and dimeric iron(I) systems are capable of the conversion of organic azides and isocyanide to produce RN=C=NR'.[18b,c,19b] Also, Hillhouse and coworkers described the catalytic formation of asymmetric carbodiimides by dimeric nickel(I) precursor supported by the N-heterocylic carbene ligand.[17c] The detailed stoichiometric and mechanistic studies of these transformations revealed that M=NR intermediates are responsible for the RN=C=NR' elimination (**Figure 1.2**).[17c, 18b,c,19b]

$$RN_3 + CNR' \xrightarrow{\text{cat.}} RNCNR' + N_2$$

Ar = 2,6-^{i}Pr$_2$Ph   L = 2-picoline   Ar = 2,6-^{i}Pr$_2$Ph
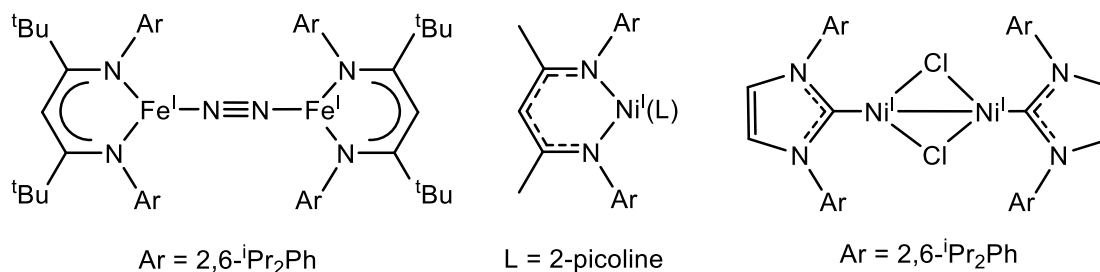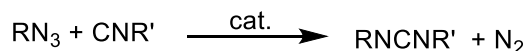
Figure 1.3. Asymmetric carbodiimide formation by coupling of azide and isocyanide (top). Selected examples of late-transition metal precatalysts in formation of carbodiimide (bottom).

Whereas the catalytic formation of asymmetric carbodiimides takes place at late-transition metal complexes via [NR] transfer to CNR', the reactivity of oxophilic early-transition-metal imido complexes with isocyanates is a well-established route to symmetric carbodiimides (**Figure 1.4**, top). Selected examples of early transition metal nitrene complexes, shown in **Figure 1.4**, are employed to synthesize symmetric carbodiimides via the condensation of isocyanates with the loss of CO_2. The vanadium tris(alkoxide) imido complex catalyze the condensation of phenyl isocyanate to diphenylcarbodiimide (PhN=C=NPh).[8b] Similarly, the catalytic formation of PhN=C=NPh can be accomplished by coupling of two isocyanates on the silica supported tantalum imido complex.[21] On the other hand, the zirconium imido compound can be only involved in the stoichiometric formation of carbodiimides (**Figure 1.4**, bottom).[22]

$$2 \text{ RNCO} \xrightarrow{\text{cat.}} \text{RNCNR} + CO_2$$
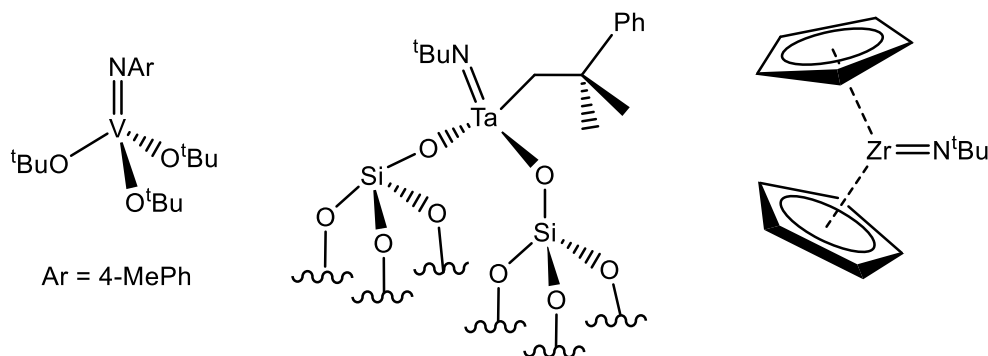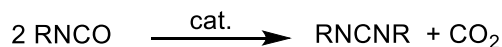
Figure 1.4. Symmetric carbodiimide formation by the coupling of two isocyanate (top). Selected examples of early transition metal imido complexes in stoichiometric and catalytic formation of carbodiimide (bottom).

It is worth noting that the imido-group transfer reactivity to form asymmetric carbodiimide through the early-transition metal complexes is not common and tend to be stoichiometric, in part because nitrene transfer requires formal two-units change in the oxidation state of the metal, and early-transition metals are generally stable mostly in high oxidation states. Recently, a new approach has been developed by Heyduk and coworkers who have explored the nitrene-isocyanide coupling using early transition metal-based Zr(IV) system. This system is capable of catalytic imido group transfer to CNR' to give the corresponding carbodiimide. However, no change in the oxidation state of the metal takes place. Instead, it is the redox active ligand that is responsible for the redox chemistry mediated by metal (**Figure 1.5**).[22,23]
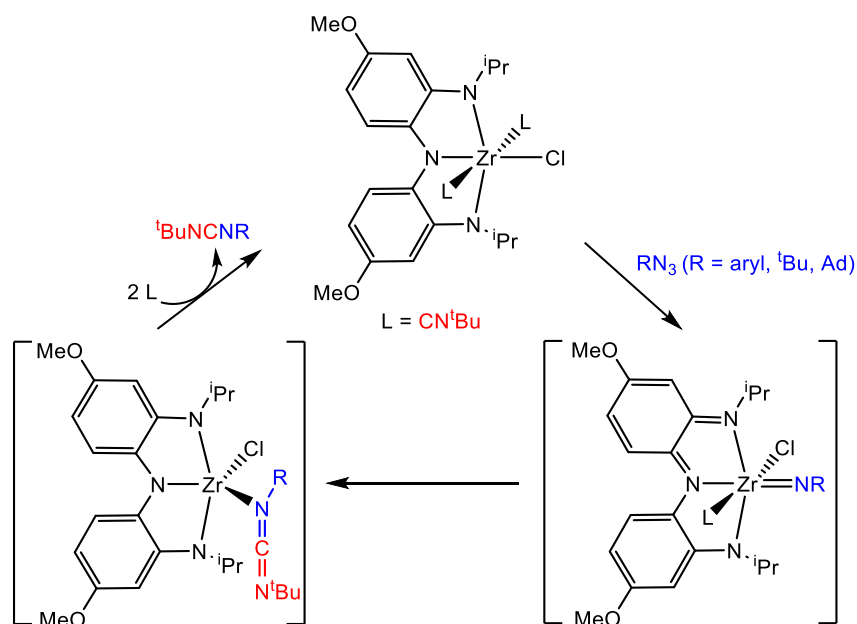
Figure 1.5. Nitrene transfer to form carbodiimide by zirconium(IV) redox-active ligand complex.

In addition to the nitrene-isocyanide coupling, organic azides can be used as an ecofriendly synthetic approach for nitrene homocoupling to form azoarenes (ArN=NAr). As azoarenes have broad industrial application as dyes or indicators and food additives,[24] efficient nitrene homocoupling can be used to form valuable azoarenes catalytically. Commonly, azoarenes are prepared by azo coupling, the Mills and Wallach reaction. These methods demonstrate many disadvantages: (1) the azo coupling requires the formation of diazonium salts that can be explosive and are hard to synthesize, (2) the Mills and Wallach reactions requires excess amounts of toxic oxidants and reductants and produce mixture of byproducts, (3) catalytic transformation by these reactions are difficult to achieve, and (4) these methods are generally limited to the scope of specific azoarenes produced.[25] In contrast, the utilization of organic azide in nitrene coupling constitutes a simple one-step reaction to form azoarenes prompting numerous efforts to develop this transformation. However, despite this interest, there are only a few known examples where azoarenes are produced catalytically in transition metal catalysis. [20,26] Peters and coworkers have reported the catalytic nitrene coupling at the trigonal bipyramid iron complex. The reactivity was

proposed to occur through iron nitrene transfer, yet due to its instability, [Fe]=NR was not isolated. However, both EPR spectroscopy and stoichiometric reactions revealed that intermediate is [Fe=NR] and it is likely to be responsible for N-N bond formation.[20] Hillhouse and Heyduk illustrated the stoichiometric formation of azoarene using nickel and tantalum imido complexes, respectively[23,27] (**Figure 1.6**).

R = Mes or Ad   R = Mes or Ad
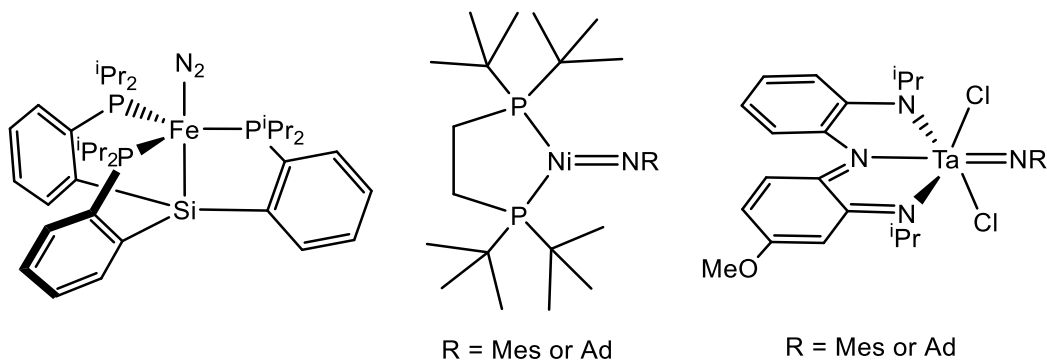
Figure 1.6. Selected low-coordinate complexes involved in stoichiometric and catalytic nitrene coupling to form azoarenes.

1.2. Activation of Heteroallenes by Low-Coordinate Transition Metal Complexes

In addition to the nitrene transfer catalysis, my dissertation also focuses on the activation of small molecules, in particular CO_2. CO_2 is the end product of the fossil fuels combustion. Therefore, it is inexpensive, readily available, and there is a significant motivation to transform it into useful organic products.[28] However, CO_2 is thermodynamically stable and kinetically inert; hence, its activation under mild conditions is among the most difficult chemical transformations.[29] In our research, we focus on the chemistry of CO_2 activation (as well as on the activation of related substrates) by its coordination to low-valent transition metal complexes. Depending on the electronic nature of the metal center, several reaction outcomes are feasible. A reductive splitting of CO_2 by a metal complex $[M^n]$ is a two-electron transformation, that leads to the formation of CO, along with $[M^{n+2}]=O$ species. Carbon monoxide is involved in the formation of carbonyl compounds and is utilized in the Fischer-Tropsch process to produce hydrocarbons.[30] CO can be

further reduced to methanol that can serve as a fuel.[31] In contrast, reductive coupling of CO_2 at the metal center $[M^n]$ is a one-electron process that can form bridging oxalate species $([M^{n+1}]_2(C_2O_4))$; oxalate can be used to make ethylene glycol, an important material in the production of polyethylene terephthalate resins and polyester fibers.[28b] **Figure 1.7** outlines an example of the reductive coupling and splitting of carbon dioxide by a reactive low-coordinate iron(I) precursor **1** to form complexes **2** and **3**, respectively.[32] Another featured example is depicted by Wolczanski and coworkers that shows the doxygenation of CO_2 at the low-valent early transition metal complexes containing Nb(III) (**4**) or Ta(III) (**5**) siloxide complexes. Compounds **4** and **5** reduce CO_2 to give oxo-metal compounds **6** and **7** along with CO release (**Figure 1.7**, bottom).[33]

Reductive coupling and splitting of CO$_2$ by late-transition metal complex
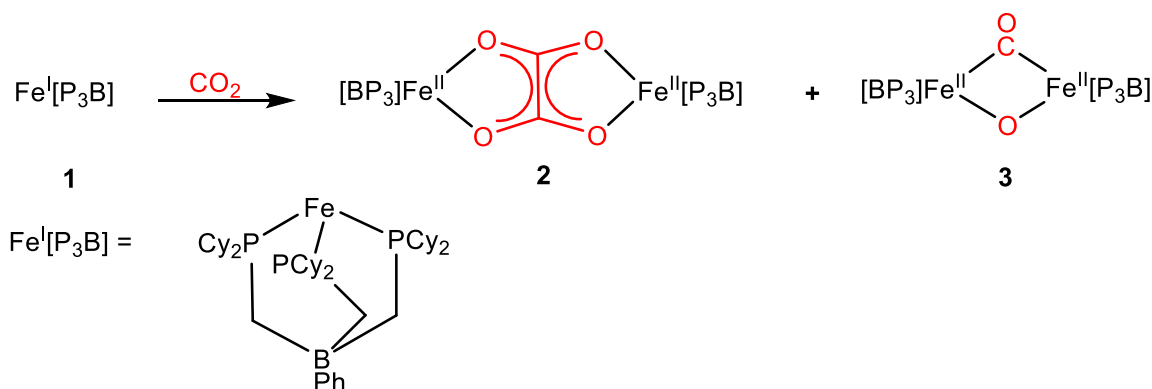
Reductive splitting of CO$_2$ by early-transition metal complexes
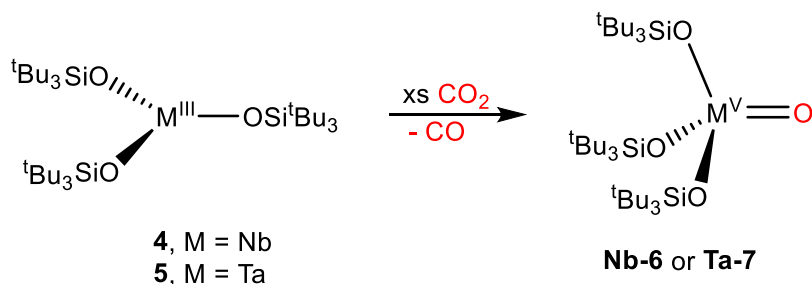
Figure 1.7. Example of reductive coupling and splitting of CO_2 by: Fe(I) precursor (top) and Nb(III) and Ta(III) tris(siloxide) complexes (bottom).

Carbon dioxide insertion into a metal-ligand bond M-X (where X = H, R, NR$_2$, OR, OH, PR$_3$ or other ligands), is another avenue for the activation of CO_2 using transition metal catalysts. There are two possible modes of CO_2 insertion into the M-X bond demonstrated in **Figure 1.8**.[29a]

when X = H or OR

(a)

(b)
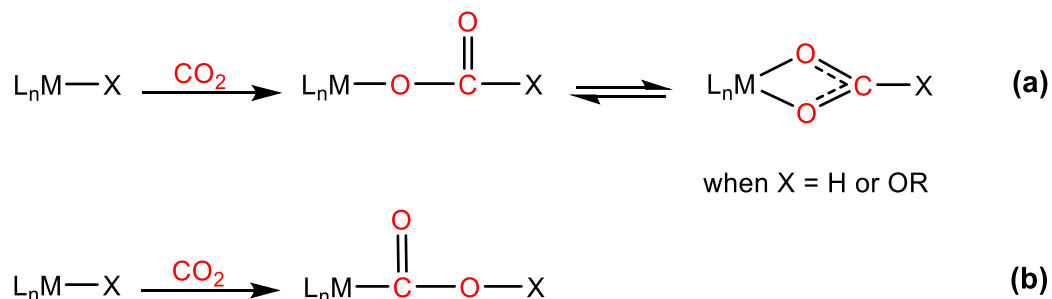
Figure 1.8. Possible modes for CO_2 insertion into M-X bond.

CO_2 insertion into the M-C bond is perhaps the most studied CO_2 insertion reactions due to their importance in C-C bond formation.[29a] When reactions follow path (a), alkyl carboxylic acids are obtained, and when path (b) is observed, metallo-acid esters are obtained (MCOOR) (See **Figure 1.8**). **Figure 1.9** illustrates the CO_2 insertion into the titanium alkyl bond to form the corresponding carboxylic acid.[34] Another example is the CO_2 insertion into the M-OR bond. This reaction is well-explored due to its importance in the CO_2 conversion to organic carbonates and polycarbonates.[35]
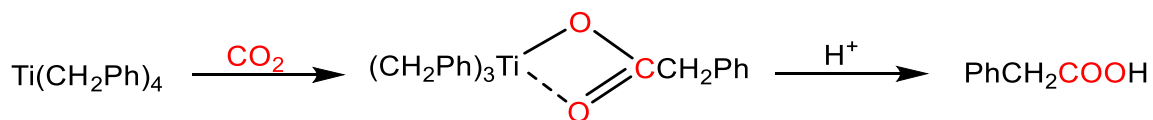
Figure 1.9. CO_2 insertion into M-X bonds: an example of C-C bond formation by CO_2 insertion into M-C bond to form alkyl carboxylic acid.

1.3. Using Bulky Alkoxides to Synthesize Reactive Low-Coordinate Transition Metal Complexes

As shown above, one commonly used approach to the activation of small molecules is the design of reactive low-coordinate transition metal centers in relatively low oxidation states.

Manipulation of the coordination environment and electronic structure at the metal center play an essential role in designing reactive precursors that will enable substrate binding and subsequent atom/group transfer chemistry. Reactive low-coordinate transition metal complexes are generally enabled by bulky ancillary ligands. The role of bulky ligand frameworks is to provide steric protection and allow for a desired electronic structure at the metal center. **Figure 1.10** demonstrates structures of isolated late-transition metal imido complexes (**8-11**) of relatively low coordination numbers. The relatively low coordination number are achieved due to the steric protection of the bulky groups in the ligand framework (**Figure 1.10**).[3d,18c,36]
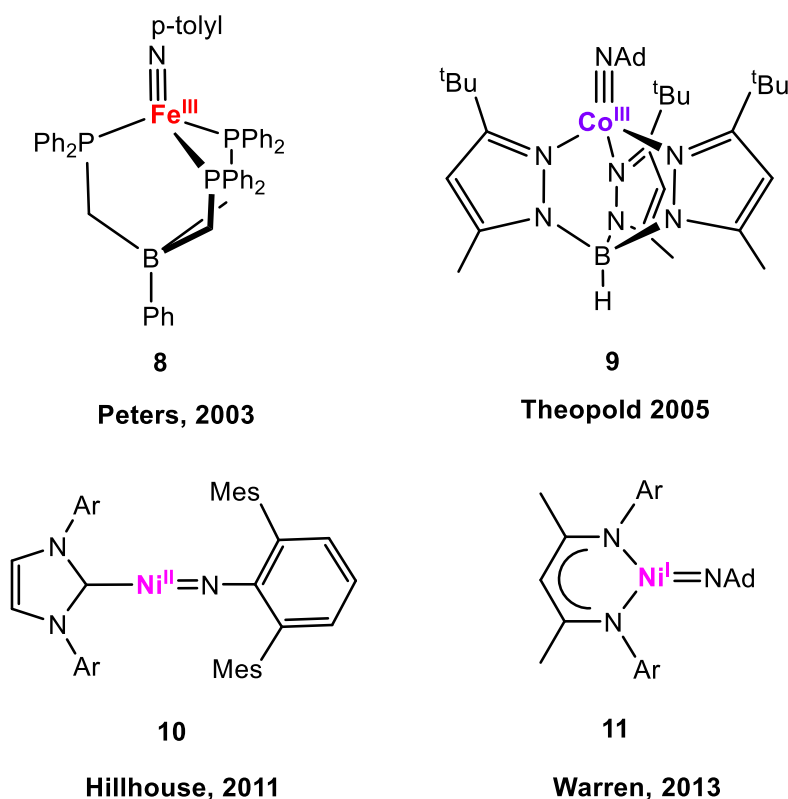
Figure 1.10. Selected examples of reactive late-transition metal-imido complexes stabilized by bulky ligands.

The Groysman group concentrates on the utilization of alkoxide ligands to design first-row transition metal complexes for group-transfer chemistry and small molecule activation. Bulky alkoxide ligands have been implicated as excellent candidates for stabilization of reactive low-

coordinate transition metal complexes.[33,37] Bulky alkoxides demonstrate multiple advantages as ancillary ligands: (1) their steric bulk protects the metal environment preventing aggregation, (2) their poor σ-donor and good π-donor ability create electrophilic reactive metal centers, (3) the ionic bonding of the alkoxides with early to mid-transition metals disfavors M-O cleavage and make them good supporting ligands, and (4) they are weak-field ligands that are capable of forming high-spin reactive metal-imido complexes; (5) their synthesis is generally straightforward. Despite these obvious advantages, the reactivity of low-coordinate first-row transition metals in bis(alkoxide) environments has not been explored thoroughly. While there is a number of isolated low-coordinate 3d metal complexes in alkoxide (or aryloxide) ligand environments, almost none of them were investigated in group-transfer chemistry (**Figure 1.11**).[38] **Figure 1.12** demonstrates an example of two-coordinate iron complex stabilized by bulky aryloxide. This complex reacts with organoazide to form transient Fe(IV)-imido, however, due to the fact the 2,6-substituents in the aryloxide ligand point toward the metal center, the imido group undergoes intramolecular reaction, thereby precluding its catalytic reactivity.[39]
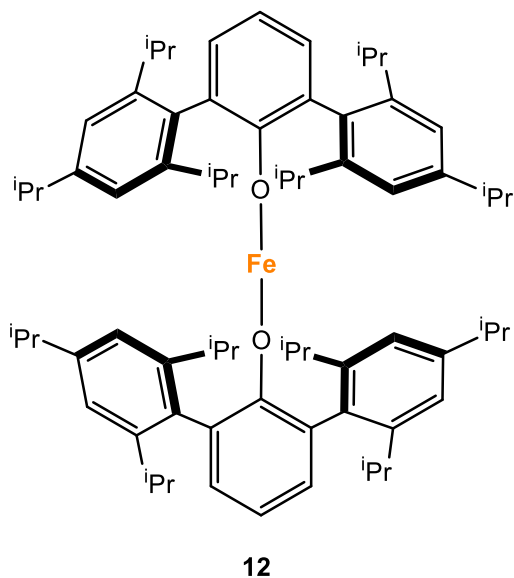
Figure 1.11. Example of a two-coordinate iron complex in the bis(aryloxide) environment.
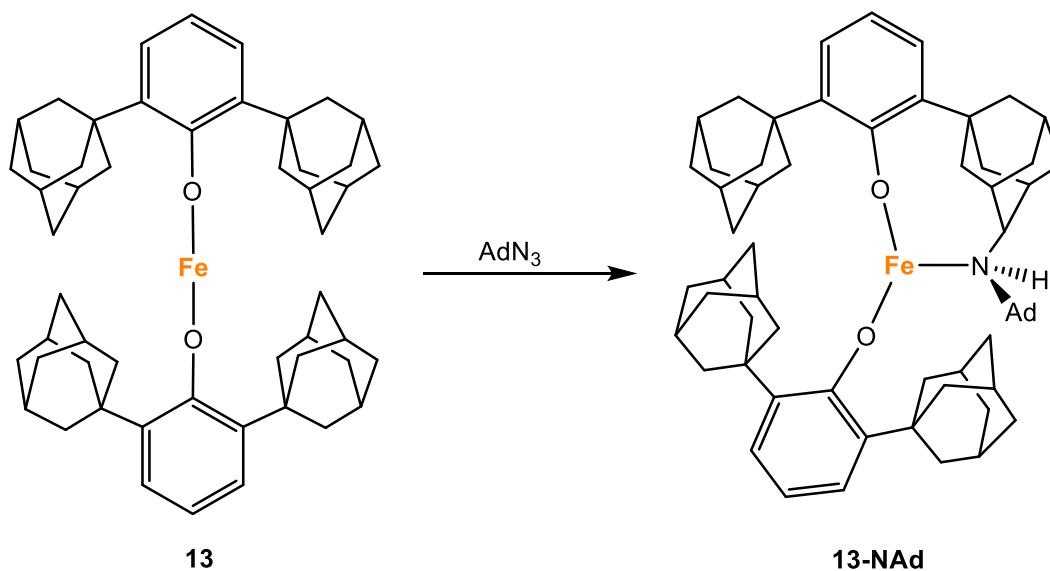
Figure 1.12. Reactivity of two-coordinate iron complex in the bis(aryloxide) environment.

Our group has previously reported the synthesis and characterization of the "first generation" bulky alkoxide ligand LiOR (R = C^{t}Bu$_2$Ph) (**Figure 1.13**).[40-42] This alkoxide ligand contains two *tert*-butyl groups that provide sufficient steric hindrance to shield the metal center and therefore create a mononuclear complex. *t*-Butyl groups also increase solubility in non-polar organic solvents generally required for the activation of small molecules. The role of the phenyl

group in [OC^{t}Bu$_2$Ph] is to (1) increase crystallinity of the resulting metal complexes; (2) allow modification of the "first-generation" ligand by the addition of substituents in the phenyl ring. Using this ligand, several reactive monomeric high-spin transition metal complexes in the bis(alkoxide) environment were isolated and characterized. These complexes had the general form M(OR)$_2$(THF)$_2$ where M = Mn - Co (selected Fe(OR)$_2$(THF)$_2$ complex (**14**) shown in **Figure 1.13**).[40-43] Our earlier studies were focused on exploring the reactivity of the "first generation" Fe(OR)$_2$(THF)$_2$ complex **14** toward organic azides. In the case of aryl azides, complex **14** displayed a selective catalytic formation of azoarenes when relatively bulky RN$_3$ were used (where R = 2,4,6-Me$_3$Ph or 2,6-Et$_2$Ph). The formation of azoarenes was accommodated by the unexpected formation of iron(III) tris(alkoxide) complex **15**. In contrast, unreactive iron(III) dimers **16-18** and compound **15** were obtained upon reactivity with less sterically hindered azides. We have attempted to intercept the transient nitrene complex by the addition of isocyanide (2,6-dimethylphenyl isocyanide, Ar'NC), in order to form a new C−N bond in the carbodiimide. However, the addition of a mixture of isocyanide and azide to the Fe(II) precursor has led instead to the formation of the stable bis(isocyanide) complex Fe(OR)$_2$(CNAr')$_2$ (**19**), which proved unreactive with excess azide (**Figure 1.13**).[42,43]
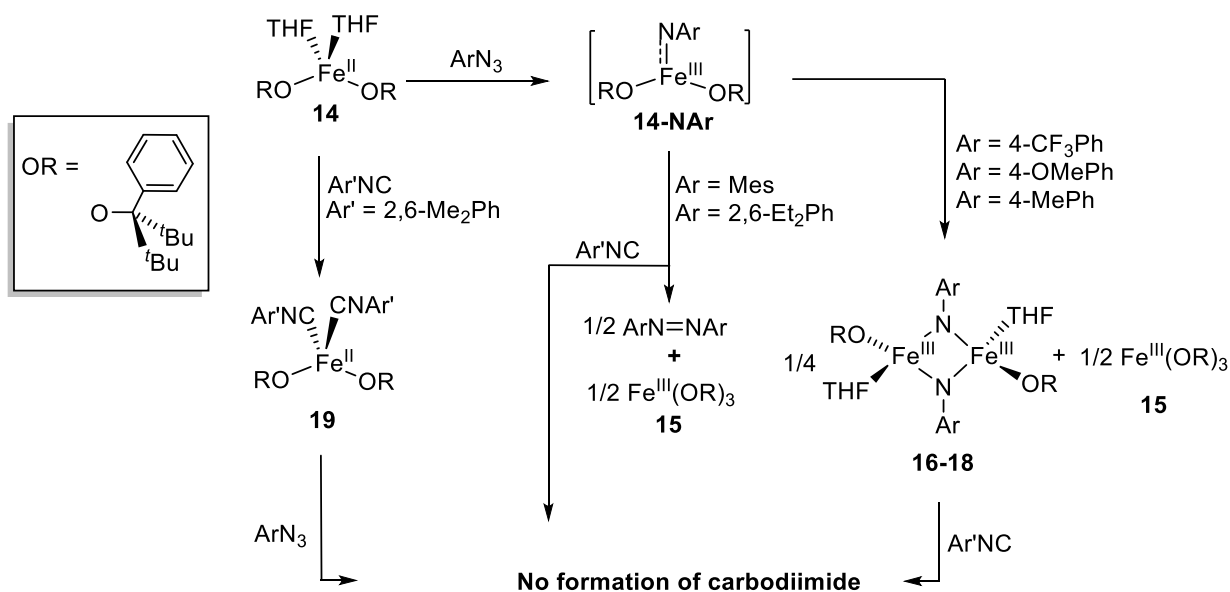
Figure 1.13. Reactivity of Fe(OR)$_2$(THF)$_2$ (**14**) explored previously by the Groysman group.

1.4. Summary and Outlook

Organoazides are versatile precursors for the catalytic formation of many useful organic compounds such as a carbodiimides, azoarenes, and aziridines. As the activation of organoazides under mild condition requires transition-metal catalysis, the development of cost-efficient low-valent first-row transition metal catalysts for the activation of organic azide is a growing field of study. Previously, the major focus of this research was on the low-valent transition metal complexes stabilized by good σ-donating/π-accepting ligands containing P-, N-, and C-based donors. In contrast, weak σ-donating/π-donating alkoxide ligands have not been well explored in these transformations. Thus, our research focuses on the use of weak-field alkoxide ligands to stabilize reactive mononuclear high-spin complexes of the M(OR)$_2$(THF)$_2$ form. Our previous investigation showed that our first-generation iron bis(alkoxide) system Fe(OR)$_2$(THF)$_2$ was indeed highly reactive with organoazides and formed transient iron-imido functionality. However, the insufficient steric bulk of [OC^{t}Bu$_2$Ph] led to formation of Fe(OR)$_3$ "sink" and therefore limited catalytic application of this precursor. Therefore, the major goal of this work was to modify our

catalytic system to enable wider range of catalytic transformations with organic azide and to explore the reactivity of the metal-alkoxide precursors with CO_2.

1.5. Research Statement and Objectives

This dissertation focuses, in large part, on N-N and N-C bond formation reactions that involve organoazides as the reactive substrate. Specifically, our primary goal is to tune the reactivity of our previous bis(alkoxide) catalysts to enable efficient catalysis of carbodiimides and azoarenes production. As mentioned earlier, the reactivity of the first-generation iron bis(alkoxide) system (**14**) is associated with two main problems: (1) the stoichiometric and catalytic transformation of organoazide to isocyanide is inhibited by the formation of $Fe(OR)_2(CNAr')_2$ (**19**), and (2) the catalytic coupling of organic azides to form azoarenes is limited to aryl azides with steric bulk in the *ortho* positions. To this end, we decided to use two approaches (outlined in **Figure 1.14**) to overcome these problems.

The first problem we encountered using complex **14**, was that the stability of iron(II) in the form of $Fe(OR)_2(CNAr')_2$ (**19**) sufficiently outweighs the stability of the obligatory intermediate $Fe(OR)_2(=NR)$ which therefore does not form. Consequently, we pursued an earlier transition metal, chromium, to synthesize stable imido complexes. Early transition metal-imido complexes are known to be more stable than later transition metal-imido compounds due to the availability of empty d orbitals that can participate in multiple bond formation between the metal center and the [NR] group (**Figure 1.2**).[44] We also anticipated that the isolable chromium imido complexes would be sufficiently reactivity to enable imido transfer to isocyanides. This hypothesis was based on two assumptions: (1) these complexes would exhibit relatively low coordination numbers, thus allowing binding of the substrate, isocyanide, and (2) the π donation to the metal, provided by

alkoxide ligands, would destabilize strong (triple) π bond between the metal center and the nitrene functionality, hence making chromium-imido complexes sufficiently reactive (**Figure 1.14**, left).

The second problem we encountered is that complex **14** showed only limited catalytic nitrene coupling to give the respective azoarene, with bulky aryl azides (MesN$_3$ and 2,6-Et$_2$PhN$_3$). In contrast, non-bulky organic azides formed unreactive dimeric complexes of Fe(OR)$_3$ **15** and (RO)(THF)Fe(μ-NAr)$_2$Fe(OR)(THF) **16-18**. Compounds **15** and **16-18** are incapable of forming azo products and hence limiting the range of azoarene formation (**Figure 1.13**).[43] We postulated that it is the slightly less than ideal size of our alkoxide [OR] enabled disproportionation of the alkoxide ligands, formed unreactive compounds Fe(OR)$_3$ and the imido dimers (RO)(THF)Fe(μ-NAr)$_2$Fe(OR)(THF), therefore shutting down the nitrene-transfer catalysis. We hypothesized that by increasing the steric profile of our alkoxide, we will disfavor the formation of these unreactive compounds, preserve the [Fe(OR)$_2$] composition of the catalyst, and therefore make our catalyst more stable and increase its substrate scope. (**Figure 1.14**, right).

Approach 1:
modifying the metal center

Approach 2:
modifying alkoxide ligand

NR

M

RO   OR
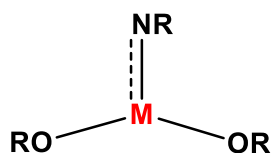
M = early transition-metal

L

Fe

R'O   OR'

R'O = bulkier alkoxide ligand

R

^{t}Bu
^{t}Bu

O$^-$

addition of
meta- substituents

R
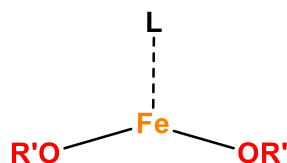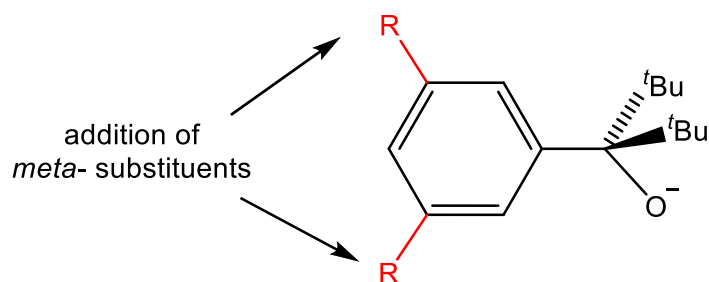
Figure 1.14. Proposed approaches to modify the "first-generation" catalyst to achieve better nitrene-transfer reactivity.

Another important goal of this research was to test the reactivity of our 3d bis(alkoxide) complexes in the activation of CO_2 and related substrates. As small molecules generally bind by the combination of weak σ-donation and π-back donation, catalysts for small molecules (CO_2 and N_2) are usually low-valent, low-coordinate metal complexes that contain strongly donating ancillary ligands. Our complexes satisfy some of these requirements, yet, alkoxides are not considered strongly donating ligands, and therefore we were curious to find out whether M(OR)$_2$-type complexes will be able to engage with CO_2. Toward this goal, we tested the reactivity of our bis(alkoxide) complexes with CO_2, as well as with organic carbonyls. As one of the possible reaction pathways with CO_2 involves oxo-transfer, we also investigated the stability of the oxo complexes in our bis(alkoxide) systems, using an oxo-transfer reaction.

To achieve these goals, we focused on the following objectives:

1. ***Catalytic nitrene transfer to isocyanides at the mononuclear chromium (II/IV) bis(alkoxide) complexes.*** Synthesis of chromium imido complexes in the bis(alkoxide) environment and their nitrene transfer reactivity to isocyanide is presented and discussed in **Chapter 2**.

2. ***Synthesis and characterization of bulkier alkoxide ligands and the preparation of the second-generation low-coordinate transition metal bis(alkoxide) complexes.*** The synthesis and characterizations of the new alkoxide ligands and bis(alkoxide) complexes is presented and discussed in **Chapter 3**.

3. ***Catalytic nitrene coupling using second-generation iron bis(alkoxide) complex and the formation of iron tetrazene complexes.*** The reactivity of the "second-generation" iron bis(alkoxide) complex toward organic azides is explored and compared to the results obtained by our "first-generation" iron(II) precursor. This objective is presented in **Chapter 4**.

4. ***The reactivity of a chromium bis(alkoxide) complex toward organic carbonyls and CO_2.*** The reductive coupling of aldehydes by chromium(II) complex is explored and compared to the reactivity of ketones at the Cr(II) center. Also, the reactivity of chromium bis(alkoxide) with CO_2 is presented and discussed. This objective is addressed in **Chapter 5**.

5. ***Exploring oxo- and sulfur- atom transfer reactions using the first-generation iron bis(alkoxide).*** The synthesis and characterization of iron oxo and sulfido complexes is presented in **Chapter 6**.

These topics were developed over the period of the last four years and constitute the body of this dissertation.

**CHAPTER 2 CATALYTIC NITRENE TRANSFER TO ISOCYANIDES AT THE
MONONUCLEAR CHROMIUM(II/IV) BIS(ALKOXIDE) COMPLEXES**

Parts of the text in this chapter were reprinted or adapted with permission from: Yousif, M.;

Tjapkes, D. J.; Lord, R. L.; Groysman, S. *Organometallics* **2015**, *34*, 5119-5128.

2.1. Introduction

As mentioned in chapter 1, our "first-generation" iron bis(alkoxide) demonstrated exciting

reactivity with various aryl azides that involved spontaneous nitrene coupling or formation of

iron(III)-bridging imido dimers. It is highly likely that this reaction proceeded via a terminal metal-

imido intermediate. However, due to the high reactivity of this intermediate, we were not able to

isolate it and investigate its reactions in a controlled fashion. For this purpose, we decided to

synthesize stable imido species with a different metal, chromium. Chromium imido complexes are

generally more stable than iron-imido due to the lower d-electron counts and therefore stronger

bonds. A stable chromium-imido in a bis(akoxide) environment could enable a snapshot of other

imido species in our system. It also gives us an opportunity to investigate the interaction of

preformed stable "metal nitrene" species in bis(alkoxide) ligand environments with isocyanides,

as we were not able to obtain this reaction with a postulated iron-imido intermediate. This chapter

focuses on the synthesis of chromium-imido complexes using a chromium bis(alkoxide) precursor

and their stoichiometric and catalytic reactivity with isocyanide to form asymmetric

carbodiimides. The detailed mechanism of carbodiimide formation catalyzed by Cr imido

(Cr=NR) species using spectroscopy and DFT calculations is discussed.

2.2. Synthesis and Characterization of the Cr(II) Precursor Cr$_2$(OR)$_4$

Groysman group has previously reported that M(OR)$_2$(THF)$_2$ (M = Mn−Co) complexes

can be obtained by treating the seesaw cluster [Cr$_2$Li$_2$X$_2$(OR)$_4$] with two equivalents of TlPF$_6$. For

Cr, this strategy failed to lead to the "Cr(OR)$_2$(THF)$_2$" species.[43] Seeking an alternative route to

Cr(OR)$_2$(THF)$_2$, we synthesized the previously reported Cr((N(SiMe$_3$)$_2$)$_2$(THF)$_2$.[45] Purple Cr(N(SiMe$_3$)$_2$)$_2$(THF)$_2$ underwent protonolysis with HOR[46] to form green homodinuclear Cr$_2$(OR)$_4$ (**20**; 60% yield). It is worth noting that the protonolysis reaction was conducted in THF, and no Cr(OR)$_2$(THF)$_2$ formation was observed (**Figure 2.1**).

$$Cr^{II}(N(SiMe_3)_2)_2(THF)_2 \xrightarrow[- 2\ HN(SiMe_3)_2]{2\ HOR,\ THF} 1/2$$
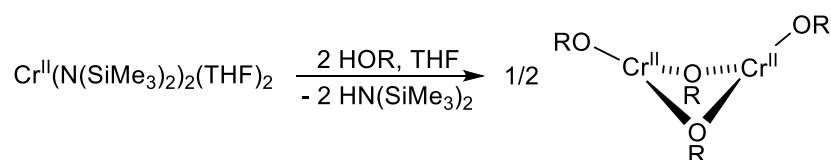
Figure 2.1. Synthesis of Cr$_2$(OC^{t}Bu$_2$Ph)$_4$ (**20**).

The structure of **20**, featuring two trigonal-planar Cr(II) centers each bridged by two alkoxides, is given in **Figure 2.2**. Compound **20** is related to the previously synthesized Cr$_2$(OSi^{t}Bu$_3$)$_4$[47] and Cr$_2$(OCH^{t}Bu$_2$)$_2$(OC^{t}Bu$_3$)$_2$.[48] The Cr–Cr separation is 2.651(1) Å in complex **20**, in comparison with 2.637(2)/2.6800(2) Å in Cr$_2$(OSi^{t}Bu$_3$)$_4$ and 3.075(1) Å in Cr$_2$(OCH^{t}Bu$_2$)$_2$(OC^{t}Bu$_3$)$_2$. The solution magnetic moment of compound **20** was found to be μ_{obs} = 2.5 ± 0.3 μ_B (2.8 μ_B in Cr$_2$(OSi^{t}Bu$_3$)$_4$), indicative of some antiferromagnetic interaction between the Cr(II) centers.[47]
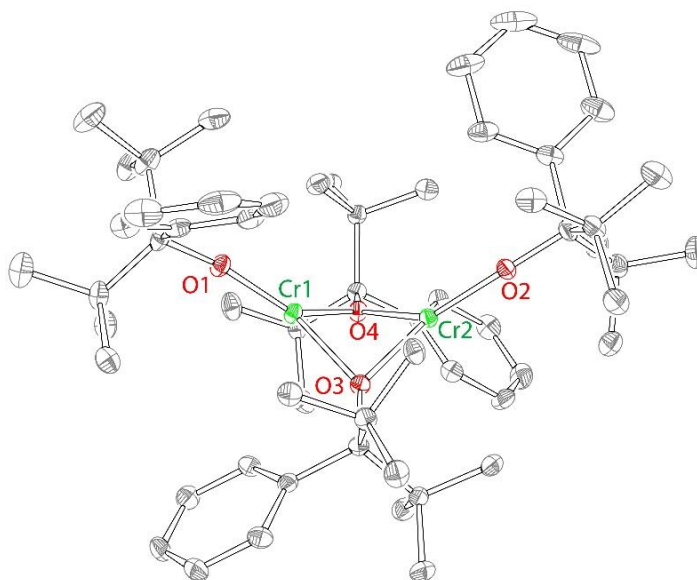
Figure 2.2. X-ray Structure of **20**.

2.3. Synthesis and Characterization of Cr(IV) Imido Complexes

To study the imido group-transfer chemistry of $Cr_2(OC^tBu_2Ph)_4$ (**20**), we treated complex

20 with 2 equivalents of mesityl azide (N_3Mes), adamantyl azide (N_3Ad), or 2,6-diethylphenyl

azide (N_3DEP). This reaction, followed by recrystallization, affords the deep red Cr mono(imido)

complexes $Cr(OR)_2(NMes)$ (**21**, 81%), $Cr(OR)_2(NAd)$ (**22**, 64%), and $Cr(OR)_2(NDEP)$ (**23**, 23%)

(**Figure 2.3**). Treatment of **20** with excess azide N_3R^1 (R^1 = Mes, Ad) does not form the

corresponding bis(imido) complexes. We also note that the treatment of **20** with bulkier azides

(2,6-diisopropylphenyl azide and 2,4,6-triphenylphenyl azide) failed to form the corresponding

imido complexes. All Cr mono(imido) compounds were found to be extremely air sensitive.

Complexes **21** and **22** were characterized by X-ray crystallography, IR spectroscopy, UV−vis

spectroscopy, solution magnetic moment measurements, and elemental analysis. Compound **23**

was isolated in low yield, due to its high solubility in pentane, and therefore was characterized

only by X-ray diffraction and IR spectroscopy. X-ray-quality crystals of the imido complexes

21−23 were obtained from pentane (**21** and **23**) and hexane (**22**) at -35 °C. The structures (**Figure**

2.4 and **Table 2.1**) display trigonal-planar Cr centers (sums of angles around Cr are 359.9° (**21**), 360.0° (**22**), and 359.6° (**23**)) with relatively short Cr−imido distances of 1.651(2) Å (**21**), 1.632(1) Å (**22**), and 1.656(2) (**23**). We note that Wolczanski and co-workers documented several related trigonal Cr imido species bearing a silox ligand, Cr(OSi^{t}Bu$_3$)$_2$(NR).[47] We also note that the structures of the Cr-imido complexes **21-23** are similar to the computationally derived iron analogue (of **21**).[43]
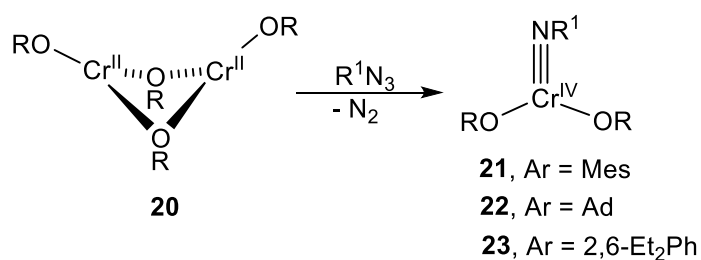
Figure 2.3. The synthesis of chromium imido complexes **21-23**.
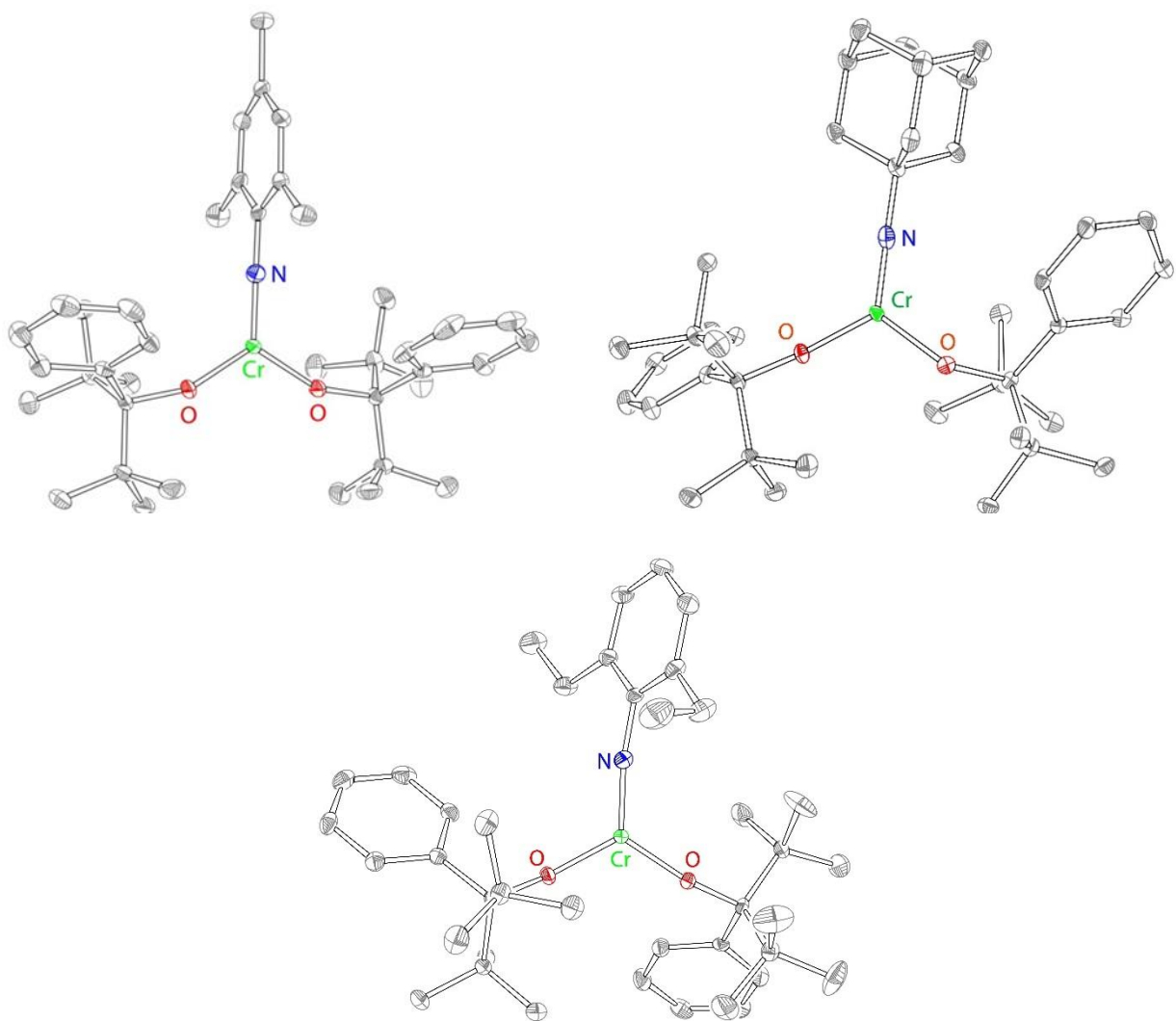
Figure 2.4. Top: molecular structures of compounds **21** (left) and **22** (right). Bottom: molecular structure of compound **23**.

The structure of Cr(OSi^{t}Bu$_3$)$_2$(N-2,6-diphenylphenyl) similarly demonstrated trigonal geometry at the Cr center and a short Cr−N bond distance of 1.649(2) Å.[47] Solution magnetic moments of compounds **21** and **22**, obtained using the Evans method,[49] were found to be μ_{obs} = 2.5 ± 0.3 μ_B and μ_{obs} = 3.3 ± 0.4 μ_B, respectively, in comparison with 2.7−2.8 μ_B values observed for Cr(OSi^{t}Bu$_3$)$_2$(NR).[47] These values are indicative of triplet ground states, which are consistent with DFT calculations discussed in the section 2.4 below.

Table 2.1. Experimental crystallographic parameters for **20-23**.

complex	20	21	22	23
formula	$C_{60}H_{92}Cr_2O_4$	$C_{39}H_{57}CrNO_2$	$C_{40}H_{61}CrNO_2$	$C_{40}H_{59}CrNO_2$
fw	981.38	623.89	639.93	637.90
crystal system	triclinic	monoclinic	triclinic	monoclinic
space group	*P-1*	*C2*	*P2$_1$/c*	*C2/c*
a (Å)	11.2537(7)	20.0987(15)	16.5562(12)	38.980(3)
b (Å)	15.7690(10)	9.4936(6)	11.6116(8)	7.9005(5)
c (Å)	18.3056(10)	23.0515(16)	19.6220(14)	23.3612(14)
α (deg)	92.830(2)	90.00	90.00	90.00
β (deg)	103.028(2)	114.717(6)	108.219(3)	94.504(2)
γ (deg)	97.627(2)	90.00	90.00	90.00
V (Å^3)	3126.3(3)	3995.47	3583.1	7172.13
D$_c$ (g cm^{-3})	1.168	1.157	1.186	1.181
Z	2	4	4	8
μ (mm^{-1})	0.394	0.322	0.353	0.353
T (K)	100(2)	100(2)	100(2)	100(2)
R$_1$	5.17	4.52	3.95	4.01
GOF	1.244	1.074	1.070	0.913

2.4. Computational Characterization

To shed light on the electronic structure of bis(alkoxide) mono(imido) complexes, we characterized them by DFT calculations. This and other DFT studies presented in this dissertation

were carried out in collaboration with the group of Prof. R. L. Lord at GVSU. The bis(alkoxide) mono(imido) species **21** and **22** were optimized as a singlet, triplet, and quintet at the B3LYP/631G(d) level of theory. No simplifications were made to the bulky alkoxide ligands. For **21**, the triplet was calculated to be lowest in free energy, followed by the singlet (+11.42 kcal/mol) and then the quintet (+20.74 kcal/mol). A similar pattern was observed for **22** with triplet < singlet (+13.31 kcal/mol) < quintet (+33.97 kcal/mol). This finding is consistent with the experimental and calculated spin states in the related Cr=NR′ species supported by siloxide ligands.[47] On the basis of the large thermodynamic preference for the triplet state that matches the experimental magnetic data, we focused on the triplet for the structural and electronic analysis. A trigonal planar arrangement about Cr was observed in the optimized structures of **21** and **22** (**Figure 2.5**). Excellent agreement with the X-ray data is observed for the Cr−N bond lengths in **21** (1.655 vs 1.651 Å) and **22** (1.635 vs 1.632 Å). It is worth noting that one of the alkoxide arms is oriented with the phenyl group *anti* to the imido group in **21**, in contrast to the crystallographic orientation, where one of the tBu groups is *anti* to the imido group in both alkoxide arms.
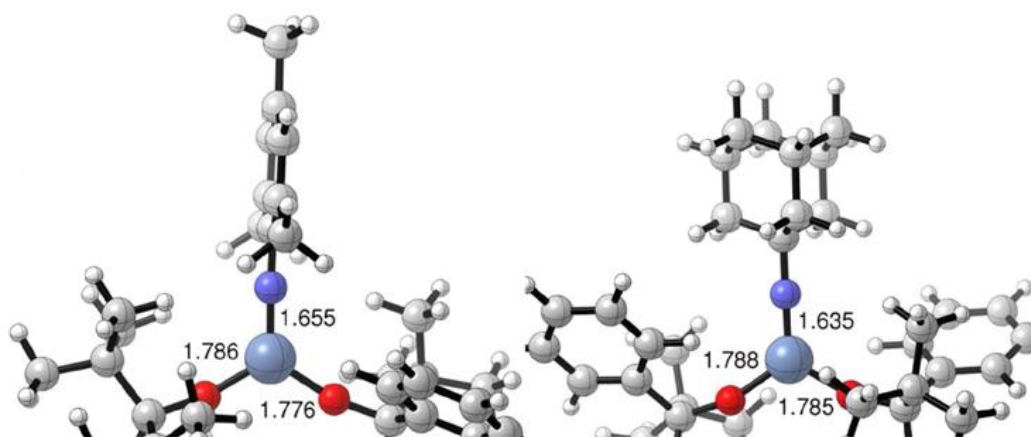
Figure 2.5. Optimized structures of triplet **21** (left) and **22** (right). Important bond lengths are given in Å. Note that parts of the alkoxide ligands are excluded from the image for clarity.

The electronic structure of **21** was investigated by calculating the corresponding orbitals[50] that are shown in **Figure 2.6**. There are two singly occupied molecular orbitals based on the Cr ion and two doubly occupied π orbitals between the imido fragment and Cr that are mainly based on NR′. Based on this orbital occupation pattern, **21** and **22** are best characterized as having a Cr(IV) ion that is triply bonded to the NR[1] fragment.[51]
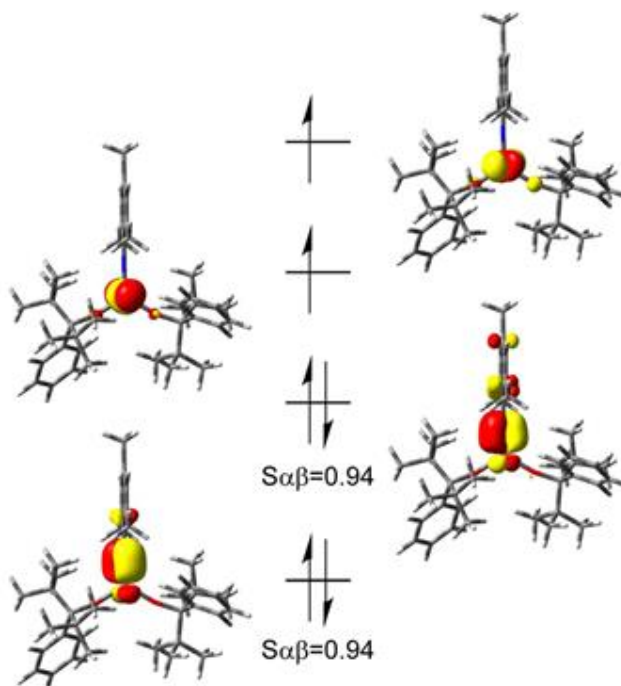
Figure 2.6. Corresponding orbitals for triple **21**. Orbital isosurfaces are plotted at isodensity value of 0.05 au.

2.5. Synthesis and Characterization of Cr(VI) Bis(imido) Complexes

Azides featuring relatively bulky R groups (R = adamantyl, mesityl, 2,6-diethylphenyl) led selectively to the formation of mono(imido) complexes. We have also investigated the reactivity of the Cr(II) precursor with selected aryl azides featuring less bulky Ar groups (Ar = 4-methoxyphenyl, 4-trifluorophenyl). The reaction of compound **20** with 2 equivalents of 4-methoxyphenyl azide or 4-trifluorophenyl azide results in the formation of deep red-brown Cr(VI)

diimido complexes $Cr(OR)_2(NAr)_2$ that are isolated as brown crystals in 46% and 30% yields, respectively (**Figure 2.7**). The reaction of **20** with 1 equivalent of 4-methoxyphenyl azide also leads to the formation of Cr(VI) bis(imido) species, as demonstrated by ^1H NMR and IR spectroscopy. We were not able to isolate or observe mono(imido) species from these reactions. For $[Cr(OSi^tBu_3)_2]$, it was also reported that bulky azides form mono(imido) species while non-bulky azides form bis(imido) complexes at room temperature.[47]
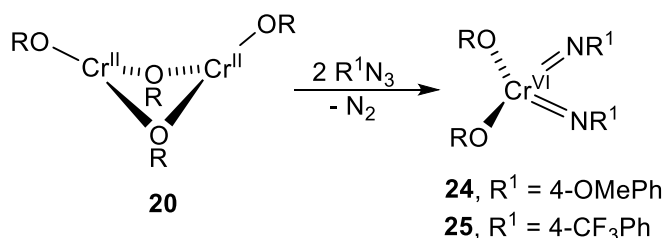
Figure 2.7. Synthesis of complexes **24** and **25**.

Cr(VI) bis(imido) complexes **24** and **25** are diamagnetic species that were characterized by ^1H and ^{13}C NMR (and ^{19}F for **25**) spectroscopy (**Appendix B**), IR spectroscopy, X-ray crystallography, and elemental analysis. NMR spectroscopy is consistent with an effective C_{2v} symmetry in solution, displaying a single type of ^tBu group and a phenyl group for both [OR] ligands. X-ray crystallography (**Figure 2.8** and **Table 2.2**) demonstrates pseudotetrahedral complexes featuring RO−Cr−OR angles of 111.4(2)° (**24**) and 113.4(3)° (**25**) and ArN−Cr−NAr angles of 104.9(3)° (**24**) and 106.6(4)° (**25**). Cr−imido bond distances are 1.641(5)/ 1.664(5) Å for **24** and 1.648(7)/1.667(7) Å for **25**.
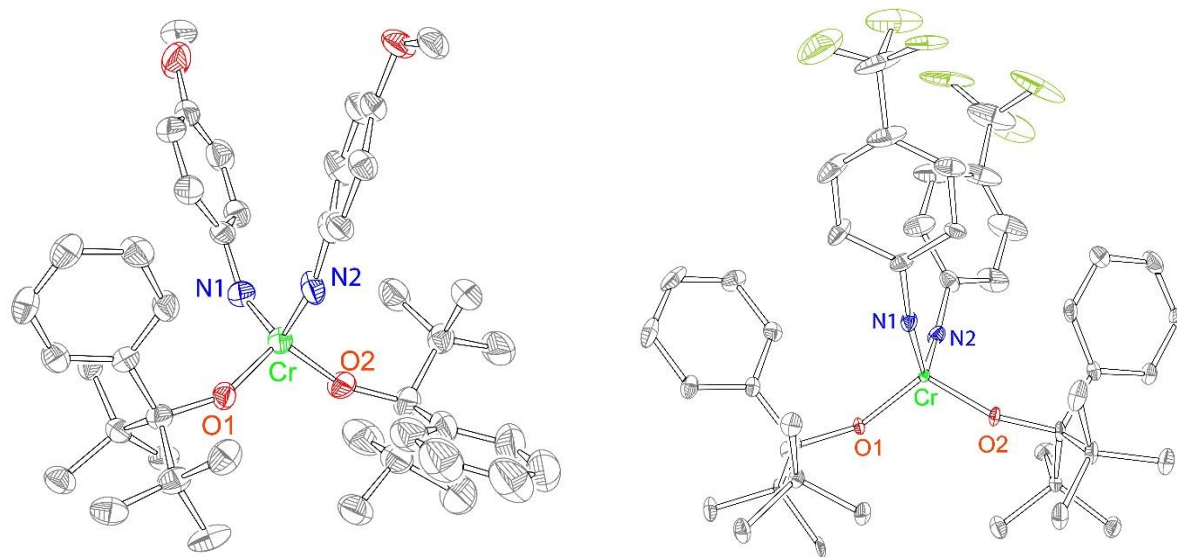
Figure 2.8. Molecular structures of complexes **24** (right) and **25** (left).

Table 2.2. Experimental crystallographic parameters for **24** and **25**.

complex	**24**	**25**
formula	$C_{44}H_{60}CrN_2O_4$	$C_{44}H_{54}CrF_6N_2O_2$
fw	732.97	808.91
crystal system	triclinic	triclinic
space group	*P-1*	*P-1*
a (Å)	12.7520(11)	8.4734(6)
b (Å)	14.2255(12)	11.3509(9)
c (Å)	22.6759(19)	11.3509(9
α (deg)	89.863(4)	99.899(4)
β (deg)	89.122(4)	91.980(4)
γ (deg)	77.243(4)	100.716(4)
V (Å^3)	4011.48	2058.7(3)
D_c (g cm^{-3})	1.213	1.305
Z	4	2
μ (mm^{-1})	0.328	0.343
T (K)	100(2)	100(2)
R_1	8.88	12.87
GOF	1.043	1.103

2.6. Reactions of Cr Imido Complexes with Isocyanides

To test the stoichiometric reactivity of the Cr mono(imido) complexes, complexes **21** and

22 were treated with 1 equivalent of 2,6-dimethylphenyl isocyanide (2,6-Me$_2$PhNC) in C$_6$D$_6$ in

the presence of an internal standard. Monitoring of the reaction by ^{1}H NMR spectroscopy (**Figure 2.9**) revealed the disappearance of the isocyanide peaks and the appearance of new peaks that were attributed to formation of the respective carbodiimides N-(2,6-dimethylphenyl)-N-mesitylmethanediimine[18] and N-adamantyl-N-(2,6-dimethylphenyl)methanediimine. The observed NMR yields of the carbodiimides were 100% and 68%, respectively. The formation of carbodiimides was also confirmed by mass spectrometry.
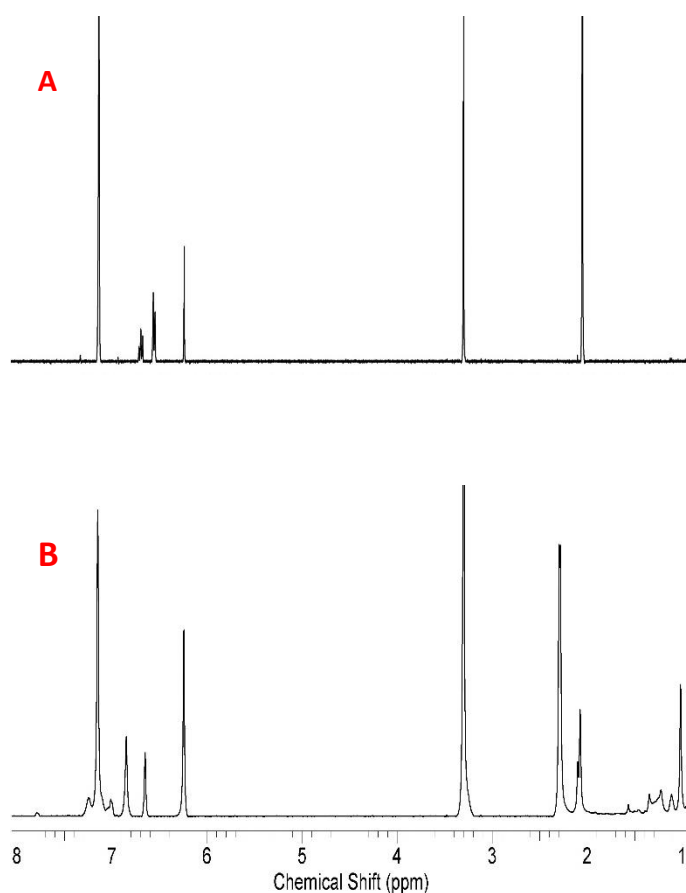
Figure 2.9. (**A**) C_6D_6 spectrum of isocyanide 2,6-Me$_2$NC (δ 6.71, 6.57, and 2.05 ppm) in the presence of an internal standard (trimethoxybenzene, δ 6.25 and 3.30 ppm) in the 1-8 ppm region. (**B**) Spectrum of the mixture (**A**) with complex **21** demonstrating the formation of (2,6-Me$_2$Ph)N=C=NMes (δ 6.85, 2.30, 2.28, and 2.07 ppm).

To gain insight into this reaction, we calculated the binding of 2,6-dimethylphenyl isocyanide to the triplet Cr(IV) imido intermediates. We denote these isocyanide-bound

intermediates as **21−CNR″** and **22−CNR″** for mesityl and adamantyl, respectively. Formation of **21−CNR″** and **22−CNR″** is slightly uphill by 11.7 and 5.3 kcal/mol. Isocyanide binding disrupts π bonding to the imido group (see **Figure 2.10**, left), as evidenced by elongation of the Cr−N bond from 1.655 to 1.672 Å for **21−CNR″** and from 1.635 to 1.653 Å for **22−CNR″**. Concurrently, the Cr−N−R′ angle decreases from 177.1 to 168.5° in **21−CNR″** and from 178.6 to 160.9° in **22−CNR″**. Next, we attempted to find a transition state for nucleophilic attack by this coordinated isocyanide on the imido group. Attempts with mesityl have been unsuccessful thus far, but the optimized transition state for adamantyl is shown in **Figure 2.10** (right). This transition state is calculated to be uphill in free energy by 23.3 kcal/mol relative to free isocyanide and **22**, which should be accessible under the experimental conditions. Elongation of the Cr−N and shortening of the Cr−C bond lengths to 1.721 and 1.924 Å is observed. The new C−N bond is still relatively long at 1.899 Å; however, visualization of the normal mode corresponding to the imaginary frequency shows significant motion along the C−N bond. The triple-bond character of isocyanide is slightly reduced, with elongation from 1.172 Å in **22−CNR″** to 1.197 Å in this transition state. An intrinsic reaction coordinate[37] calculation demonstrated that this transition state connects **22−CNR″** to a species with carbodiimide bound to $Cr(OR)_2$. Optimization of the carbodiimide adducts for both mesityl and adamantyl resulted in structures that are uphill relative to free isocyanide and **21**/**22** by 9.2 and 0.6 kcal/mol, respectively. The endergonic reaction energy for **21** may indicate why we have been unable to identify the transition state for carbodiimide formation with this species.
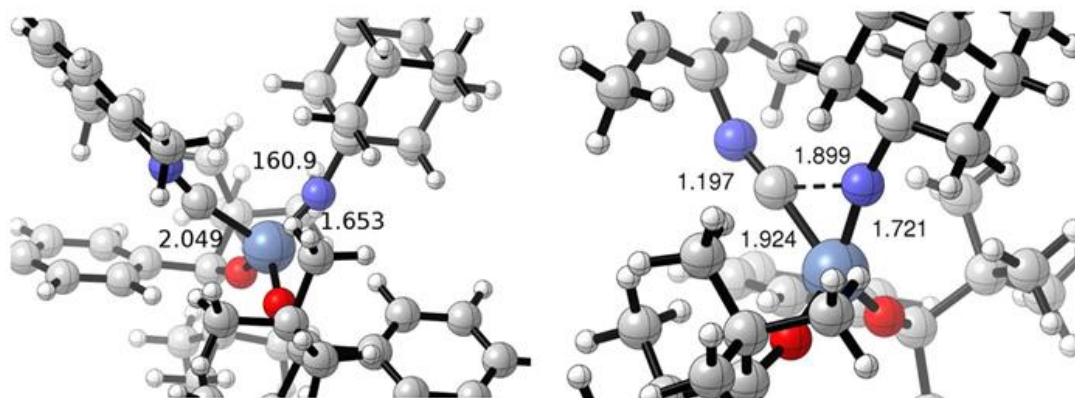
Figure 2.10. Optimized structure of **22-CNR''** (left) and the transition state for carbodiimide formation for **22** (right). Important bond lengths are labeled in and bond angles in deg. Note that parts of the alkoxide ligands and isocyanide/imido substituents are excluded from the image for clarity.

Using 1 equivalent of isocyanide, we observed the formation of carbodiimide; however, we were not able to isolate the Cr-containing product. Thus, we decided to treat Cr mono(imido) species with excess isocyanide. The reaction of complex **21** with 5 equivalents of 2,6-dimethylphenyl isocyanide resulted in complete conversion to the respective carbodiimide, as indicated by ^{1}H NMR spectroscopy (**Figure 2.11,** top). Solvent removal and crystallization at -35 °C from hexanes produced deep brown crystals of $Cr^{II}(OR)_2(CNR_2)_4$ (**26**; 56%). Chromium-ligated isocyanides can be further converted to carbodiimides: the reaction of complex **26** with 5 equiv of MesN$_3$ produced the corresponding carbodiimide in 96% yield (based on isocyanide), as indicated by ^{1}H NMR spectroscopy (**Figure 2.11,** bottom). We were not able to isolate a chromium-containing product from this reaction (**Appendix B**).
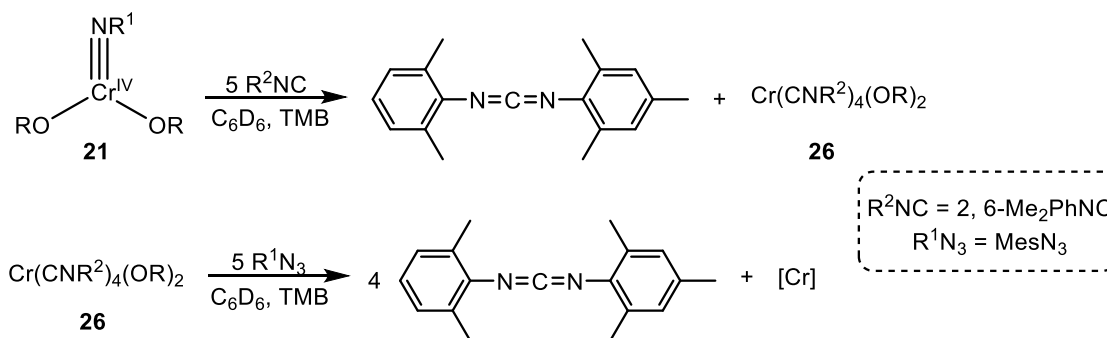
Figure 2.11. Reactivity of **21** with isocyanide (top) and **26** with azide (bottom).

Compound **26** was characterized by X-ray crystallography, IR spectroscopy, and solution magnetic moment measurements. The X-ray structure of compound **26** (**Figure 2.12**) reveals a pseudooctahedral Cr(II) complex containing two alkoxide ligands and four isocyanides. This compound is a rare example of a Cr complex combining isocyanide and alkoxide ligands.[52] Wolczanski and co-workers synthesized [Cr(OSi^{t}Bu$_3$)$_2$(CN^{t}Bu)$_2$]. Due to the two observed CN absorptions (major peak at 2192 cm^{-1}, minor peak at 2099 cm^{-1}), the compound was proposed to exist as a mixture of *cis* and *trans* (major) isomers.[47] In **26**, the bulky alkoxides occupy mutually *trans* (axial) positions, whereas isocyanides form an equatorial plane. The IR spectrum of **26** reveals the CN group absorption at 2063 cm^{-1} (singlet), versus 2116 cm^{-1} in free 2,6-dimethylphenyl isocyanide.[53,54] Other Cr(II) isocyanide complexes generally demonstrate lower CN stretching frequencies,[55] thus indicating relatively electron-deficient isocyanides in the bis(alkoxide) complex **26** or in [Cr(OSi^{t}Bu$_3$)$_2$(CN^{t}Bu)$_2$].
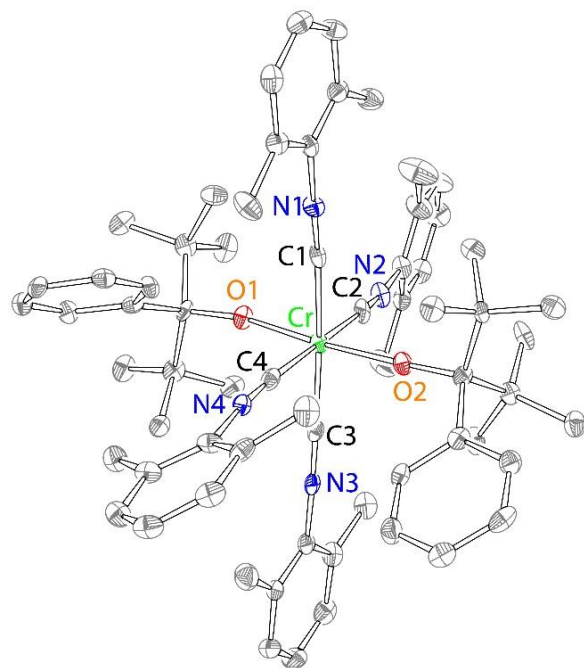
Figure 2.12. X-ray structure of complex **26**.

Table 2.3. Experimental crystallographic parameters for **26**.

complex	26
formula	$C_{66}H_{82}CrN_4O_2$
fw	1015.38
crystal system	triclinic
space group	*P*-1
a (Å)	11.411(2)
b (Å)	11.8024(18)
c (Å)	21.695(4)
α (deg)	93.822(5)
β (deg)	99.414(6)
γ (deg)	102.134(6)
V (Å^3)	2802.57
D_c (g cm^{-3})	0.997
Z	2
μ (mm^{-1})	0.240
T (K)	100(2)
R_1	7.75
GOF	0.821

2.7. Reactions of Cr(VI) Bis(imido) Complexes with Isocyanides

We have also investigated the reactivity of Cr(VI) bis(imido) complexes **24** and **25** with 2,6-dimethylphenyl isocyanide. The experiments were conducted in a manner similar to the

experiments involving [NR] transfer from Cr(IV) mono(imido) complexes: C_6D_6 solutions of the relevant Cr(VI) complexes were treated with C_6D_6 solutions containing 6 equivalents of 2,6-dimethylphenyl isocyanide and the internal standard trimethoxybenzene. In both cases, no reaction was observed (**Figure 2.13**). The ^1H NMR spectrum of complex **25** in the range 1−9 ppm (A), the spectrum of the isocyanide in the presence of the internal standard in the same range (B), and the ^1H NMR spectrum resulting upon mixing a solution of the isocyanide/standard from A with the solution of the complex from B (C) are given in **Figure 2.14**. Spectrum C clearly demonstrates that no change takes place, as it appears as a superposition of spectra A and B (**Figure 2.14**). We therefore conclude that the formation of Cr(VI) bis(imido) complexes encumbers the imido group transfer to isocyanides. It is possible that, due to the steric hindrance, Cr(VI) bis(imido) cannot bind an additional ligand (isocyanide), thus preventing formation of carbodiimide. We note that Wilkinson, Hursthouse, and co-workers reported imido group transfer to an isocyanide at the Cr(VI) bis(imido) complex $Cr(N^tBu)_2(Mes)_2$ at room temperature to form an isolable metal-bound carbodiimide.[56]

RO—Cr^{VI}(=NR^1)$_2$(OR) + CNR^2 ⟶ ✗ ⟶ R^1-N=C=N−R^2

24, R^1 = 4-OMePh
25, R^1 = 4-CF$_3$Ph

R^2 = 2,6-Me$_2$Ph
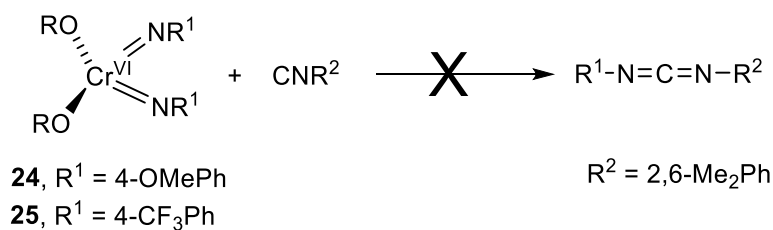
Figure 2.13. Reaction of complex **24** or **25** with R^2NC does not lead to the formation of the corresponding carbodiimide.
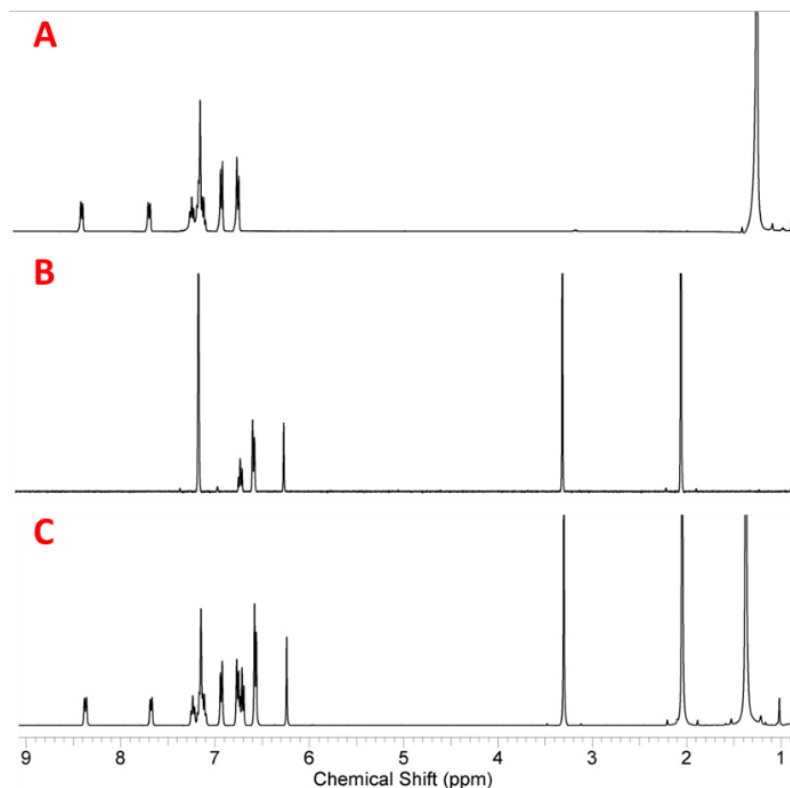
Figure 2.14. (**A**) ^{1}H NMR spectrum of complex **25** in 1-9 ppm range. (**B**) Spectrum of 2,6-dimethylphenyl isocyanide in the presence of internal standard (TMB). (**C**) Spectrum of the mixture of the isocyanide and compound **25**, demonstrating the lack of formation of the corresponding carbodiimide.

We have also investigated the possibility of carbodiimide formation by treating complex **26** with the non-bulky azides N_3R^1 (R^1 = 4-methoxyphenyl, 4trifluorophenyl). Monitoring the reaction by ^{1}H NMR spectroscopy indicated no formation of the respective carbodiimide.

Our stoichiometric and DFT experiments suggested that the mechanism for the formation of carbodiimides proceeds via the formation of Cr(IV) imido complex first. This compound then reacts with isocyanide(s) to form carbodiimide along with chromium(II) tetrakis(isocyanide) complex. Cr(II) complex reacts next with another azide to release N_2 and form the respective carbodiimide and the Cr(IV) complex (**Figure 2.15**).

$$\text{NR}^1$$
$$\text{Cr}^{\text{IV}}(\text{OR})_2$$

4 R^1NCNR^2

N_2

5 CNR^2

5 N_3R^1

R^1NCNR^2

$\text{Cr}^{\text{II}}(\text{OR})_2(\text{CNR}^2)_4$
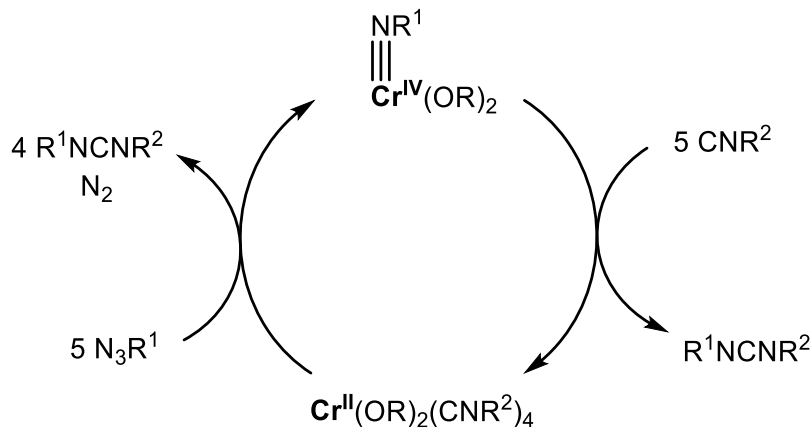
Figure 2.15. Catalytic cycle for the carbodiimide formation via the precatalyst Cr$_2$(OR)$_4$ (**20**).

2.8. Catalytic Formation of Carbodiimides

Having established the stoichiometric reactivity modes of bis(alkoxide) Cr imido complexes with 2,6-dimethylphenyl isocyanide, we turned to investigate the catalytic reactivity of the Cr(II) precursor with various mixtures of aryl/alkyl azides and isocyanides. The experiments were conducted by treating 2.5 mol % of complex **20** with R^{2}NC (R^2 = 2,6-Me$_2$Ph, 4-OMePh, Ad, 2-Cl-6-MePh) and various organoazides at room temperature for 24 h in C$_6$D$_6$. In selected cases (**Table 2.4**, entries 4, 8, and 9), the mixture was heated to 60 °C. The results of the catalytic experiments are given in **Table 2.4**.

Table 2.4. Catalytic Formation of Asymmetric Carbodiimides.

$$ArN_3 + CNR^2 \xrightarrow[- N_2]{\substack{[\mathbf{Cr^{II}}] \\ 2.5\ mol\%}} ArN=C=NR^2$$
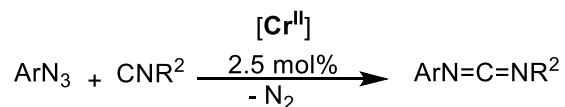
Entry	Azide	Isocyanide	NMR Yield (%)	Isolated Yield (%)
1	MesN$_3$	2,6-Me$_2$PhNC	100	63
2	2,6-Et$_2$PhN$_3$	2,6-Me$_2$PhNC	93	56
3	2-^{i}PrPhN$_3$	2,6-Me$_2$PhNC	94	63
4	AdN$_3$	2,6-Me$_2$PhNC	24 / 23[a]	--- / ---
5	MesN$_3$	4-OMePhNC	100	40
6	2,6-Et$_2$PhN$_3$	4-OMePhNC	71	---
7	MesN$_3$	2-Cl, 4-MePhNC	62	32
8	MesN$_3$	AdNC	0[b] / 50[c]	--- / ---
9	AdN$_3$	AdNC	0 / 0[d]	--- / ---
10	4-F$_3$CPhN$_3$	2,6-Me$_2$PhNC	0	---
11	4-OMePhN$_3$	2,6-Me$_2$PhNC	0	---
12	2,6-^{i}Pr$_2$PhN$_3$	2,6-Me$_2$PhNC	0	---

[a]Heated to 60 °C for 15 h. [b]The reaction at room temperature produced only a small amount of the product; we were not able to quantify the amount of carbodiimide formed due to its small amount, and peaks overlap with those of the starting materials. [c]Heated to 60 °C for 8 h. [d]Heated to 60 °C for 14 h. [e]We were not able to obtain this carbodiimide in pure form due to the presence of a small unknown impurity. [f]All of the experiments were conducted at room temperature for 24 h unless otherwise indicated.

The combination of organoazides R^1N_3 (entries 1-3 and 5-7) featuring relatively bulky aryl substituents (R^1 = Mes, 2,6-Et$_2$Ph, 2-^{i}PrPh) with aryl isocyanides R^2NC (R^2 = 2,6-Me$_2$Ph, 4-OMePh, 2-Cl-6-MePh) successfully forms carbodiimides in high yields. In contrast, combination of adamantyl group at either azide or isocyanide with a mesityl/2,6-dimethylphenyl counterpart produced only low yields of the resulting carbodiimide product (see entries 4 and 8) at room temperature. The yield can be somewhat increased for R^1 = Mes and R^2 = Ad by heating to 60 °C for several hours; further heating leads to the decomposition of starting materials (entry 8). As expected from the stoichiometric experiments, no carbodiimides form for aryl azides with aryl groups lacking ortho substituents (R^1 = 4-CF$_3$Ph, 4-OMePh; entries 10 and 11). Similarly, no carbodiimides form for the very bulky aryl azides 2,6-diisopropylphenyl azide and 2,4,6-triphenylphenyl azide (for an example of 2,6-diisopropylphenyl azide, see entry 12), for which no Cr(IV) imido formation was observed. The carbodiimides N-(2,6-dimethylphenyl)-N′-mesitylmethanediimine (entry 1), N-(2,6-diethylphenyl)-N′-(2,6 dimethylphenyl)methanediimine (entry 2), N-(2,6-dimethylphenyl)-N-(2-isopropylphenyl)methanediimine (entry 3), N-mesityl-N-(4-methoxyphenyl)methanediimine (entry 5), and N-mesityl-N-(2-chloro-6-methylphenyl)methanediimine (entry 7) were isolated in moderate yields and characterized by ^{1}H and ^{13}C NMR spectroscopy, IR spectroscopy, mass spectrometry, and elemental analysis. We also obtained catalytic formation of N-(2,6diethylphenyl)-N-(4-methoxyphenyl)methanediimine (entry 6) in good yield; however, we were not able to obtain this carbodiimide in pure form due to a persistent unknown impurity (**Appendix B**). The product was detected by ESI-MS. Whereas catalytic formation and isolation of N-(2,6-dimethylphenyl)-N′mesitylmethanediimine was previously reported by Warren and co-workers,[18c] other carbodiimides are new compounds that have not been reported before. All newly synthesized carbodiimides appear to be mildly air

sensitive. The most notable IR feature of carbodiimides involves strong signals around 2140 cm^{-1} attributed to the N=C=N stretch.[57]

2.9. Summary and Conclusions

We have demonstrated that bulky aryl and alkyl azides form selectively Cr(IV) imido complexes supported by two bulky alkoxides, whereas nonbulky aryl azides lead to the formation of Cr(VI) bis(imido) complexes. Trigonal-planar Cr(IV) imido bis(alkoxide) complexes are capable of nitrene transfer to isocyanides to form carbodiimides, whereas Cr(VI) bis(imido) complexes are inert to this transformation. DFT calculations indicate a possible mechanism for carbodiimide formation; however, the calculated product with carbodiimide coordinated to Cr(OR)$_2$ was unable to be isolated experimentally. The reaction is catalytic for selected azides and aryl isocyanides, with two major limitations: (1) relatively small azides do not form carbodiimide product due to the formation of unreactive Cr(VI) bis(imido) complexes and (2) excessively bulky azides do not form any carbodiimide product, as they are incapable of imido formation. Our future endeavors in this project will focus on bulkier alkoxide ligands which may restrict even small azides to the formation of mono(imido) complexes, thus increasing the scope of possible substrates for carbodiimide formation.

2.10. Experimental Section

Computational Details. Electronic structure calculations were carried out using density functional theory as implemented in Gaussian09.[58] Geometry optimizations were initially performed at the B3LYP[46−49] level of theory using the 6-31G(d) basis set. No symmetry constraints were imposed during geometry optimizations, and optimized structures were confirmed to have stable wave functions[59,60] and to be local minima by analyzing the harmonic

frequencies.[61,62] Thermodynamic quantities assumed standard approximations[63] and a temperature of 298.15 K to estimate the free energy of each species.

X-ray Crystallographic Details. The structures of **20-26** were confirmed by X-ray analysis. The crystals were mounted on a Bruker APEXII/Kappa three circle goniometer platform diffractometer equipped with an APEX-2 detector. A graphic monochromator was employed for wavelength selection of the Mo Kα radiation ($\lambda = 0.71073$ Å). The data were processed and the structure was solved using the APEX-2 software supplied by BrukerAXS. The structure was refined by standard difference Fourier techniques with SHELXL (6.10 v., Sheldrick G. M., and Siemens Industrial Automation, 2000). Hydrogen atoms were placed in calculated positions using a standard riding model and refined isotropically; all other atoms were refined anisotropically. The structure of **21** contained partially disordered solvent that was modelled as pentane molecule in three orientations. The crystals of **24** diffracted to ~0.9 Å only; the data was therefore cut at 0.87 Å resolution. The crystals of **25** were of overall low quality resulting in high R factors.

General Methods and Procedures. All reactions involving air sensitive materials were performed under inert atmosphere using N_2-filled glovebox. LiOR,[40] mesityl azide,[18c] 2-isopropylphenyl azide,[64a] 2,6-diisopropylphenyl azide,[44b] 2,6-diethylphenyl azide,[44c] and $Cr[N(SiMe_3)_2]_2(THF)_2$[45] were synthesized according to previously reported procedures. Chromium(II) chloride was purchased from Strem. Lithium bis(trimethylsilyl)amide, adamantyl azide, 4-(trifluoromethyl)phenyl azide solution, 4-azidoanisole solution, 2,6-dimethylphenyl isocyanide, 4-methoxyphenyl isocyanide, 1-adamantyl isocyanide, and 2-chloro-6-methylphenyl isocyanide were purchased from Aldrich and used as received. All solvents were purchased from Fisher Scientific and were of HPLC grade. The solvents were purified using an MBraun solvent purification system and stored over 3 Å molecular sieves. Compounds **20-22** and **24-26** were

characterized by IR and UV-Vis spectroscopy, state magnetic susceptibility, X-ray crystallography, and elemental analysis. Isolated carbodiimides were characterized by ^{1}H and ^{13}C NMR, IR, and mass spectrometry and elemental analysis. UV-Vis spectra for complexes **20-22** and **24-26** were obtained in THF. NMR spectra were recorded at the Lumigen Instrument Center (Wayne State University) on a Varian Mercury 400 MHz NMR spectrometer in C_6D_6 at room temperature. Chemical shifts and coupling constants (J) are reported in parts per million (δ) and hertz, respectively. IR spectra of powdered samples were recorded on a Shimadzu IR Affinity-1 FT-IR spectrometer outfitted with a MIRacle10 attenuated total reflectance accessory with a monolithic diamond crystal stage and pressure clamp. Solution state effective magnetic moments were determined using the Evans method. Low-resolution mass spectra were obtained at the Lumigen Instrument Center utilizing a Waters Micromass ZQ mass spectrometer (direct injection, with capillary at 3.573 kV and cone voltage of 20.000 V). Only selected peaks in the mass spectra and in the IR spectra are reported below. Analyses were performed by Midwest Microlab LLC and Galbraith Laboratories, Inc.

Synthesis and Characterization of Chromium Complexes

[Cr₂(OR)₄](20). A solution of 5 mL of HOR^{46} (57.6 mg, 0.261 mmol) in THF was added at once to $Cr[N(SiMe_3)_2]_2(THF)_2$ (67.5 mg, 0.131 mmol) in THF. The solution gradually turned from light violet to green. The reaction mixture was stirred for 6 h, upon which the solvent was removed, and crystallization from hexanes at -35 °C overnight produced green crystals of $Cr_2(OR)_4$ (38.2 mg, 60% yield). IR (cm^{-1}): 2996 (m), 2916 (m), 2349 (m), 1059 (m), 949 (s), 745 (s), 706 (s). Anal. Calcd for $C_{60}H_{92}Cr_2O_4$: C, 73.4; H, 9.5. Found: C, 72.8; H, 9.2. $\mu_{eff} = 2.5 \pm 0.3\ \mu_B$ (calcd 2.8 μ_B).

Cr(OR)₂(NMes) (21). A solution of 74 µL of $MesN_3$ in ether (0.764 M) was added to a solution of complex **20** (28.1 mg, 0.0286 mmol) in toluene in one portion. The solution immediately

changed color from green to deep red. The reaction mixture was stirred for 4 h, upon which the solvent was removed. Crystallization from pentane at $-35\ ^\circ$C gave crystals of deep red $Cr(OR)_2(NMes)$ (29.1, 81% yield). IR (cm^{-1}): 2943 (m), 2877 (w), 2122 (m), 1601 (m), 1479 (m), 1389 (m), 1202 (s), 1094 (s), 1053 (m), 1012 (m), 893 (w), 851 (m), 777 (s), 702 (s), 762 (s). μ_{eff} = 2.5 ± 0.3 μ_B (calcd 2.8 μ_B). Anal. Calcd for $C_{39}H_{57}CrNO_2$: C, 75.1; H, 9.2. Found: C, 74.9; H, 9.4.

$Cr(OR)_2(NAd)$ (22). A solution of 5 mL of AdN_3 (4.7 mg, 0.0265 mmol) in toluene was added to a solution of compound **20** (12.3 mg, 0.0125 mmol) in toluene in one portion. The solution immediately changed color from green to deep red. The reaction mixture was stirred for 4 h, upon which the solvent was removed. Crystallization from hexanes at $-35\ ^\circ$C overnight gave crystals of deep red $Cr(OR)_2(NAd)$ (10.1 mg, 64% yield). IR (cm^{-1}): 2900 (m), 2891 (m), 1487 (m), 1440 (m), 1387 (m), 1360 (m), 1206 (m), 1053 (s), 1009 (s), 901 (m), 771 (s), 704 (s). μ_{eff} = 3.3 ± 0.4 μ_B (calcd 2.8 μ_B). Anal. Calcd for $C_{40}H_{61}CrNO_2$: C, 75.1; H, 9.6, N, 2.2. Found: C, 75.2; H, 9.8, N, 2.2.

$Cr(OR)_2(NDEP)$ (23). A solution of 5 mL of N_3DEP (2.4 mg, 0.014 mmol) in toluene was added to a solution of compound **20** (28.0 mg, 0.029 mmol) in toluene in one portion. The solution immediately changed color from green to deep red. The reaction mixture was stirred for 4 h, upon which the solvent was removed. Crystallization from pentane at $-35\ ^\circ$C over 2 weeks gave crystals of deep red $Cr(OR)_2(NDEP)$ (8.5 mg, 23% yield). The low isolated yield of compound **23** is likely due to its high solubility. The crystallized compound was characterized by X-ray crystallography and IR spectroscopy; the low isolated yield of the compound and prolonged crystallization times prevented us from further characterization of this compound. IR (cm^{-1}): 2967 (w), 2878 (w), 2832 (w), 1597 (w), 1474 (w), 1432 (w), 1204 (m), 1092 (w), 1067 (s), 744 (s), 706 (s).

Cr(OR)₂(N(4-CH₃OPh))₂ (24). A solution of 4-azidoanisole (0.5 M in tert-butyl methyl ether, 0.110 mL) was added to a 5 mL solution of complex **20** (26.0 mg, 0.0265 mmol) in toluene. The solution color changed immediately from green to deep brown. The reaction mixture was stirred for 4 h, upon which the volatiles were removed. Crystallization from hexanes at −35 °C overnight gave deep brown crystals of Cr(OR)₂(N(4-CH₃OPh))₂ (18.2 mg, 46%). IR (cm^{-1}): 2963 (w), 1585 (s), 1485 (m), 1250 (s), 1157 (s), 991 (m), 829 (s). ^{1}H NMR (C₆D₆): δ 8.66 (d, $^3J_{HH}$ = 7.6 Hz, 2H), 7.75 (d, $^3J_{HH}$ = 8.8 Hz, 2H), 7.39 (m, 2H), 7.17 (m, 8H), 6.37 (d, $^3J_{HH}$ = 8.8 Hz, 4H), 3.05 (s, 6H), 1.49 (s, 36H). ^{13}C NMR (C₆D₆): δ 147.76, 130.17, 129.00, 127.11, 127.05, 125.88, 125.69, 113.61, 54.81, 44.59, 31.05 ppm. Anal. Calcd for complex **24**: C, 72.1; H, 8.3, N, 3.8. Found: C, 72.3; H, 8.4; N, 3.7.

Cr(OR)₂(N(4-CF₃Ph))₂ (25). To a solution of 5.0 mL of complex **20** (37.2 mg, 3.79 mmol) in toluene was added 4-(trifluoromethyl)phenyl azide solution (0.5 M in tert-butyl methyl ether, 0.30 mL) dropwise. Immediately gas evolution was observed, along with a change in solution color to deep brown. The reaction mixture was stirred for 4 h, upon which the solvents were removed in vacuo to yield a brown residue. Crystallization from hexanes at −35 °C overnight gave deep brown crystals of Cr(OR)₂(N(4-CF₃Ph))₂ (15.6 mg, 30%). IR (cm^{-1}): 2966 (w), 1597 (w), 1319 (s), 1165(m), 1103 (m), 975 (s), 833 (m). ^{1}H NMR (C₆D₆): δ 8.38 (d, $^3J_{HH}$ = 9.2 Hz, 2H), 7.68 (d, $^3J_{HH}$ = 6.8 Hz, 2H), 7.01 (m, 4H), 7.22 (m, 2H), 6.93 (d, $^3J_{HH}$ = 8.0 Hz, 4H), 6.76 (d, $^3J_{HH}$ = 8.4 Hz, 4H), 1.38 (s, 36H). ^{13}C NMR (C₆D₆): δ 163.76, 146.44, 129.73, 129.00, 127.03, 126.40, 126.18, 126.00, 124.21, 100.70, 44.86, 30.91 ppm. Anal. Calcd for complex **25**: C, 65.3; H, 6.7, N, 3.5. Found: C, 65.4; H, 6.6; N, 3.4.

Reaction of Cr(OR)₂(NMes) (21) with 1 Equiv of 2,6-Dimethyl Isocyanide. To a solution of 5.0 mL of complex **21** (35.2 mg, 0.056 mmol) in C₆D₆ were added 1 equiv of 2,6-dimethylphenyl

isocyanide (7.3 mg, 0.056 mmol) and 1 equiv of 1,3,5-trimethoxybenzene (TMB, 9.3 mg, 0.055 mmol) in C_6D_6. The solution changed color from green to deep brown and was stirred for 2 h, upon which a ^1H NMR spectrum was taken to show complete conversion to the corresponding carbodiimide.

Reaction of Cr(OR)$_2$(NMes) (21) with 5 Equivalents of 2,6-Dimethylphenyl Isocyanide: Observation of Carbodiimides and Isolation of Compound 26. To a solution of 5.0 mL of complex **21** (19.8 mg, 0.032 mmol) in C_6D_6 were added 5 equivalents of 2,6-dimethylphenyl isocyanide (19.5 mg, 0.149 mmol) and 1 equiv of TMB (5.6 mg, 0.0333 mmol) in C_6D_6. The solution changed color from green to deep brown and was stirred for 2 h, upon which a ^1H NMR spectrum was taken to show complete conversion to the corresponding carbodiimide. Once the complete conversion was established, the volatiles were removed in vacuo to yield a brown residue. The residue was dissolved in hexanes and placed in the freezer at −35 °C to produce deep orange crystals of complex **26** (16.9 mg, 56%).

Independent Synthesis of Cr(OR)$_2$(CN(2,6-Me$_2$Ph))$_4$ (26) from the Cr(II) Precursor Cr$_2$(OR)$_4$ (20). A solution of 5 mL of CN(2,6Me$_2$Ph) (34.0 mg, 0.259 mmol) in toluene was added to a solution of compound **20** (30.9 mg, 0.0315 mmol) in toluene in one portion. The solution immediately changed color from green to deep brown. The reaction mixture was stirred for 4 h, upon which the solvent was removed. Crystallization from hexanes at −35 °C overnight produced crystals of deep orange Cr(OR)$_2$(CN(2,6-Me$_2$Ph))$_4$ (40.1 mg, 65% yield). $\mu_{eff} = 2.3 \pm 0.2 \ \mu_B$ (calcd 2.8 μ_B). Anal. Calcd for complex **26**: C, 78.1; H, 8.1, N, 5.5. Found: C, 77.2; H, 8.6; N, 5.4.

Reaction of Cr(OR)$_2$(N(4-CH$_3$OPh))$_2$ (24) with 2,6-Dimethylphenyl Isocyanide. To a solution of 5.0 mL of complex **24** (12.7 mg, 0.0173 mmol) in C_6D_6 were added 6 equivalents of 2,6-dimethylphenyl isocyanide (14.4 mg, 0.110 mmol) and 1 equiv of TMB (5.30 mg, 0.0315 mmol)

in C_6D_6. The solution was stirred for 2 days, upon which an ^1H NMR spectrum was taken to show no formation of the corresponding carbodiimide and no consumption of the starting isocyanide and complex **24**.

Reaction of Cr(OR)₂(N(4-CF₃Ph))₂ (25) with 2,6-Dimethylphenyl Isocyanide. To a solution of 5.0 mL of complex **25** (26.6 mg, 0.033 mmol) in C_6D_6 were added 6 equivalents of 2,6-dimethylphenyl isocyanide (2.5 mg, 0.192 mmol) and 1 equiv of TMB (6.0 mg, 0.036 mmol) in C_6D_6. The solution was stirred for 2 days, upon which a ^1H NMR spectrum was taken to show no formation of the corresponding carbodiimide and no consumption of the starting isocyanide and complex **25**.

General Procedure for Catalytic Formation of Carbodiimides. NMR-Scale Reactions. All the reactions were performed in an N_2-filled glovebox by the addition of 24 equivalents of isocyanide, 20 equivalents of organoazide, and TMB standard solution in C_6D_6 to a solution of 2.5 mol % of complex **20** (approximately 15−30 mg) in C_6D_6. The reaction mixture was stirred for 24 h and a ^1H NMR spectrum was taken to calculate the percent yield of the carbodiimide produced.

Synthesis of the Isolated Carbodiimides. The isolated carbodiimides were synthesized according to the following procedure: all of the reactions were performed in an nitrogen filled glovebox by the addition of 20 equivalents of isocyanide and 20 equivalents of organoazide in THF to a solution of 2.5 mol % of complex **20** (approximately 15−30 mg) in THF. The reaction mixture was stirred for 24 h, upon which volatiles were removed in vacuo. The brown residue was purified on silica under an inert atmosphere using hexanes. Carbodiimides were isolated by collecting the light orange or pale yellow layer and subsequent evaporation (oils) or recrystallization at −35 °C (solids). Full characterization data for the isolated carbodiimides are found in the Appendix B.

CHAPTER 3 SYNTHESIS AND CHARACTERIZATION OF BULKIER ALKOXIDE LIGANDS AND THE PREPARATION OF THE SECOND-GENERATION LOW-COORDINATE TRANSITION METAL COMPLEXES

Parts of the text in this chapter were reprinted or adapted with permission from: Yousif, M.; Cabelof, A. C.; Lord, R. L.; Martin, P. D.; Groysman, S. *Dalton Trans.* **2016**, *45*, 9794-9804.

3.1. Introduction

Our next goal was to synthesize new, bulkier, alkoxide ligand which might stabilize bis(alkoxide) complexes and thereby help to solve problems encountered in nitrene coupling. As stated above (in **1.5. Research Statement and Objectives**), we hypothesized that increasing the size of the alkoxide would prevent the formation of iron tris(alkoxide) "sink" in nitrene coupling and thereby increase catalyst reactivity and substrate scope. In addition, all the previous $M(OR)_2$-type complexes were isolated in $M(OR)_2(THF)_2$ form. We hoped that bulkier alkoxide ligands will be able to "expel" neutral THF ligands, enable formation of three-coordinate or two-coordinate $M(OR)_2$ complexes and thus open up coordination sphere of the metal to bind small inert molecules such as CO_2 or N_2. This chapter focuses on the synthesis and characterization of bulkier alkoxide ligands and their coordination with first row transition metals (M = Cr-Co).

3.2. Synthesis and Characterization of Alkoxide Ligands

We modified our first generation alkoxides by targeting new ligands with different alkyl substituents in *meta* positions (R = Me, ^{t}Bu, Ph) on the phenyl ring of the alkoxide (**Figure 3.1**). The synthetic route leading to the new alkoxide ligands shown in **Figure 3.1**. Treatment of ArBr precursors with two equivalents of *t*-butyllithium followed by the addition of hexamethylacetone formed the lithium salt of the ligand, LiOR'. Subsequent aqueous work-up afforded the protonated ligands **27-29** as white solid.
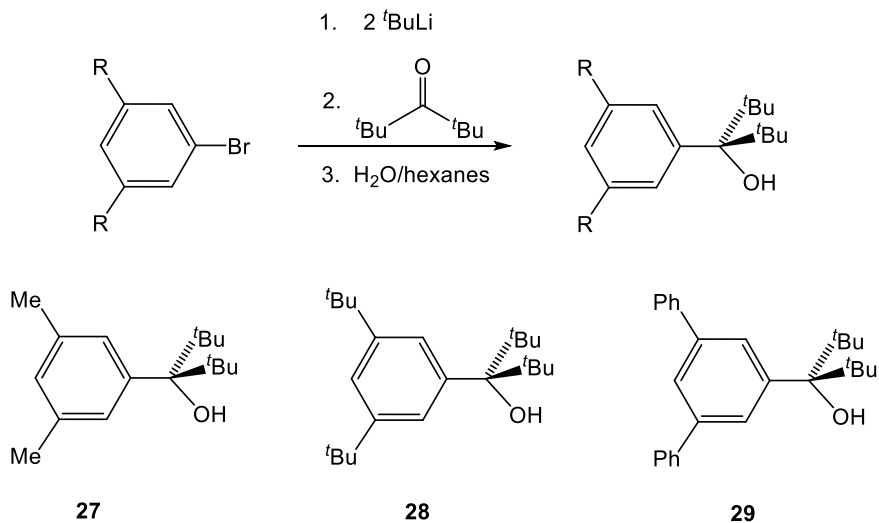
Figure 3.1. Synthesis of bulky alkoxide ligands (Top). The different alkoxide ligands investigated (Bottom).

As demonstrated in **Figure 3.1**, all R groups were added in the *meta* positions of the phenyl ring. The *meta* substituents are expected to increase the steric "volume" of the ligand. At the same time, they point away from the metal and therefore are not likely to engage in ligand deactivation processes commonly encountered in bulky (2,6-substituted) aryloxides (one of each is shown in **Figure 1.11**). Adding methyl groups in these positions led to formation of compound **27** in 50% yield. As the methyl groups did not increase the steric volume of the ligand significantly, we turned to the bulkier *t*-butyl substituents. The resulting compound (**28**) was isolated in 82% yield. However, the presence of two *t*-butyl groups on ligand periphery generated a relatively "greasy" ligand and made isolation of the crystalline metal complexes with this ligand difficult. Compounds **27** and **28** are fully characterized by elemental analysis, IR, ^{1}H and ^{13}C NMR spectroscopy (see **Appendix C**). Based on these results, we synthesized an additional alkoxide ligand, HOR', containing phenyl groups in the 3,5 positions. HOR' (**29**) displayed phenyl groups in the *meta* positions that did not only increase the steric volume of the ligand, but also improved the crystallinity of the ligand-bearing *meta* complexes. The ligand (HOR') is obtained as white solid

in 77% yield and fully characterized by IR, ^{1}H and ^{13}C NMR, X-ray crystallography, and elemental analysis. As the properties of this ligand [OC^{t}Bu$_2$(3,5-Ph$_2$Ph)], or [OR'] henceforth, proved superior to [OC^{t}Bu$_2$(3,5-Me$_2$Ph)] and [OC^{t}Bu$_2$(3,5-^{t}Bu$_2$Ph)], the other two ligands were not pursued further.

The ^{1}H NMR spectrum of HOR' demonstrates three singlets for the central phenyl (δ 8.19, 7.90, 7.64 ppm) integrating to one proton each, consistent with the restricted rotation of the Ph$_2$Ph group (see **Appendix C**). The structure of HOR' (**Figure 3.2** and **Table 3.1**) demonstrates slightly twisted lateral phenyl groups (dihedral angles of 26° and 37° with the central phenyl); other intramolecular bond distances and angles are unremarkable. The structure also demonstrates intramolecular OH–π interaction of 2.5 Å between two neighboring alcohols.
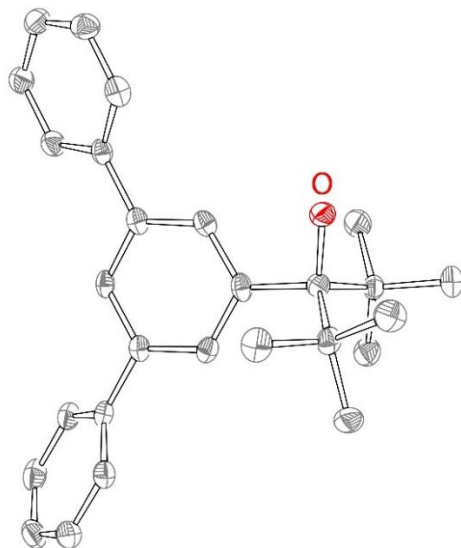
Figure 3.2. Molecular structure of HOR' (**29**). H atoms are omitted for clarity.

Table 3.1. Experimental crystallographic parameters for **29**.

complex	29
formula	$C_{27}H_{32}O$
fw	372.54
crystal system	monoclinic
space group	$P2_1/c$
a (Å)	12.9525(6)
b (Å)	13.8945(7)
c (Å)	12.3884(6)
α (deg)	90.00
β (deg)	106.686(2)
γ (deg)	90.00
V (Å^3)	2135.64(18)
D_c (g cm^{-3})	1.159
Z	4
μ (mm^{-1})	0.068
T (K)	100(2)
R_1	5.65
GOF	1.030

3.3. Synthesis and Characterization of Cr(OR')$_2$(THF)$_2$

We previously reported that Cr(N(SiMe$_3$)$_2$)$_2$(THF)$_2$ undergoes protonolysis with "first-generation" HOR in THF to yield Cr$_2$(μ_2-OR)$_2$(OR)$_2$ (**Chapter 2**, **Figure 2.1**). Similarly, treatment of Cr(N(SiMe$_3$)$_2$)$_2$(THF)$_2$ with HOR′ leads to a facile protonolysis reaction. However, in contrast to OR, the bulkier OR′ forms a mononuclear Cr(II) complex Cr(OR′)$_2$(THF)$_2$ **30** (**Figure 3.3**). Compound **30** was obtained as pale green crystals from hexanes in 81% yield, and was characterized by IR and UV-vis spectroscopy, solution magnetic measurements (by Evans' method) and elemental analysis. Evans' method measurements (in C$_6$D$_6$) displays μ_{eff} value of 4.2 $\pm$ 0.5μ_B which is somewhat lower than the value of ~4.8 μ_B generally found for the square-planar Cr(II) complexes.[45,47,65-69] We confirmed this value by conducting Evans' measurements in C$_7$D$_8$ (toluene-d$_8$), which gave the same μ_{eff} value of 4.2 $\pm$ 0.5μ_B. Several reasons can explain these lower than expected values for a Cr(II) complex, including orbital contribution to the magnetic moment possible in d^4 species, potential experimental error associated with a large diamagnetic contribution (of a large organic ligand), or the geometry significantly different (see below) from the one usually found for Cr(II) complexes.
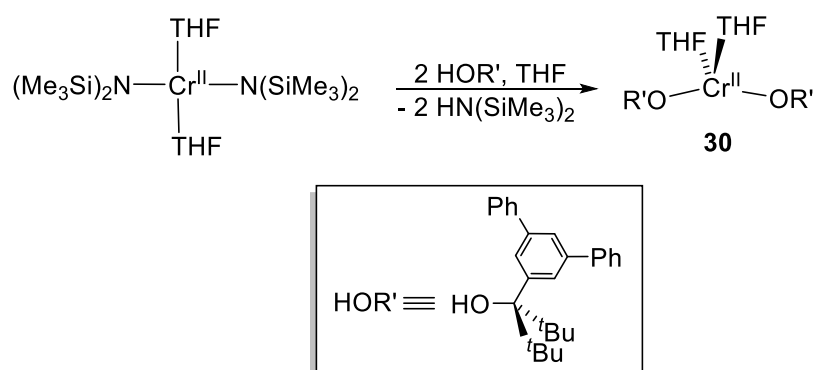
Figure 3.3. Synthesis of compound **30**.

The identity of **30** was further verified by X-ray crystallography (**Figure 3.4**). The solid-state structure of **30** demonstrates that $Cr(OR')_2(THF)_2$ is a mononuclear, tetra-coordinate species ligated by two alkoxides and two THF molecules.
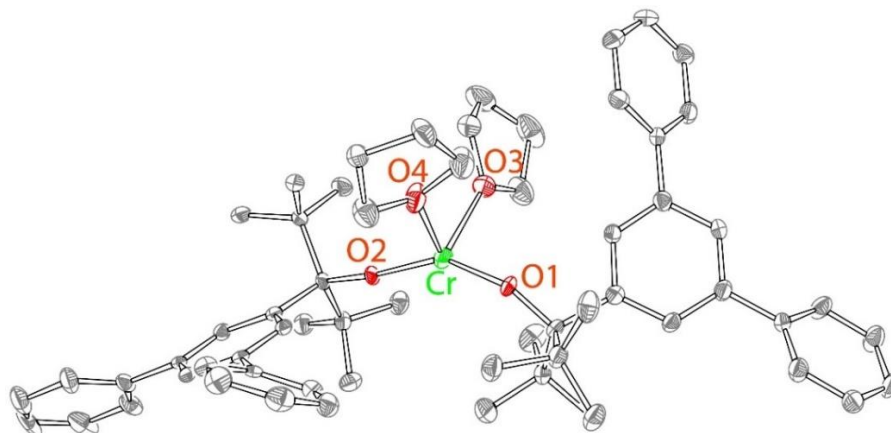
Figure 3.4. X-ray structure for complex **30** with 50% probability ellipsoids.

Most previously reported tetracoordinate Cr(II) complexes were square-planar, as may be anticipated for a d^4 metal ion. [45,47,65-69] As shown in **Figure 3.5**, a significant number of bulky amide, aryl, and aryloxide ligands have been demonstrated to form mononuclear Cr complexes.[65-67] For amide ligands,[45,65] examples of such complexes include square-planar trans-Cr(N$(SiMe_3)_2)_2(THF)_2$,[45] $Cr(N(SiMe_2Ph)_2)_2(THF)_2$ and two-coordinate $Cr(N(SiMe_2Ph)_2)_2$,[65a] and $Cr(N(Si^iPr_3)(DIPP))_2$ where DIPP = 2,6-diisopropylphenyl.[65b] Examples of mononuclear Cr(II) complexes stabilized by aryl ligands include square-planar trans-$Cr(Mes)_2(PMe_3)_2$,[66a] and cis-$Cr(Mes)_2(THF)_2$,[66b] among other compounds (Mes = mesityl).[66] A mononuclear, square-planar Cr(II) complex stabilized by bulky aryloxide ligands was reported by Gambarotta and coworkers and Osborn and coworkers.[67] The situation is different for alkoxide ligands. Alkoxide is an intrinsically less bulky ligand due to a single O substituent that points away from the metal center.[42] Power reported synthesis of $Cr(OR)_2L_2$ (L = OC^tBu_3; L = THF) species, that analyzed as mononuclear bis(ligand) adducts.[48] However, structurally characterized low-coordinate alkoxide

complexes of chromium(II) were found to be dinuclear or polynuclear (selected structures are given in **Figure 3.5**).[70] We note that mononuclear complexes of bulky siloxide ligands are known,[47,68] including crystallographically characterized square-planar trans-$Cr(OSiO^tBu_3)_2(NHEt_2)_2$.
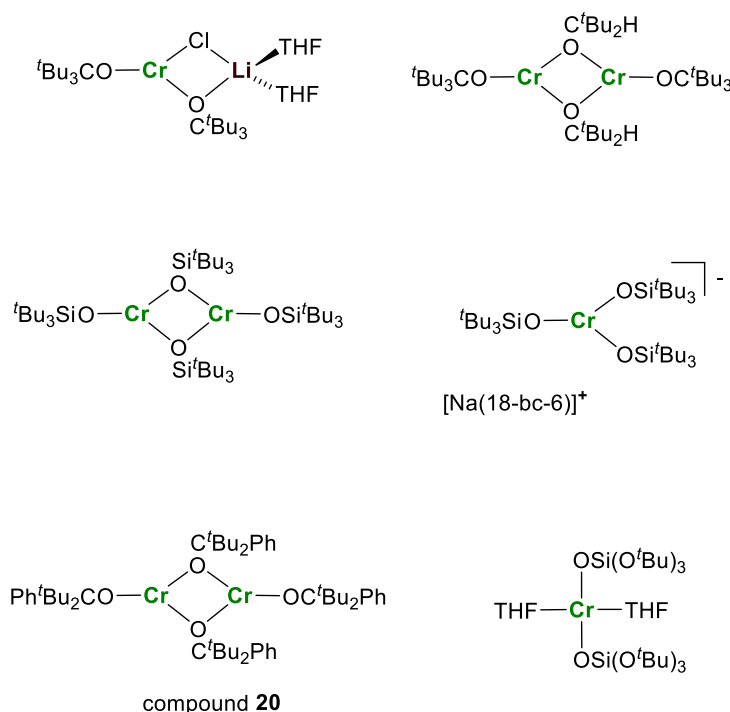
Figure 3.5. Examples of structurally characterized Cr(II) complexes with bulky alkoxides and siloxides, including $Cr_2(\mu_2-OR)_2(OR)_2$ (OR = OC^tBu_2Ph, compound **20**).

Compound **30**, however, is clearly not square-planar. Instead, it appears to adopt distorted seesaw (cis-divacant octahedral) geometry: the angle between the alkoxides (O1–Cr–O2) is relatively wide (147.5(1)°), while all the other angles are relatively close to 90° (89.6(1)– 105.0(1), see **Table 3.2** for details).

This geometry is reminiscent of related first generation $M(OR)_2(THF)_2$ complexes (M = Mn–Co) that we recently reported.[42] It is likely that the steric bulk of OR′ is primarily responsible for the destabilization of square-planar geometry that requires the presence of four ligands in one plane (a hypothetical plane [CrO1O2O3O4] for the hypothetical square-planar structure of **30**).

Most of the aforementioned Cr(II) complexes contain relatively planar bulky ligands (such as $N(SiR_3)_2$, Mes or OAr), that can remove most of their steric bulk from the plane by adopting an orientation "perpendicular" to the plane of the ligands. For instance, in the structure of trans-$Cr(N(SiMe_3)_2)_2(THF)_2$, dihedral angles between the two $CrNSi_2$ planes and the CrN_2O_2 plane were 73° and 56°. In contrast, there is no possibility to remove the bulk of OR′ from the hypothetical $[CrO1O2O3O4]$ plane, therefore, the complex must adopt a different geometry.

Table 3.2 Selected bond distances (Å) and angles (º) for complex **30**.

complex	**30**
Cr1-O1	1.910(2)
Cr1-O2	1.869(2)
Cr1-O3	2.292(3)
Cr1-O4	2.161(3)
O1-Cr1-O2	147.5(1)
O4-Cr1-O1	89.6(1)
O3-Cr1-O4	95.0(1)
O2-Cr1-O4	103.0(0)
O1-Cr1-O3	103.5(1)
O3-Cr1-O2	105.0(1)

3.4. Synthesis and Characterization of Fe(OR')$_2$(THF)$_2$ and Co(OR')$_2$(THF)$_2$

Similar to complex **30**, low-coordinate Fe(OR')$_2$(THF)$_2$ (**31**) and Co(OR')$_2$(THF)$_2$ (**32**) precursors are synthesized using one-step approach, that involves protonolysis of

Fe(N(SiMe$_3$)$_2$)$_2$(THF)$_X$[71] and Co(N(SiMe$_3$)$_2$)$_2$(THF)$_X$[72] with two equivalents of HOR',

respectively (**Figure 3.6**).
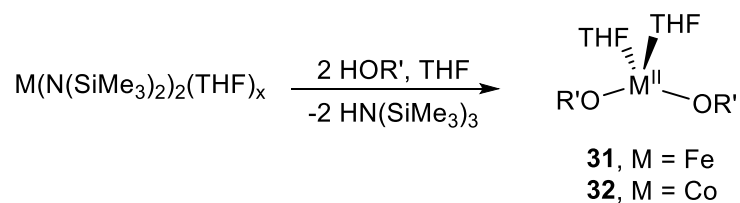
Figure 3.6. Synthesis of complexes **31** and **32**.

Complex **31** is obtained as light-gold crystals isolated in 82% yield by recrystallization

from hexanes, while complex **32** is obtained as purple crystals isolated in 92% yield from hexanes.

X-ray crystal structures of compound **31** (**Figure 3.7**) and **32** (see **Appendix C**) demonstrate

highly distorted tetrahedral geometry. Compound **31** display a wide inter-alkoxide (R'O-Fe-OR')

angle of 141.4(1)°. This value is only slightly larger than the inter-alkoxide angle of 138.7(1)° in

first generation Fe(OR)$_2$(THF)$_2$.[41] Magnetic susceptibility value of $\mu_{\text{eff}} = 4.7 \pm 0.3\mu_B$ for **31**

obtained by Evans measurements, is consistent with the expected high-spin configuration for the

d^6 Fe(II) center in a weak-field ligand environment.
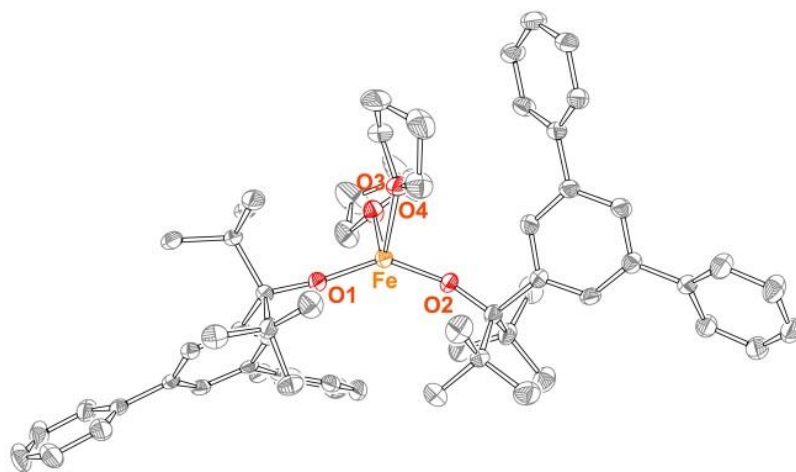
Figure 3.7. X-ray structure of compound **31**, 50% probability ellipsoids.

Table 3.3. Experimental crystallographic parameters for **30** and **31**.

complex	30	31
formula	$C_{62}H_{78}CrO_4$	$C_{62}H_{78}FeO_4$
fw	939.28	943.13
crystal system	triclinic	triclinic
space group	*P* -1	*P* -1
a (Å)	13.2611(6)	13.1801(8)
b (Å)	13.2611(6)	13.5550(8)
c (Å)	16.2082(6)	16.2336(10)
α (deg)	100.689(2)	101.004(3)
β (deg)	102.137(2)	101.633(3)
γ (deg)	109.316(2)	108.976(2)
V (Å^3)	2580.86(19)	2581.27
D_c (g cm^{-3})	1.206	0.272
Z	2	2
μ (mm^{-1})	0.269	0.339
T (K)	100(2)	100(2)
R_1	6.99	4.51
GOF	1.019	0.814

3.5. Summary and Conclusions

In this chapter, we demonstrated the synthesis and characterization of our "second-generation" alkoxide ligand, HOR'. We showed that the OR' is sufficiently bulky to enable the

formation of a rare mononuclear non-square-planar Cr(II) bis(alkoxide) complex Cr(OR')$_2$(THF)$_2$. However, OR' did not allow for the isolation of strictly two-coordinate complexes of the "M(OR')$_2$" form, instead we were able to isolate tetrahedral complexes of M(OR')$_2$(THF)$_2$ for M = Co and Fe.

3.6. Experimental Section

General Methods and Procedures. Cr(N(SiMe$_3$)$_2$)$_2$(THF)$_2$[45], Fe(N(SiMe$_3$)$_2$)$_2$(THF)[71], and Co(N(SiMe$_3$)$_2$)$_2$(THF)$_2$[72] were synthesized according to previously reported procedure. ^{t}Butyllithium solution, chromium(II) chloride, cobalt(II) chloride, lithium bis(trimethylsilyl)amide, potassium bis(trimethylsilyl)amide, and 1-bromo-3,5-dimethylbenzene were purchased from Aldrich and used as received. Iron(II) chloride was purchased from Strem. 1-Bromo-3,5-diphenylbenzene and 1-bromo-3,5-di-tert-butyllbenzene were purchased from AK Scientific. Hexamethylacetone was purchased from Alfa Aesar. All solvents were purchased from Fisher Scientific and were of HPLC grade. The solvents were purified using an MBRAUN solvent purification system and stored over 3 Å molecular sieves. Compounds **27–32** were characterized by IR and UV-Vis spectroscopy, and elemental analysis; selected compounds (**29-32**) were characterized by X-ray crystallography and solution state magnetic susceptibility measurements (**30-32**). NMR spectra were recorded at the Lumigen Instrument Center (Wayne State University) on a Varian Mercury 400 MHz NMR Spectrometer in C$_6$D$_6$ at room temperature. Chemical shifts (*J*) were reported in parts per million (δ) and Hertz respectively. All of the UV-visible spectra were obtained on Shimadzu UV-1800 spectrometer in THF. IR spectra of powdered samples were recorded on a Shimadzu IR Affinity1 FT-IR Spectrometer outfitted with a MIRacle10 attenuated total reflectance accessory with a monolithic diamond crystal stage and pressure clamp. Only selected peaks in the IR spectra are reported below. Solution state effective magnetic moments

were determined using the Evans method. Elemental analyses were performed under ambient conditions by Midwest Microlab LLC Laboratory, Inc. See **Appendix C** for details on the synthesis and characterizations of compound **32**.

Synthesis of C$_{17}$H$_{28}$O (27). To a solution of 1-bromo-3,5-dimethylbenzene (0.430 g, 2.33 mmol) in 4 ml ether and 2 ml THF, solution of *t*-BuLi in pentane (2.7 ml, 1.7 M) was added dropwise at −35 °C. The solution changed color from clear to yellow. This reaction stirred for one hour and slowly warm to room temperature, upon which it was cooled again to −35 °C and added to a cold solution of hexamethylacetone (0.4 mL, 2.31 mmol). The reaction was stirred for 24 hours, upon which all solvents were removed under in vacuo to yield yellow residue. The residue was dissolved in hexanes and extracted with water and hexanes (3 × 10 mL). The organic layer was concentrated to yield to white solid. (0.286 g, 50% yield). Anal. Calcd: C, 82.2; H, 11.4. Found: C, 81.6; H, 11.2. ^{1}H NMR (C$_6$D$_6$, 400 MHZ) δ 7.48 (s, 1H), 7.21 (s, 1H), 6.74 (s, 1H), 2.20 (s, 1H), 2.17 (s, 1H), 1.59 (s, 1H), 1.06 (s, 1H). ^{13}C NMR (C$_6$D$_6$): δ 145.72, 136.43, 134.70, 125.96, 125.41, 82.81, 41.41, 29.57, 21.54, 21.47. IR (cm^{-1}): 2959 (m), 1601 (w), 1481 (w), 1385 (w), 1366 (w), 1207 (w), 1146 (w), 1061 (m), 999 (m), 856 (w), 710 (w).

Synthesis of C$_{23}$H$_4$O (28). To a solution of 1-bromo-3,5-di-*t*-butylbenzene (0.622 g, 2.31 mmol) in 4 ml ether and 2 ml THF, solution of *t*-BuLi in pentane (2.7 ml, 1.7 M) was added dropwise at −35 °C. The solution changed color from clear to yellow. This reaction stirred for one hour and slowly warm to room temperature, upon which it was cooled again to −35 °C and added to a solution of hexamethylacetone (0.4 mL, 2.32 mmol). The reaction was stirred for 24 hours, upon which all solvents were removed under in vacuo to yield yellow residue. The residue was dissolved in hexanes and extracted with water and hexanes (3 × 10 mL). The organic layer was concentrated to yield to white solid. (0.570 g, 82% yield). Anal. Calcd: C, 83.1; H, 12.1. Found: C, 82.7; H,

12.4. ^{1}H NMR (C$_6$D$_6$, 400 MHZ) δ 7.84 (s, 1H), 7.53 (s, 1H), 7.43 (s, 1H), 1.68 (s, 1H), 1.35 (s, 18H), 1.13 (s, 18H). ^{13}C NMR (C$_6$D$_6$): δ 149.21, 147.36, 144.70, 122.94, 121.96, 118.96, 83.20, 41.45, 34.76, 31.45, 31.33, 29.60. IR (cm^{-1}): 2959 (s), 1593 (m), 1454 (m), 1389 (m), 1361 (s), 1246 (w), 1173 (w), 1057 (m), 995 (s), 876 (s).

Synthesis of C$_{27}$H$_{32}$O (29). To a solution of 1-bromo-3,5-diphenylbenzene (0.448 g, 1.45 mmol) in 4 ml ether and 2 ml THF, solution of *t*-BuLi in pentane (1.7 ml, 1.7 M) was added dropwise at −35 °C. The solution changed color from clear to gold. This reaction stirred for one hour and slowly warm to room temperature, upon which it was cooled again to −35 °C and added to a solution of hexamethylacetone (0.25 mL, 1.45 mmol). The reaction was stirred for 24 hours, upon which all solvents were removed under in vacuo to yield yellow residue. The residue was dissolved in hexanes and extracted with water and hexanes (3 × 10 mL). The organic layer was concentrated to yield to white solid. Crystallization from concentrated solution of hexanes at −35 °C overnight gave colorless crystals of HOR′ (0.416 g, 77% yield). Anal. Calcd: C, 87.1; H, 8.7. Found: C, 87.0; H, 8.6. IR (cm^{-1}): 2955 (w) 2916 (w), 1454 (w), 1416 (m), 1389 (m), 1369 (m), 1261 (w), 1030 (w), 880 (m), 760 (s), 689 (s), 613 (m). ^{1}H NMR (C$_6$D$_6$, 400 MHZ) δ 8.19 (s, 1H), 7.90 (s, 1H), 7.64 (s, 1H), 7.62 (t, *J* = 8 Hz, 4H), 7.22 (t, *J* = 8 Hz, 4H), 7.13 (m, 2H), 1.64 (s, 1H), 1.06 (s, 18H). ^{13}C NMR (C$_6$D$_6$): δ 147.25, 142.48, 141.59, 139.99, 129.24, 129.08, 127.66, 127.55, 127.48, 126.56, 126.23, 124.60, 83.53, 41.85, 29.96.

Cr(OR)$_2$(THF)$_2$ (30). To a solution of 5.0 mL of Cr(N(SiMe$_3$)$_2$)$_2$(THF)$_2$ (35.6 mg, 0.069 mmol) in THF, the solution of HOR′ (53.0 mg, 0.142 mmol) in THF was added dropwise. The solution changed color slowly from light purple to blue then to light green. The reaction was stirred for six hours, upon which the solvents were removed in vacuo to yield green residue. Crystallization from hexanes at −35 °C overnight gave green crystals of complex **30** (52.40 mg, 81%). $\mu_{\text{eff}} = 4.2 \pm 0.5 \mu_{\text{B}}$.

IR (cm^{-1}): 2974 (w), 1589 (w), 1497 (m), 1415 (w), 1385 (w), 1099 (m), 1060 (w), 1029 (m), 876 (m), 748 (s), 694 (s). Anal. Calcd: C, 79.3; H, 8.4. Found: C, 78.9; H, 8.4.

Fe(OR')$_2$(THF)$_2$ (31). To a solution of 5.0 mL of Fe[N(SiMe)$_3$]$_2$(THF) (47.8 mg, 0.107 mmol) in THF, HOR' (69.0mg, 0.185 mmol) in THF was added slowly. The solution gradually changed color from muddy green to light gold-brown. The reaction was stirred for two hours, upon which the solvents where removed in vacuo to yield light gold residue. Crystallization from hexanes at −35 °C overnight gave crystals of light gold of **31** (82.3 mg, 82%). IR (cm^{-1}): 2878 (m), 1589 (m), 1416 (m), 1138 (m), 1103 (s), 1018 (s), 979 (s), 872 (m), 760 (d), 694 (s). $\mu_{eff} = 4.7 \pm 0.3\mu_B$ Anal. Calcd: C, 88.0; H, 8.3. Found: C, 78.7; H, 8.2.

CHAPTER 4 CATALYIC NITRENE COUPLING USING SECOND-GENERATION IRON BIS(ALKOXIDE) COMPLEX AND THE FORMATION OF IRON TETRAZENE COMPLEXES

4.1. Introduction

As described in the introduction, our "first-generation" iron bis(alkoxide) complex $Fe(OR)_2(THF)_2$ (OR = OC^tBu_2Ph, **14**, **Figure 1.12**) catalyzed efficient transformation of bulky aryl azides ArN_3 (Ar = 2,4,6-Me_3Ph or 2,6-Et_2Ph) to the corresponding azoarenes. Intriguingly, no azoarene formation was observed for smaller aryl azides (Ar = 2-MePh, 3,5-Me_2Ph, 4-MePh). Instead, formation of bridging imido mono(alkoxide) complexes $Fe_2(\mu_2\text{-}NAr)_2(OR)_2(THF)_2$ was observed, along with tris(alkoxide) $Fe(OR)_3$ by-product (**Figure 1.12**).[43] We postulated that favorable alkoxide disproportionation to form the thermodynamic "sink", $Fe(OR)_3$, was largely responsible for the lack of catalysis with smaller aryl azides. To prevent this disproportionation and to shed light on the reaction mechanism, we synthesized the bulkier alkoxide HOR' (OR' = $OC^tBu_2(3,5\text{-}Ph_2Ph)$, **Figure 3.1**). We anticipated that the larger size of [OR'] would preclude the formation of hypothetical "$Fe(OR')_3$" species, and as a result would prevent alkoxide disproportionation and enable better-defined catalytic performance with organoazides. In this chapter, we explore the reactivity of the "second-generation" $Fe(OR')_2(THF)_2$ (**31**) with aryl azides and compare those results to the "first-generation" iron(II) complex (**14**).

4.2. Catalytic Reactivity of Fe(OR')₂(THF)₂ in Nitrene Coupling

Our group previously demonstrated that compound **14** was able to conduct highly efficient formation of azoarenes from aryl azides containing two *ortho* substituents (i. e. mesityl and 2,6-diethylphenyl). In contrast, no reactivity was observed for the less bulky aryl azides (such as 2-methylphenyl, 3,5-dimethylphenyl or 4-methylphenyl). Not surprisingly, **31** is also able to efficiently couple mesityl and 2,6-diethylphenyl nitrenes to give the corresponding azoarenes

(**Table 4.1,** entries 1 and 2) in high yields. As previously observed for **14**, catalysis with **31** proceeds at room temperature to give azomesitylene and azo(2,6-diethylbenzene) in high yields. More significantly, **31** is also capable of coupling of other azides, albeit higher catalyst loadings and heating is required in these cases. Thus, 3,5-dimethylphenylazide forms azo(3,5-dimethylbenzene) in 47% yield after 8 hours at 60 °C; heating for 24 h brings the yield of the product to 66%. 4-tolyl azide gives azo(4-methylbenzene) in 16% yield after 8 h; longer heating (24 h) improves the yield to 47%. In other cases, longer heating times do not improve the yield, leading instead to the decomposition of starting materials. Thus, the 4-trifluoromethylazide forms the corresponding azoarene in 20% yields after 8 h. Heating for 24 h keeps the yields of azoarene products low while producing black insoluble material, which we were unable to identify. Also, no product formation was observed for 4-methoxyphenyl azide (entry 9).

Table 4.1. Complex **31** catalyzed formation of azoarenes from the corresponding azides.

Entry	Azide	Catalytic Loading (mol%)	Time (H)	Temperature (°C)	^{1}H NMR Yield (%)
1	MesN$_3$	5	4	25[a]	100
2	2,6-Et$_2$PhN$_3$	5	24	25[a]	100
3	3,5-Me$_2$PhN$_3$	10	8	60[a]	47
4	3,5-Me$_2$PhN$_3$	10	24	60[a]	66
5	2-^{i}PrPhN$_3$	10	8	60[a]	53
6	4-MePhN$_3$	10	8	60[a]	16
7	4-MePhN$_3$	10	24	60[a]	47
8	4-CF$_3$PhN$_3$	10	8	60[a]	20[b]
9	4-OMePhN$_3$	10	8	60[a]/100[c]	0

[a]The reactions were conducted in C$_6$D$_6$ in the presence of an internal standard (trimethoxybenzene) and the yields were determined by ^{1}H NMR spectroscopy. [b]Longer heating of these samples produced insoluble materials; no yield improvement was observed by ^{1}H NMR spectroscopy. [c]The reaction at 100 °C was conducted in C$_7$D$_8$ in the presence of an internal standard.

4.3. Synthesis, Characterization, and Reactions of Iron Tetrazene Complexes

Fe(RNNNNR)(OR')$_2$

As the catalytic reactivity of complex **31** with some aryl azides differs significantly from that of **14**, we became interested in the interrogation of the reaction mechanism. To gain an initial insight, we investigated stoichiometric reactivity of complex **31** with bulky and non-bulky aryl azides. Treatment of the pale-yellow solution of **31** with two equivalents of mesityl azide or 2,6-diethylphenyl azide leads to N$_2$ evolution and color change to red-drown. ^{1}H NMR spectroscopy indicates nearly quantitative formation of the corresponding diazene products. These results are consistent with the results previously obtained for **14**. In contrast to the compound **14**, however, compound **31** does not lead to the formation of the iron tris(alkoxide) complex Fe(OR')$_3$ (**15**) as a

by-product of nitrene coupling. Following mesityl nitrene coupling, we were able to re-isolate compound **31.** We were not able to determine its yield as it co-crystallized with the azomesitylene.

The reaction of **31** with non-bulky aryl azides takes an entirely different route from that of compound **14**. Treatment of **31** with two equivalents of aryl azides N$_3$Ar lacking *ortho* substituents (azidobenzene, 4-azidotoluene, 4-azidoanisole, 3,5-dimethylphenyl azide) leads to the formation of deep-green solutions. Recrystallization of the crude products from ether or hexanes solutions leads to the isolation of dark-green tetrazene complexes **33-36** (**Figure 4.1**). Compound **33-36** were characterized by elemental analysis, solution magnetic measurements by Evans' method, and IR spectroscopy. Solution magnetic measurements of the tetrazene compounds indicate magnetic moments consistent with S = 2. Selected compounds (**33** and **35**) were also characterized by X-ray crystallography (**Figures 4.2** and **4.3,** respectively).

Ar = Ph, **33**, 34% yield
4-MePh, **34**, 52% yield
4-MeOPh, **35**, 46% yield
3,5-MePh, **36**, 68% yield
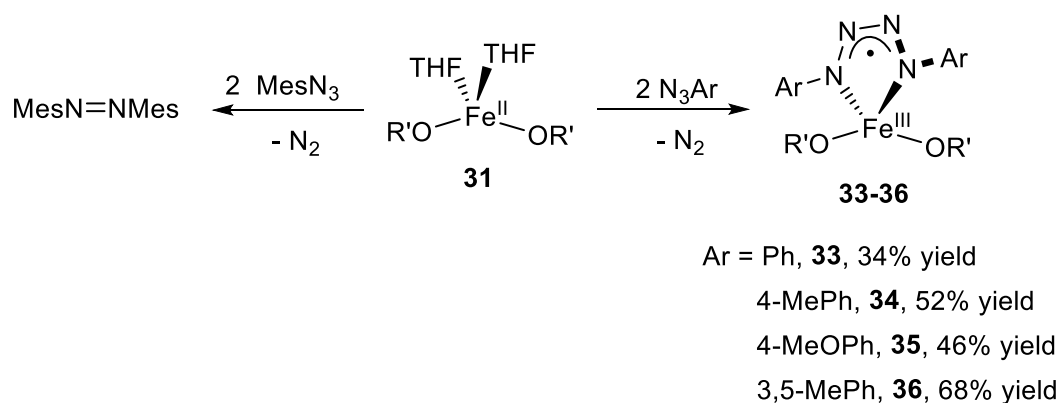
Figure 4.1. Synthesis of iron tetrazene complexes **33-36**.
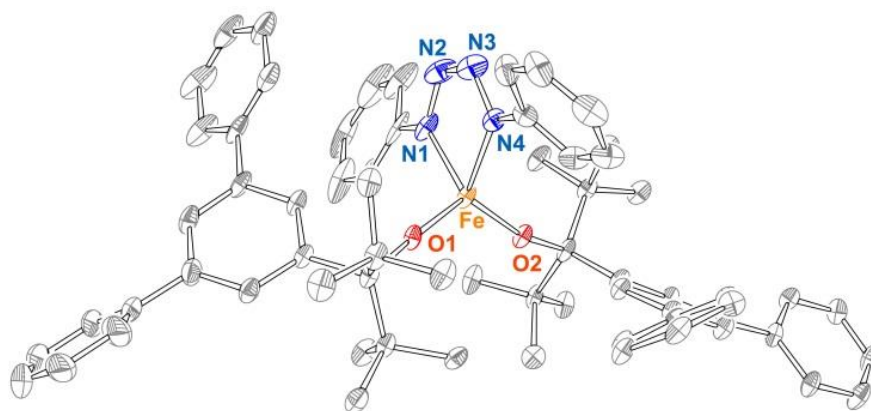
Figure 4.2. X-ray structure of complex **33**.
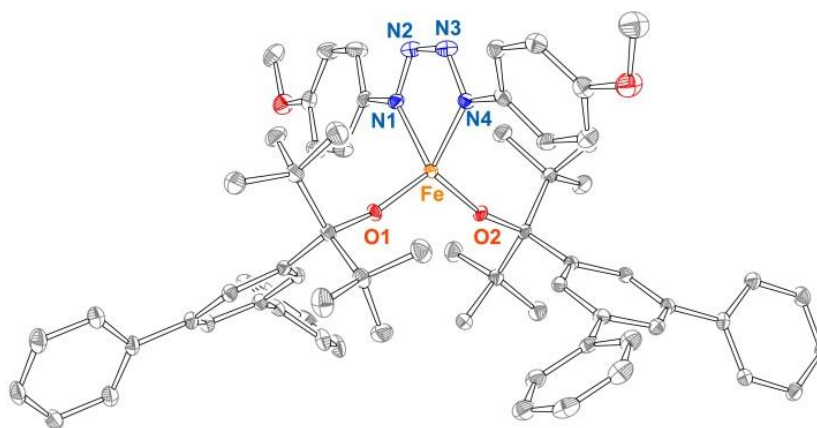
Figure 4.3. X-ray structure of complex **35**.

Both structures confirm coordination of 1,4-tetrazene ligand to the distorted tetrahedral iron center. Due to the lower quality of the structure of **33**, only the metric parameters of **35** are discussed in details. However, metric parameters for **33** follow the trends described below for **35**. The iron-alkoxide bond distances in **35** are slightly shorter than the corresponding distances in **31**: 1.792(1)/1.795(1) Å vs. 1.828(2)/1.854(2) Å. The iron-1,4-tetrazene chelate is planar, with flanking anisole groups displaying different torsion angles of 14 and 31 degrees. The structure is nearly C_2-symmetric, albeit C_2 symmetry is not crystallographic due to the different torsion angles of the anisole groups (see **Table 4.2**). The bond distances in the 1,4-tetrazene fragment indicate

that N1-N2 and N3-N4 distances of 1.322(2) and 1.316(2) Å are similar to the N2-N3 distance of 1.325(2) Å, all being intermediate between N-N and N=N bonds.[73] The redox-active nature of metal-bound tetrazene, that is capable of adopting three different oxidation states (2-/1-/0, **Figure 4.4**), has been previously discussed by Holland and coworkers,[74] and Riordan and coworkers.[75] The similarity in the tetrazene N-N bond distances in **35** suggests that tetrazene ligand is in the radical anion (1-) state, which leads to the Fe(III) center. Thus, compound **35** constitutes the first structurally characterized Fe(III)-tetrazene complex. Other reported iron tetrazene complexes include Fe(II)-tetrazene radical anion reported by Holland and coworkers, and Riordan and coworkers, and Fe(IV)-tetrazene dianion, reported by Jenkins and coworkers.[74-76]

Table 4.2. Experimental crystallographic parameters for **33 and 34**.

complex	33	35
formula	$C_{66}H_{72}FeN_4O_2$	$C_{68}H_{76}FeN_4O_4$
fw	1009.17	1069.23
crystal system	monoclinic	triclinic
space group	$P\,2_1/n$	$P\,$-1
a (Å)	12.1405(14)	11.5932(8)
b (Å)	11.5971(13)	15.3654(9)
c (Å)	42.075(5)	18.0327(11)
α (deg)	90.00	80.380(2)
β (deg)	96.367(4)	85.537(2)
γ (deg)	90.00	76.194(2)
V (Å^3)	5887.39	3073.15
D_c (g cm^{-3})	0.290	0.401
Z	4	2
μ (mm^{-1})	0.307	0.300
T (K)	100(2)	100(2)
R_1	6.56	4.14
GOF	1.011	1.023

4.4. [57]Fe Mössbauer Spectroscopy and Density Function Theory Calculations of Tetraznes

To further study the electronic properties of tetrazene complexes, we have collaborated

with Dr. Sebastian Stoian at the National High Magnetic Field Laboratory to obtain [57]Fe

Mössbauer and EPR spectrum for complex **36.** The zero-field [57]Fe Mössbauer spectra recorded for

36 exhibit a well-defined quadrupole doublet (**Figure 4.4**). This doublet accounts for ~ 85% of the iron present in the sample. The remaining iron amount is associated with an EPR-silent species that exhibits a very broad magnetic hyperfine splitting typically associated with iron(III)-based nanoparticles. At 4.2 K the quadrupole doublet is characterized by an isomer shift $\delta = 0.49$ mm/s, quadrupole splitting $\Delta E_Q = 2.21$ mm/s, and a relatively narrow linewidth $\Gamma = 0.28$ mm/s. While the isomer shift is typical of high-spin iron(III) ions the observed ΔE_Q is unusually large for $S = 5/2$ ferric compounds.[79]
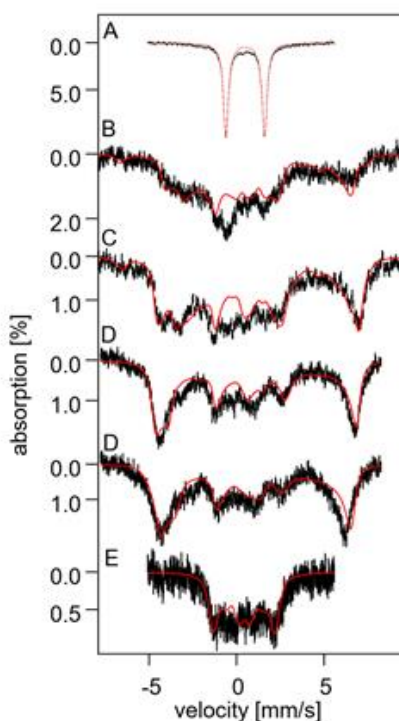
Figure 4.4. Field- and temperature-dependent ^{57}Fe Mössbauer spectra recorded for a neat sample of **36** at 4.2 K, 0 T (**A**); 4.2 K, 0.5 T (**B**); 4.2 K, 1.0 T (**C**); 4.2 K, 4.0 T (**D**); 4.2 K, 8.0 T (**E**); 180.0 K, 8.0 T (**F**). The solid red lines are simulations obtained using a standard $S = 2$ spin. Hamiltonian using D = 1.6 cm-1, E/D = 0.2, $\Delta E_Q = -2.21$ mm/s, $\delta = 0.49$ mm/s, $\eta = 1.3$; $\alpha_{EFG} = 14^o$, $\beta_{EFG} = 78^o$, $\gamma = 0^o$, $A_x/g_n\beta_n = -12.5$ T, $A_y/g_n\beta_n = -19.1$ T, $A_z/g_n\beta_n = -22.1$ T, and $\Gamma = 0.4(1)$ mm/s.

Our combined analysis of the field-dependent ^{57}Fe Mössbauer and high-field EPR spectra (see **Appendix D**) demonstrates that **36** exhibits a quintet, $S = 2$ ground spin state which is characterized by a small zero-field splitting (ZFS) and isotropic g tensor. Thus, our current best

estimates of the ZFS parameters are D = 2.2(6) cm^{-1}, E/D = 0.26(4) and of the intrinsic g-tensor components $g_x \approx g_y \approx g_z \approx$ 2.03(4). These values reveal the presence for **36** of an isolated orbital state and are in stark contrast to those expected for a bona fide high-spin iron(IV) ion. In contrast, a small ZFS parameter D and $g_{x,y,z} \sim g_e$ = 2.0023 is typically associated with high-spin iron(III) ions that have a half-filled valence shell and thus a 6A singlet orbital ground state. Together with the value of the isomer shift the magnetic properties of **36** strongly support the presence for this compound of a high-spin ferric ion with a sextet, S = 5/2 ground spin state. Consequently, the observed S = 2 ground spin state of **36** originates not from a S = 2 iron(IV) site but from the presence of a ligand based S = 1/2 radical that is strongly antiferromagnetically coupled to the S = 5/2 of the iron(III) ion.

In order to explore the origin of the observed spectroscopic parameters we have performed a series of DFT calculations using an unabridged structural model and the B3LYP/6-311G functional/basis set combination. Our investigation revealed that the predicted ground state of **36** is of a broken-symmetry type for which one beta, spin-down electron is delocalized on the nitrogen atoms of the tetrazene ligand and nearly five spin-up, alpha electrons are localized on the iron ion. Furthermore, both the predicted zero-field Mössbauer parameters and predicted structures are in good agreement with those observed experimentally. Consequently, these calculations further corroborate the presence for this complex of a high-spin iron(III) ion and suggest that the S = 1/2 ligand-based spin is localized on the tetrazene moiety (**Figure 4.5**). Finally, these calculations also allow us to rationalize the observed ΔE_Q value. Thus, the predicted EFG tensor is dominated by the presence of a large ligand contribution to the EFG tensor generated by the two alkoxo ligands.
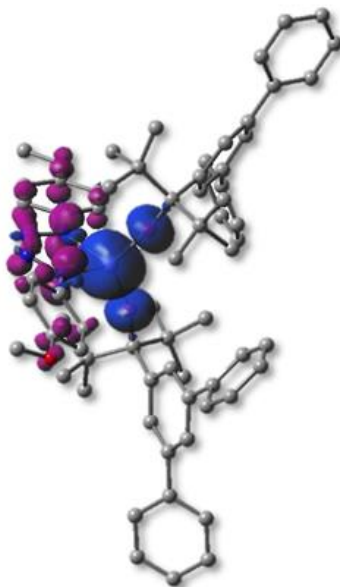
Figure 4.5. Spin-density predicted for the X-ray structure at B3LYP/6-311G level. Positive, alphaspin density is shown in blue and negative, beta-spin density is shown in purple. When compared to the ferromagnetic (F), S = 3 state the broken-symmetry (BS), S = 2 state for which the spin density is shown here is stabilized by 6.7 kcal/mol. In the $J\mathbf{\hat{S}}1 \cdot \mathbf{\hat{S}}2$ formalism this energy difference corresponds to an exchange coupling constant between the iron-based S = 5/2 spin and the tetrazene-localized S = 1/2 spin of J = 941 cm-1. Geometry optimizations performed for the BS and F states lead to a lower difference that is, 3.92 kcal/mol corresponding to J = 550 cm^{-1}.

4.5. Formation of Azoarene from Tetrazene Complexes

It is generally accepted that tetrazenes are formed by [2+3] cycloaddition of metal-nitrene complex with an organoazide,[73,77] which indicates that Fe(OR')$_2$ system forms Fe(OR')(Ar) (nitrene) species first. What is the role of 1,4-tetrazene species in the formation of diazenes in Fe(OR')$_2$ system? One could propose three possible roles of tetrazene: (1) an obligatory reaction intermediate on the path to diazenes; (2) a "masked form" of reactive iron-nitrene species, whose formation is reversible, and which may not directly lead to diazenes, but which may enable their formation by reforming reactive nitrene or some other species; (3) a side product that is not relevant to the main reaction path that leads to the diazenes, and whose formation is irreversible. We note

that Jenkins and coworkers have recently demonstrated that in their tetracarbene (TC) system, Fe(TC)(ArNNNNAr) (tetrazene) complex forms diazene upon heating; it also forms aziridines upon reaction with olefins (**Figure 4.6a**). Zdilla and coworkers have demonstrated that the formation of Mn-tetrazene in Mn(ArNNNNAr)$_2$ was reversible, and detected the ring-opened Mn-imido-azide intermediate (**Figure 4.6b**)[78] albeit no formation of azoarenes were detected in their system. Hillhouse and Cundari proposed that formation of diazenes takes place via a 1,2-tetrazene in nickel-diphosphine system (**Figure 4.6c**).[17a] Finally, Peters and coworkers have thoroughly investigated the mechanism of catalytic formation of diazenes in their iron and ruthenium systems, and found no evidence for tetrazene participation. Instead, mechanistic evidence pointed to the direct nitrene coupling for ruthenium, and for metal-imido coupling for iron (**Figure 4.6d**).[20]
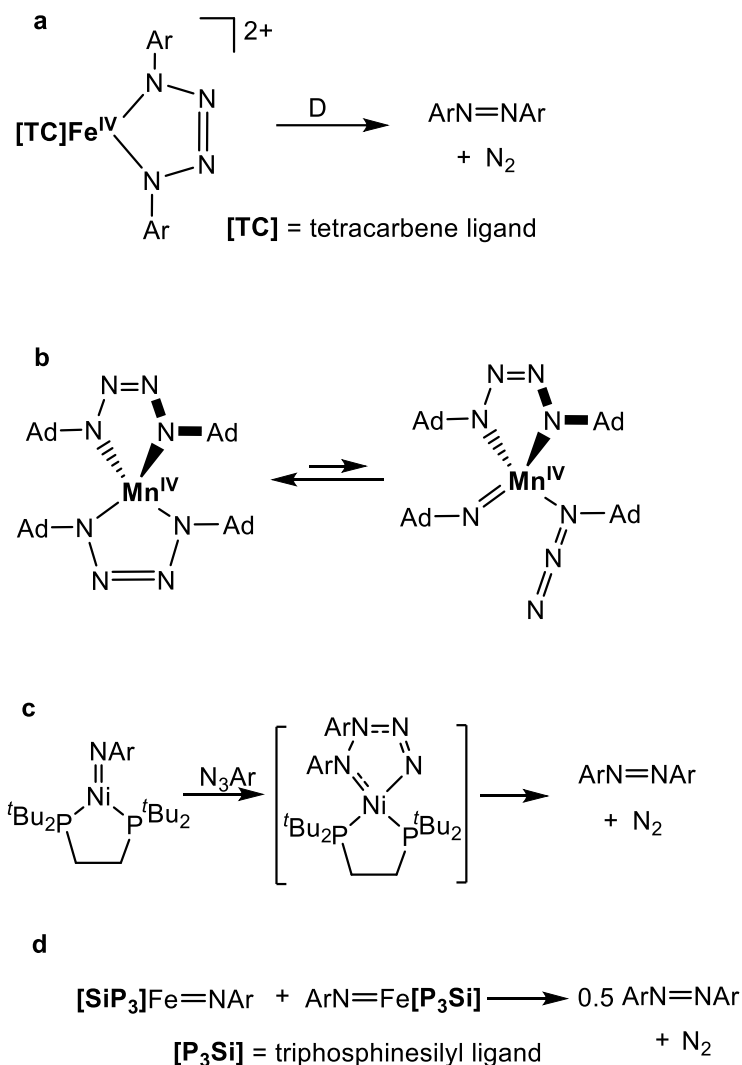
Figure 4.6. Previously reported reactions of metal-imido of relevance to tetrazene or diazene chemistry.

To shed light on the role of 1,4-tetrazene in our system, we interrogated whether the Fe(OR)$_2$(ArNNNNAr) complexes are capable of forming diazenes. We specifically focused on the reactivity of complexes **34** or **36**, as there can be isolated in a relatively good yield. Heating C$_6$D$_6$ solution of **34** or **36** to 50 °C for 8 h produces the corresponding azoarene. The formation of aroarene was also confirmed by mass spectrometry (**Appendix D**). Next, we interrogate the reactivity of preformed tetrazene complex with a different azide. Treatment of complex **36** with the C$_6$D$_6$ solution of azidotoluene results in the formation of three different diazenes, two

symmetric and one asymmetric (**Figure 4.7**), as confirmed by mass spectrometry (see **Appendix D**). These experiments seem to suggest that while (*i*) tetrazenes are relevant to the catalytic cycle that produces diazenes, (*ii*) they appear to be in equilibrium with Fe-imido which can then upon a reaction with a different azide form mixed diazene product. For further insight into the reaction mechanism, we will use DFT calculations in collaboration with the Lord lab to explain the mechanism of these reactions.
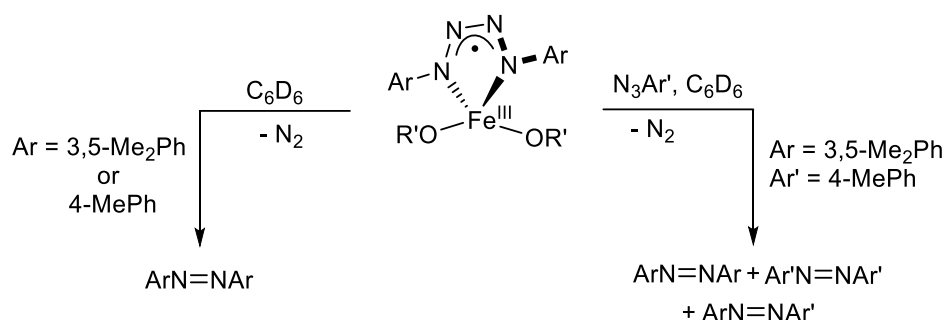
Figure 4.7. Stoichiometric reactions of tetrazene complexes forming diazenes.

4.6. Summary and Conclusions

Our second-generation iron bis(alkoxide) complex Fe(OR')$_2$(THF)$_2$ allows catalytic diazene formation for a variety of aryl azides. We specifically show that, due to the lack of alkoxide disproportionation/formation of Fe(OR')$_3$ species, even smaller aryl azides are transformed into azoarenes, albeit somewhat less efficiently than bulkier azides (i. e. mesityl). We also demonstrate that the reaction proceeds via the formation of iron-tetrazene intermediates, which were isolated and characterized structurally and spectroscopically. Presently, we are investigating the mechanism in which azorenenes are formed by the second-generation iron(II) precursor **31**.

4.7. Experimental Section

Mössbauer Spectroscopy. The field- and temperature - dependent Mössbauer spectra were recorded using a spectrometer operated in a constant acceleration mode. The instrument was fitted with a Janis Super-Varitemp, 8DT flow-type cryostat equipped with a superconducting magnet

and was cooled using liquid helium. This setup allowed for reaching temperatures between 1.7 and 220 K as well as for the generation of magnetic fields with a strength of up to 8 T. The field was applied parallel to the propagation direction of the 14.4 keV γ-ray. The light source was incorporated in a vertical velocity transducer system and consisted of a 100 mCi ^{57}Co dispersed in a rhodium foil. The spectra recorded at 4.2 K were obtained while the sample space of the cryostat was flooded with liquid helium. At higher temperatures the sample was cooled using a stream of cold helium gas with a flow controlled by a needle-type valve. The sample temperature was determined using a Cernox® sensor and was maintained using a 50 Ω heater powered by a Cryocon 32B temperature controller. The isomer shift is reported against the center of the α-iron metal foil spectrum recorded at room temperature. The spectra were analyzed in the framework of a standard $S = 2$ spin-Hamiltonian as implemented in by the SpinHam option of the WMOSS spectral analysis software (See Co., formerly Web Research Co., Edina, MN). The samples investigated by ^{57}Fe Mössbauer spectroscopy consisted of about 20 mg neat polycrystalline material contained in custom-made Delrin® cups. The samples were prepared using unenriched, natural abundance iron in Detroit and shipped to Tallahassee while kept at 77 K in a dry LN2 shipping dewar. Subsequently, the samples were stored and handled under LN2.

Density Functional Theory. The DFT calculations were performed using the Gaussian 09 (revisions A02 and C01) quantum chemical software package. Moreover, for this computational investigation we used the spin unrestricted formalism, the B3LYP/6-311G functional/basis set combination, and an unabridged structural model. Single point self-consistent field (SCF) calculations and geometry optimizations were completed using standard convergence criteria. The ground state character of a particular electronic configuration was assessed on the basis of time-dependent (TD) DFT calculations, that is, all one-electron excitations were found to be positive.

The theoretical exchange coupling constants, J, were estimated from the comparison of the predicted SCF energies of the ferromagnetic (F) and broken-symmetry (BS) states.[80] The initial electronic guesses of the starting SCF calculations were obtained using the default guess option in the case of the F configuration and the *fragment* option of the *guess* keyword for the BS states. While the F state had a septet, $S_T = 3$ configuration, the BS state corresponds to a $S_T = 2$ configurations for which 5α, spin-up, electrons are localized on the iron site while 1β, spin-down, electron was localized on the tetrazene ligand. The value of the exchange coupling constant was obtained using the expression $J = 2(E_F - E_{BS})/5$ where the E_{BS} and E_F energies were obtained from single-point calculations performed either on the X-ray structure or on the geometry optimized structures. Charge and spin distributions were assessed on the basis of the Mulliken atomic spin densities and charges. The predicted ΔE_Q and η values describing the electric field gradient and the predicted ^{57}Fe hyperfine coupling constants were estimated using the standard *prop* keyword of the Gaussian code. The predicted isomer shift values were determined using the calibration given by Vrajmasu et al.[81]

General Methods and Procedures. All reactions involving air-sensitive materials were executed in a nitrogen-filled glovebox. The synthesis of HOR' and Fe(OR')$_2$(THF)$_2$ are described in chapter 3. Mesityl azide,[18c] 2-isopropylphenyl azide, [64a] 2,6-diethylphenyl azide,[44c] and 3,5-dimethylphenyl azide,[82] were synthesized according to previously reported procedures. Azidobenzene solution, 4-azidotoluene, 4-(trifluoromethyl)phenyl azide solution, 4-azidoanisole solution, and 2,6-dimethylphenyl isocyanide were purchased from Aldrich and used as received. All solvents were purchased from Fisher Scientific and were of HPLC grade. The solvents were purified using an MBraun solvent purification system and stored over 3 Å molecular sieves. Complexes **33** and **35** were identified by X-ray crystallography. Compounds **33-36** were

characterized by UV-Vis and IR spectroscopy, solution magnetic susceptibility, and elemental analysis. NMR spectra were recorded at the Lumigen Instrument Center (Wayne State University) on a Varian Mercury 400 MHz NMR spectrometer in C_6D_6 at room temperature. Chemical shifts and coupling constants (J) are reported in parts per million (δ) and hertz, respectively. IR spectra of powdered samples were recorded on a Shimadzu IR Affinity-1 FT-IR spectrometer outfitted with a MIRacle10 attenuated total reflectance accessory with a monolithic diamond crystal stage and pressure clamp. Magnetic moments were determined using the Evans method.[49] Low resolution mass spectra were obtained at the Lumigen Instrument Center utilizing a Waters Micromass ZQ mass spectrometer (direct injection, with capillary at 3.573 kV and cone voltage of 20.000 V). Elemental analyses were performed by Midwest Microlab LLC.

Synthesis of Fe(OR')₂(PhNNNNPh) (33). To a solution of 3.0 mL of Fe(OR′)₂(THF)₂ (32.0 mg, 0.0339 mmol) in toluene, azidobenzene (0.14 mL, 0.5 M) in toluene was added slowly. The solution changed color immediately from light gold to deep green-black. The reaction was stirred for 30 minutes, upon which the solvents were removed in vacuo to yield green-black residue. Crystallization from ether at −35 °C over two days gave green-black crystals of **33** (11.5 mg, 34%). IR (cm^{-1}): 2920 (m), 1524 (s), 1489 (s), 1454 (s), 1339 (s), 1123(m), 1057 (s), 976 (s), 849 (s). $\mu_{eff} = 4.3 \pm 0.2\mu_B$. Anal. Calcd: C, 78.6; H, 7.2; N, 5.6. Found: C, 78.4; H, 7.3; N, 5.5.

Fe(OR')₂((4-CH₃C₆H₄)NNNN(4-CH₃C₆H₄)) (34). To a solution of 3.0 mL of Fe(OR′)₂(THF)₂ (40.9 mg, 0.0434 mmol) in toluene, 4-azidotoluene (0.17 mL, 0.5 M) in toluene was added slowly. The solution changed color immediately from light gold to deep green-black. The reaction was stirred for 30 minutes, upon which the solvents were removed in vacuo to yield green black residue. Crystallization from ether at −35 °C over two days gave dark green crystals of **34** (23.2 mg, 52%). IR (cm^{-1}): 2970 (m), 1593 (s), 1489 (m), 1416 (s), 1389 (s), 1177 (s), 1119 (m), 1045 (s), 1003 (s),

880 (s), 822 (s), 823 (s), 703 (s). $\mu_{eff} = 4.3 \pm 0.1\mu_B$. Calcd: C, 78.7; H, 7.4; N, 5.4. Found: C, 78.4; H, 7.5; N, 5.1.

Fe(OR')$_2$((4-OCH$_3$C$_6$H$_4$)NNNN(4-OCH$_3$C$_6$H$_4$)) (35). To a solution of 3.0 mL of Fe(OR')$_2$(THF)$_2$ (40.5 mg, 0.0429 mmol) in toluene, 4-azidoanisole (0.20 mL, 0.5M) in toluene was added slowly. The solution changed color immediately from light gold to deep green black. The reaction was stirred for one hour, upon which the solvents were removed in vacuo to yield green black residue. Crystallization from ether at −35 °C over two days gave crystals of dark green crystals of **35** (21.0 mg, 46%). IR (cm^{-1}): 2955 (m), 1497 (m), 1389 (s), 1370 (s), 1246 (m), 1057 (m), 880 (s), 760 (s), 698 (s). $\mu_{eff} = 4.1 \pm 0.4\ \mu_B$. Anal. Calcd: C, 76.4; H, 7.2; N, 5.2. Found: C, 76.0; H, 7.4; N, 5.2.

Fe(OR')$_2$((3,5-Me$_2$C$_6$H$_3$)NNNN(3,5-Me$_2$C$_6$H$_3$)) (36). To a solution of 3.0 mL of Fe(OR')$_2$(THF)$_2$ (41.9 mg, 0.044 mmol) in toluene, 3,5-dimethylphenyl azide (1.42 mg, 0.088 mmol) in toluene was added slowly. The solution changed color immediately from light gold to deep green black. The reaction was stirred for 30 minutes, upon which the solvents were removed in vacuo to yield green-black residue. Crystallization from hexanes at −35 °C over two days gave dark green crystals of **36** (31.3 mg, 68%). IR (cm^{-1}): 2970 (m), 1593(s), 1489 (m), 1119 (m), 1045 (s), 999 (s), 880 (s), 822 (s), 768 (s), 702 (s). $\mu_{eff} = 4.4 \pm 0.2\mu_B$. Calcd: C, 78.9; H, 7.6; N, 5.3. Found: C, 79.1; H, 8.0; N, 5.1.

General Procedure for Catalytic Formation of Azoarenes. All the reactions were performed by the addition of 10 or 20 equivalents of organic azide and TMB standard solution in C$_6$D$_6$ to a solution of 10 or 5 mol % of complex **31** (approximately 30-35 mg) in C$_6$D$_6$ in an N$_2$-filled

glovebox. The reaction mixture was then stirred at the noted temperature for 8 or 24 hours. The yields of azoarene products were determined by ^{1}H NMR spectroscopy.

Formation of Azoarene from Tetrazene Complex 34. A solution of complex **34** (45.6 mg, 0.0439 mmol) and TMB in C_6D_6 was heated at 60 ^{o}C. The reaction mixture was stirred for 8 h after which ^{1}H NMR spectrum was taken to calculate the percent yield of azoarene produced (17%). To further analyze the product, all solvents were removed under vacuo and the residue was separated on silica gel using hexanes. The collected orange solution was characterized by mass spectroscopy to confirm the formation of $(4\text{-MeC}_6H_4)N=N(4\text{-MeC}_6H_4)$ (see **Appendix D**).

Formation of Azoarene from Tetrazene Complex 36. A solution of complex **36** (28.6 mg, 0.0268 mmol) and TMB in C_6D_6 was heated at 60 ^{o}C. The reaction mixture was stirred for 8 h after which ^{1}H NMR spectrum was taken to calculate the percent yield of azoarene produced (30%). To further analyze the product, all solvents were removed under vacuo and the residue was separated on silica gel using hexanes. The collected orange solution was characterized by mass spectroscopy to confirm the formation of $(3,5\text{-Me}_2C_6H_3)N=N(3,5\text{-Me}_2C_6H_3)$ (see **Appendix D**).

Reaction of Tetrazene Complex 36 with 4-methylphenylazide. To a solution of complex **36** (66.2 mg, 0.0621 mmol) in C_6D_6, TMB and azidotoluene (0.2 mL, 0.5 *M*) in C_6D_6 was added. The reaction was heated at 60 ^{o}C for 4 h, upon which ^{1}H NMR spectrum was taken to show the formation of several azoarenes. To analyze the reaction mixture, all solvents were removed and the crude product was separated on silica gel using hexanes. The obtained orange solution was characterized by mass spectroscopy to show the formation of three different diazenes (see **Appendix D**).

CHAPTER 5 THE REACTIVITY OF A CHROMIUM BIS(ALKOXIDE) COMPLEX TOWARD ORGANIC CARBONYLS AND CO$_2$

The text in this chapter were reprinted or adapted with permission from: Yousif, M.; Cabelof, A. C.; Lord, R. L.; Martin, P. D.; Groysman, S. *Dalton Trans.* **2016**, *45*, 9794-9804.

5.1. Introduction

Cr(II) complexes are highly versatile reagents in catalysis and small molecule activation,[83] that enable reductive coupling of aldehydes and ketones (including pinacol coupling),[84,85] oligomerization and polymerization of olefins,[86] activation of dinitrogen,[87] and other transformations. Some of these transformations are enabled by the simplest Cr(II) compound, CrCl$_2$.[88] However, while CrCl$_2$ is among the cheapest Cr(II) sources available, its heterogeneous nature hampers mechanistic perception of the catalyzed processes. Hence, there is a significant interest in homogeneous well-defined chromium(II) complexes capable of providing molecular insight into the reactivity of chromium(II) with various substrates. Low-coordinate complexes are particularly useful in this regard, as their coordinative unsaturation facilitates substrate fixation. As a result, significant efforts are invested into the design of mononuclear low-coordinate chromium(II) complexes in different ligand environments. One of the major hurdles in the design of low-coordinate Cr(II) species is their tendency to form multiply-bonded dimers.[89] Having synthesized a distinct and reactive monomeric Cr(II) bis(alkoxide) complex, Cr(OR')$_2$(THF)$_2$ (**30**), we decided to explore its reactivity toward reduction of carbonyl compounds and CO$_2$. The reductive coupling of carbonyl compounds (ketones and aldehydes) to form diol compounds is a well-established transformation that is suggested to occur either by monometallic or bimetallic pathways depending on the transition metal ability to engage in one- or two-electron(s) transfer reduction, respectively.[90] However, direct investigation of the catalytic coupling mechanism performed by simple Cr(II) compounds (i.e. CrCl$_2$) is rather complicated due to the heterogeneous

nature of the Cr(II) chloride and the ability of the chromium to behave as one or two electron reducing agent. In this chapter, we used our Cr(II) bis(alkoxide) complex **30** as a model to examine and explore the reductive coupling of carbonyl compounds. DFT calculations will be used to explain the mechanism of these reactions. Also, we interrogated the reactivity of Cr bis(alkoxide) with CO_2.

5.2. Reactivity of Cr(OR')$_2$(THF)$_2$ with Aldehydes and Ketones

As described previously, mixtures of $CrCl_2$ with various co-catalysts serve as effective catalysts for the reductive coupling of organic carbonyls.[84,85] However, due to the heterogeneous nature of the multi-component mixtures, mechanistic details on these transformations are scarce. In general, pinacol coupling can proceed via a "monometallic" or a "bimetallic" mechanism (**Figure 5.1**),[84a,c] where each metal center functions as a two- or a one-electron donor, respectively. For certain metals (i.e. K(0), Ti(III)), pinacol coupling must proceed via a bimetallic mechanism, as the metals are obligatory one-electron reductants. For Cr(II), however, the answer is far from certain as Cr(II) can function as a one- or a two-electron reductant. Under certain reaction conditions, Cr(III) was postulated to be the product of pinacol coupling originating in Cr(II), thus implying a "bimetallic mechanism".[84a,85b,f,g] Having in hand a well-defined Cr(II) precursor that may provide a homogeneous reactivity model for the $CrCl_2$-derived pinacol coupling, we decided to interrogate the stoichiometric reactivity of Cr(OR′)$_2$(THF)$_2$ with aldehydes and ketones.
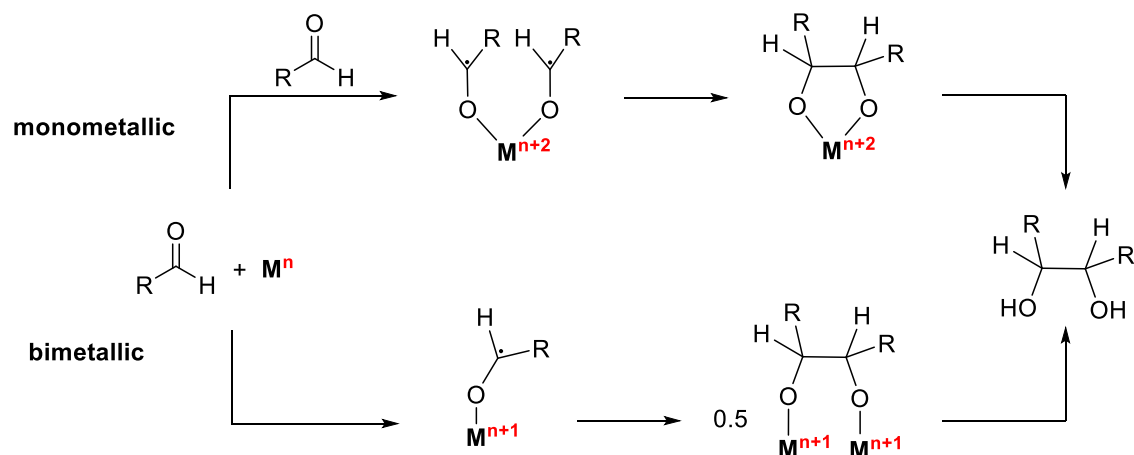
Figure 5.1. Proposed mechanism for the pinacol coupling. Top: monometallic mechanism. Bottom: bimetallic mechanism.

Treatment of Cr(OR')$_2$(THF)$_2$ (**30**) with two equivalents of benzaldehyde in toluene or hexane affords green solution, from which the Cr(IV) complex Cr(OR')$_2$(O$_2$C$_2$H$_2$Ph$_2$) (**37**) is isolated as deep-green crystals in 67% yield. Similarly, treatment of **30** with 4-anisaldehyde, 4-(trifluoromethyl)benzaldehyde, and 2,4,6-trimethylbenzaldehyde (**Figure 5.2**) yields corresponding diolate complexes **38-40** (74%, 35%, and 66%, respectively). Thus, the Cr(II) complex Cr(OR')$_2$(THF)$_2$ functions as a two-electron reductant in the reactions with aldehydes; no Cr(III) products were isolated. Since compounds **37-40** are isolated in good yields, it is unlikely that any Cr(III) products form in appreciable amounts. We also attempted the reaction of complex **30** with an aliphatic aldehyde, hexanal. A similar color change was observed; however, we were not able to isolate products of this reaction.
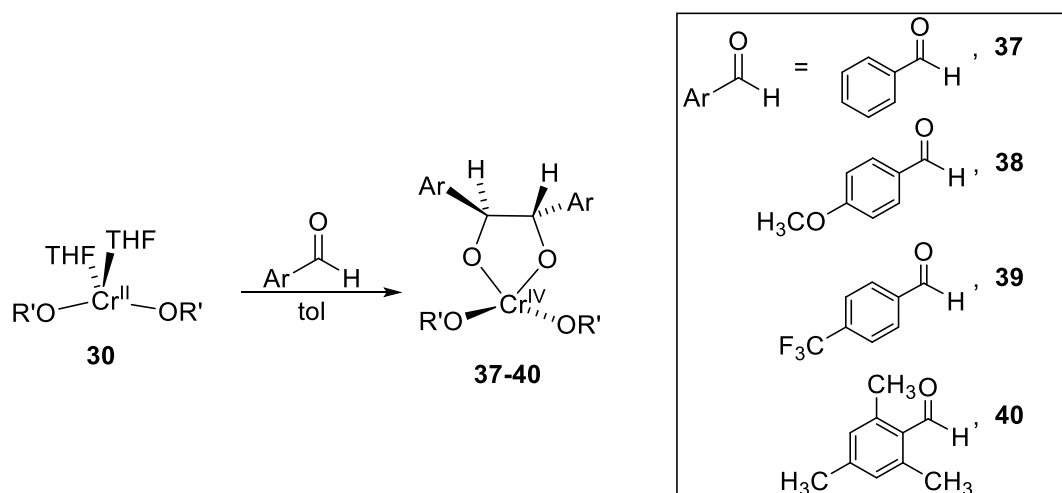
Figure 5.2. Synthesis of the complexes **37-40**.

Complexes **37-40** were characterized by IR and UV-vis spectroscopy, solution magnetic measure measurements, and elemental analyses. In addition, representative complexes **37** and **38** (see **Appendix E**) are characterized by X-ray crystallography. The structure of **37** (**Figure 5.3**) illustrates a tetra-coordinate Cr(IV) center ligated by two monodentate alkoxides OR′ and a bidentate racemic deprotonated hydroxybenzoin ligand that results from the reductive coupling of two benzaldehydes (C1–C2 bond of 1.546(3) Å). In contrast to the structure of **30**, the metal geometry in **37** is distorted tetrahedral, with the largest angle of 116.1(1)° between the bulky alkoxides OR′. The complex adopts nearly C_2-symmetrical structure, albeit non-crystallographic due to the presence of two solvent (ether) molecules (**Table 5.1**). Chromium–oxygen bonds are within 1.747(2)-1.786(2) Å range, typical for the Cr(IV)–OR distances.[91]
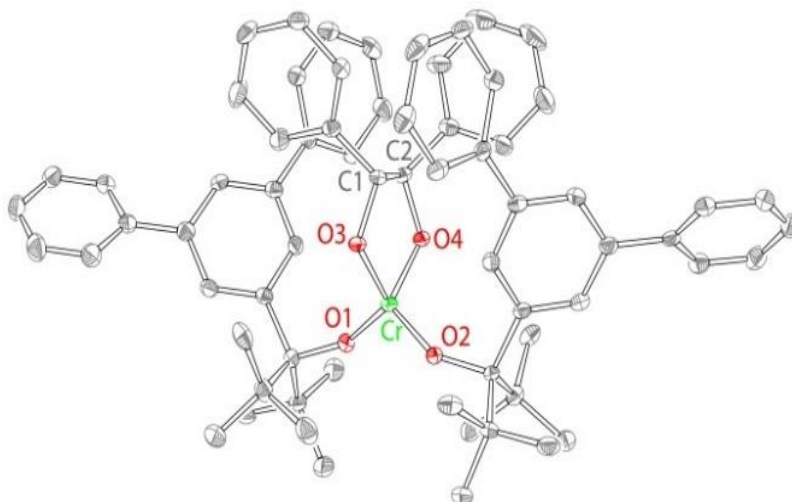
Figure 5.3. X-ray structure of **37**, 50% probability ellipsoids.

We also investigated the reactivity of compound **30** with ketones. Treatment of the green

hexane solution of $Cr(OR')_2(THF)_2$ with benzophenone led to an immediate color change to deep

blue. Recrystallization of the reaction product from hexanes afforded blue-green crystals of

benzophenone adduct $Cr(OR')_2(OCPh_2)$ (**41**) in 78% yield (**Figure 5.4**).
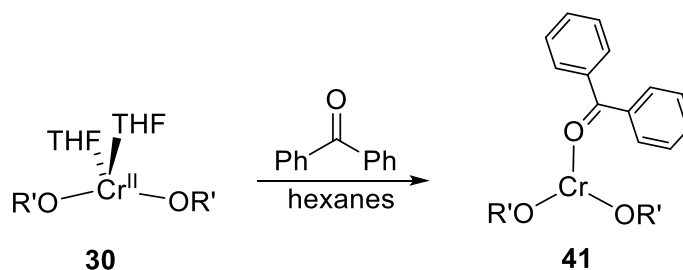
Figure 5.4. Synthesis of complex **41**.

The structure of **41**, presented in **Figure 5.5**, reveals a trigonal-planar complex with a single

benzophenone ligand coordinated to chromium. The structure also indicates that there is a slight

elongation of the benzophenone C=O bond from 1.222 in free benzophenone[92] to 1.254(3) Å in

41. This distance is, however, significantly shorter that in a true metal-bound "ketyl".[92,93] Thus, it

appears that, in contrast to the aldehydes, no benzophenone coupling takes place. We postulate

that the reason behind this is the steric requirements of two benzophenone equivalents vs. two

benzaldehyde equivalents. This hypothesis is supported by calculations (vide infra). We note that the treatment of complex **30** with a smaller ketone – acetophenone – exhibited a different color change (from green to brown), which may indicate a different reactivity pattern. We were not able to isolate the chromium product from this reaction. Instead, recrystallization led to the isolation of the colorless crystals of HOR′ (confirmed by IR and X-ray).
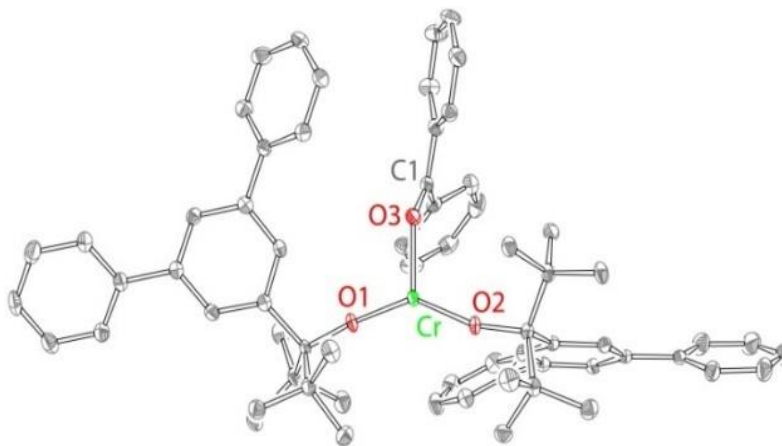
Figure 5.5. X-ray structure of complex **41**.

Table 5.1. Experimental crystallographic parameters for **37** and **41**.

complex	37	41
formula	$C_{68}H_{74}CrO_4$	$C_{67}H_{72}CrO_3$
fw	1007.31	977.28
crystal system	triclinic	triclinic
space group	*P -1*	*P 2₁/c*
a (Å)	14.3588(8)	11.9901(5)
b (Å)	15.5398(8)	13.5092(5)
c (Å)	16.5005(9)	32.9625(14)
α (deg)	72.971(3)	90.00
β (deg)	76.079(3)	94.836(2)
γ (deg)	69.182(3)	90.00
V (Å^3)	3251.9(3)	5320.1(4)
D_c (g cm^{-3})	1.180	1.220
Z	2	4
μ (mm^{-1})	0.228	0.263
T (K)	100(2)	100(2)
R_1	5.34	4.75
GOF	1.268	1.105

5.3. Computational Studies

To better understand why the aldehyde undergoes pinacol coupling but the ketone does not, we explored the C–C bond formation step at a single Cr center using a QM/MM approach due

to the size of the ligand.[44] Initially, the diolate product with the benzaldehyde substrate was optimized for comparison to the experimental X-ray structure. The optimized structure compares well to the experimental one, with the largest discrepancy in one of the Cr–O bonds being 0.015 Å (**Figure 5.6**).

The critical C–C bond only differs by 0.001 Å. This triplet species is a d^2-Cr(IV) complex based on the Mulliken spin of 2.00 at the metal ion. The transition state and bis-aldehyde reactant were located by elongating the C–C bond in this species (**Figure 5.7**). Alternative spin states were explored for the bis-aldehyde reactant, however, the triplet was found to be lower in Gibbs energy than the singlet (+32.6 kcal mol^{-1}) and quintet (+0.6 kcal mol^{-1}). When combined with the fact that the only sensible spin state for the Cr(IV) diolate is a triplet, we focused exclusively on the triplet surface for reactivity despite examples of Cr chemistry spanning multiple spin surfaces.[94]
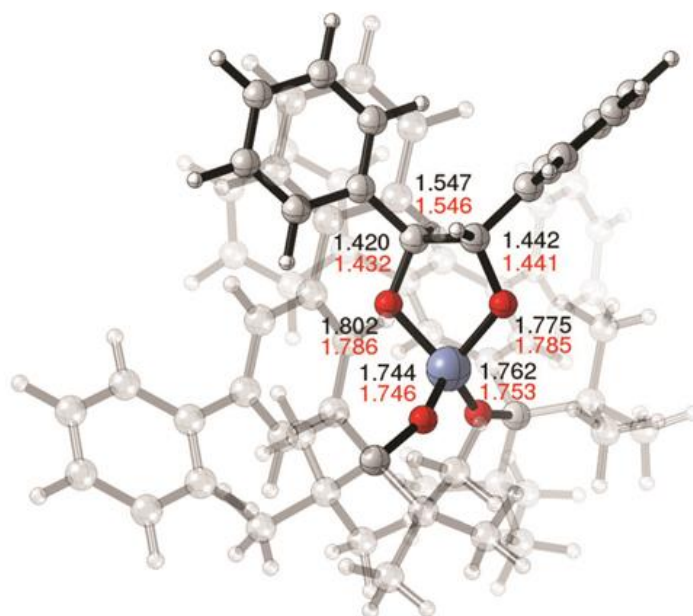
Figure 5.6. Comparison of the calculated (black) and experimental (red) bond lengths (Å) for **37**. The QM region of the molecule is highlighted and the MM region is transparent.

The bis-aldehyde reactant has longer Cr–O contacts to the alkoxide ligands (1.81 Å vs. 1.75 Å) and carbonyls (1.92 Å vs. 1.79 Å) when compared to the diolate product. Carbonyl bond lengths of 1.276 and 1.274 Å vs. 1.216 Å in free benzaldehyde (calculated at this level of theory) suggest only partial reduction of the aldehyde ligands. Mulliken spin densities of 2.82 at Cr, and −0.28/−0.22 at the carbonyl Cs suggest this species is a Cr(III) complex with two half-reduced aldehydes. A corresponding orbital analysis[95] shows that the metal is antiferromagnetically coupled to the radical spread between the aldehyde ligands. This finding is consistent with recent examples of formally Cr(II) species forming Cr(III) complexes in the presence of redox-active ligands.[96] The transition state shows Cr–O bond lengths of 1.79 Å to the alkoxides and 1.90 Å to the carbonyls, intermediate between reactant and product, and the forming C–C bond distance is 1.940 Å. Mulliken spin densities of 2.77 at Cr and −0.14/−0.13 at the carbonyl Cs suggest that the complex is still a Cr(III) ion and the final electron transfer must occur after the transition state. Thus, it appears that partial reduction of the aldehydes is sufficient for reductive coupling to occur. This transition state is 10.5 kcal mol^{-1} higher than the bis-aldehyde reactant, and the diolate product is downhill by −13.3 kcal mol^{-1}; these Gibbs energies are consistent with the mild experimental conditions.
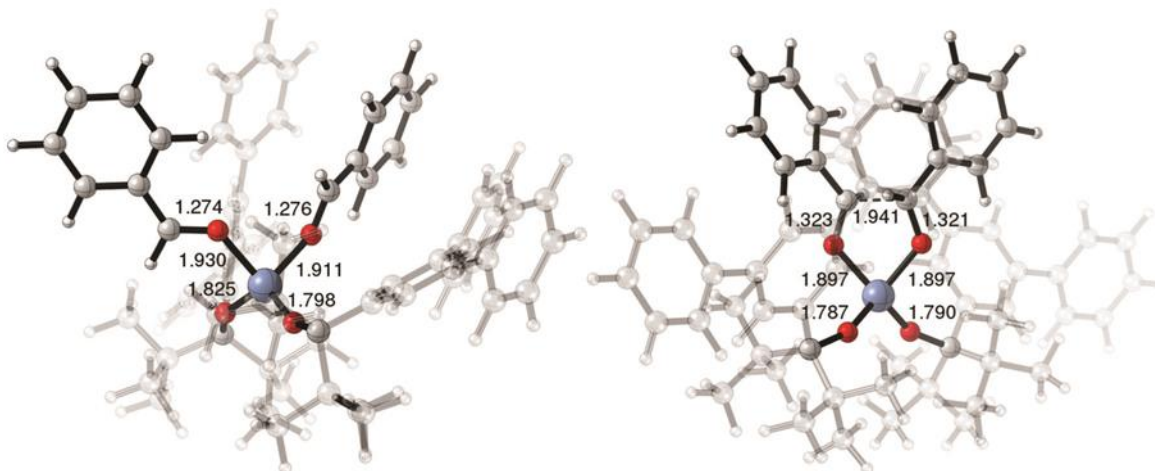
Figure 5.7. Optimized structure for the bis-aldehyde species (left) and the transition state for C–C coupling (right) with bond lengths in Å. The QM region of the molecule is highlighted and the MM region is transparent.

Next, we explored the unobserved coupling of two equivalents of benzophenone. Again, we started with the optimized diolate product. This product shows marked differences when compared to the aldehyde product: (i) a much longer C–C bond length of 1.651 vs. 1.547 Å and (ii) significant rotation of both alkoxide ligands to accommodate the much bulkier substrate. Before, the aldehyde hydrogens could point toward the aryl moiety of the ligand whereas the phenyl groups disallow such an orientation (see **Figure 5.8** for top-down comparison of these diolate products). The Mulliken spin density of 2.00 at the Cr center confirms a Cr(IV) species once again. Elongation of the C–C bond afforded the bis-ketone reactant and transition state. Once again the triplet was lowest in energy for this reactant, and we thus focus exclusively on this spin surface. The bis-ketone reactant shows Cr–O bond lengths of 1.81 Å to the alkoxides and 1.95 Å to the carbonyls, consistent with the aldehyde reactant. Mulliken spin densities of 2.90 at Cr and −0.31/−0.21 for the carbonyl Cs suggests again that this is a Cr(III) complex with partially reduced ketones. The thermodynamics of this reaction highlight why ketone coupling is not observed with the transition state and product being +29.9 and +12.7 kcal mol^{-1} in Gibbs energy, respectively,

relative to the bis-ketone reactant. The transition state has a longer C–C distance (2.097 Å) than the aldehyde but similar Cr–O bond lengths and Mulliken spin densities of 2.51 at Cr and −0.10/−0.08 at the carbonyl Cs.

Why then do aldehydes couple but not ketones? Both of the bis-ligated reactants show partial reduction of the carbonyls. This is perhaps not that surprising since benzophenone and benzaldehyde are known to have standard reduction potentials that only differ by 0.01 V.[97] Thus, the inability for ketones to couple is not an electronic issue. The much longer C–C bond in the product, along with the congestion of the catalyst center (**Figure 5.8**), suggest that sterics prevent ketone coupling at a single metal center. In addition to the thermodynamic penalty from the bis-benzophenone species to the diolate complex, binding of a second benzophenone equivalent to the mono-benzophenone complex is uphill by 9.5 kcal mol^{-1} in Gibbs energy while binding of the second benzaldehyde equivalent to the monobenzaldehyde species is thermoneutral ($\Delta G = -0.3$ kcal mol^{-1}). These analyses have focused exclusively on coupling of the carbonyl substrates at a single chromium center; we cannot rule out a bimetallic mechanism but the monometallic mechanism for benzaldehyde is consistent with the experimental observation of a mononuclear Cr(IV) diolate and the mild reaction conditions.
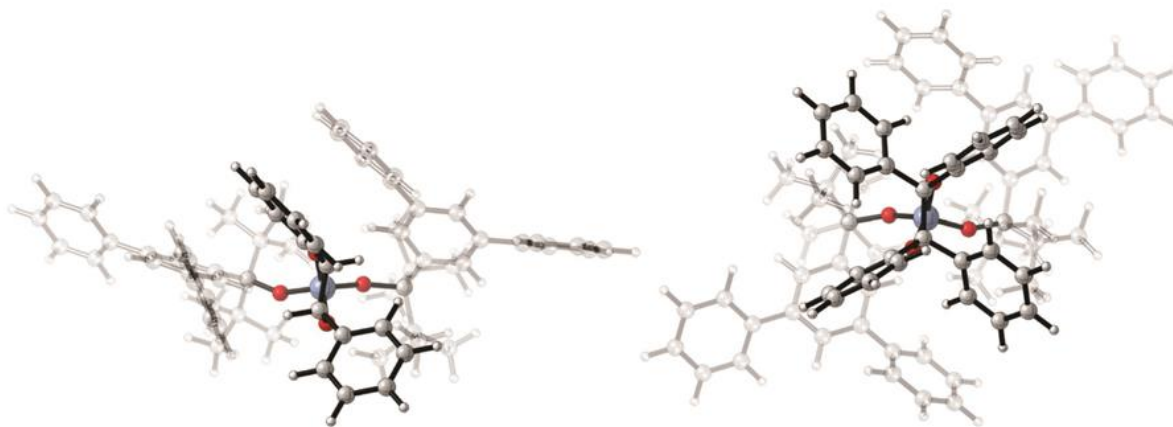
Figure 5.8. Top down view of the calculated diolate products for benzaldehyde (left) and benzophenone (right). The QM region of the molecule is highlighted and the MM region is transparent.

5.4. Reactivity of Cr(OR')$_2$(THF)$_2$ with CO$_2$

Following the investigation of reactivity of Cr(OR')$_2$(THF)$_2$ (**30**) with the organic carbonyls, we turned to study its reactivity with carbon dioxide. The reaction with CO$_2$ was carried out by bubbling dry CO$_2$ through the toluene solution of complex **30** for 5 minutes, during which the initial pale green color of the solution changed to pink. Subsequent work-up followed by recrystallization from ether and THF led to the isolation of pale pink Cr$_2$(O$_2$COR')$_4$(THF)$_2$ (**42**) in 50% yield (**Figure 5.9**), whose identity was verified by X-ray crystallography (**Figure 5.10**). In addition to the X-ray crystallography, compound **42** was also characterized by UV-vis, IR, and NMR spectroscopies, and combustion analysis.
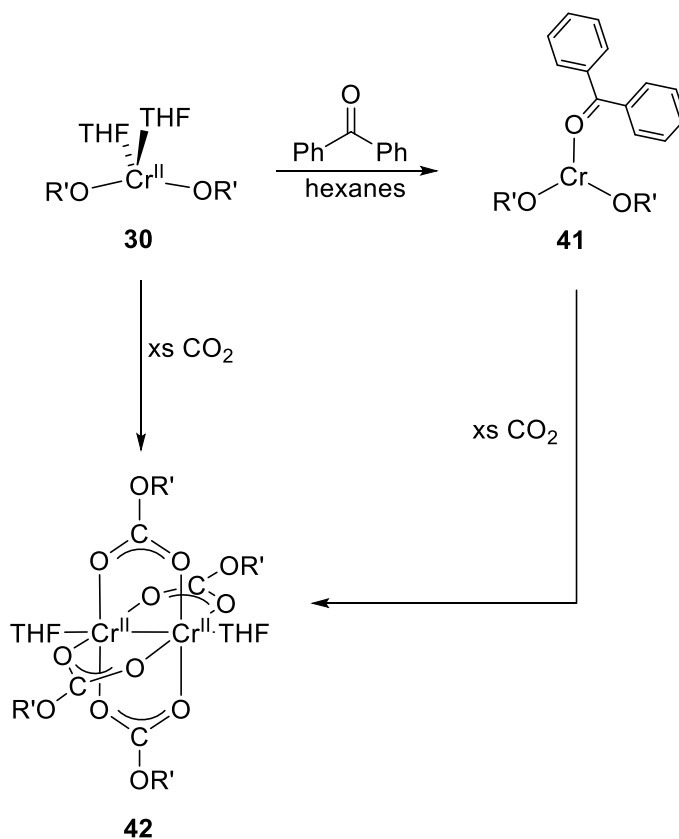
Figure 5.9. Synthesis of complex **42** from complexes **30** and **41**.

^{1}H NMR spectroscopy demonstrates that **42** is a diamagnetic complex, with all the resonances in the 1–8 ppm spectral window. Most of the signals, especially the signals associated with the ^{t}Bu groups of O_2COR' (1.23 ppm) and THF ligands (3.47) appear as broad resonances. We postulate that a dynamic process (such as the rotation around the O–C bonds in O_2COR') leads to the line broadening in the spectrum of **42** (**Appendix E**).
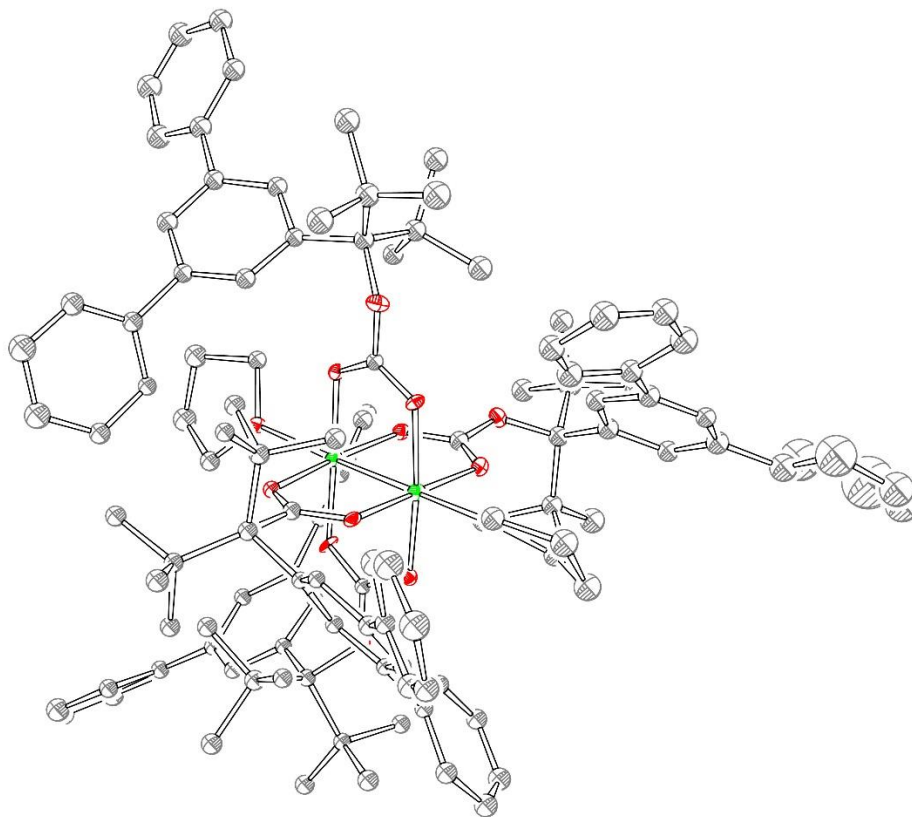
Figure 5.10. Molecular structure of complex **42**. One of the lateral phenyl groups was found to be disordered over two conformations, only one is shown for clarity.

The structure of **42** (**Figure 5.10**) demonstrates a dinuclear paddlewheel complex in which two Cr(II) centers are bridged by four bidentate alkyl carbonate ligands O_2COR'. $Cr_2(O_2COR')_4(THF)_2$ (**42**) results from CO_2 insertion into a chromium–alkoxide bond to form an alkyl carbonate, followed by complex rearrangement to a paddlewheel structure. Insertion of CO_2 into a M–OR bond is a well-known reaction that has been previously reported.[98] However, there is only one precedent for CO_2 insertion into a Cr(II)–OR bond.[99] Chisholm, Cotton, and coworkers reported that a dinuclear complex $(C_5H_5)_2Cr_2(O^tBu)_2$ reacts with CO_2 to afford red $Cr_2(O_2CO^tBu)_4(THF)_2$. The X-ray structure of $Cr_2(O_2CO^tBu)_4(THF)_2$ exhibited paddlewheel structure with a quadruple Cr–Cr bond of 2.4 Å, that is similar to the Cr1–Cr2 bond distance 2.3 Å in $Cr_2(O_2COR')_4(THF)_2$. We note that in the present case the mononuclear precursor

(Cr(OR′)$_2$(THF)$_2$) leads to the dinuclear product, whereas for Cr$_2$(O$_2$CO^{t}Bu)$_4$(THF)$_2$, the precursor

was also dinuclear, Cr$_2$(C$_5$H$_5$)$_2$(O^{t}Bu)$_2$, with the Cr–Cr bond of 2.65(2) Å. Furthermore, complex

42 Cr(OR′)$_2$(OCPh$_2$) also reacted with CO$_2$ under similar reaction conditions to produce pink

crystals of Cr$_2$(O$_2$COR′)$_4$(THF)$_2$, whose nature was confirmed by NMR spectroscopy (**Figure 5.9**).

Table 5.2. Experimental crystallographic parameters for **42**.

complex	**42**
formula	C$_{12}$H$_{140}$Cr$_2$O$_4$
fw	1910.42
crystal system	triclinic
space group	*P -1*
a (Å)	13.8974(15)
b (Å)	16.8586(18)
c (Å)	28.648(4)
α (deg)	78.612(6)
β (deg)	85.689(6)
γ (deg)	76.473(5)
V (Å^3)	6394.3(12)
D$_c$ (g cm^{-3})	0.988
Z	4
μ (mm^{-1})	0.221
T (K)	100(2)
R$_1$	11.73
GOF	1.149

5.5. Summary and conclusions

To summarize this chapter, the reactivity of $Cr(OR')_2(THF)_2$ with organic carbonyls (aldehydes and ketones) and carbon dioxide was interrogated. With aldehydes, $Cr(OR')_2(THF)_2$ functions as a two-electron reagent, enabling their reductive coupling to yield the corresponding Cr(IV) bis(alkoxide) 1,2-diolate products. Calculations suggest that this reaction proceeds via a bis-aldehyde adduct that is best described as a Cr(III) complex with partially reduced aldehydes. It appears that partial reduction of the aldehydes at a single metal center is sufficient to drive bond formation. With ketones, the fate of the reaction was less clear, but modeling suggests that the steric constraints of a ketone may be incompatible with our bulky alkoxide ligand. For benzophenone, coordination of a single equivalent of ketone to the metal was observed. For smaller ketones, only complex decomposition (free ligand) was observed. Finally, CO_2 undergoes insertion into a Cr–OR′ bond to furnish alkylcarbonate complexes, in which four alkylcarbonate ligands [OCO_2R'] bridge two quadruply-bonded Cr centers.

5.6 Experimental Section

General Methods and Procedures. a nitrogen-filled glovebox. HOR' and $Cr(OR)_2(THF)_2$ (**30**) were synthesized according to previously reported procedure in Chapter 3. Benzaldehyde, 4-trifluorbenzaldehyde, p-anisaldehyde, benzophenone, and acetophenone were purchased from Aldrich and used as received. 2,4,6-trimethylbenzaldehyde were purchased from AK Scientific. Instrument grade carbon dioxide was purchased from Airgas and passed through drying agent (drierite) prior to use. All solvents were purchased from Fisher Scientific and were of HPLC grade. The solvents were purified using an MBRAUN solvent purification system and stored over 3 Å molecular sieves. Compounds **37–40** were characterized by IR and UV-Vis spectroscopy, and elemental analysis; selected compounds **37**, **38**, **41**, and **42** were characterized by X-ray

crystallography and solution state magnetic susceptibility measurements. Diamagnetic compound **42** was also characterized by ^{1}H and ^{13}C NMR spectroscopy (see **Appendix E**). NMR spectra were recorded at the Lumigen Instrument Center (Wayne State University) on a Varian Mercury 400 MHz NMR Spectrometer in C_6D_6 at room temperature. Chemical shifts and coupling constants (*J*) were reported in parts per million (δ) and Hertz respectively. UV-visible spectra were obtained on Shimadzu UV-1800 spectrometer in THF (**37–40**) or toluene (**41**, **42**). IR spectra of powdered samples were recorded on a Shimadzu IR Affnity-1 FT-IR Spectrometer outfitted with a MIRacle10 attenuated total reflectance accessory with a monolithic diamond crystal stage and pressure clamp. Solution state effective magnetic moments were determined using the Evans method. Only selected peaks in the IR spectra are reported below. Analyses were performed under ambient conditions by Midwest Microlab LLC Laboratory, Inc.

Computational details. Substrate(s) and the catalyst up to the α carbon of the alkoxide (see **Figures 5.6**, **5.7**, and **5.8** for visualization of this partitioning generated by CYLView[100]) were treated at the B3LYP/6-31G(d) level of theory,[101] while the whole molecule was treated with the Universal Force Field.[102] This was done within the ONIOM formalism[103] using mechanical embedding as implemented in Gaussian 09.[104] All geometric structures were confirmed to be minima by analyzing the harmonic frequencies,[105] and confirmed to have stable wavefunctions within the QM region.[106]

X-ray crystallographic details. Structures of ligand HOR′ and compounds **37**, **39**, **32**, and **41** were confirmed by X-ray structure determination. The crystals were mounted on a Bruker APEXII/Kappa three circle goniometer platform diffractometer equipped with an APEX-2 detector. A graphic monochromator was employed for wavelength selection of the molybdenum Kα radiation (λ = 0.71073 Å). The data were solved and refined using the APEX2 software.

Structures were determined by direct methods in SHELXS and refined by standard difference Fourier techniques in the SHELXTL program suite (6.10 v., Sheldrick G. M., and Siemens Industrial Automation, 2000). Hydrogen atoms were placed in calculated positions using the standard riding model and refined isotropically; all other atoms were refined anisotropically. The structure of **37** co-crystallized with two ether molecules which were fully refined. Crystals of compound **42** diffracted poorly, resulting in the overall low quality of the structure. In addition, the structure of **42** contained several THF solvent molecules in the asymmetric unit, of which two were relatively ordered, three were modeled by finding two alternative conformations, and the other two were found to be severely disordered. One of the lateral phenyl groups in the main molecule (of **42**) was found to be disordered; the disorder was modeled by two conformations.

Synthesis of Cr(OR′)$_2$(O$_2$C$_2$H$_2$Ph$_2$) (37). To a solution of 5.0 mL of Cr(OR′)$_2$(THF)$_2$ (38.7 mg, 0.041 mmol) in toluene, the solution of benzaldehyde (9.0 mg, 0.085 mmol) in toluene was added slowly. The solution changed color immediately from light green to deep green. The reaction was stirred for four hours, upon which the solvents were removed in vacuo to yield green residue. Crystallization from ether at −35 °C for two days gave crystals of deep green Cr(OR′)$_2$(O$_2$C$_2$H$_2$Ph$_2$) (**37**) (42.2 mg, 67%). $\mu_{eff} = 2.4 \pm 0.3\mu_B$. Anal. Calcd: C, 81.1; H, 7.4. Found: C, 81.4; H, 7.6. IR (cm^{-1}): 2967 (w), 2874 (w), 1593 (m), 1497 (m), 1454 (w), 1281 (w), 1196 (w), 1161 (w), 1119 (w), 1076 (w), 1038 (w), 961 (s), 756 (s), 694 (s).

Synthesis of Cr(OR′)$_2$(O$_2$C$_2$H$_2$(4-CH$_3$OPh)$_2$) (38). To a solution of 5.0 mL of Cr(OR′)$_2$(THF)$_2$ (45.3 mg, 0.0482 mmol) in toluene, the solution of 4-anisaldehyde (13.2 mg, 0.097 mmol) in toluene was added slowly. The solution changed color immediately from light green to deep green. The reaction was stirred for four hours, upon which the solvents were removed in vacuo to yield green residue. Crystallization from ether at −35 °C overnight gave crystals of deep blue-green Cr

(OR′)$_2$(O$_2$C$_2$H$_2$(4-CH$_3$OPh)$_2$) (**38**) (37.9 mg, 74%). $\mu_{eff} = 2.3 \pm 0.3\mu_B$. Anal. Calcd: C, 78.8; H, 7.4. Found: C, 78.6; H, 7.6. IR (cm^{-1}): 2967 (w), 2882 (w), 1609 (w), 1593 (w), 1393 (w), 1254 (m), 1231 (w), 1173 (m) 961 (s). 833 (w), 760 (s), 737 (m).

Synthesis of Cr(OR′)$_2$(O$_2$C$_2$H$_2$(4-F$_3$CPh)$_2$) (39). To a solution of 5.0 mL of Cr(OR′)$_2$(THF)$_2$ (34.5 mg, 0.037 mmol) in hexanes, 4-(trifluoromethyl)benzaldehyde (14.2 mg, 0.082 mmol) in hexanes was added slowly. The solution changed color immediately from light green to deep green. The reaction was stirred for four hours, upon which the solvents were removed in vacuo to yield green residual. Crystallization from ether and hexanes at −35 °C over two days gave crystals of deep blue green of Cr(OR′)$_2$(O$_2$C$_2$H$_2$(4-F$_3$CPh)$_2$) (**39**) (16.1 mg, 35%). $\mu_{eff} = 2.5 \pm 0.3\mu_B$. Anal. Calcd: C, 73.5; H, 6.4. Found: C, 73.7; H, 6.6. IR (cm^{-1}): 2970 (w), 2820 (w), 1420 (w), 1393 (w), 1323 (s), 1165 (m), 1111 (m), 964 (s), 880 (m), 837 (m), 760 (s), 698 (m).

Synthesis of Cr(OR′)$_2$(O$_2$C$_2$H$_2$(2,4,6-Me$_3$Ph)$_2$) (40). To a solution of 5.0 mL of Cr(OR′)$_2$(THF)$_2$ (52.3 mg, 0.056 mmol) in hexanes, the solution of 2,4,6-timethylbenzaldehyde (16.4 mg, 0.11 mmol) in hexanes was added slowly. The solution changed color immediately from light green to deep green. The reaction was stirred for four hours, upon which the solvents were removed in vacuo to yield green residue. Crystallization from ether at −35 °C overnight gave crystals of deep blue-green Cr(OR′)$_2$(O$_2$C$_2$H$_2$(2,4,6-Me$_3$Ph)$_2$) (**40**) (40.1 mg, 66%). $\mu_{eff} = 2.6 \pm 0.3\mu_B$. Anal. Calcd: C, 81.4; H, 7.9. Found: C, 81.2; H, 8.1. IR (cm^{-1}): 3001 (w), 2878 (w), 1578 (w), 1485 (w), 1153 (w), 1119 (w), 1072 (w), 1034 (m), 957 (s), 926 (m), 876 (m), 756 (s), 694 (s).

Synthesis of Cr(OR′)$_2$(OCPh$_2$) (41). To a solution of 5.0 mL of Cr(OR′)$_2$(THF)$_2$ (34.8 mg, 0.037 mmol) in hexanes, benzophenone (8.5 mg, 0.047 mmol) in hexanes was added slowly. The solution changed color immediately from light green to deep green. The reaction was stirred for four hours, upon which the solvents were removed in vacuo to yield green residue. Crystallization from ether

at -35 °C for one day gave crystals of deep blue-green $Cr(OR)_2(OCPh_2)$ (**41**) (28.6 mg, 78%). Anal. Calcd: C, 82.3; H, 7.5. Found: C, 82.4; H, 7.4. $\mu_{eff} = 3.8 \pm 0.4\mu_B$. IR (cm^{-1}): 2951 (w), 1531 (w), 1497 (w), 1408 (w), 1381 (w), 1331 (m), 1292 (w), 1080 (m), 1061 (s), 1018 (m), 872 (s), 756 (s), 694 (s).

Synthesis of $Cr_2(O_2COR')_4(THF)_2$ (42). To a solution of 6.0 mL of $Cr(OR')_2(THF)_2$ (47.8 mg, 0.051 mmol) in THF, CO_2 was bubbled into the solution for 5 minutes while the solution was stirring. The solution slowly change color from pale green to blue to pink. The reaction was stirred for additional hour under CO_2 atmosphere, upon which all THF was removed in vacuo to yield pink residue. Crystallization from ether at -35 °C for two days gave crystals of pink $Cr_2(O_2COR')_4(THF)_2$ (24.2 mg, 50%). Anal. Calcd: C, 75.4; H, 7.4. Found: C, 75.6; H, 7.5. IR (cm^{-1}): 2974 (w), 1686 (w), 1612 (m), 1524 (w), 1358 (s), 1165 (w), 1123 (w), 1076 (m), 941 (w), 875 (m), 760 (m), 725 (s), 698 (m). ^1H (C_6D_6): δ 7.89, 7.67, 7.50, 7.28, 7.19, 3.47, 1.23 ppm. ^{13}C NMR (C_6D_6): 141.98, 141.85, 141.10, 139.93, 137.51, 130.15, 129.05, 128.88, 127.07, 126.96, 126.64, 99.20, 29.53 ppm.

Reaction of complex 41 with CO_2. To a solution of 5.0 mL of complex **41** (25.8 mg, 0.026 mmol) in toluene, CO_2 was bubbled into the solution for 5 minutes while the solution was stirring. The solution changed color from deep blue to gold-brown. The reaction was stirred for additional one hour under CO_2 atmosphere, upon which toluene was removed. The solid residue was dissolved in THF. Crystallization from THF at -35 °C for one day gave pink crystals of $Cr_2(O_2COR')_4(THF)_2$ (8.0 mg, 32%).

CHAPTER 6 EXPLORING OXO- AND SULFUR- ATOM TRANSFER REACTIONS USING THE "FIRST GENERATION" IRON BIS(ALKOXIDE) COMPLEX

Portions of the text in this chapter were reprinted or adapted with permission from: Bellow, A. B.; [¶]Yousif, M.; [¶]Fang, D.; Kratz, E. G.; Cisneros, G. A.; Groysman, S. *Inorg. Chem.* **2015**, *54*, 5624-5633. ([¶]indicates equally contributing authors)

6.1. Introduction

As described above, our iron catalysts were capable of nitrene group-transfer chemistry upon reactions with organoazides. Next, we decided to investigate the reactivity of previously synthesized "first-generation" iron bis(alkoxide) complex $Fe(OR)_2(THF)_2$ **14** (where [OR] = [OC^{t}Bu$_2$Ph]) complexes toward [O] and [S] atom transfer. The motivation for this research is two-fold. First, studying oxygen and sulfur atom transfer reactions may serve as a model for the reduction of heteroallenes CX_2 (X = O, S) via the "reductive splitting" mechanism ($CX_2 \rightarrow CX + [X]$) that necessitates an X-atom transfer. Also, the interest in examining well-defined metal-oxo complexes in the "oxygen-type" ligand environments is encouraged by the fact that these are proposed to serve as important intermediate in many transformations[107] including activation of alkanes on the surface of metal oxide materials.[108] This chapter focuses on the synthesis and characterization of iron oxo- and sulfido- complexes.

6.2. Synthesis and Characterization of Dinuclear Iron-oxo and Iron-sulfido Complexes

First-generation iron bis(alkoxide) complex **14** undergoes a reaction with an oxo-transfer reagent (PhIO) and a sulfur-atom transfer reagent (Ph_3SbS) to furnish $Fe_2(O)(OR)_4(THF)_2$ (**43**) and $Fe_2(S)(OR)_4(THF)_2$ (**44**), respectively (**Figure 6.1**). The structures of **43** and **44** are given in **Figure 6.2**. Both complexes feature distorted tetrahedral Fe(III) centers ligated by two terminal alkoxides, one THF ligand, and a bridging oxo (**43**) or sulfido (**44**) ligand. Thus, the Fe centers retain their bis(alkoxide) ligation upon chemical transformation. Complex **43** displays

crystallographic C_2 symmetry, with only half the molecule occupying the asymmetric unit. The Fe−O−Fe angle is 176.4(1)°, and the Fe−(μ_2-O) distance is 1.8031(3) Å. The Fe−S−Fe angle in the non-C_2-symmetric **44** is 164.8°, and the Fe−S bond distances are 2.1821(5) and 2.1901(5) Å. While Fe$_2$(μ_2-O) compounds are common in the literature, compound **44** is one of the few known di-Fe(III) complexes in which the Fe centers are bridged by a single sulfide.[109]
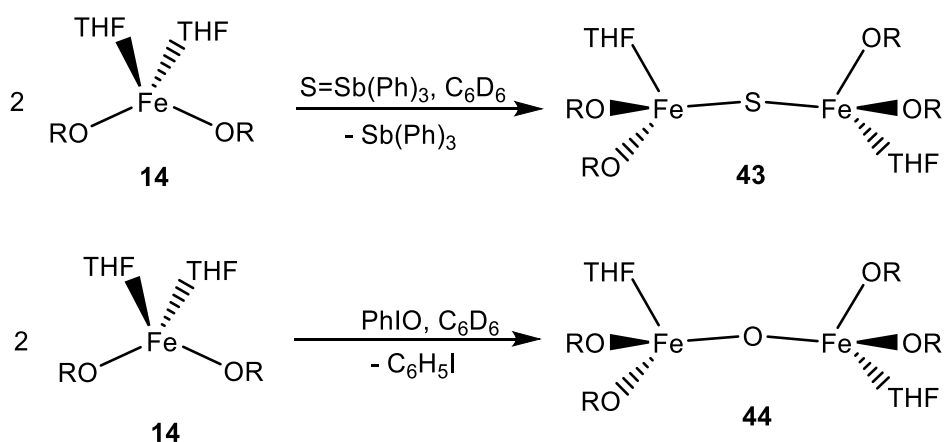
Figure 6.1. reactivity of **14** to produce **43** and **44**.
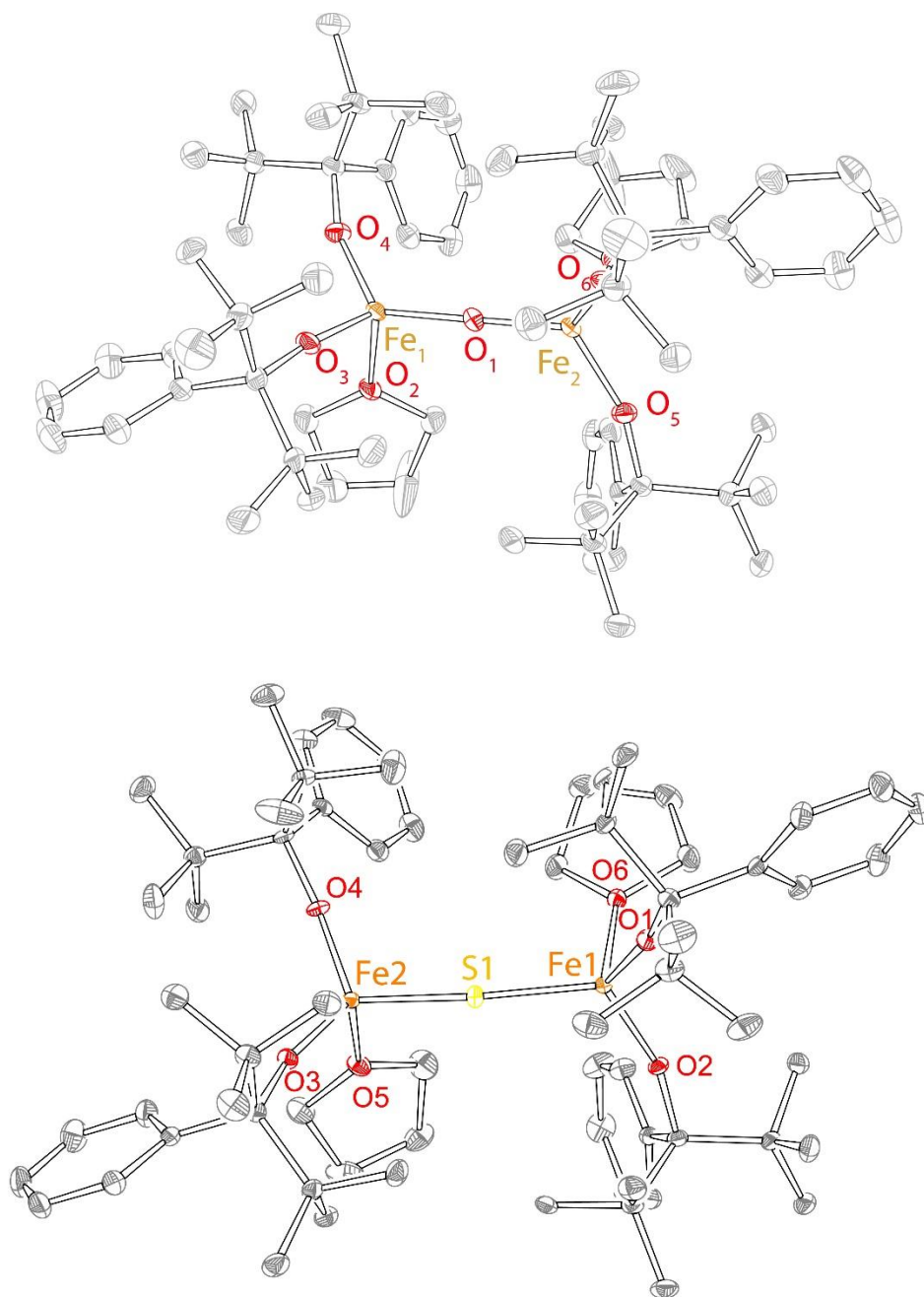
Figure 6.2. X-ray structures of complexes **43** (top) and **44** (bottom).

The IR spectra of compounds **43** and **44** in the $600-1700$ cm^{-1} region are presented in

Figure 6.3 below. The overlay of the spectra demonstrates a significant structural similarity, with

the exception of the strong peak at 795 cm^{-1} that is observed only for compound **43** and is therefore

assigned to the Fe−oxo stretch. The Fe−sulfido stretch is expected to occur in the far-IR region

(<500 cm^{-1}) and was not observed. The UV-vis spectrum of pale yellow-orange **43** exhibits a weak absorption (shoulder) around 500 nm. Unlike Fe$_2$(S)(OR)$_4$(THF)$_2$; the deep red sulfur-containing compound **44** demonstrates relatively intense absorptions around 497 (21350 M^{-1} cm^{-1}) and 339 (7570 M^{-1} cm^{-1}) nm (see **Appendix F**). It is worth noting that the investigation of the reactivity of the **43** and **44** dimers toward phosphines or olefins indicated stable and unreactive complexes.
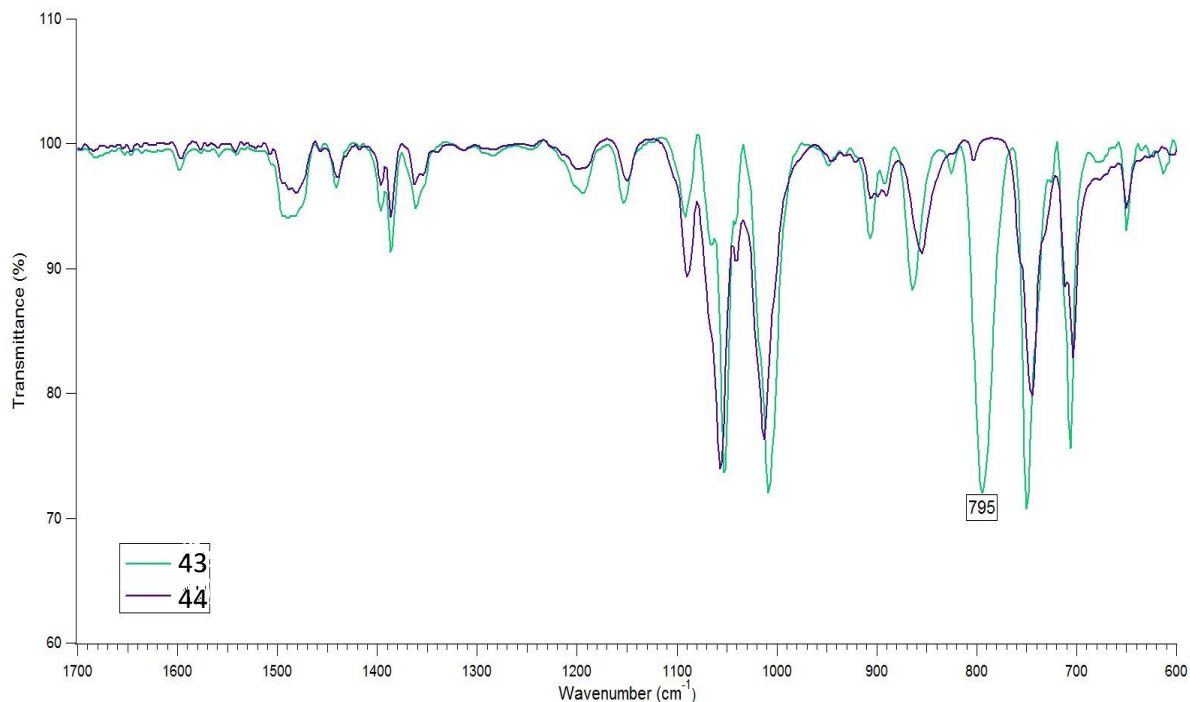
Figure 6.3. IR spectra of compounds **43** and **44** in the 600−1700 cm^{-1} range.

Table 6.1. Experimental crystallographic parameters for **43** and **44**.

complex	**43**	**44**
formula	$C_{68}H_{108}Fe_2O_7$	$C_{68}H_{108}Fe_2O_6S$
fw	1149.30	1165.36
crystal system	monoclinic	monoclinic
space group	*C2*	*P2$_1$/n*
a (Å)	22.7688(12)	15.8313(5)
b (Å)	15.7928(8)	22.0960(7)
c (Å)	11.0352(6)	18.6495(5)
α (deg)	90.00	90.00
β (deg)	117.190(2)	102.2450(10)
γ (deg)	90.00	90.00
V (Å^3)	3529.6(3)	6375.3(3)
D$_c$ (g cm^{-3})	1.136	1.214
Z	4	4
μ (mm^{-1})	1.136	0.537
T (K)	100(2)	100(2)
R$_1$	4.39	3.65
GOF	1.092	0.941

6.3 Summary and Conclusion

In this chapter, we have investigated the formation of iron oxo- and sulfido complexes in the bis(alkoxide) environment. The bis(alkoxide) ligation led to the rapid formation of stable μ_2-oxo and sulfido iron(III) dimers, which were found to be unreactive in atom-transfer reactions.

6.4 Experimental Section

General Methods and Procedures. All manipulations were executed in a nitrogen-filled glovebox. Complex $Fe(OR)_2(THF)_2$ (**14**) was synthesized according to previously reported procedures.[40,43] Triphenylstibine sulfide were purchased from Aldrich and iodosobenzene was purchased from TCI. All materials were used as received. All solvents were purchased from Fisher Scientific and were of HPLC grade. The solvents were purified using an MBRAUN solvent purification system and stored over 3 Å molecular sieves. Compounds **43** and **44** were characterized by IR spectroscopy, UV−vis spectroscopy, solution-state magnetic susceptibility, X-ray crystallography, and elemental analysis. NMR spectra were recorded at the Lumigen Instrument Center (Wayne State Univ.) on a Varian Mercury 400 MHz NMR spectrometer in C_6D_6 at RT. Solution-state effective magnetic moments were determined using the Evans method.[20] IR spectra were recorded on a Shimadzu IR-Affnity-1 FT-IR spectrometer as paratone oil mull suspensions. UV−vis spectra were obtained in a Shimadzu UV-1800 spectrometer. Elemental analyses were performed by Midwest Microlab LLC.

$Fe_2(O)(OR)_4(THF)_2$ (43). To a stirred solution of $Fe(OR)_2(THF)_2$ (60.2 mg, 0.0943 mmol), 5 mL solution of PhIO (13.0 mg, 0.0591 mmol) in toluene was added at once. The reaction changed color slowly from light brown to orange brown. The reaction was stirred for 4 h, after which the solvent was removed. The residue was dissolved in hexanes and filtered. Crystallization from concentrated hexanes produced orange crystals at -35 °C overnight (13.0 mg, 24% yield). IR (cm⁻

[1]): 2970 (m), 2878 (m), 1483 (s), 1387 (s), 1053 (m), 1009 (m), 864 (s), 795 (m), 750 (m), 706 (m). λmax (ε): 734 (176), 578 (64), 472 (40), 386 (98) M^{-1} cm^{-1}. No discernible features in the UV−vis spectrum, except for the shoulder around 480 nm. μ_{eff} = 2.8 ±0.1 μ_B. Anal. Calcd for $C_{68}H_{108}Fe_2O_7$: C, 71.1; H, 9.5. Found: C, 71.2; H, 9.3%.

$Fe_2(S)(OR)_4(THF)_2$ (44). To a stirred solution of $Fe(OR)_2(THF)_2$ (86.8 mg, 0.136 mmol) in toluene, 5 mL solution of triphenylstibine sulfide (26.7 mg, 0.0693 mmol) in toluene was added at once. The solution color immediately changed from light brown to deep red. The reaction was stirred for 4 h, after which the solvent was removed. The residue was dissolved in hexanes and filtered. Crystallization from hexanes at -35 °C produced deep red X-ray quality crystals (47.3 mg, 60% yield). IR (cm−1): 2990 (s), 2879 (s), 1481(s), 1150 (m), 1013 (m), 891 (s), 745 (m), 704 (m). λmax (ε): 339 (7570), 497 (21350) M^{-1} cm^{-1}. μ_{eff} = 2.8 ± 0.2 μ_B. Anal. Calcd for $C_{68}H_{108}Fe_2O_6S$: C, 70.1; H, 9.3. Found: C, 70.3; H, 9.5%.

CHAPTER 7 CONCLUSIONS AND OUTLOOK

In this work, we demonstrated the N-C, N-N, and C-C bond formation by our first and second generation first-row transition metal bis(alkoxide) complexes. While our "first-generation" Fe(II) bis(alkoxide) displayed selective reactivity toward azo compounds formation, this system is associated with several problems that limited the catalytic reactivity of organoazides. For this reason, we sought two approaches to modify the reactivity of this complex. First, replacing the iron center with chromium allowed for the isolation of reactive dinuclear Cr(II) complex. The chromium complex served as a pre-catalyst for the selective catalytic formation of asymmetric carbodiimides at the mononuclear chromium(IV) center. DFT studies showed that the coordination of isocyanide to the well-defined Cr(IV) imido complexes was responsible for the initiation of the C-N bond formation.

In the second approach, we synthesized "second-generation" HOR' ligand by lithium-halogen exchange reaction. The ligand was modified by the addition of Ph groups in the *meta* positions of the phenyl ring in LiOR (R = C^tBu_2Ph). The synthesis of the bulkier alkoxide ligand, HOR', enabled the isolation and characterization of the "second-generation" bis(alkoxide) complexes for the first row-transition metals.

Consequently, we investigated the "second-generation" iron bis(alkoxide) precursor reactivity with organoazides. Due to the stabilization of the bis(alkoxide) ligation at the expense of the tris(alkoxide) by-product, our second-generation iron exhibited broader spectrum of reactivity in the catalytic coupling of organic azides. It also enabled isolation and characterization of tetrazene complexes. The iron tetrazene compounds were identified to be the first structurally characterized Fe(III)-tetrazene complexes. Following this study, our primary goal is understanding the role that tetrazenes play in the azoarenes formation and mechanism in which catalytic reactions

take place. Both spectroscopy and DFT calculations will be performed to better examine this system.

Furthermore, using the "second-generation" alkoxide ligand, we were able to isolate a rare and well-defined example of monomeric Cr(II) bis(alkoxide) complex, $Cr(OR')_2(THF)_2$, having a distorted see-saw geometry identified by X-ray crystallography. This compound activates the reductive coupling of aldehydes to form Cr(IV) bis(alkoxide) diolate complexes. In contrast, reactivity with benzophenone showed the formation of chromium adduct without further activation. Interestingly, CO_2 undergoes insertion into the Cr-OR bond to yield bridging carbonate complex. Future work will focus on investigating the possibility of using chromium (II) bis(alkoxide) complex in the activation and coupling of CO_2 and organic azides to form isocyanates (RNCO).

The research described in this dissertation had mainly focused on the utilization of aromatic azides for N-N (azoarene) and N-C (carbodiimiide) bond formation. This chemistry can be further extended to the exploration of the different types of azides and different transformation. One potential research direction involves targeting simple linear aliphatic organic azides (having allylic and benzylic C-H bonds) to intramolecular cyclization to form N-heterocylic compounds. Thus, this direction can expand our research toward exploring C-H bond activation using iron and chromium bis(alkoxide) complexes.

Future direction of the alkoxide project could be also aimed toward the synthesis of true two-coordinate bis(alkoxide) transition metal complexes of the form $M(OR)_2$. We notice that increasing the steric bulk of the "first-generation" alkoxide ligand LiOR (R = C^tBu_2Ph), did not permit the formation of the two-coordinate $M(OR)_2$ complexes. Therefore, our future research should focus on the synthesis of other bulky ligands [OR]. One potential and relatively easily

accessible alteration involves replacement of t-butyl groups with two adamantyl substituents to synthesize a new alkoxide ligand with OR = OCAd$_2$Ph. We expect the steric profile of this new ligand to be significantly different from the first- and second-generation ligand, and will be sufficient to eliminate THF binding at the metal center and produce more reactive mononuclear two-coordinate M(OR)$_2$ complexes. This, in turn, may pave the way for exploring activation of new substrates for group-transfer reactions including small molecules CO_2 and N_2.

APPENDIX A

PERSONAL/LICENSE AGREEMENTS FOR COPYRIGHTED MATERIAL

Portions of **Chapters 1, 2** and **3** have been reproduced from **Yousif, M.;** Tjapkes, D. J.; Lord, R.

L.; Groysman, S. *Organometallics* **2015**, *34*, 5119-5128.

Title:	Catalytic Formation of Asymmetric Carbodiimides at Mononuclear Chromium(II/IV) Bis(alkoxide) Complexes
Author:	Maryam Yousif, Daniel J. Tjapkes, Richard L. Lord, et al
Publication:	Organometallics
Publisher:	American Chemical Society
Date:	Oct 1, 2015

Copyright © 2015, American Chemical Society

PERMISSION/LICENSE IS GRANTED FOR YOUR ORDER AT NO CHARGE

Portions of **Chapters 5** have been reproduced from **Yousif, M.**; Cabelof, A. C.; Lord, R. L.;

Martin, P. D.; Groysman, S. *Dalton Trans.* **2016**, *45*, 9794-9804.

Author reusing their own work published by the Royal Society of Chemistry

You do not need to request permission to reuse your own figures, diagrams, etc, that were originally published in a Royal Society of Chemistry publication. However, permission should be requested for use of the whole article or chapter <u>except if reusing it in a thesis.</u> If you are including an article or book chapter published by us in your thesis please ensure that your co-authors are aware of this.

Reuse of material that was published originally by the Royal Society of Chemistry must be accompanied by the appropriate acknowledgement of the publication. The form of the acknowledgement is dependent on the journal in which it was published originally, as detailed in 'Acknowledgements'.

Portions of **Chapters 6** have been reproduced from Bellow, A. B.;[¶] **Yousif, M.**;[¶] Fang, D.;

Kratz, E. G.; Cisneros, G. A.; Groysman, S. *Inorg. Chem.* **2015**, *54*, 5624-5633.

Title: Synthesis and Reactions of 3d Metal Complexes with the Bulky Alkoxide Ligand [OC^{t}Bu$_2$Ph]

Author: James A. Bellow, Maryam Yousif, Dong Fang, et al

Publication: Inorganic Chemistry

Publisher: American Chemical Society

Date: Jun 1, 2015

Copyright © 2015, American Chemical Society

PERMISSION/LICENSE IS GRANTED FOR YOUR ORDER AT NO CHARGE

This type of permission/license, instead of the standard Terms & Conditions, is sent to you because no fee is being charged for your order. Please note the following:

- Permission is granted for your request in both print and electronic formats, and translations.
- If figures and/or tables were requested, they may be adapted or used in part.
- Please print this page for your records and send a copy of it to your publisher/graduate school.
- Appropriate credit for the requested material should be given as follows: "Reprinted (adapted) with permission from (COMPLETE REFERENCE CITATION). Copyright (YEAR) American Chemical Society." Insert appropriate information in place of the capitalized words.
- One-time permission is granted only for the use specified in your request. No additional uses are granted (such as derivative works or other editions). For any other uses, please submit a new request.

APPENDIX B: SUPPLEMENTARY MATERIAL FOR CHAPTER 2

1. Evans method formula and procedure

The Evans method was accomplished on all compounds using a Wilmad coaxial insert (purchased from Aldrich) and a standard NMR tube. The sample was carefully weighed, and a precise amount of the suitable NMR solvent was added to give solutions with known concentrations for the calculations. The solutions were added to the insert, and the insert was placed inside the outer NMR tube, which contained blank NMR solvent. NMR spectra were taken as indicated previously. The molar susceptibility χ_m of the complexes was first calculated using Equation 1: [49]

$$\chi_m = [\ 3\Delta\nu\ 4\pi m\nu_0 + \chi_0]\ M \qquad (1)$$

where $\Delta\nu$ is the peak separation in Hertz, m is the concentration of the solution in grams per milliliter, ν_0 is the spectrometer operating frequency in Hertz, χ_0 is the molar susceptibility of the solvent (in cm^3/g), and M is the molar mass of the compound (g/mol). The solution state effective magnetic moment (μ_{eff}) was calculated using Equation 2:

$$\mu_{eff} = \sqrt{(2.383 \times 10^3)(\chi_m)} \qquad (2)$$

Three measurements were taken; the average of the three and the corresponding standard deviation were calculated. However, we estimated the error to be at least 10% due to the uncertainty in weighing; the larger of the two values was used for the final estimate of the error.

Table B.1. Spin-only magnetic moments calculated for **20-22** and **26** using Evans method.

Complex	μ_{obs} (1) (μ_B)	μ_{obs} (2) (μ_B)	μ_{obs} (3) (μ_B)	μ_{obs} (average) (μ_B)
20	2.2	2.4	2.7	2.4±0.3
21	2.4	2.4	2.8	2.5±0.3
22	3.2	3.1	3.6	3.3±0.4
26	2.4	2.4	2.2	2.3±0.2

2. Spectroscopic and elemental analysis characterization of carbodiimide products

MesN=C=N(2,6-Me$_2$C$_6$H$_3$).

^{1}H NMR (C$_6$D$_6$): δ 6.85 (m, 3H), 6.65 (s, 2H), 2. 29 (d, 12H), 2.08 (s, 3H). ^{13}C NMR (C$_6$D$_6$): δ 136.57, 134.02, 133.47, 132.82, 132.62, 129.67, 129.32, 128.57, 124.66, 20.78, 19.02, 18.96 ppm. Anal. Calcd.: C,81.8; H, 7.6, N, 10.6. Found: C, 82.1; H, 7.5; N, 10.6

MesN=C=N(6-H$_3$OC$_6$H$_4$).

^{1}H NMR (C$_6$D$_6$): δ 7.06 (m, 2H), 6.63 (m, 4H), 3.23 (s, 3H), 2.28 (s, 6H), 2.06 (s, 3H). ^{13}C NMR (C$_6$D$_6$): δ 157.35, 134.55, 133.25, 133.13, 133.07, 132.79, 129.33, 124.93, 115.09, 55.00, 20.78, 19.00 ppm. Anal. Calcd.: C, 76.7; H, 6.8, N, 10.5. Found: C, 76.3; H, 7.1; N, 10.1

(2,6-Et$_2$C$_6$H$_3$)N=C=N(2,6-Me$_2$C$_6$H$_3$).

^{1}H NMR (C$_6$D$_6$): δ 6.91 (m, 3H), 6.85 (m, 3H), 2.73 (m, 4H), 2.30 (s, 6H), 1.16 (t, 6H). ^{13}C NMR (C$_6$D$_6$): 142.58, 137.60, 133.04, 128.57, 127.07, 126.54, 125.41, 125.22, 124.76, 29.03, 23.17, 19.05 ppm. Anal. Calcd.: C, 82.0; H, 8.0, N, 10.1. Found: C, 81.7; H, 8.1; N, 10.0

(2-^{i}PrC$_6$H$_3$)N=C=N(2,6-Me$_2$C$_6$H$_3$).

^{1}H NMR (C$_6$D$_6$): δ 7.11 (m, 2H), 6.93 (m, 2H), 6.81 (s, 3H), 3.55 (m, 1H), 2.24 (s, 6H), 1.18 (d, 6H). ^{13}C NMR (C$_6$D$_6$): 142.60, 137.62, 133.06, 128.56, 127.09, 126.56, 125.43, 125.24, 124.79, 29.05, 23.19, 19.08 ppm. Anal. Calcd.: C, 81.8; H, 7.6, N, 10.6. Found: C, 81.9; H, 7.7; N, 10.6

NMes=C=N(2-Cl,6-MeC$_6$H$_3$).

^{1}H NMR (C$_6$D$_6$): δ 7.00 (d, 1H), 6.59 (d, 2H), 6.63 (s, 2H), 2.31 (s, 6H), 2.18 (s, 3H), 2.06 (s, 3H). Anal. Calcd.: C, 71.7; H, 6.0, N, 9.8. Found: C, 71.9; H, 6.1; N, 9.9

3. NMR Spectra
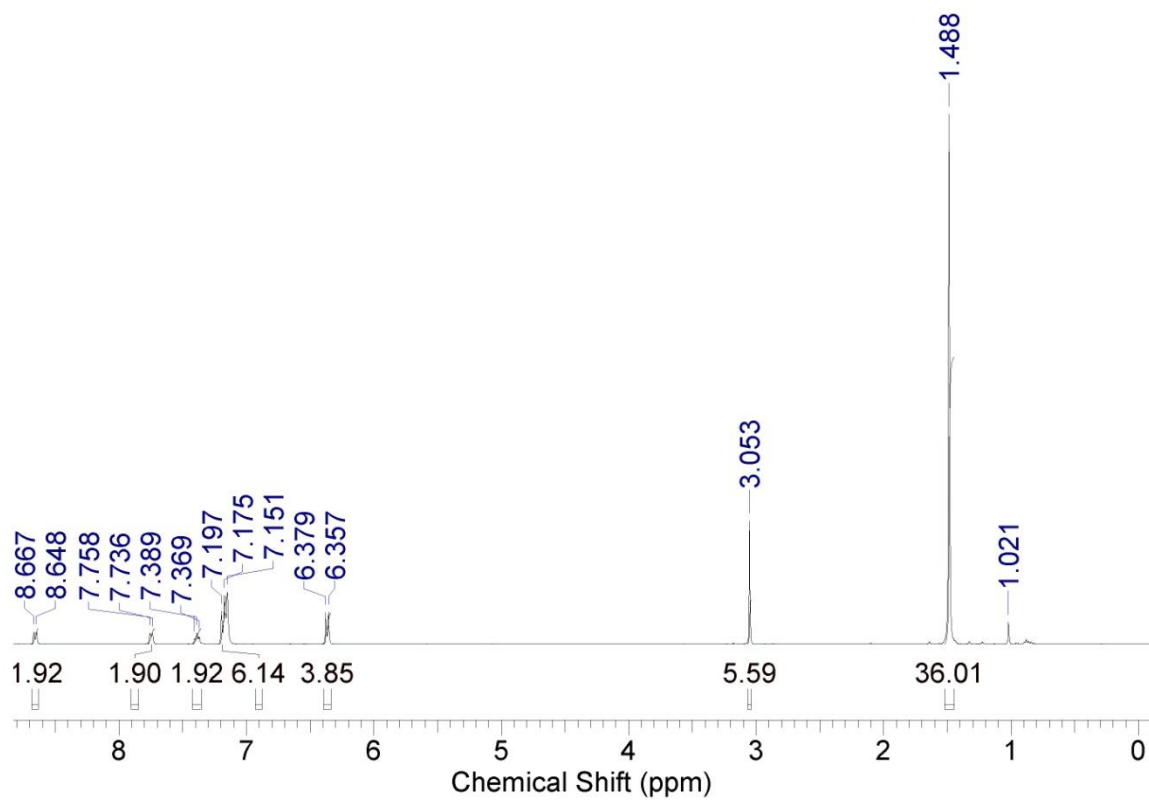
Figure B.1. ^{1}H NMR spectrum of complex **24**.
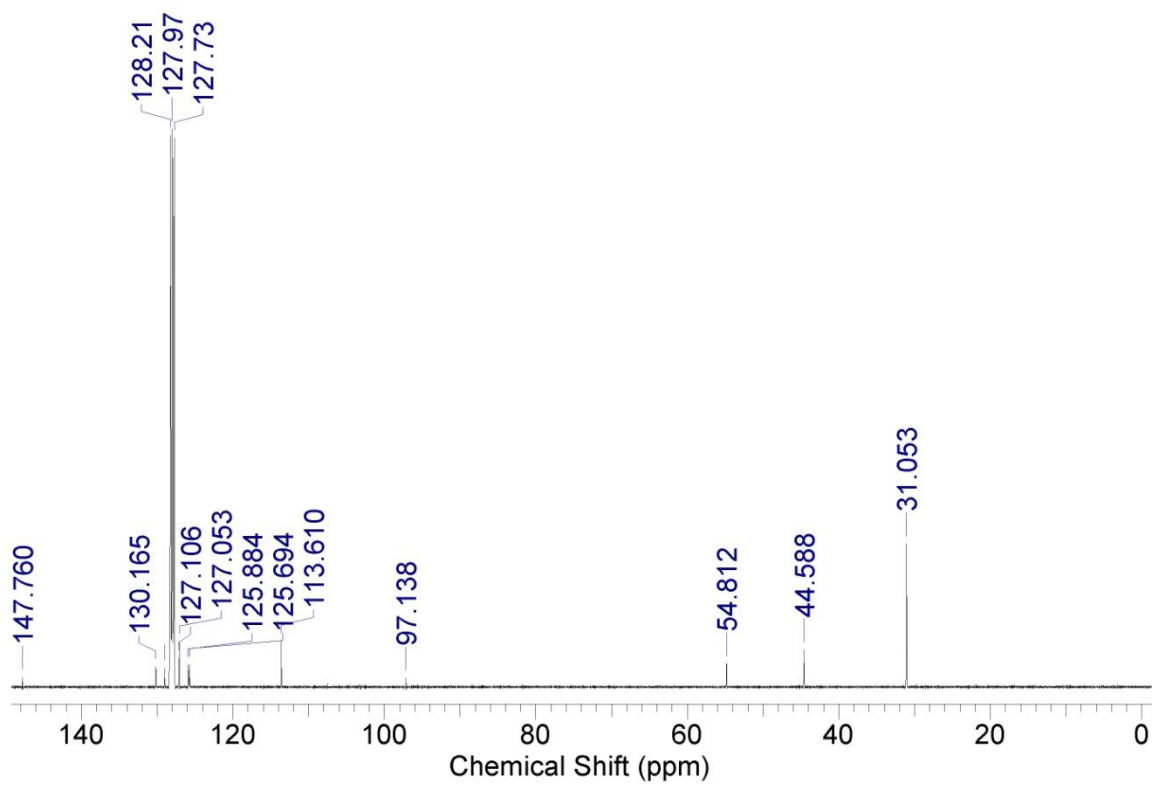
Figure B.2. ^{13}C NMR spectrum of complex **24**.
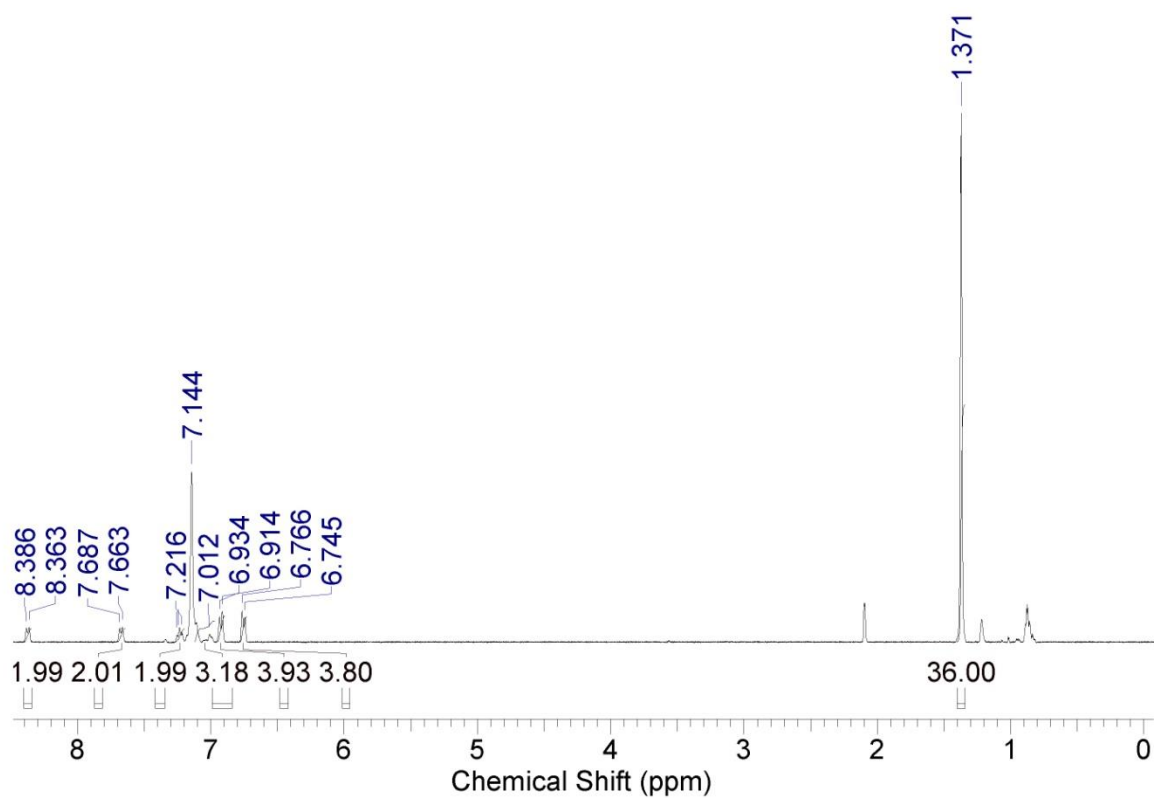
Figure B.3. ^{1}H NMR spectrum of complex **25**.
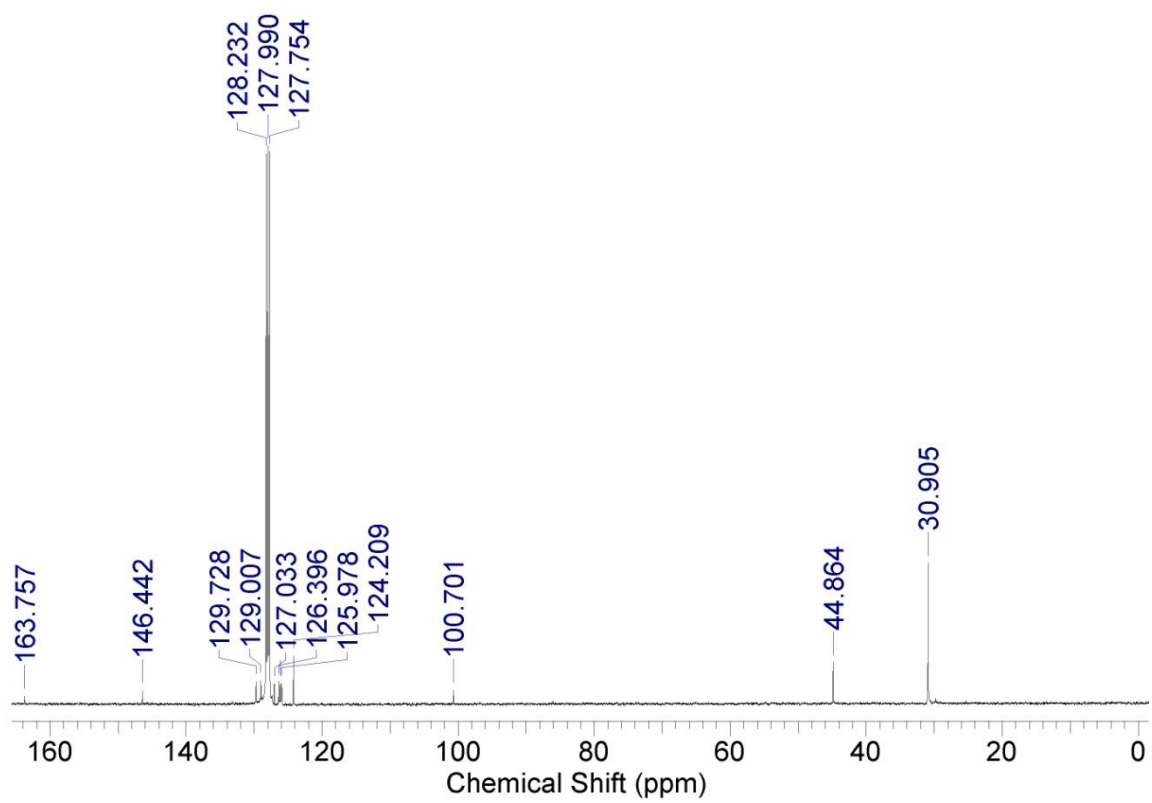
Figure B.4. ^{13}C NMR spectrum of complex **25**.
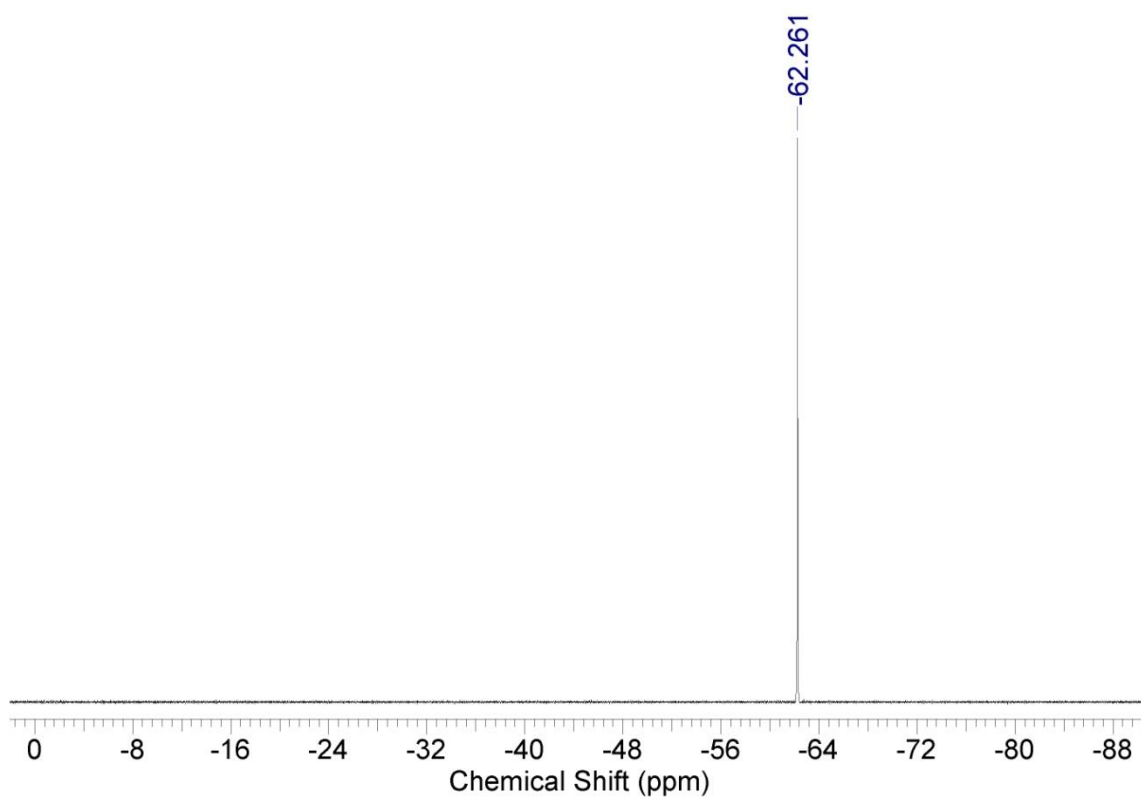
Figure B.5. ¹⁹F NMR spectrum of complex **25**.
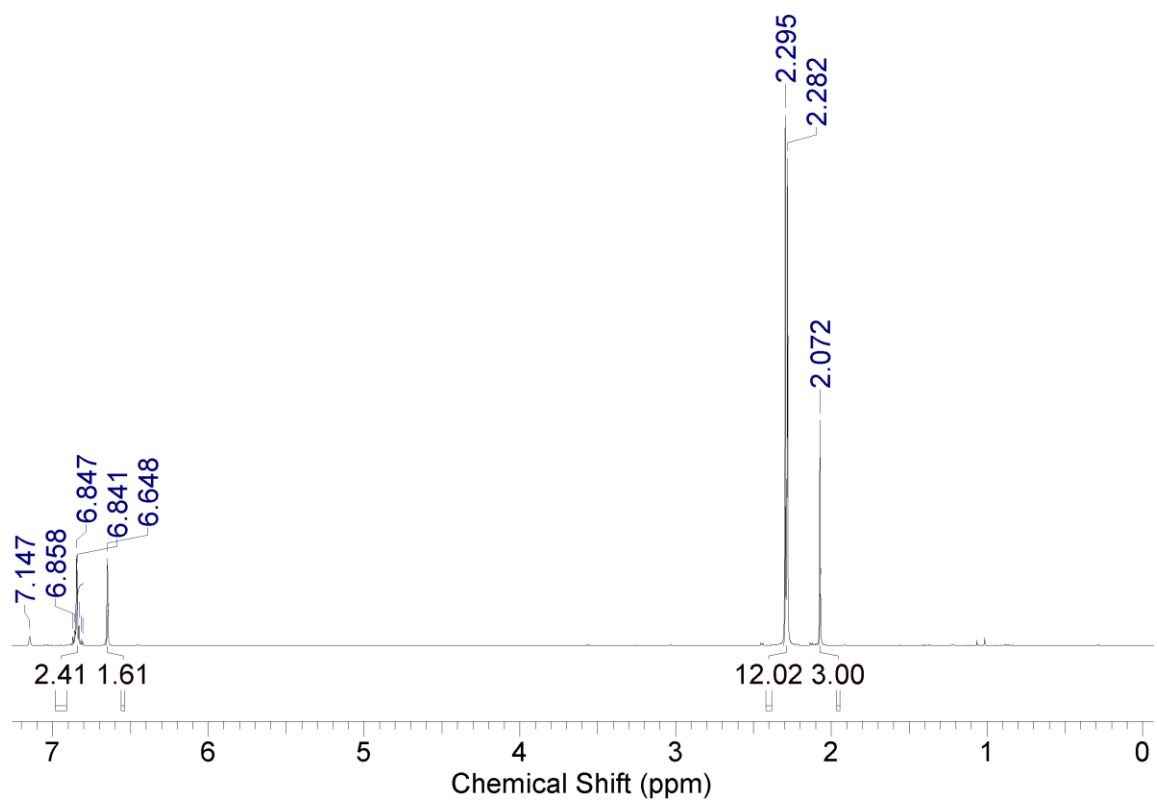
Figure B.6. ^{1}H NMR spectrum of MesNCN(2,6-Me$_2$C$_6$H$_3$).
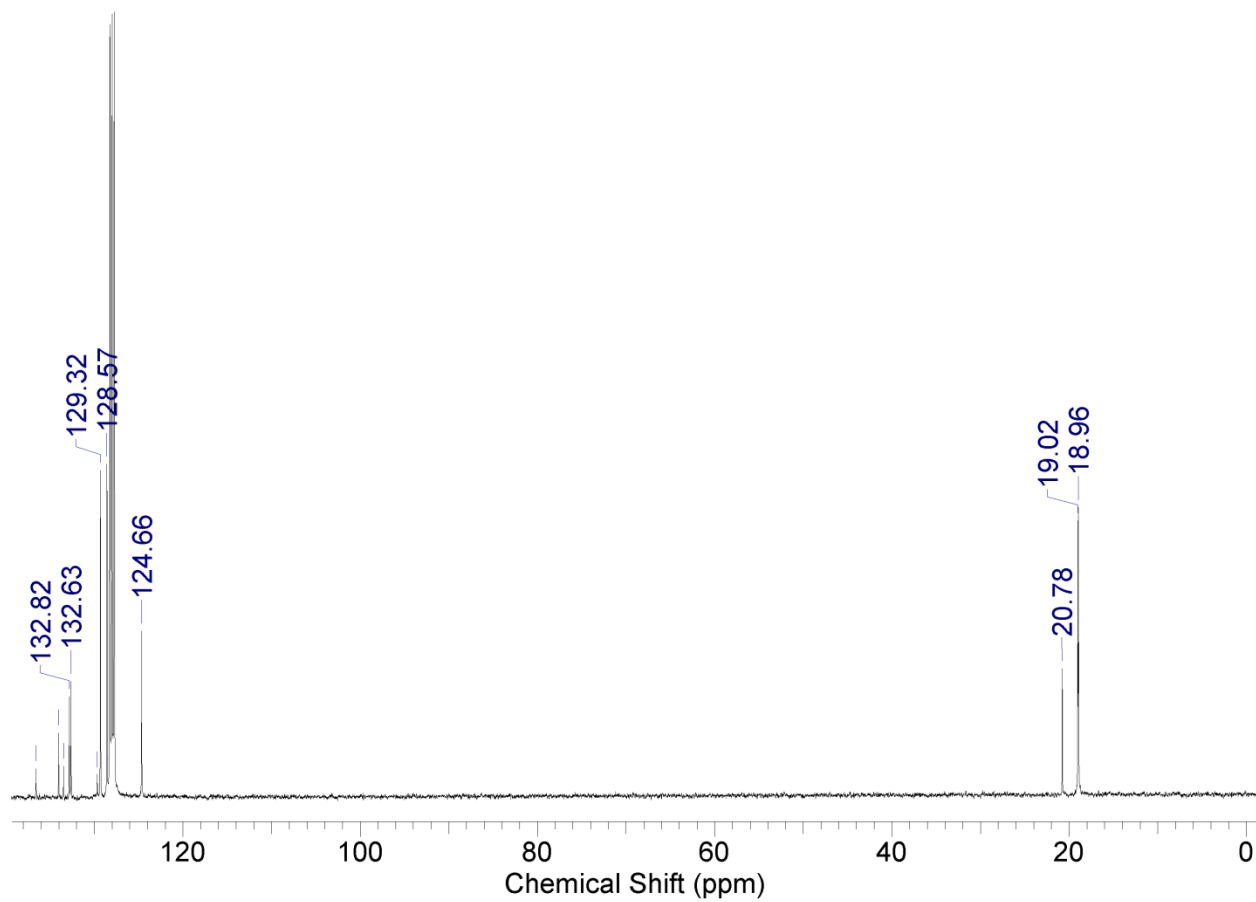
Figure B.7. ^{13}C NMR spectrum of MesNCN(2,6-Me$_2$C$_6$H$_3$).
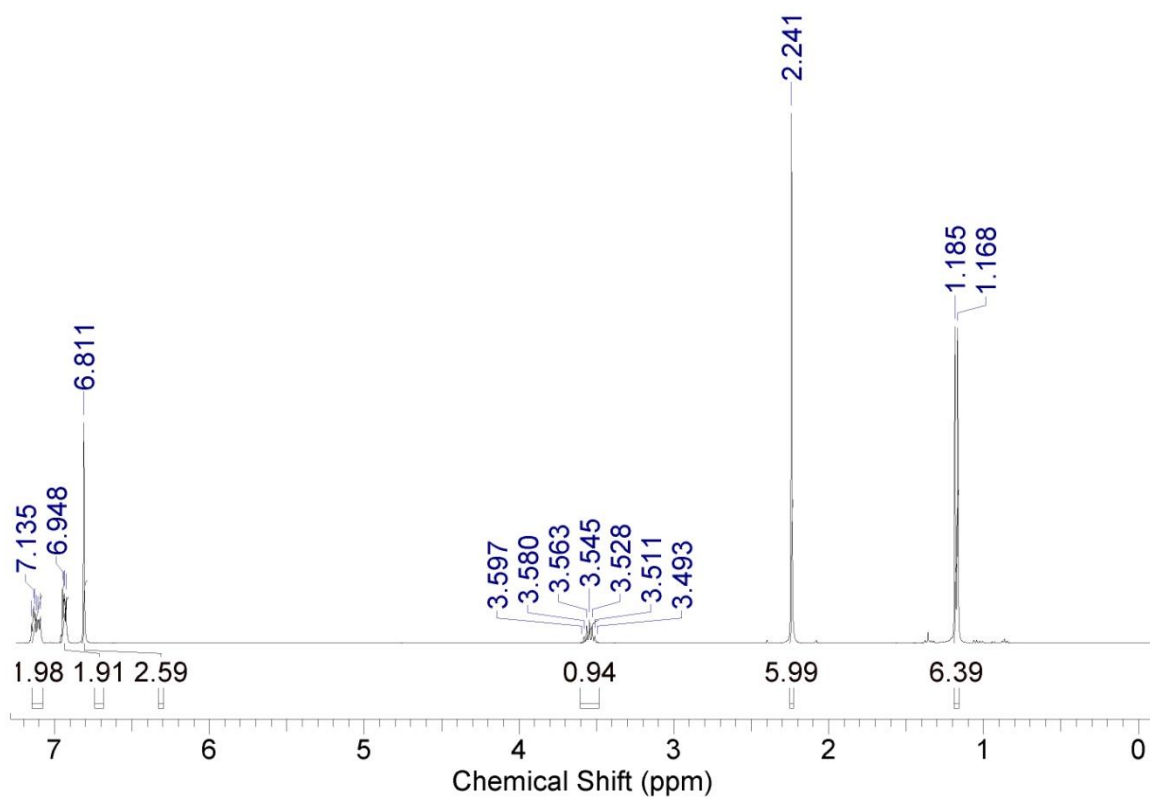
Figure B.8. ^{1}H NMR of spectrum 2-[i]PrPhNCN(2,6-Me$_2$C$_6$H$_3$).
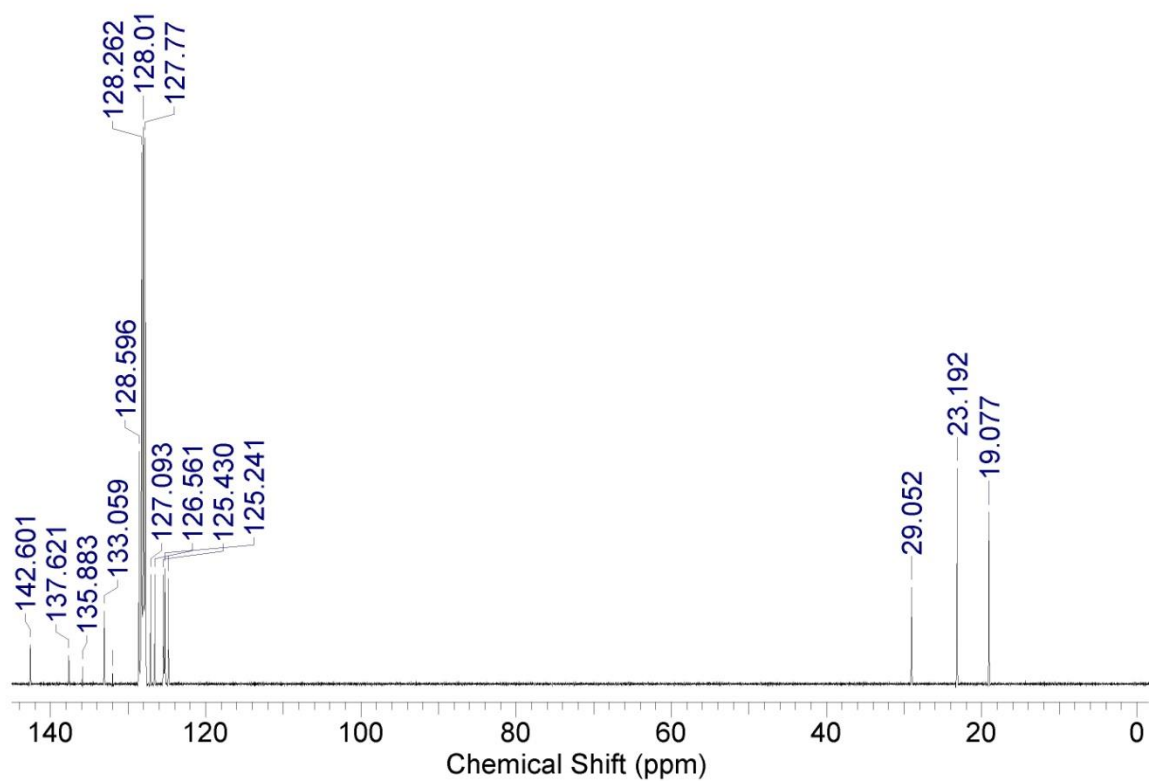
Figure B.9. ^{13}C NMR of spectrum 2-^{i}PrPhNCN(2,6-Me$_2$C$_6$H$_3$).
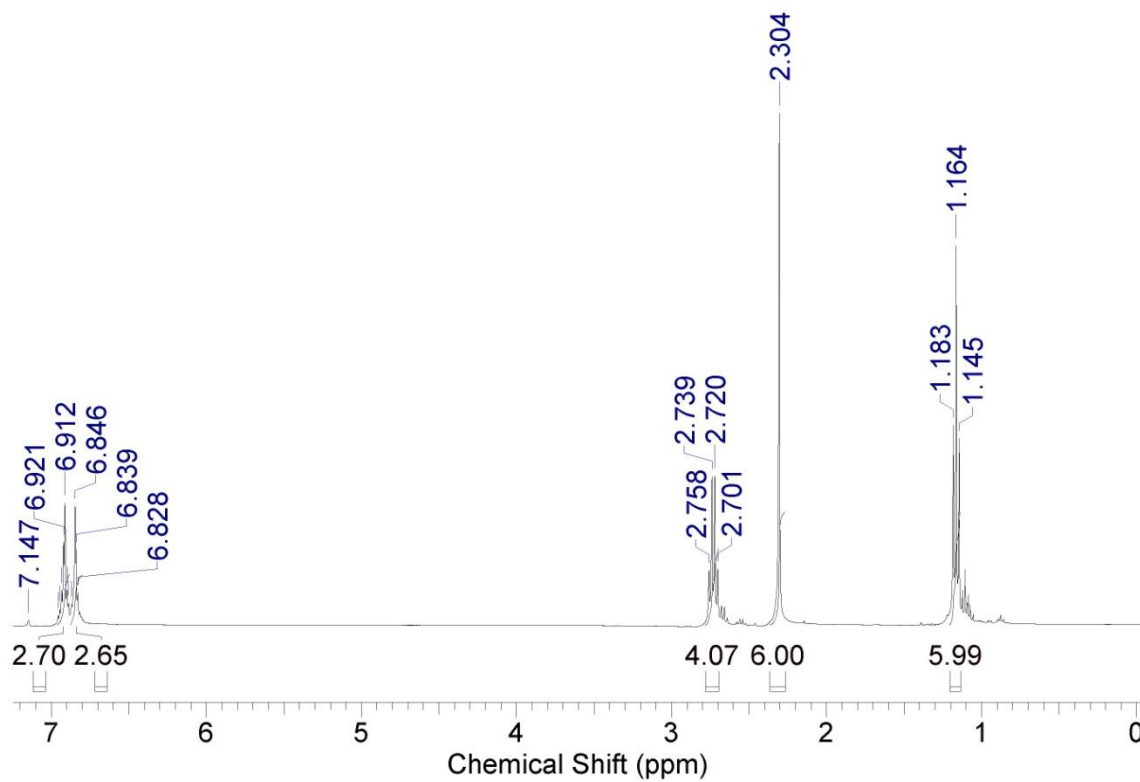
Figure B.10. ^{1}H NMR spectrum of (2,6-Et$_2$C$_6$H$_3$)NCN(2,6-Me$_2$C$_6$H$_3$).
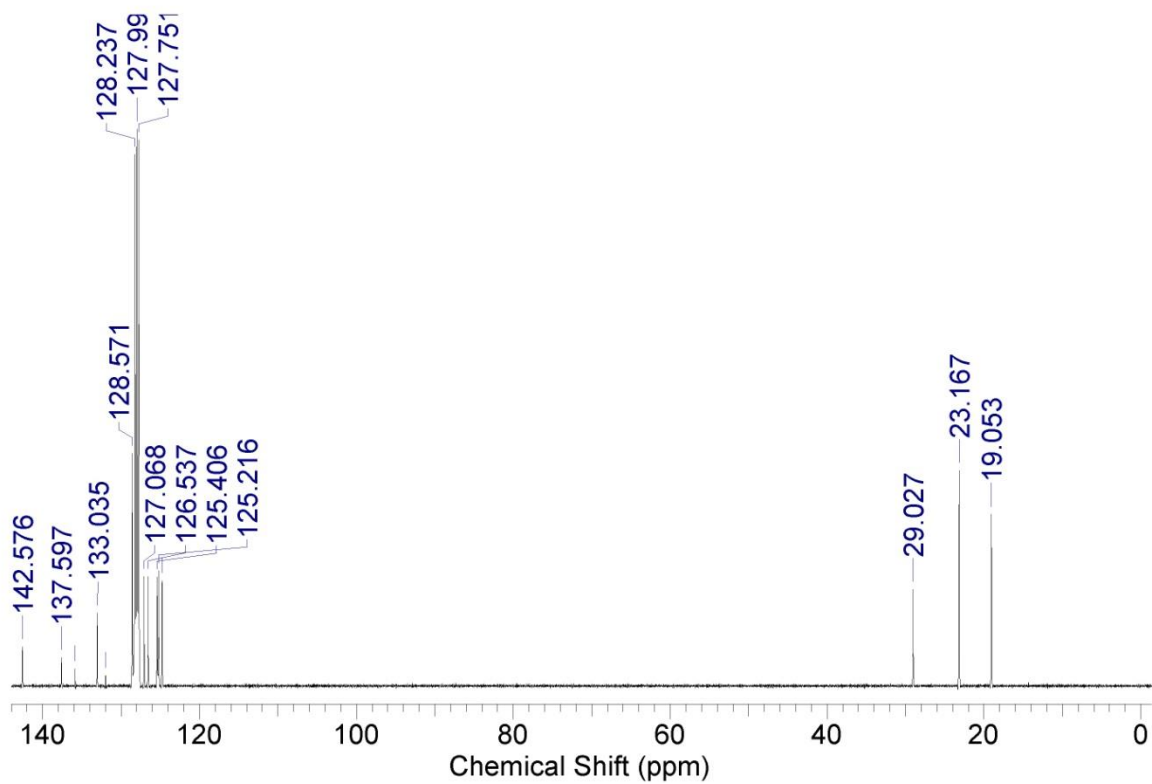
Figure B.11. ^{13}C NMR spectrum of (2,6-Et$_2$C$_6$H$_3$)NCN(2,6-Me$_2$C$_6$H$_3$).
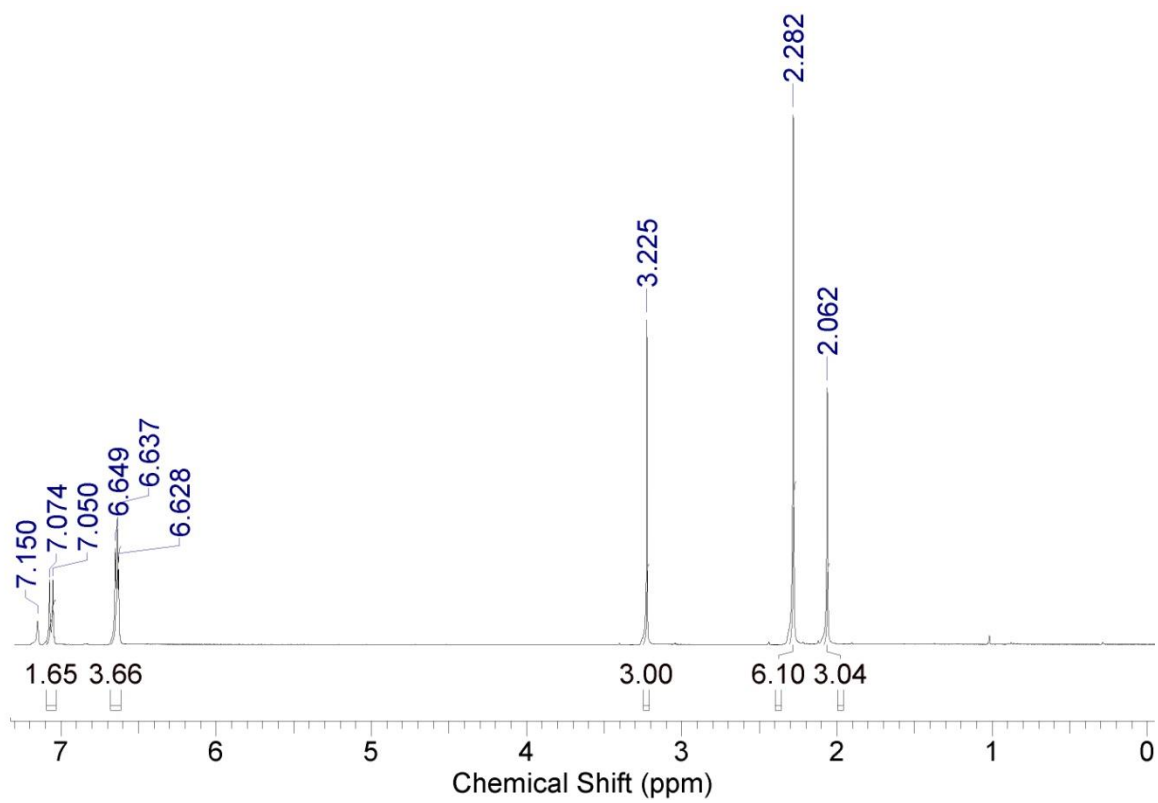
Figure B.12. ^{1}H NMR spectrum of MesNCN(4-OCH$_3$C$_6$H$_3$).
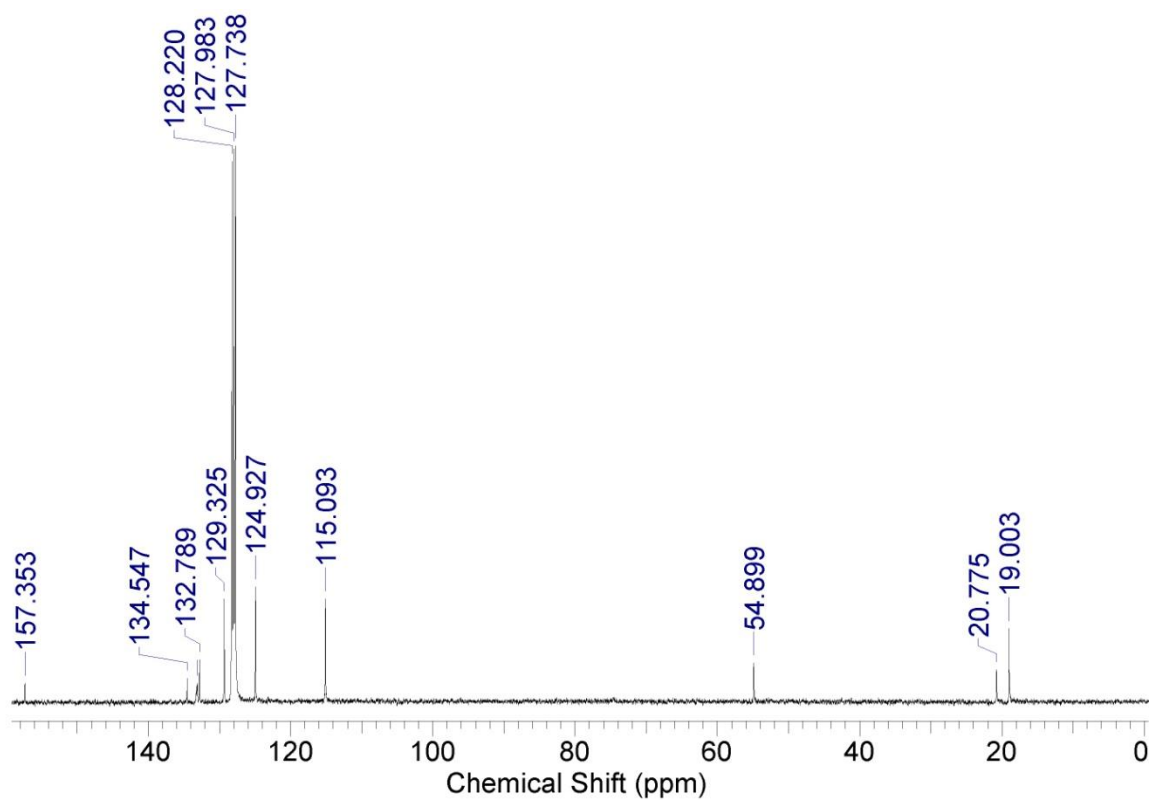
Figure B.13. ^{13}C NMR spectrum of MesNCN(4-OCH$_3$C$_6$H$_3$).
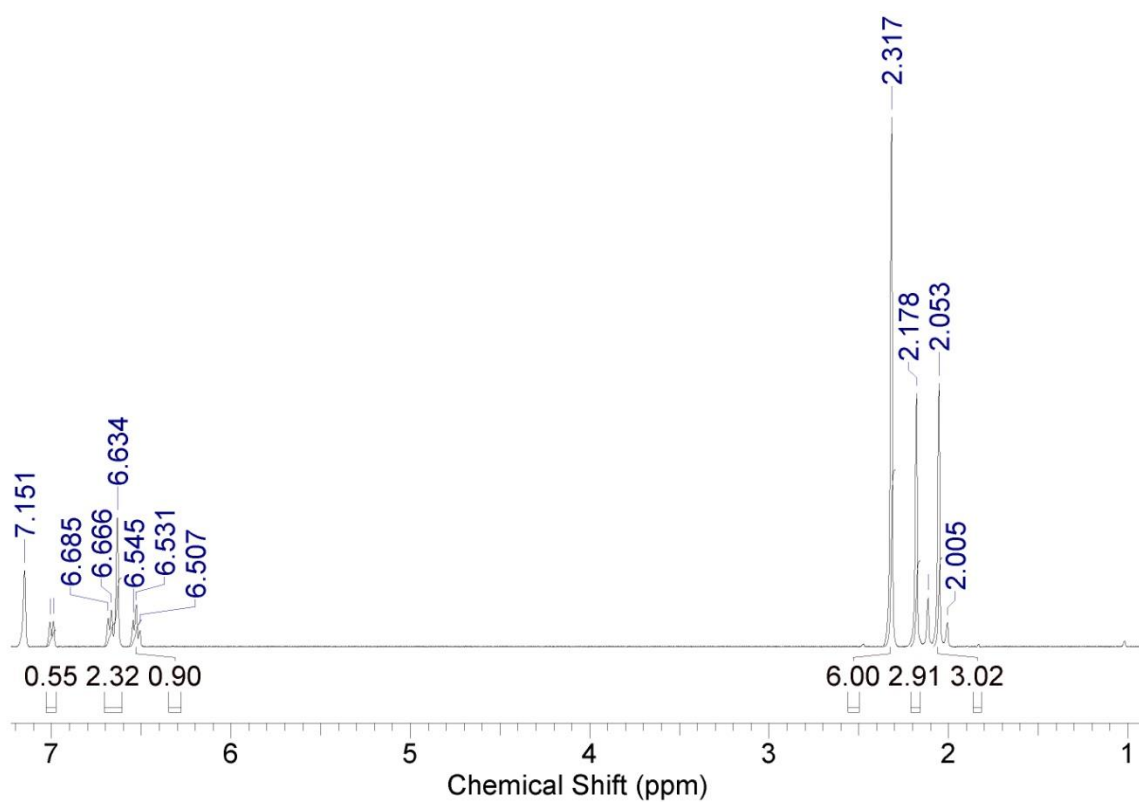
Figure B.14. ^{1}H NMR spectrum of MesNCN(2-Cl, 6-MeC$_6$H$_3$). Peaks at 6.531, 2.113, 2.005 ppm correspond to small amounts of unreacted MesN$_3$.
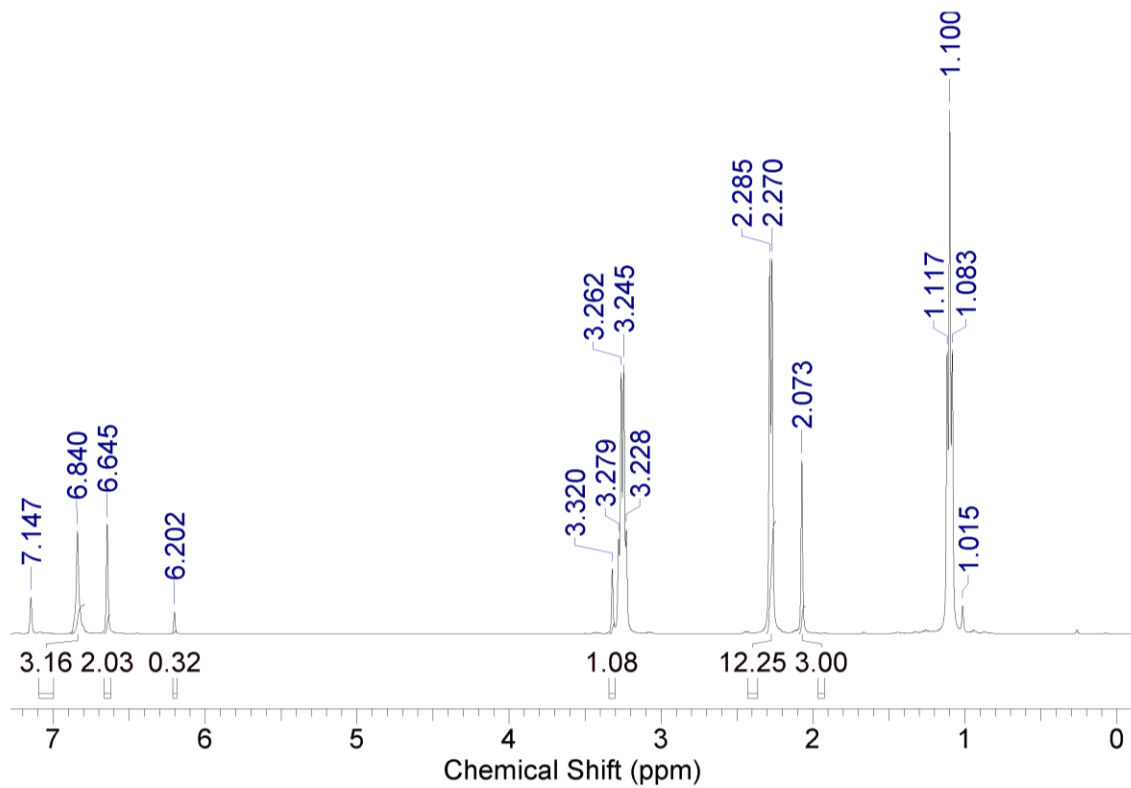
Figure B.15. ^{1}H NMR spectrum showing catalysis to form MesPhNCN(2,6-Me$_2$C$_6$H$_3$).
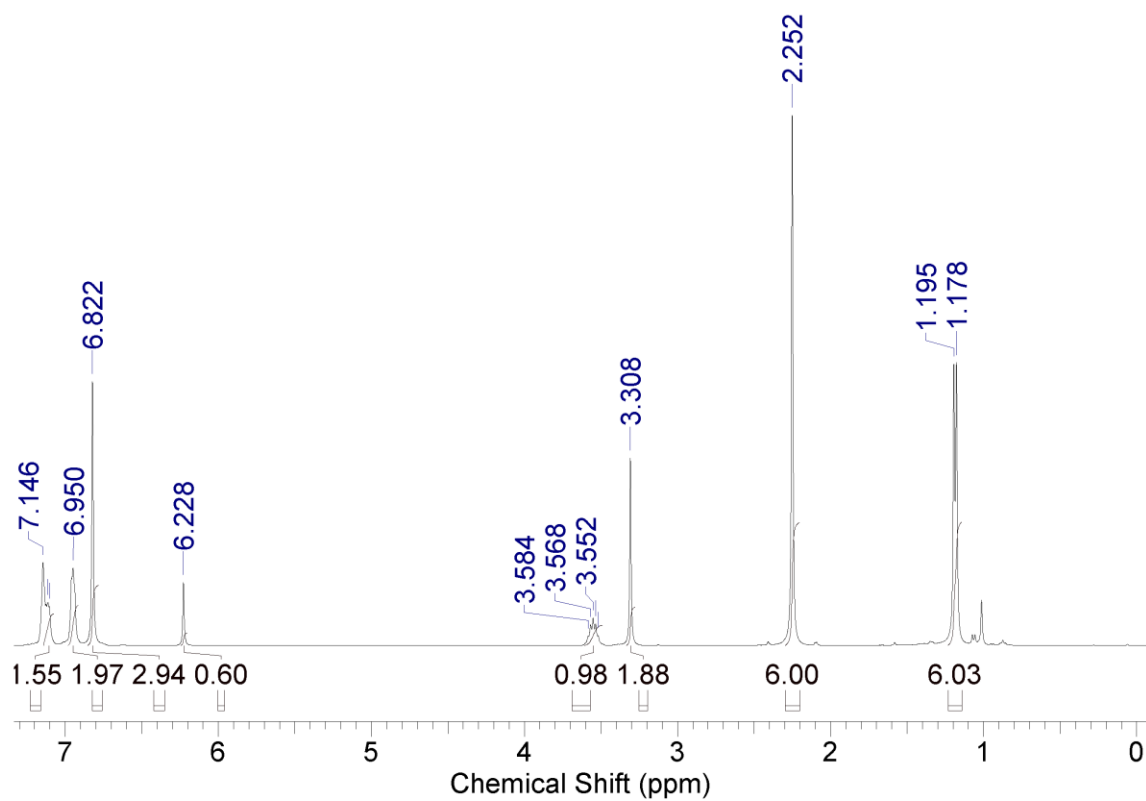
Figure B.16. ^{1}H NMR spectrum showing catalysis to form (2-[i]prC$_6$H$_4$)NCN(2,6-Me$_2$C$_6$H$_3$).
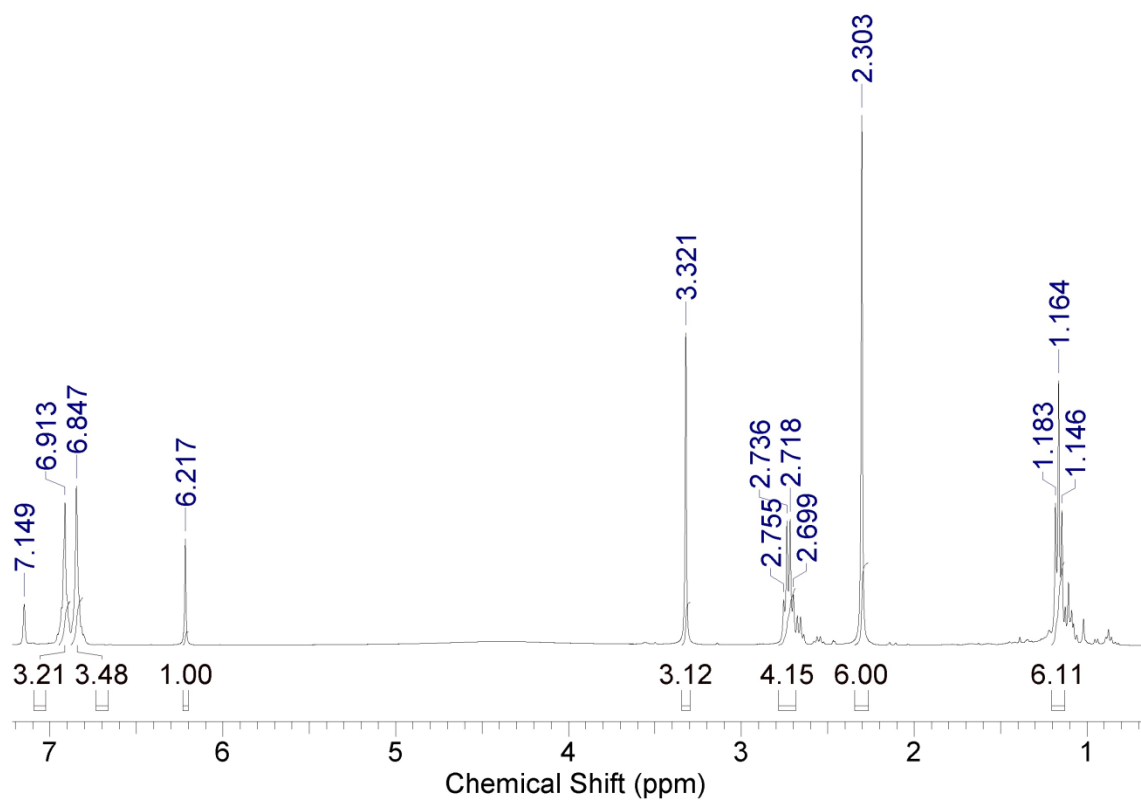
Figure B.17.^{1}H NMR spectrum showing catalysis to form (2,6-Et$_2$C$_6$H$_3$)NCN(2,6-Me$_2$C$_6$H$_3$).
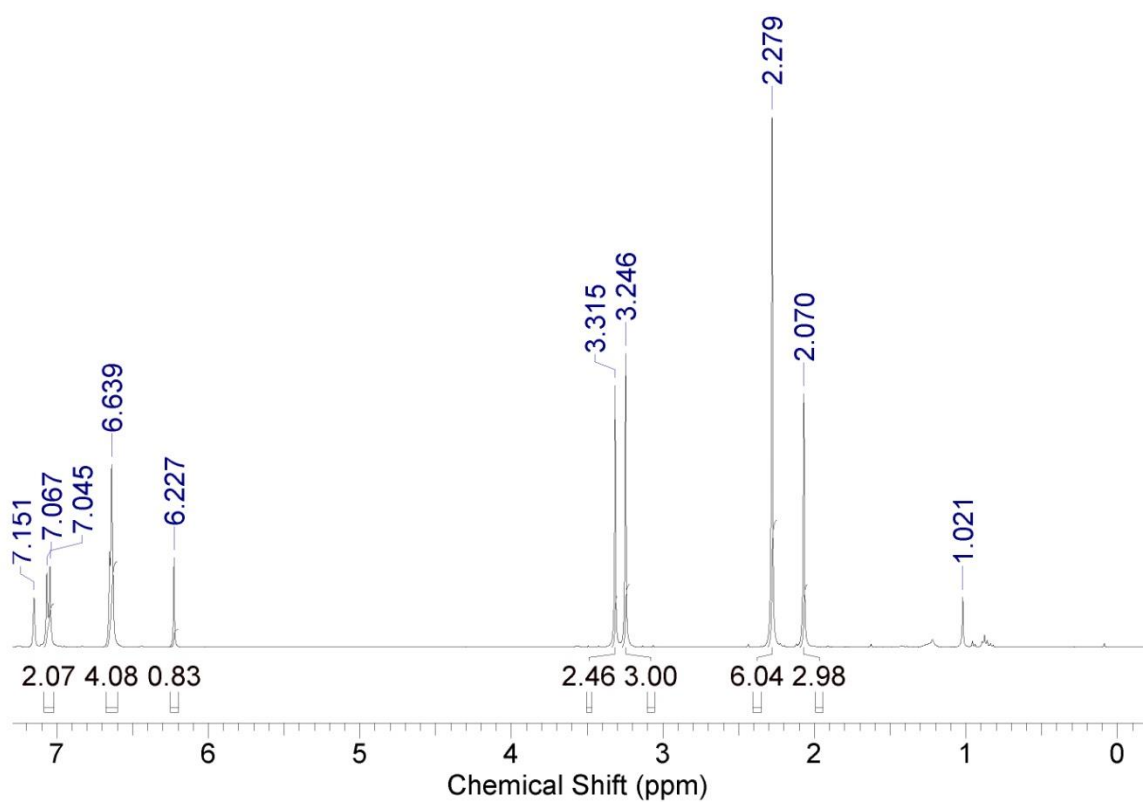
Figure B.18. ^{1}H NMR spectrum showing catalysis to form MesNCN(4-OCH$_3$C$_6$H$_4$).
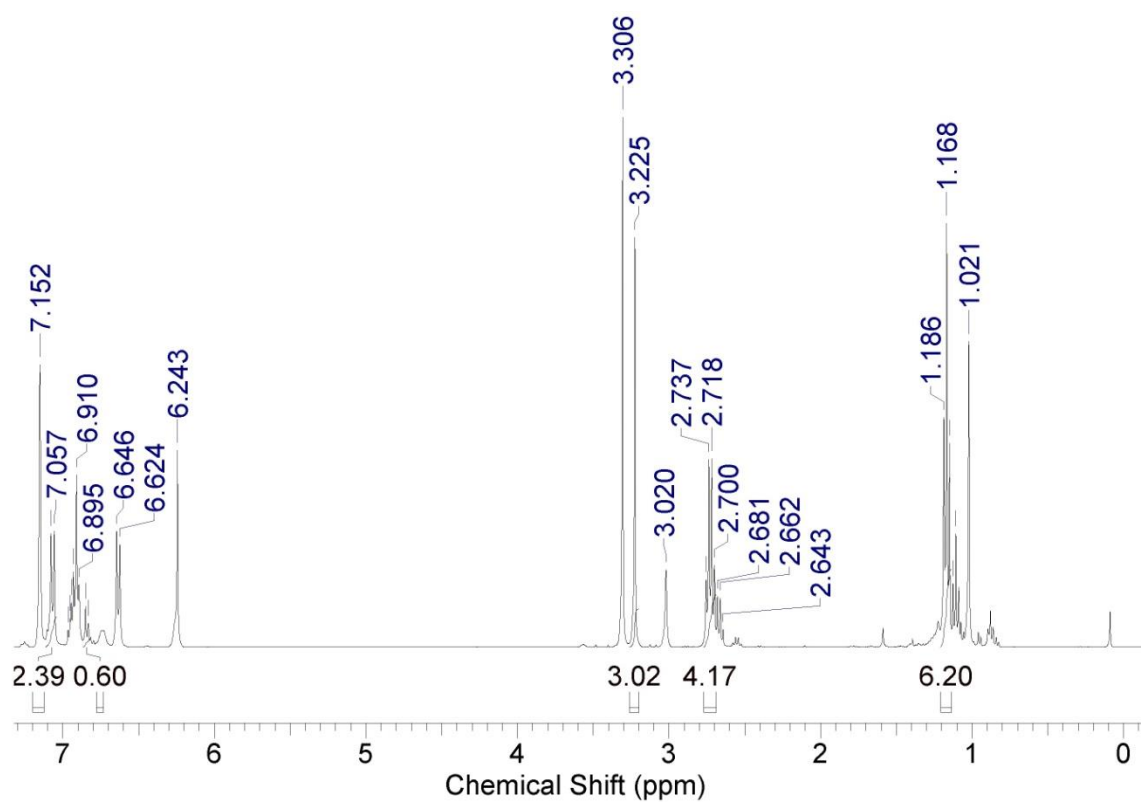
Figure B.19. ^{1}H NMR spectrum showing catalysis to form (2,6-Et$_2$C$_6$H$_3$)NCN(4-OCH$_3$C$_6$H$_4$).
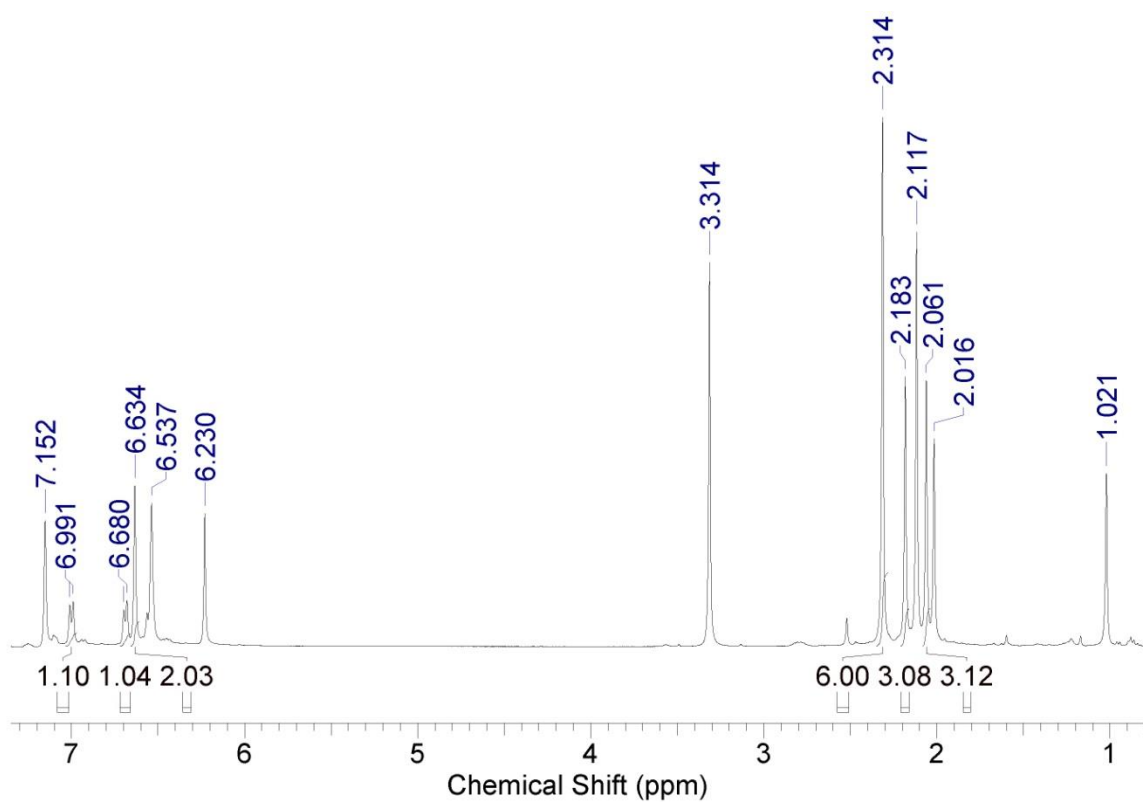
Figure B.20. ^{1}H NMR spectrum showing catalysis to form MesNCN(2-Cl, 6-MeC$_6$H$_3$).
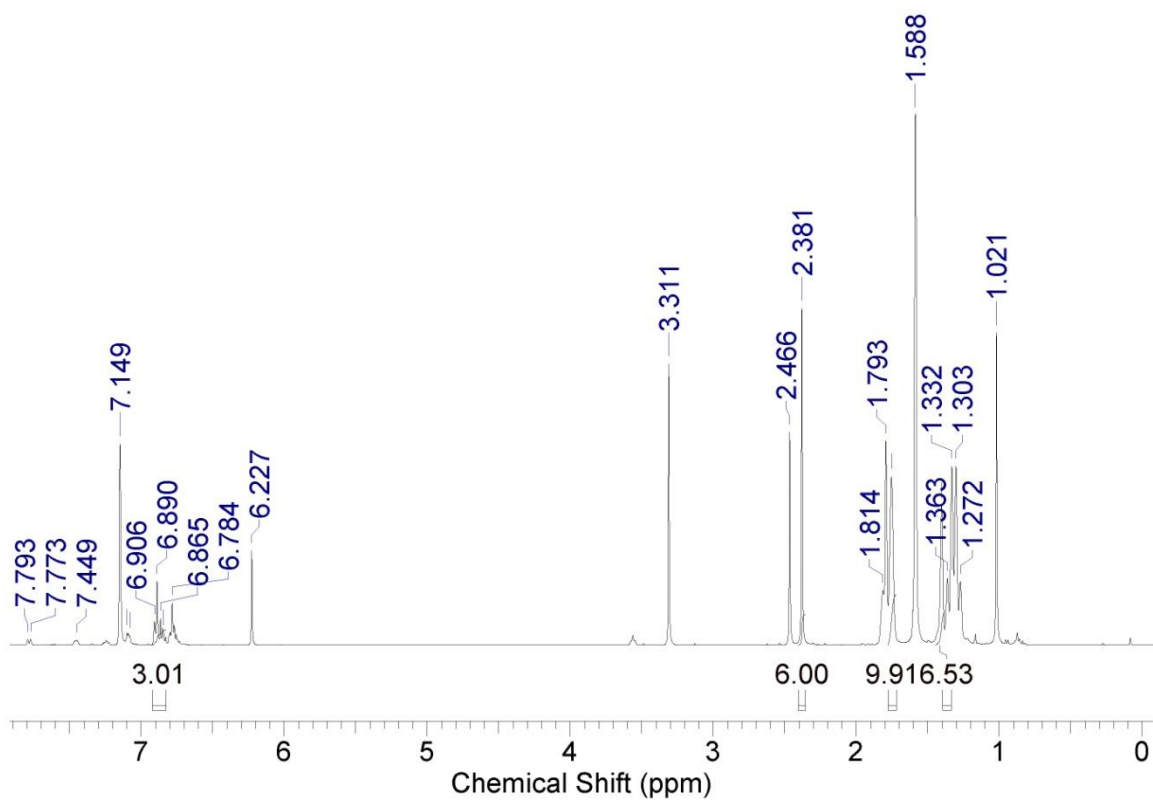
Figure B.21. ^{1}H NMR spectrum showing catalysis to form AdNCN(2,6-Me$_2$C$_6$H$_3$) at room temperature.
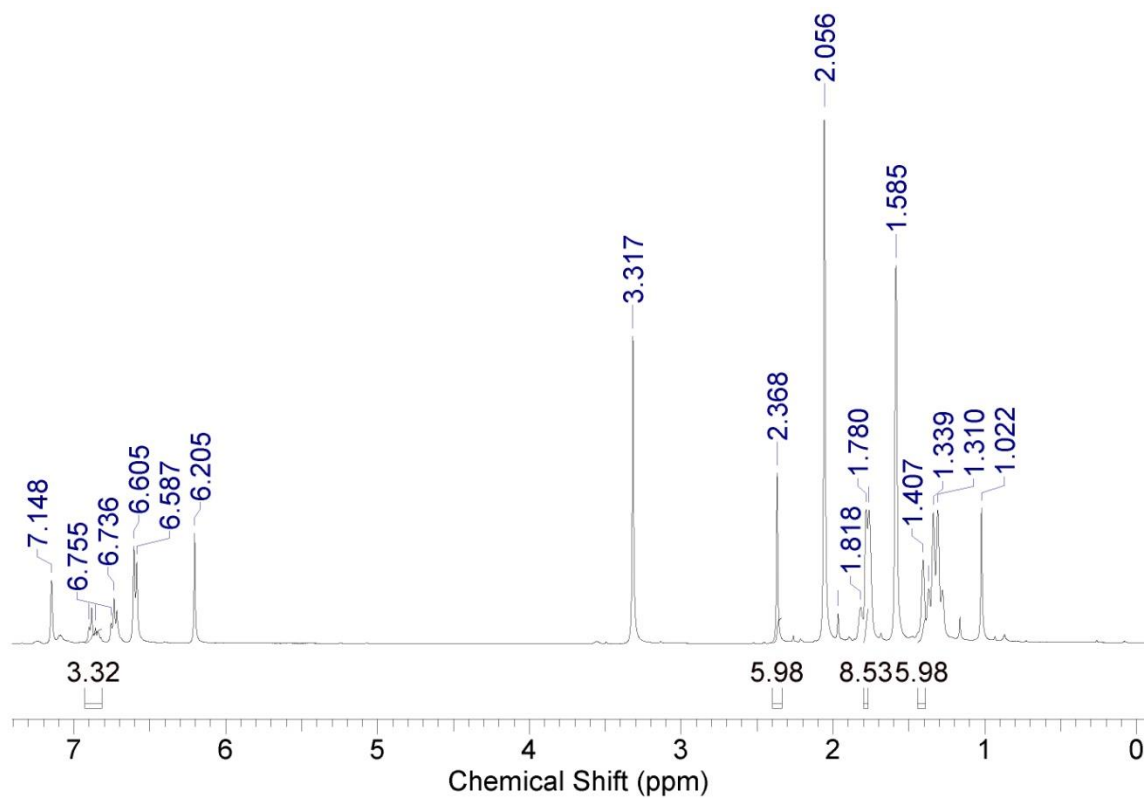
Figure B.22. ^{1}H NMR spectrum showing catalysis to form AdNCN(2,6-Me$_2$C$_6$H$_3$) at 60 ^{o}C for 15 h.
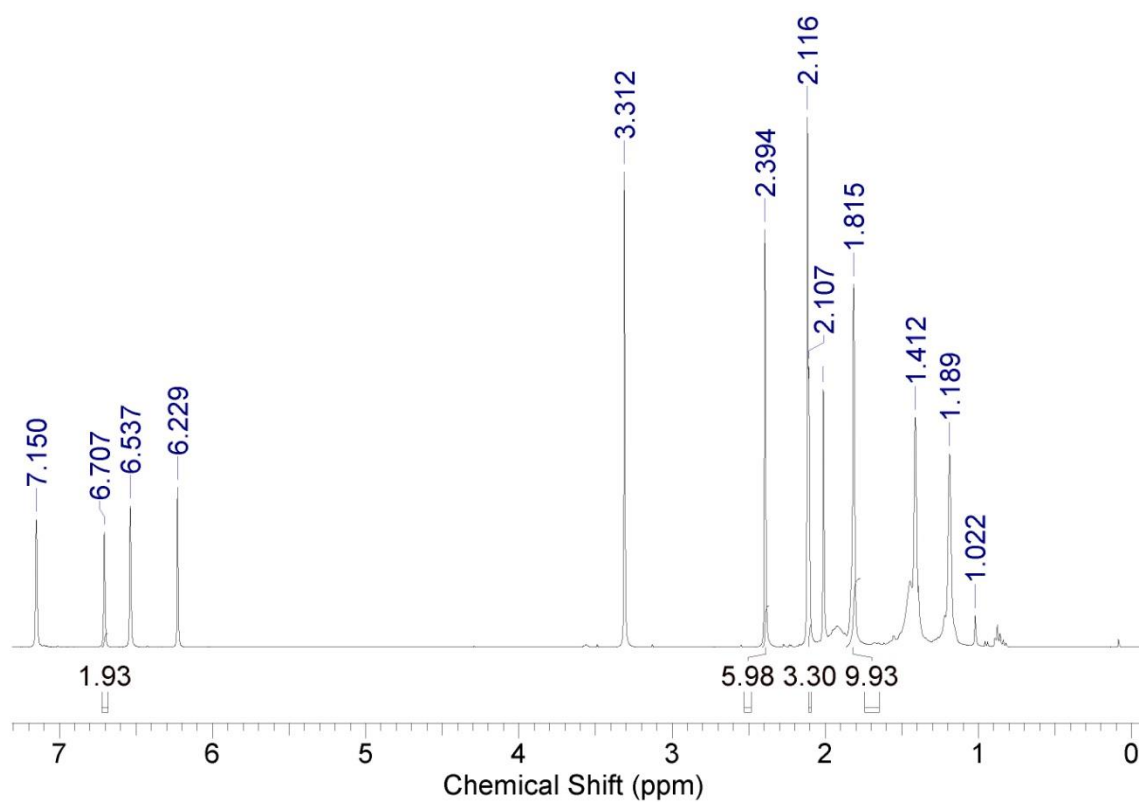
Figure B.23. ^{1}H NMR spectrum showing catalysis to form MesNCNAd at 60 ^{o}C for 8 h .
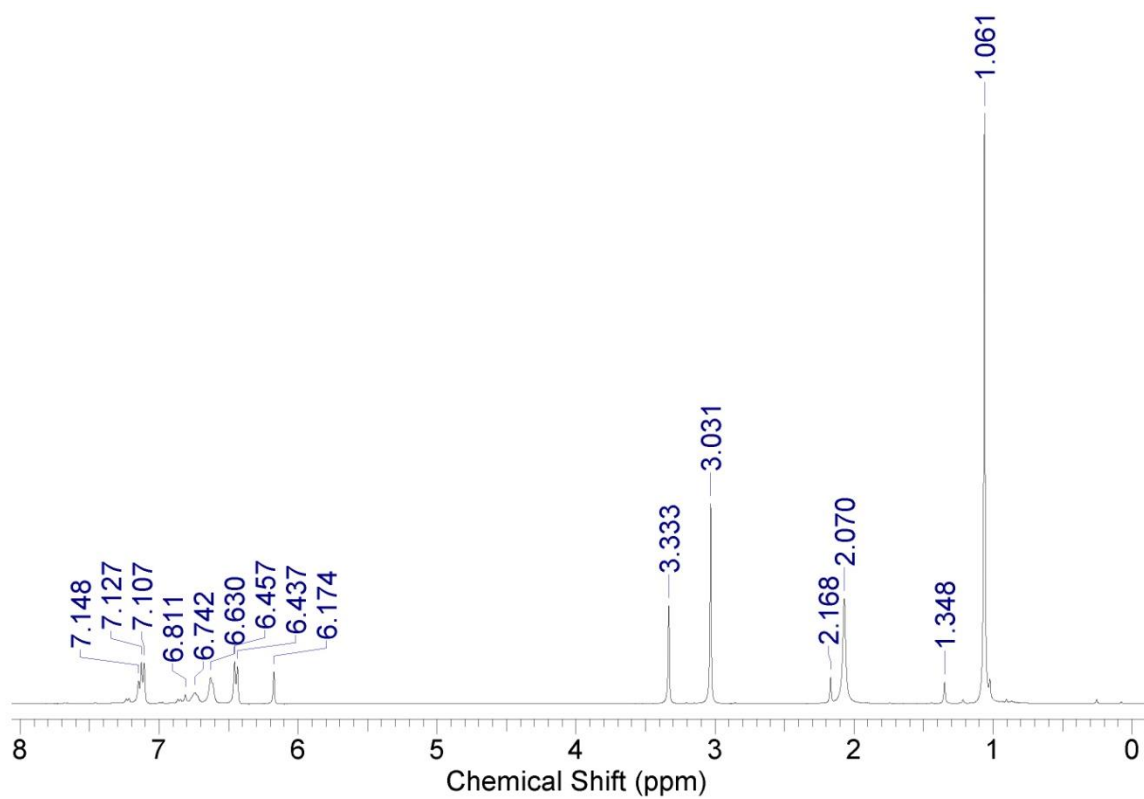
Figure B.24. ^{1}H NMR spectrum of the reaction mixture of 4-F$_3$CPhN$_3$ and 2,6-Me$_2$PhNC showing no catalysis to form the respective carbodiimide. Peaks at 3.301 and 1.061 ppm correspond to the tertbutyl methyl ether solvent.
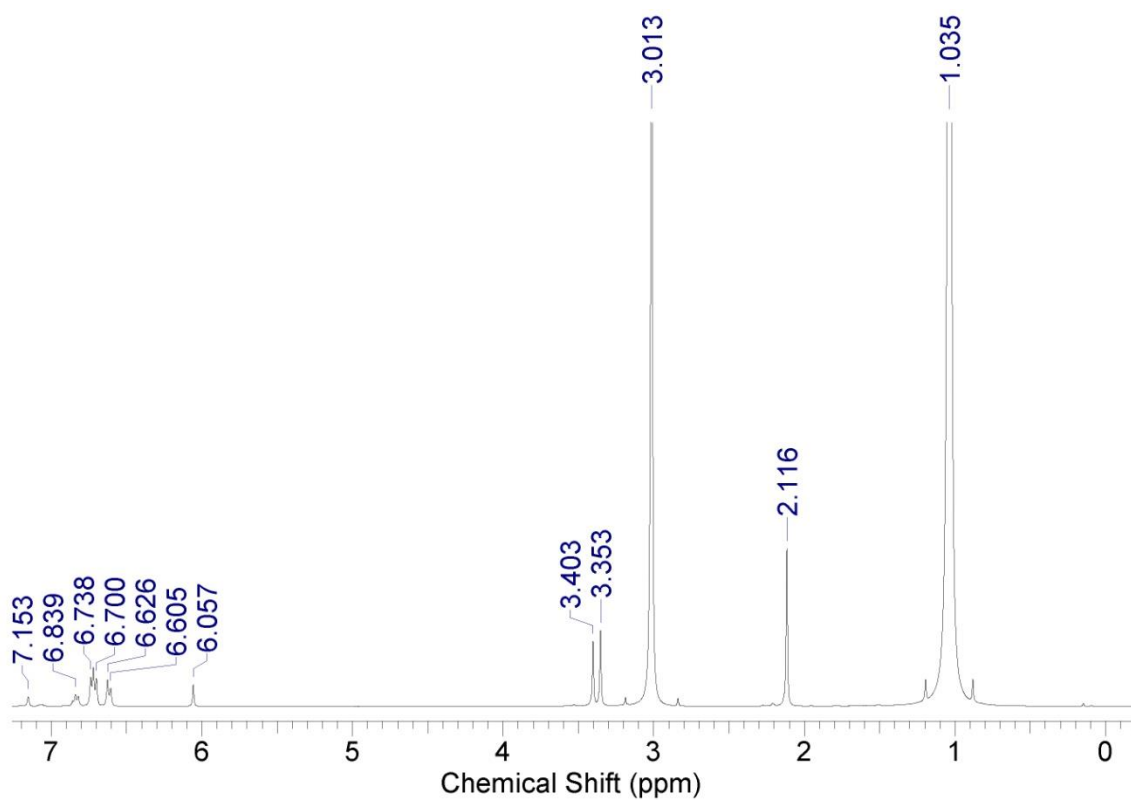
Figure B.25. ^{1}H NMR spectrum of the reaction mixture of 4-OCH$_3$PhN$_3$ and 2,6-Me$_2$PhNC showing no catalysis to form the respective carbodiimide.
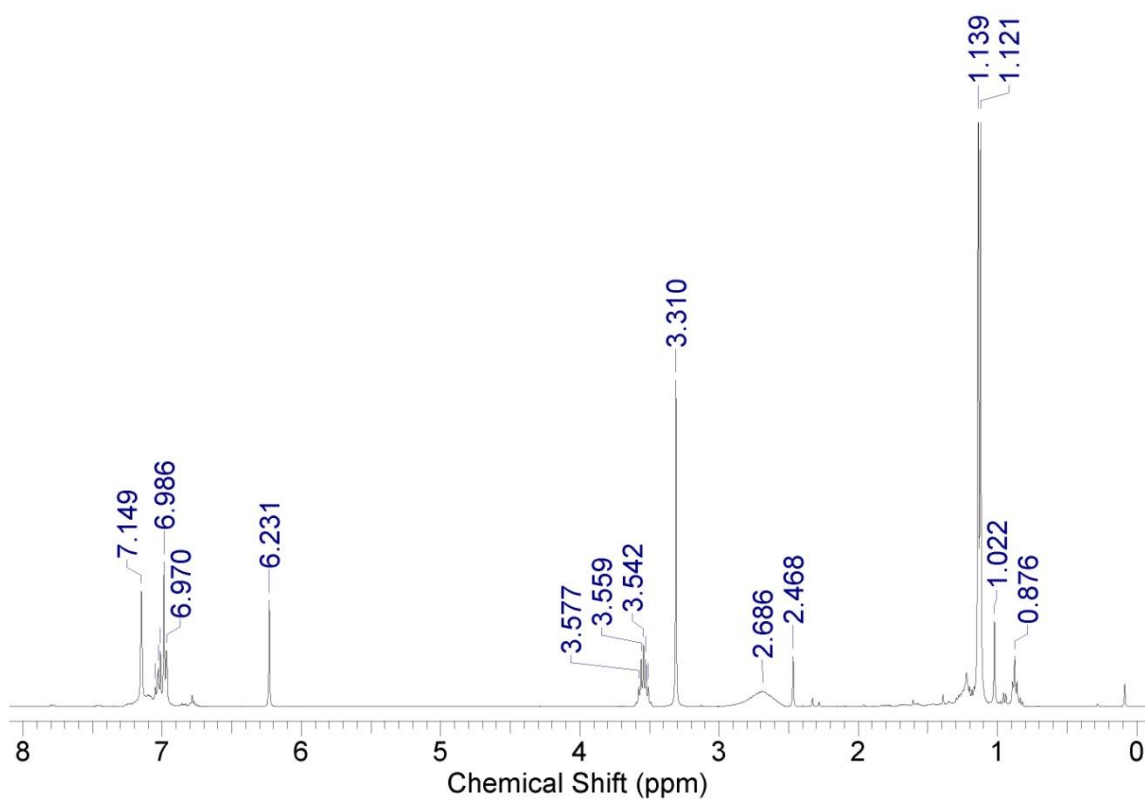
Figure B.26. ^{1}H NMR spectrum of the reaction mixture containing 2,6-^{i}Pr$_2$PhN$_3$ and 2,6-Me$_2$PhNC showing no catalysis to form the respective carbodiimide.
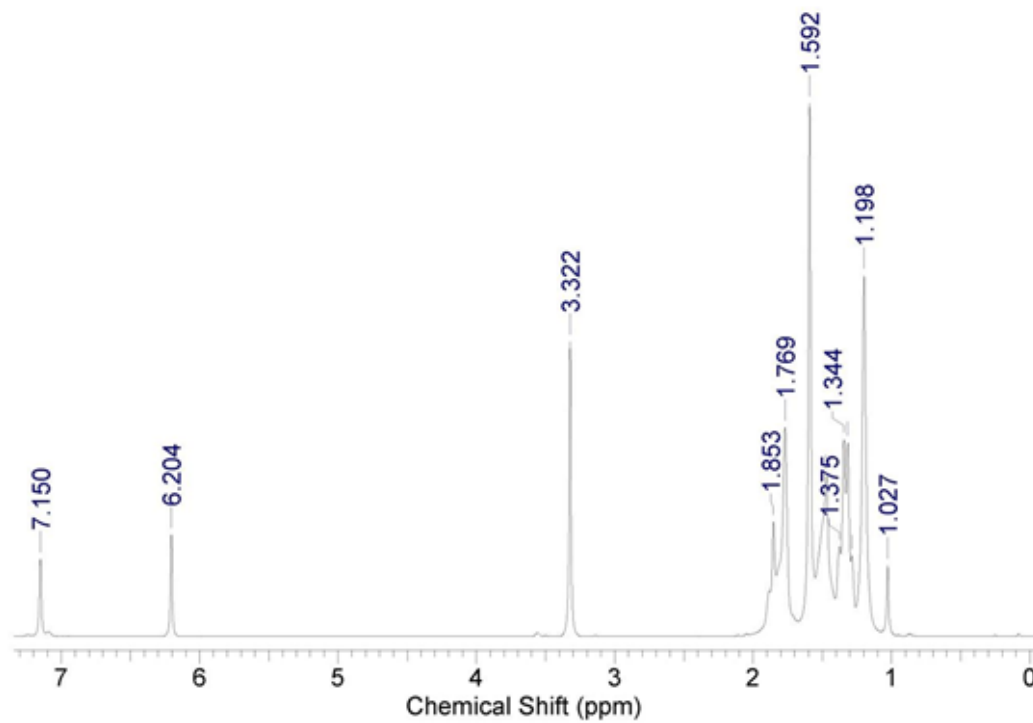
Figure B.27. ^{1}H NMR spectrum of the reaction mixture containing AdN$_3$ and AdNC showing no catalysis to form the respective carbodiimide at room temperature.
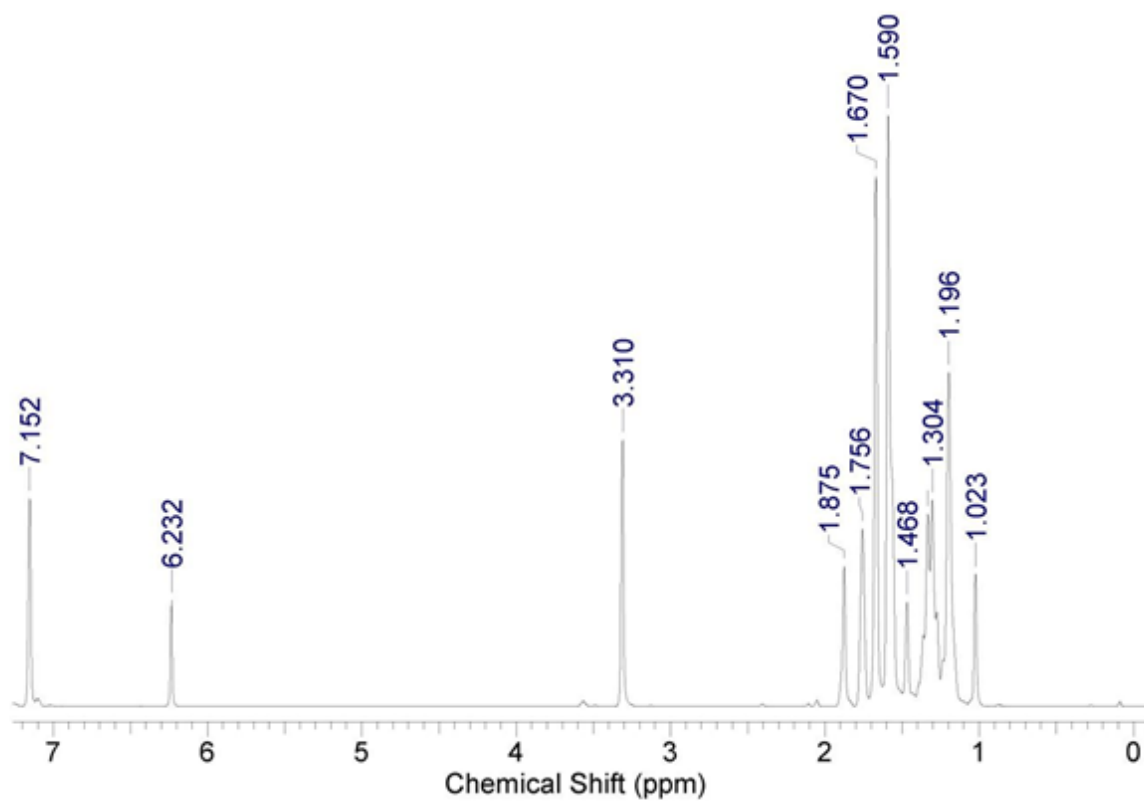
Figure B.28. ^{1}H NMR spectrum of the reaction mixture containing AdN$_3$ and AdNC following heating to 60 °C for 14 hours showing no catalysis to form the respective carbodiimide.
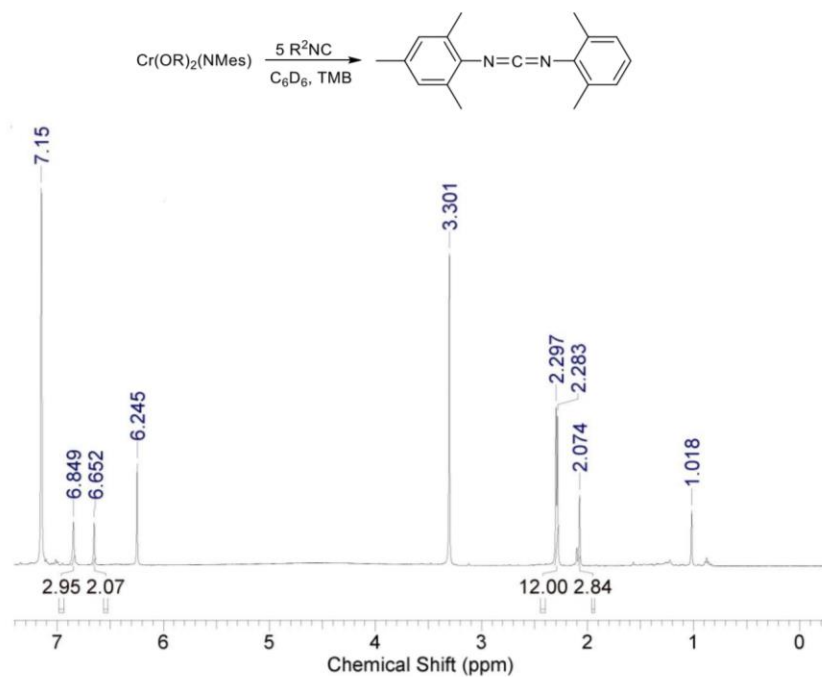
Figure B.29.^{1}H NMR spectrum of complex **21** with 5 equivalent of 2,6-Me2PhNC showing the formation of MesN=C=N(2,6-Me$_2$C$_6$H$_3$).
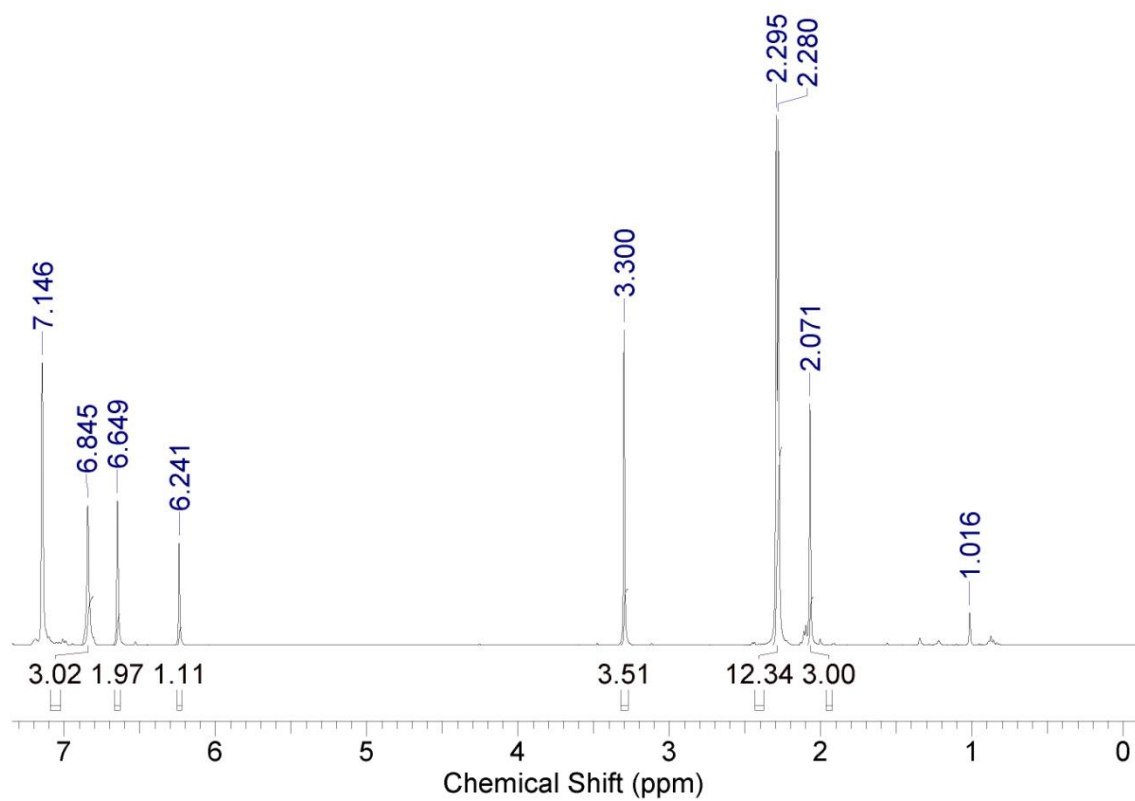
Figure B.30. ^{1}H NMR spectrum of complex **26** (RO)$_2$Cr(CNR)$_4$ and 5 equiv. of MesN$_3$ showing the formation of MesN=C=N(2,6-Me$_2$C$_6$H$_3$).
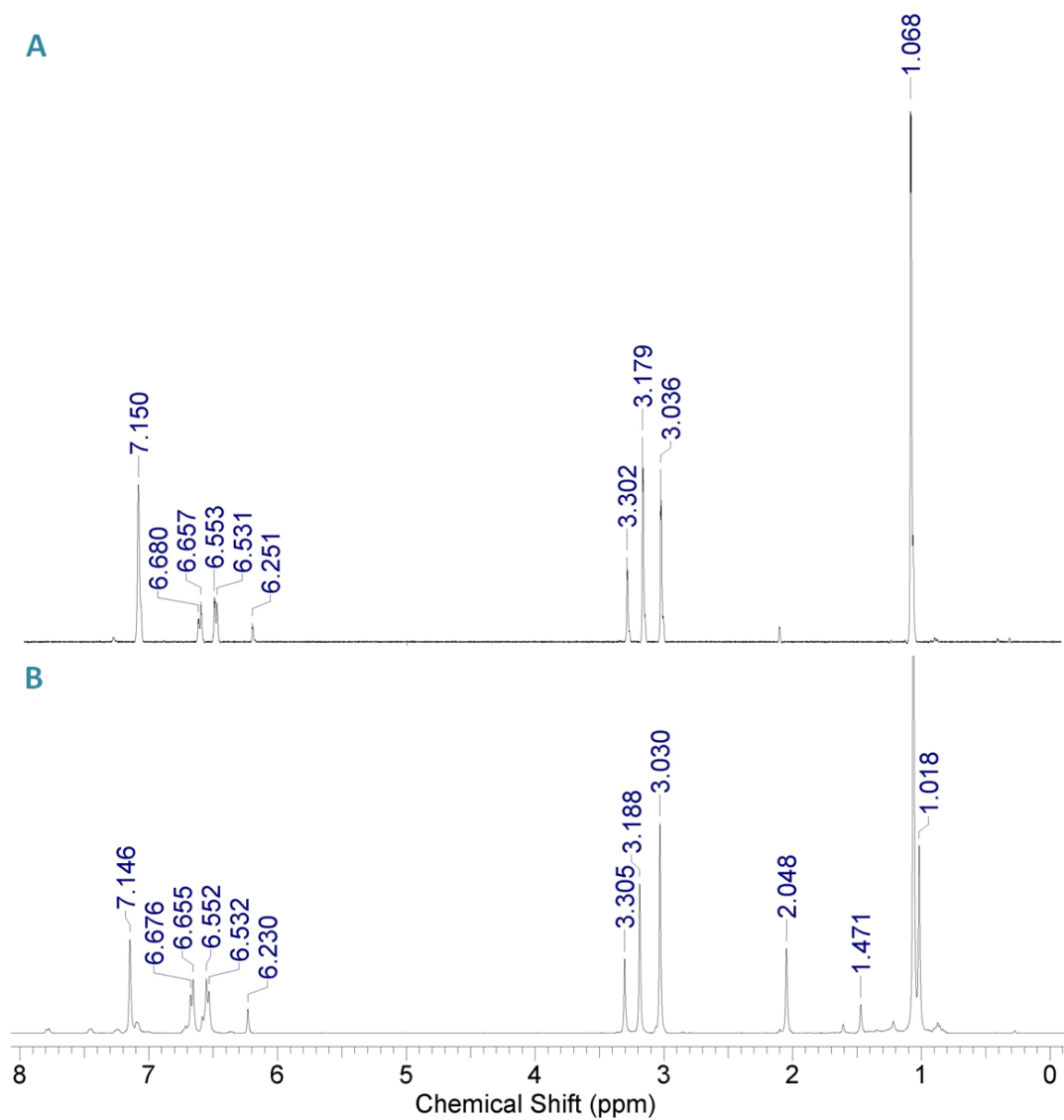
Figure B.31. Top (**A**) ^{1}H NMR spectrum of 4-CF$_3$PhN$_3$ in the presence of internal standard (TMB). Bottom: (**B**) the spectrum of the mixture from (A) with complex Cr(CNR$_2$)$_4$(OR)$_2$ (**26**) demonstrating no formation of the respective carbodiimide. Note: peaks at 3.302 and 1.068 ppm correspond to the *tert*-butyl methyl ether solvent.
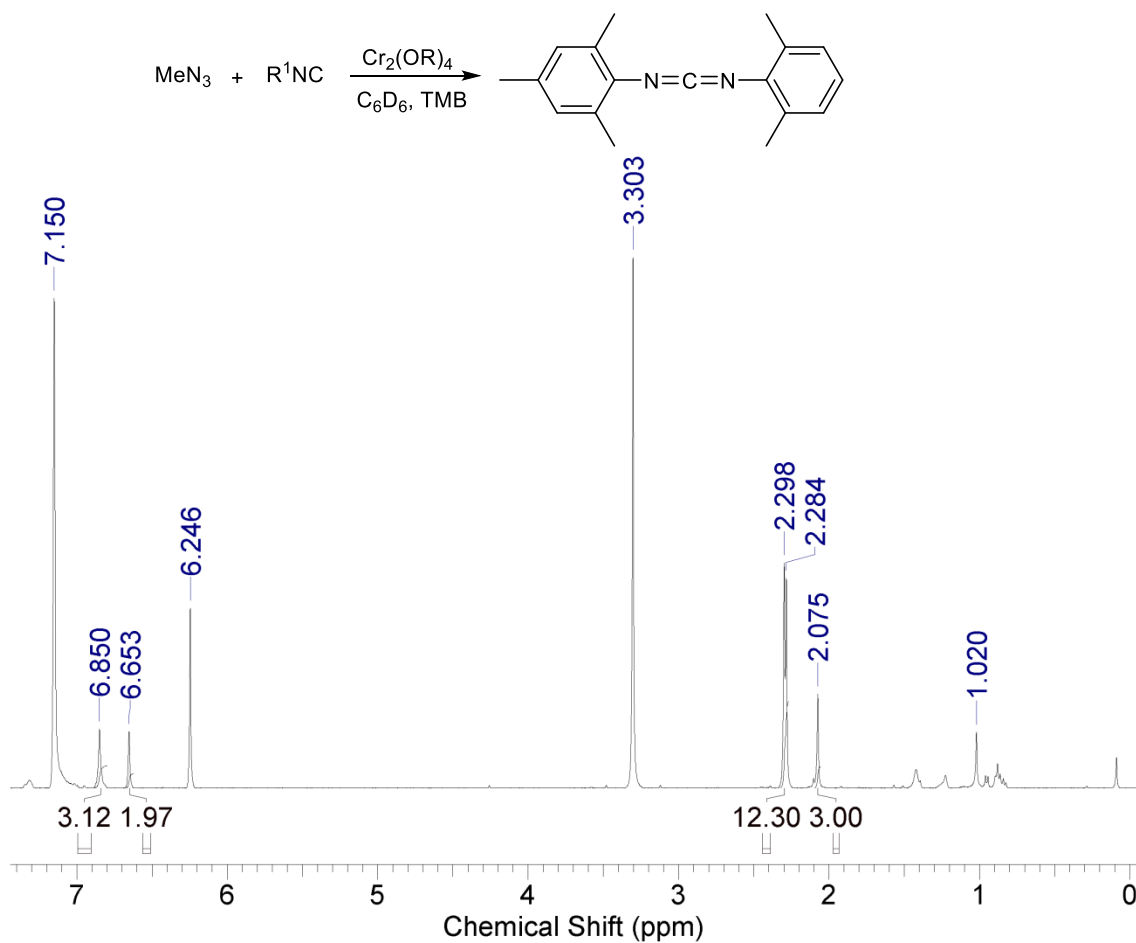
Figure B.32. ^{1}H NMR spectrum of the reaction of complex **20** with one equivalent of MesN$_3$ and 2,6-Me$_2$PhNC showing the formation of MesN=C=N(2,6-Me$_2$C$_6$H$_3$).
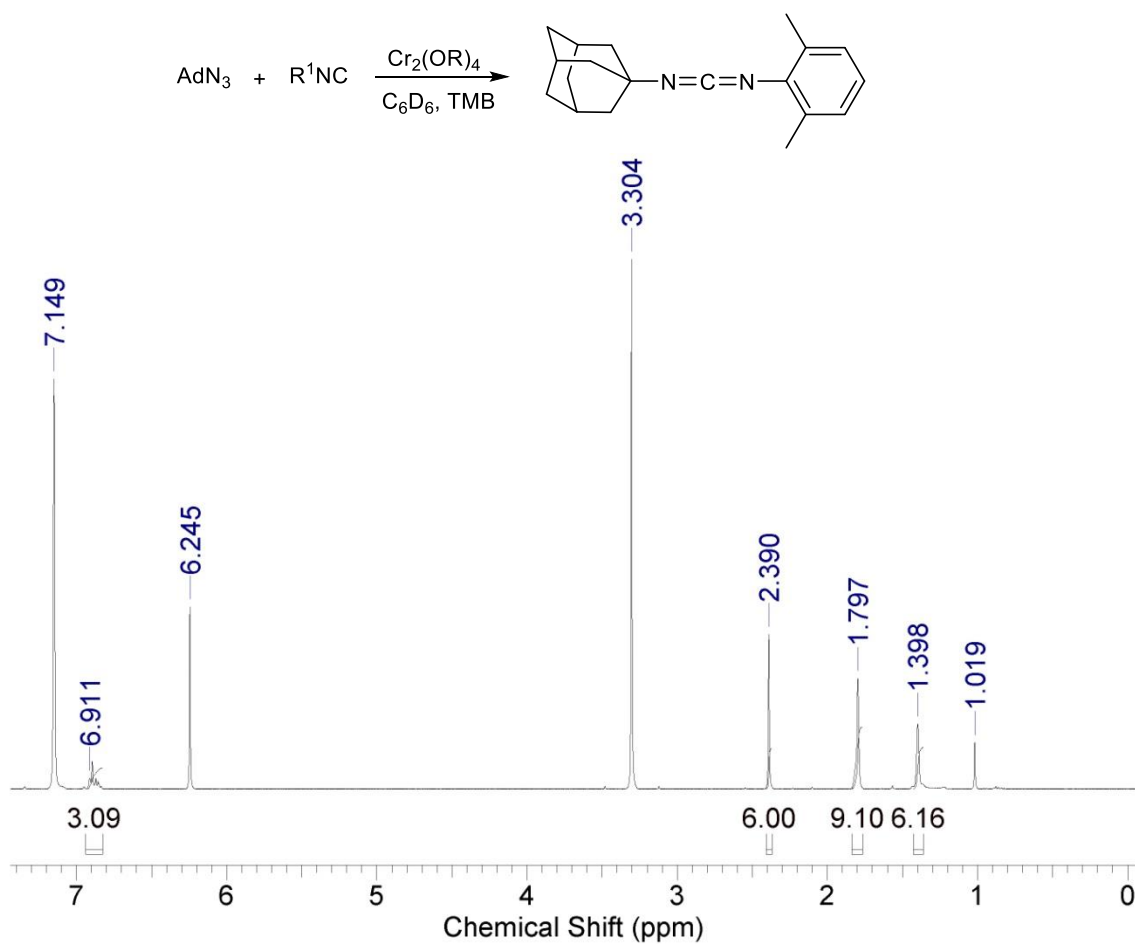
Figure B.33. ^{1}H NMR spectrum of the reaction of complex **20** with one equivalent of AdN$_3$ and 2,6-Me$_2$PhNC showing the formation of AdN=C=N(2,6-Me$_2$C$_6$H$_3$).

4. IR Spectra
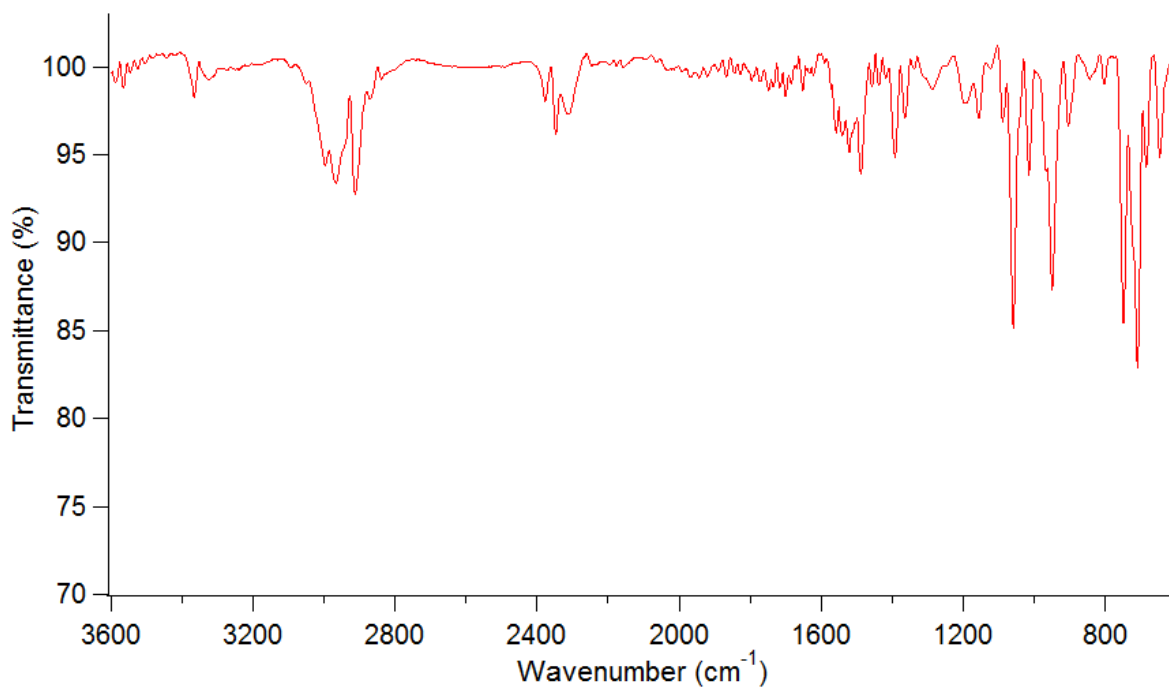
Figure B.34. IR spectra of complex **20** $Cr_2(OR)_4$.
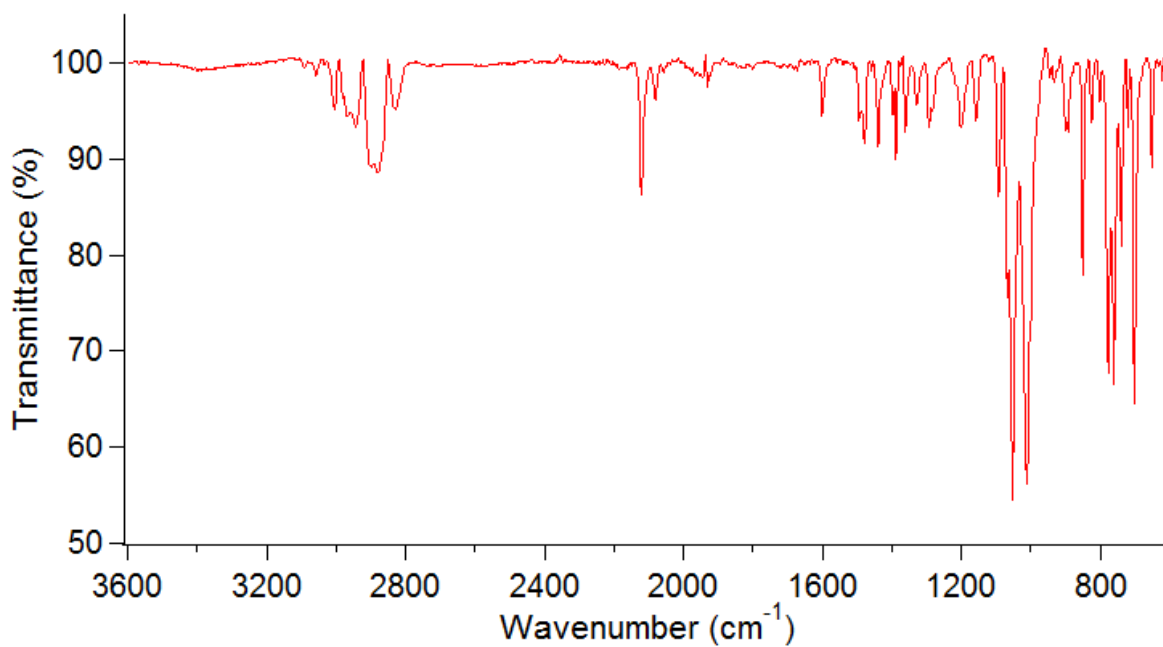
Figure B.35. IR spectra of complex **21** $Cr(OR)_2(NMes)$.
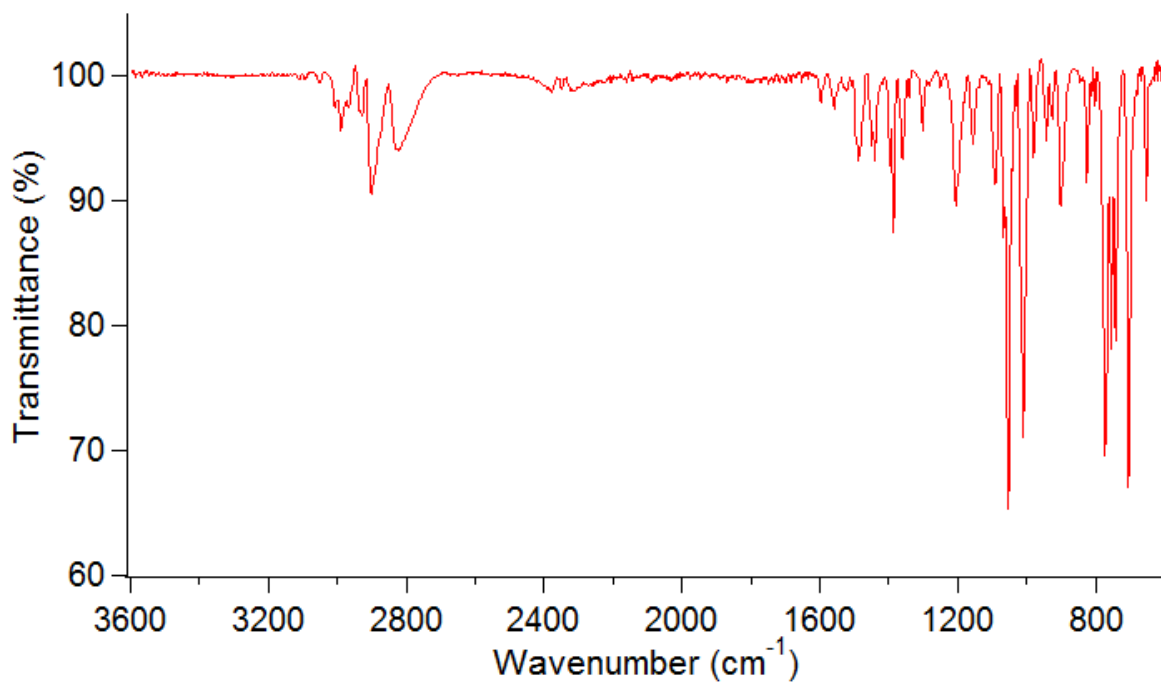
Figure B.36. IR spectra of Complex **22** Cr(OR)$_2$(NAd).
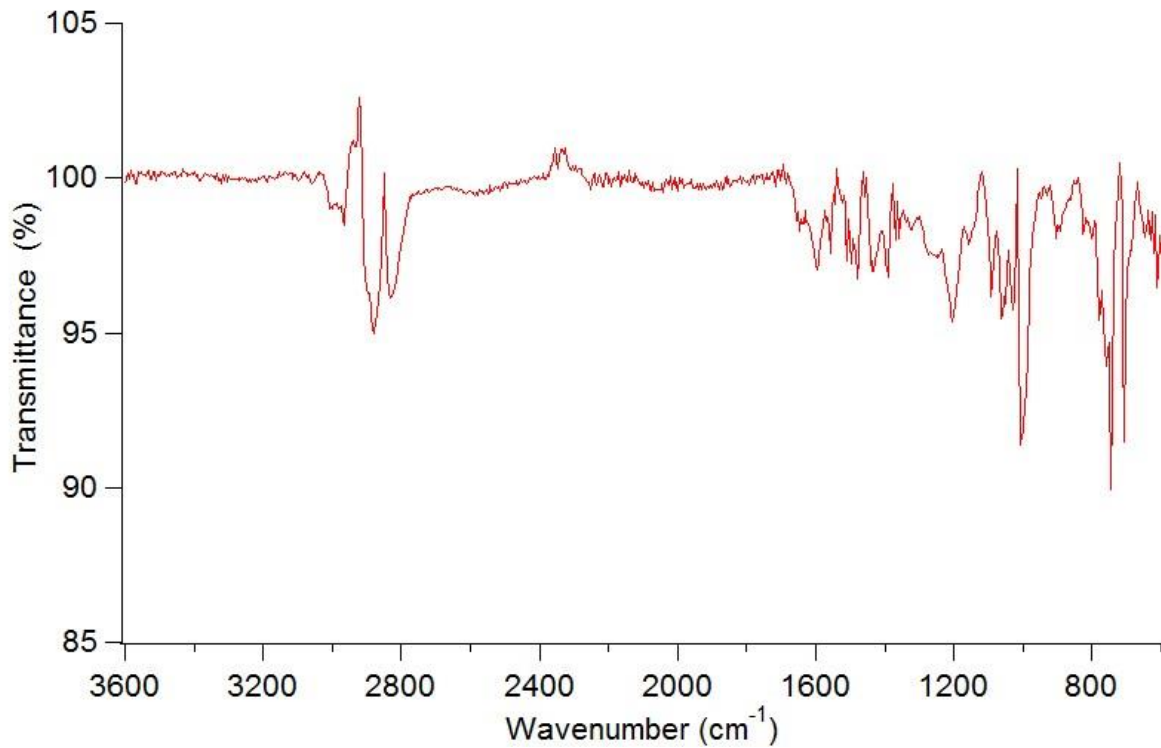
Figure B.37. IR spectra of complex **23** Cr(OR)$_2$(NDEP) in the 3400-600 cm^{-1} range.
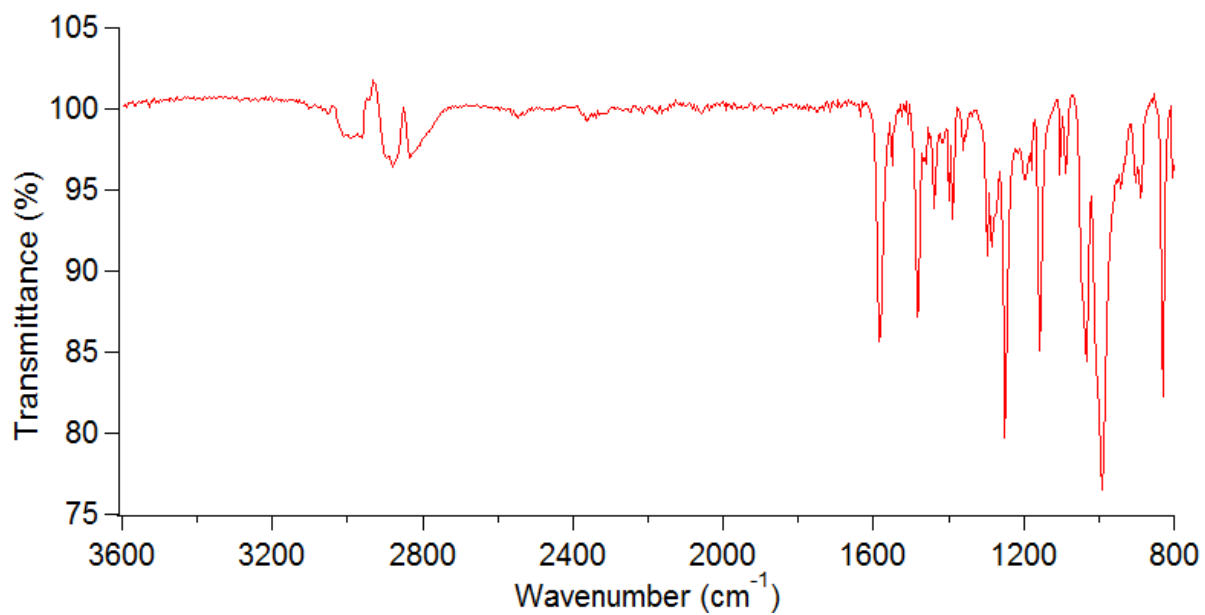
Figure B.38. IR spectra of complex **24** Cr(OR)$_2$(NPhOCH$_3$)$_2$.
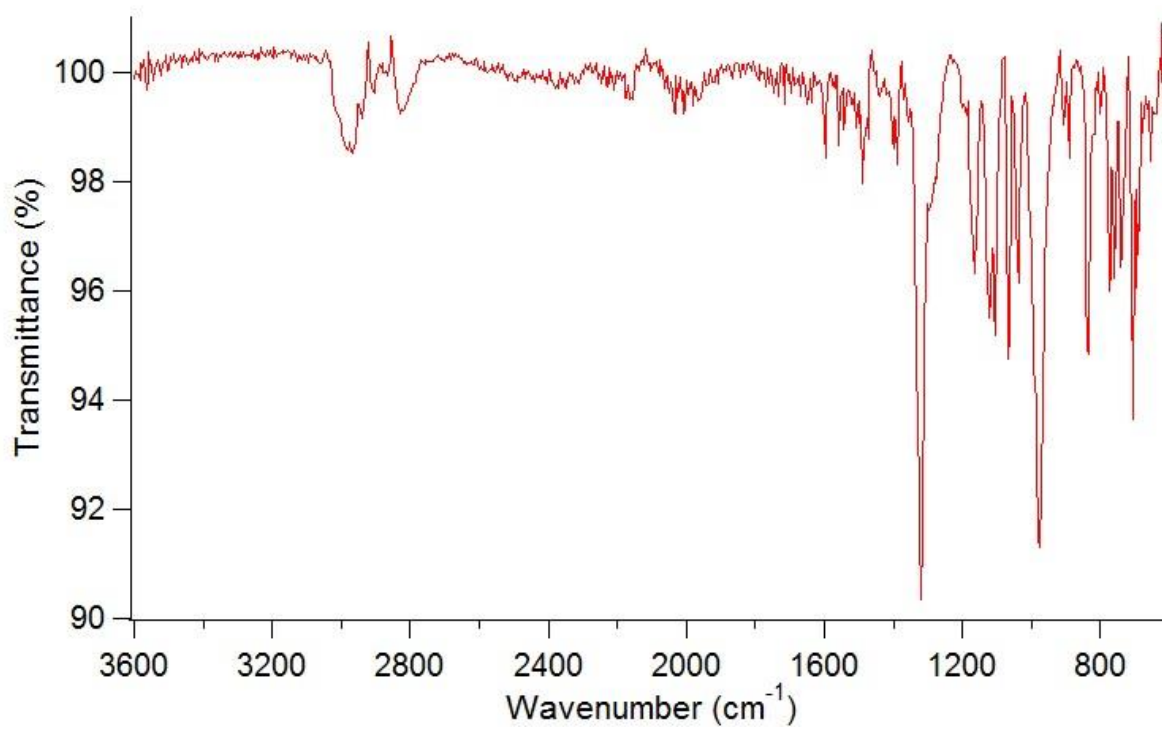
Figure B.39. IR spectra of complex **25** Cr(OR)$_2$(NPhCF$_3$)$_2$.
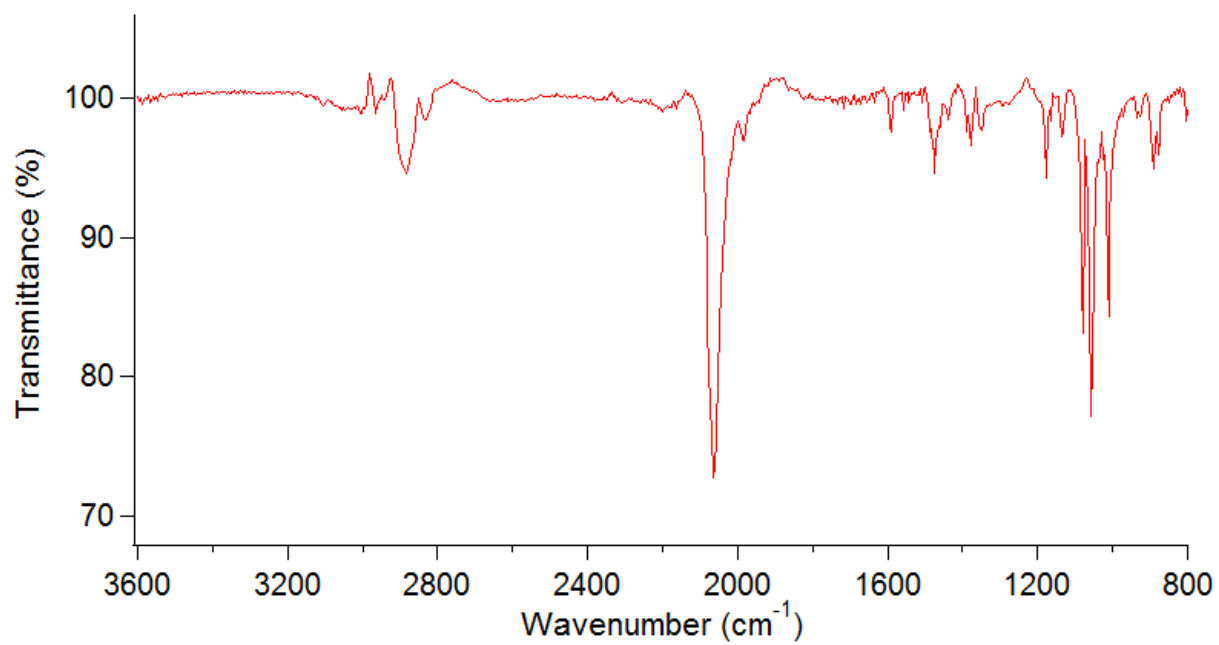
Figure B.40. IR spectra of complex **26** Cr(OR)$_2$(CNR)$_4$.

5. UV-Vis Spectra
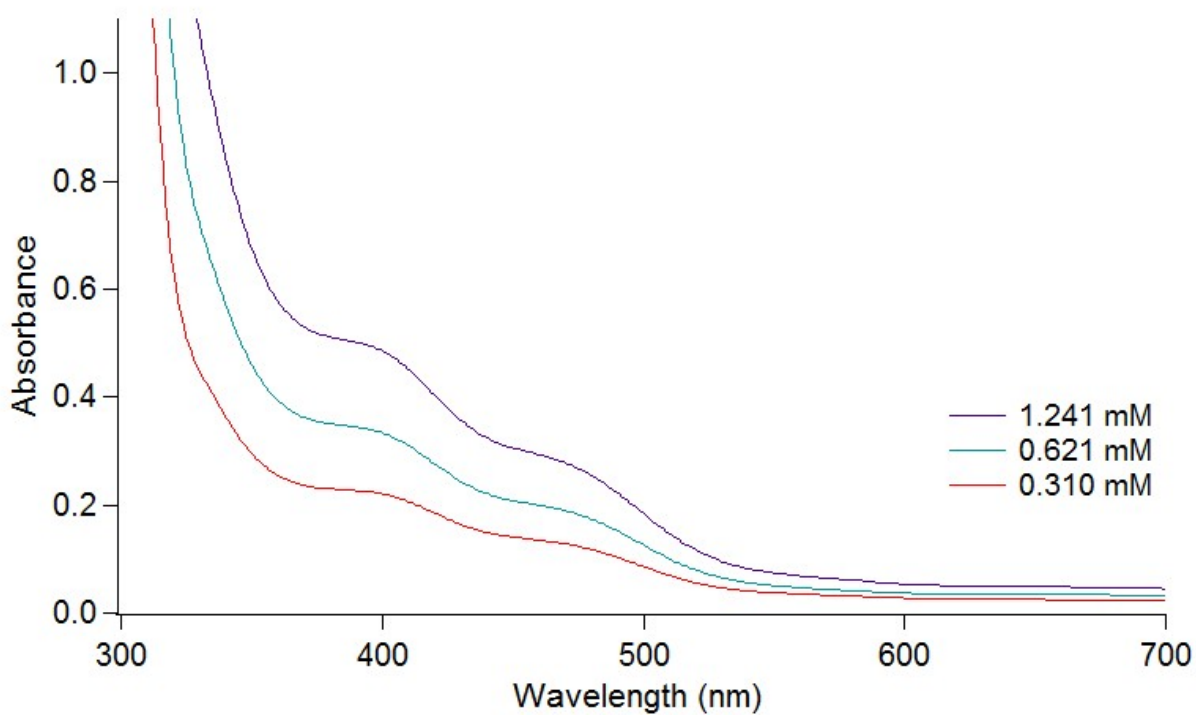
Figure B.41. UV-vis spectrum for complex **20** $Cr_2(OR)_4$ at three different concentrations. λ_{max} (εM): 726 (67).
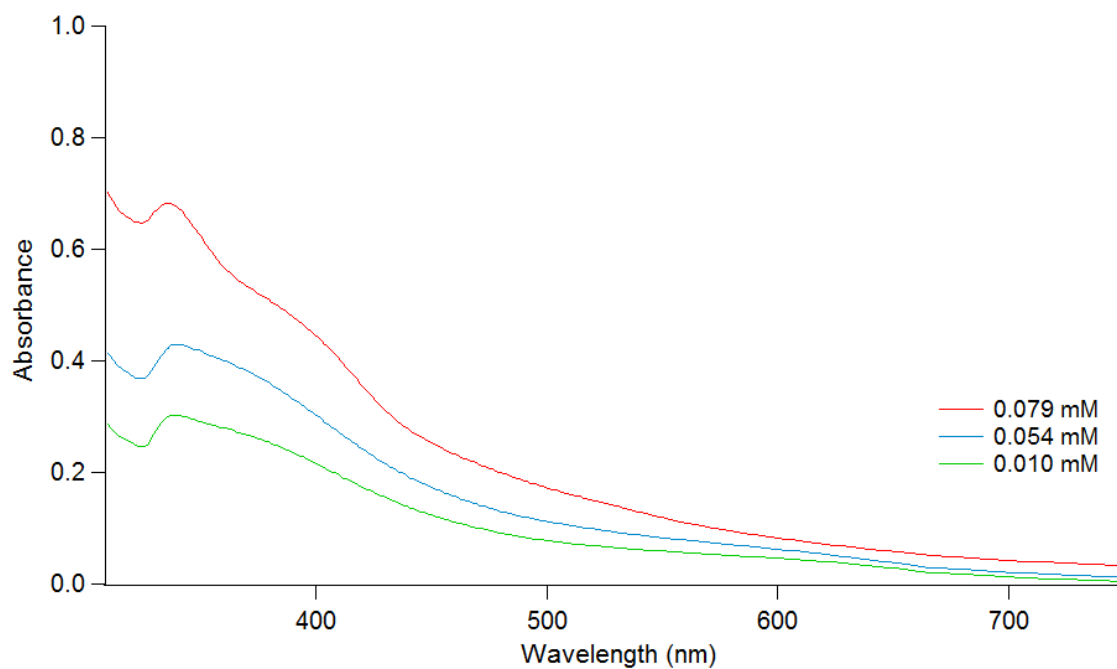
Figure B.42. UV-vis spectrum for complex **21** $Cr(NMes)(OR)_2$ at three different concentrations. λ_{max} (εM): 339 (14728).
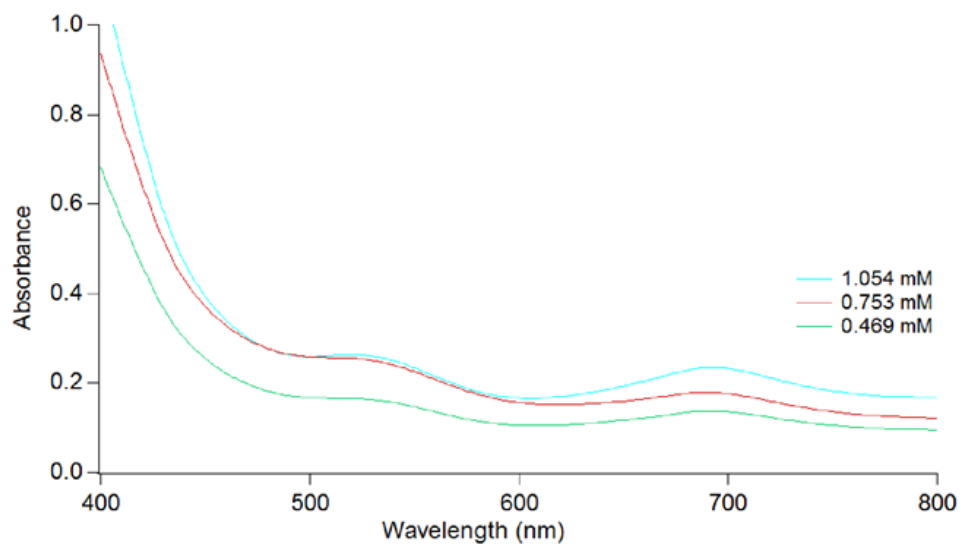
Figure B.43.UV-vis spectrum for complex **22** (Cr (OR)$_2$(NAd)) at three different concentrations. λ_{max} (ϵM): 530 (309), 695(250)
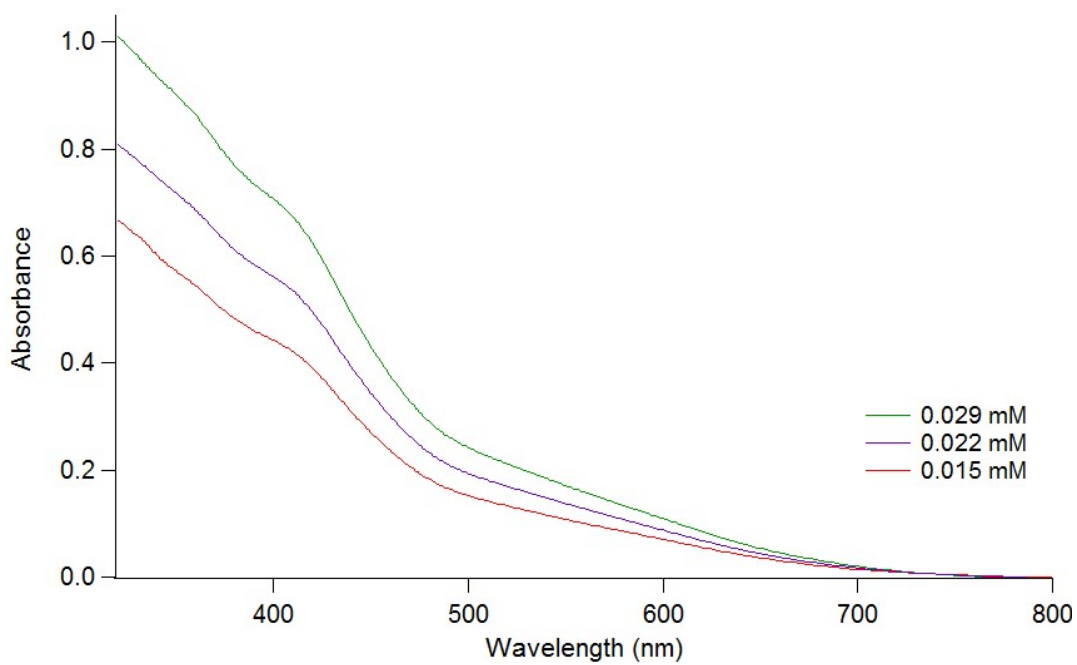
Figure B.44.UV-vis spectrum for complex **24** Cr(OR)$_2$(NPhOMe)$_2$ at three different concentrations. λ_{max} (ϵM): 415 (24409).
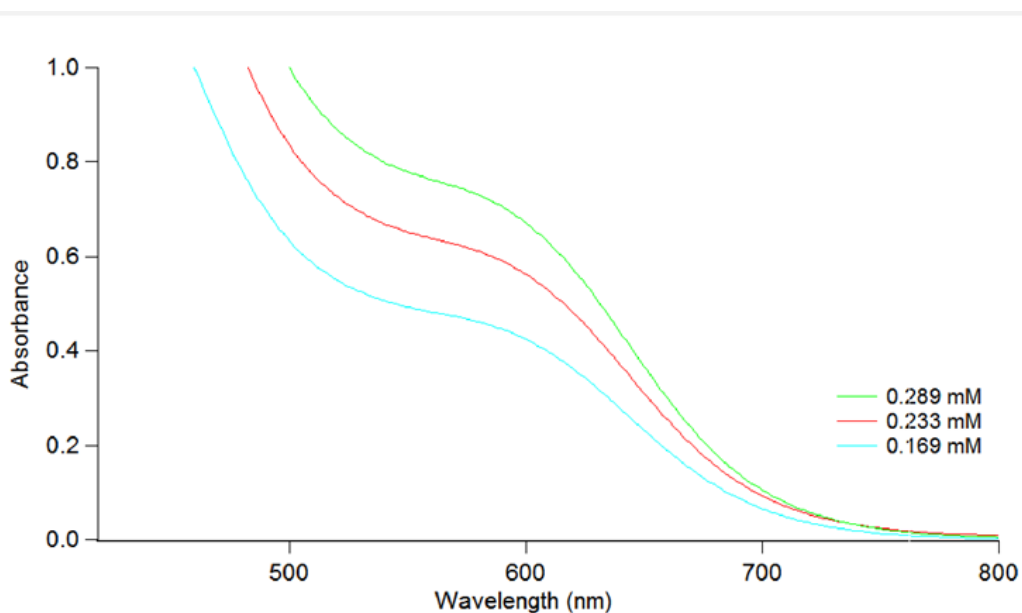
Figure B.45. UV-vis spectrum for complex **25** (Cr(OR)$_2$(NPhCF$_3$)$_2$). λ_{max} (εM): 600 (2415).
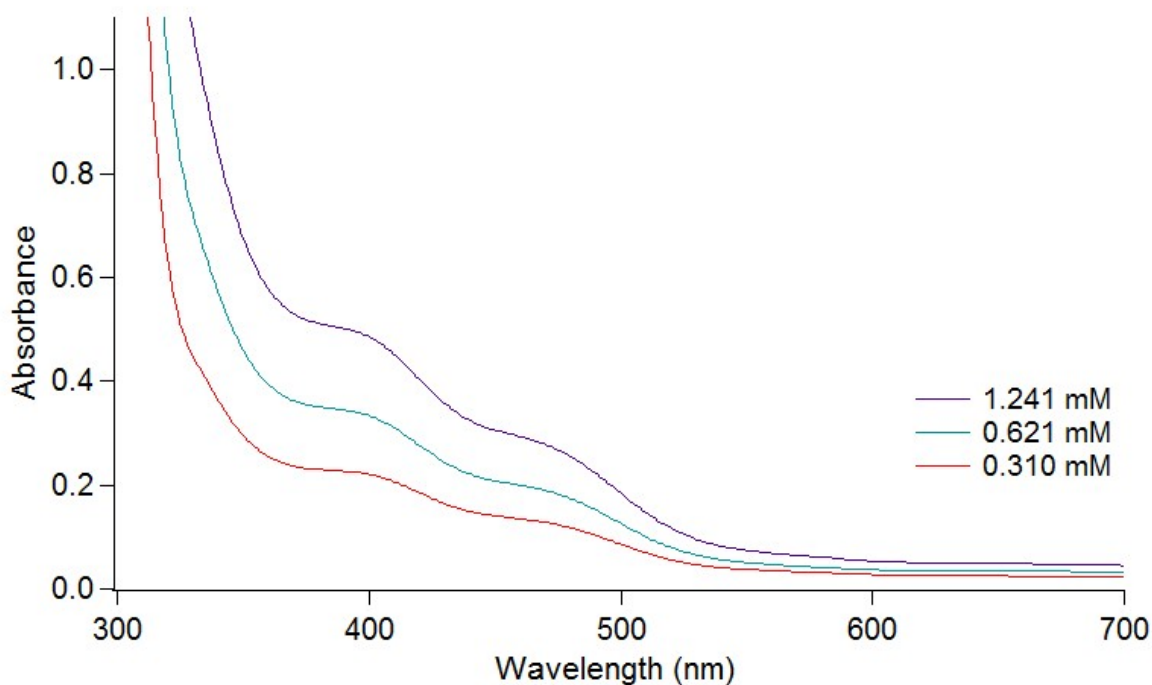
Figure B.46. UV-vis spectrum for complex **26** Cr(OR)$_2$(CNR)$_4$ at three different concentrations. λ_{max} (εM): 401 (544), 479 (296).

6. Mass Spectra
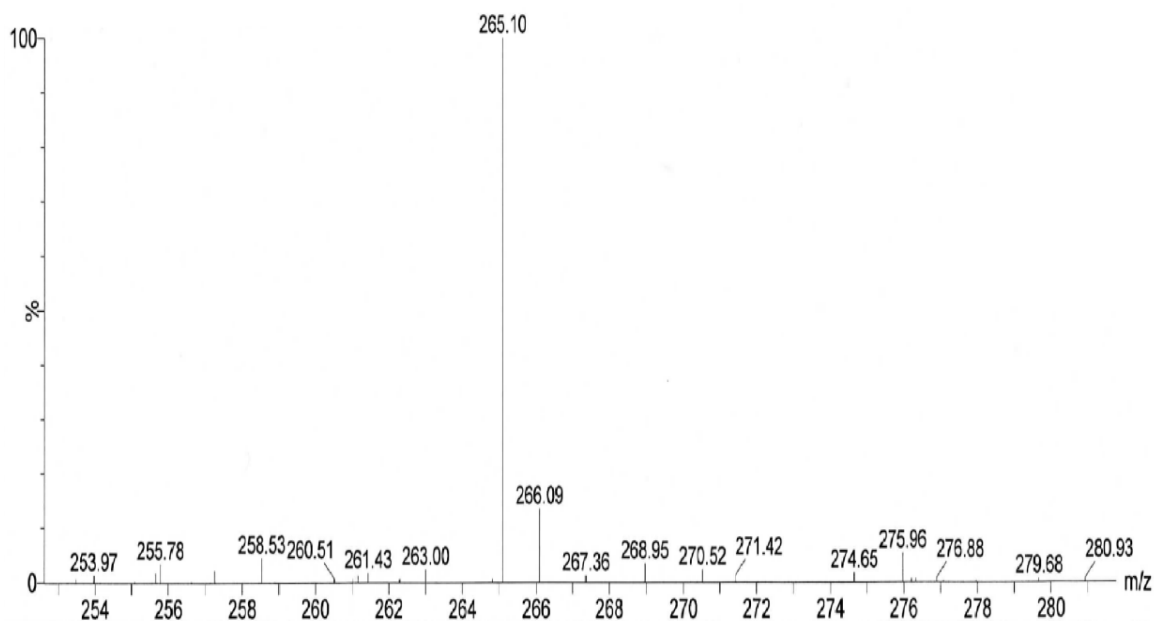
Figure B.47. MesPhNCN(2,6-Me$_2$C$_6$H$_3$). [M+H] = 265.
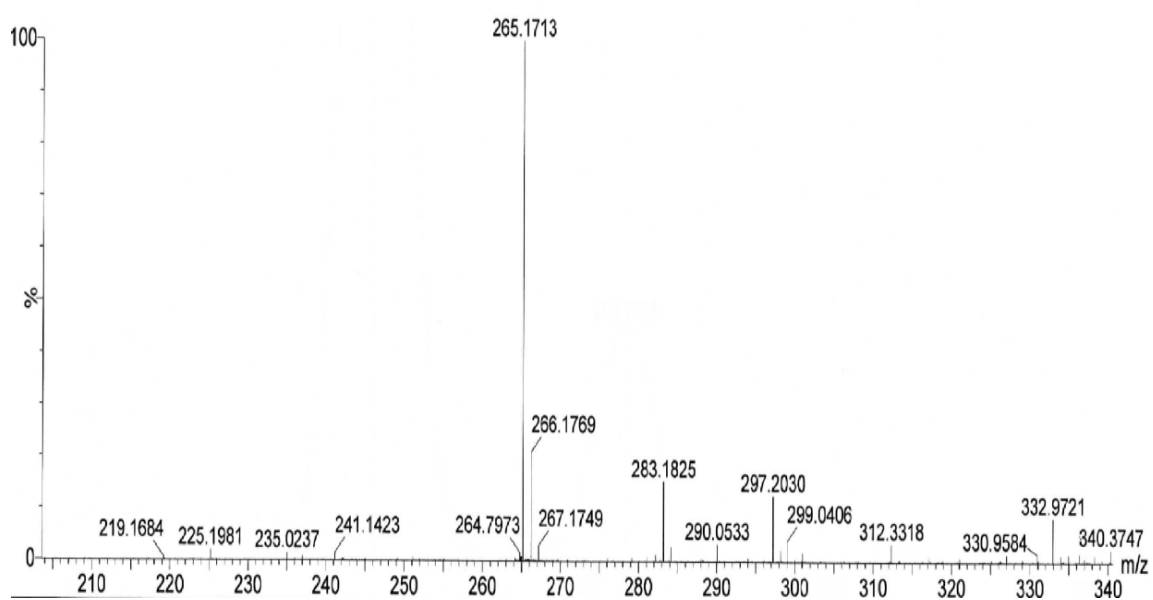
Figure B.48. 2-^{i}PrPhNCN(2,6-Me$_2$C$_6$H$_3$). [M+H] = 265.
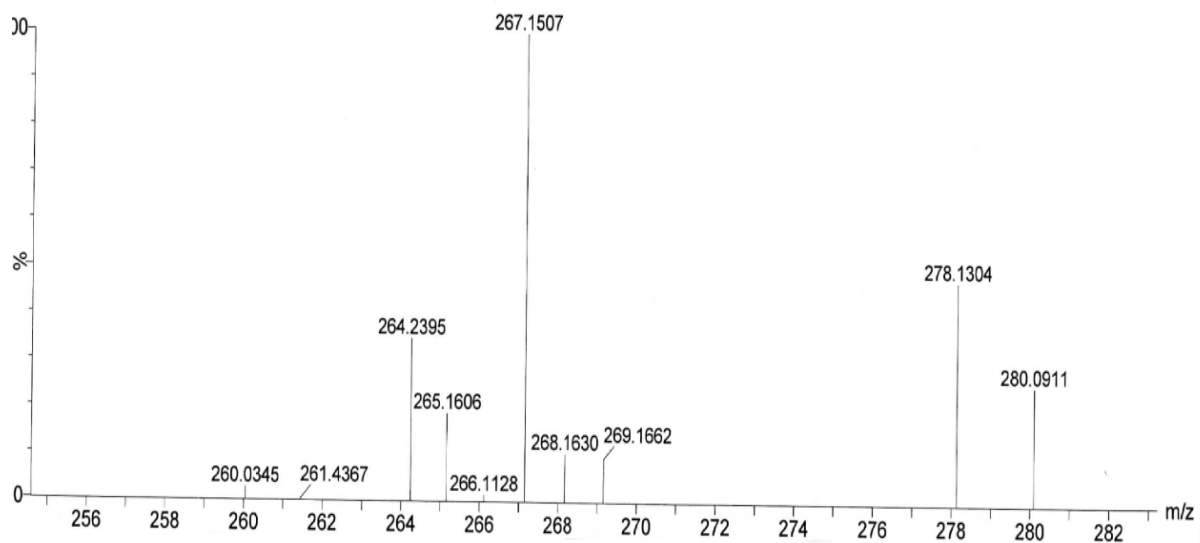
Figure B.49. MesPhNCN (4-OCH$_3$C$_6$H$_4$). [M+H] = 267.
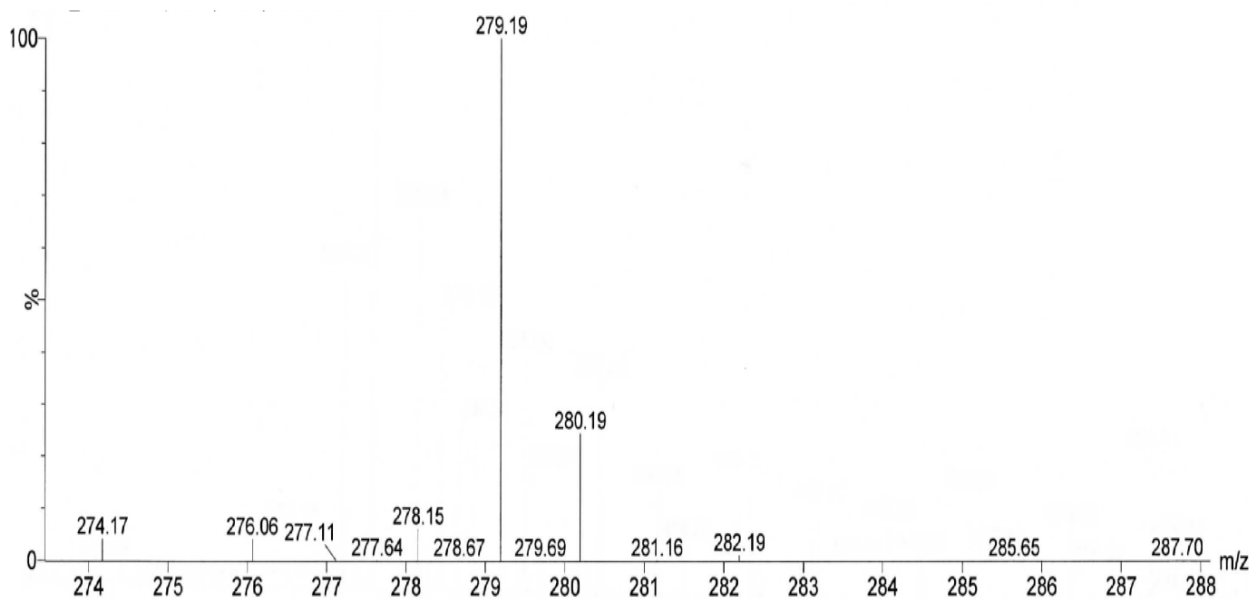
Figure B.50. (2,6-Et$_2$ C$_6$H$_3$)NCN(2,6-Me$_2$C$_6$H$_3$). [M+H] = 279.
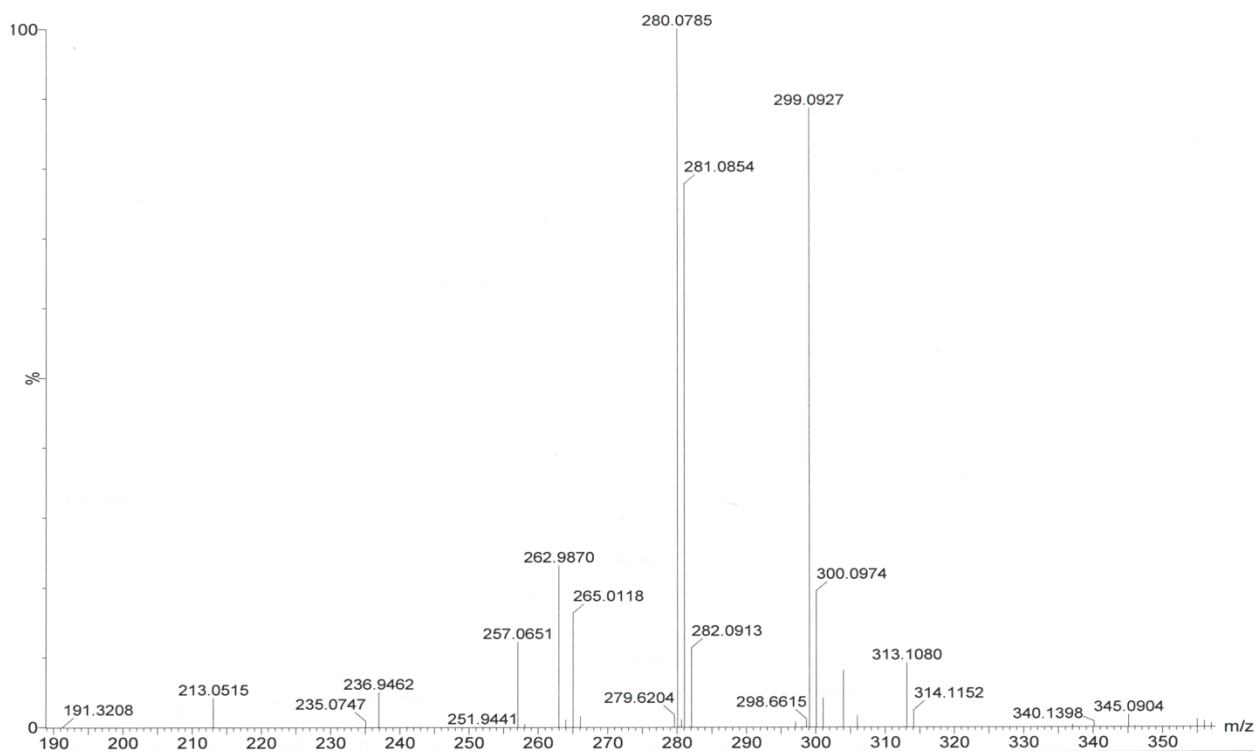
Figure B.51. (2,6-Et$_2$C$_6$H$_3$)NC N(4-OCH$_3$C$_6$H$_4$). [M+H] = 281.
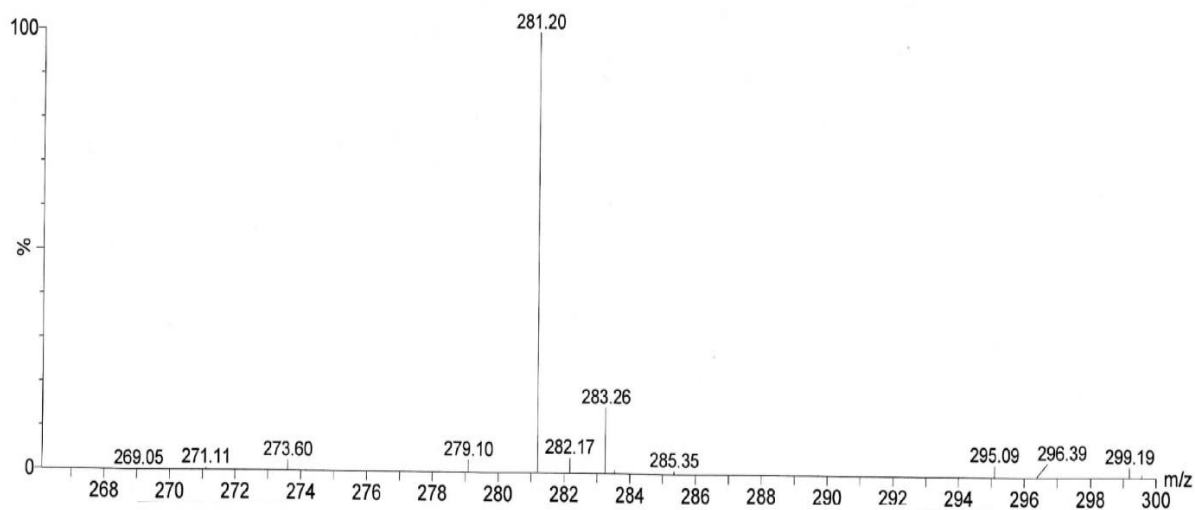
Figure B.52. AdPhNCN(2,6-Me$_2$C$_6$H$_3$)**.** [M+H] = 281.
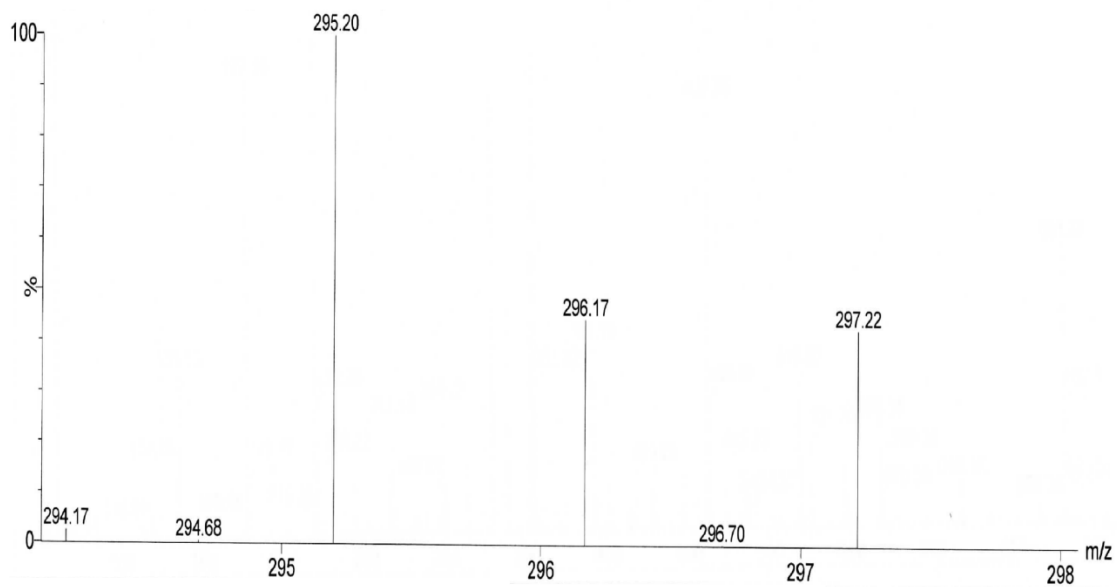
Figure B.53. MesNCNAd. [M+H] = 295.

APPENDIX C: SUPPLEMENTARY MATERIAL FOR CHAPTER 3

1. Crystal Structure Not Shown in Chapter 3
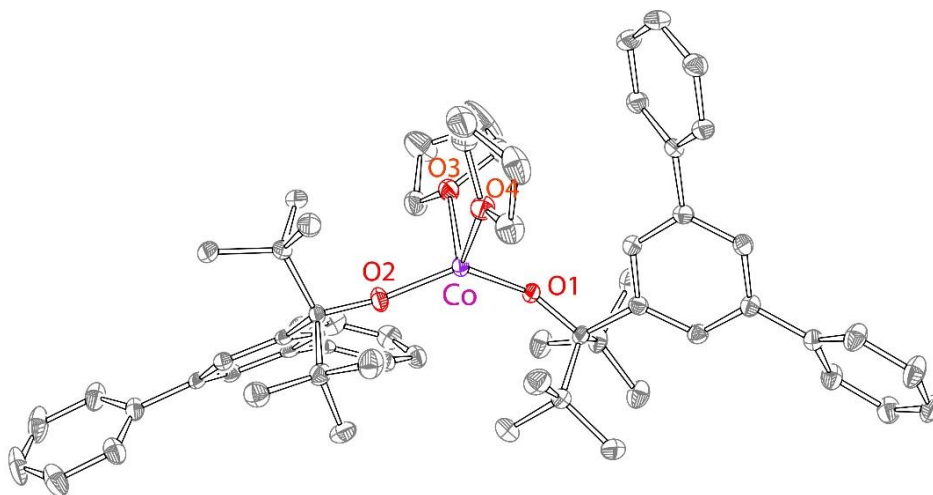
Figure C.1. X-ray structure of Co(OR')$_2$(THF)$_2$ (**32**).

2. Synthesis of Co(OR')$_2$(THF)$_2$ (32). Reaction was carried in N$_2$-filled glovebox. To a solution of 5.0 mL of Co(N(SiMe$_3$)$_2$)$_2$(THF)$_2$ (38.20mg, 0.073 mmol) in THF, the solution of HOR' (57.1 mg, 0.153 mmol) in THF was added dropwise. The solution changed color slowly from green to purple. The reaction was stirred for two hours, upon which the solvents were removed in vacuo to yield purple residue. Crystallization from hexanes at −35 °C overnight gave purple crystals of complex **32** (63.3 mg, 92%). $\mu_{eff} = 3.71\mu_B$. IR (cm^{-1}): 2882 (m), 1589 (w), 1497 (m), 1416 (m), 1358 (w), 1134 (w),1015 (s), 864 (s), 745 (s). Anal. Calcd: C, 78.7; H, 8.31. Found: C, 76.8; H, 8.3.

3. Evans Method and Procedure

Table C.1. Spin-only magnetic moments calculated for **30** and **31** using Evans method.

Complex	μ_{obs} (1) (μ_B)	μ_{obs} (2) (μ_B)	μ_{obs} (3) (μ_B)	μ_{obs} (average) (μ_B)
30	4.2	4.2	4.2	4.2±0.5
31	4.7	5.0	4.4	4.7±0.3

4. NMR Spectra
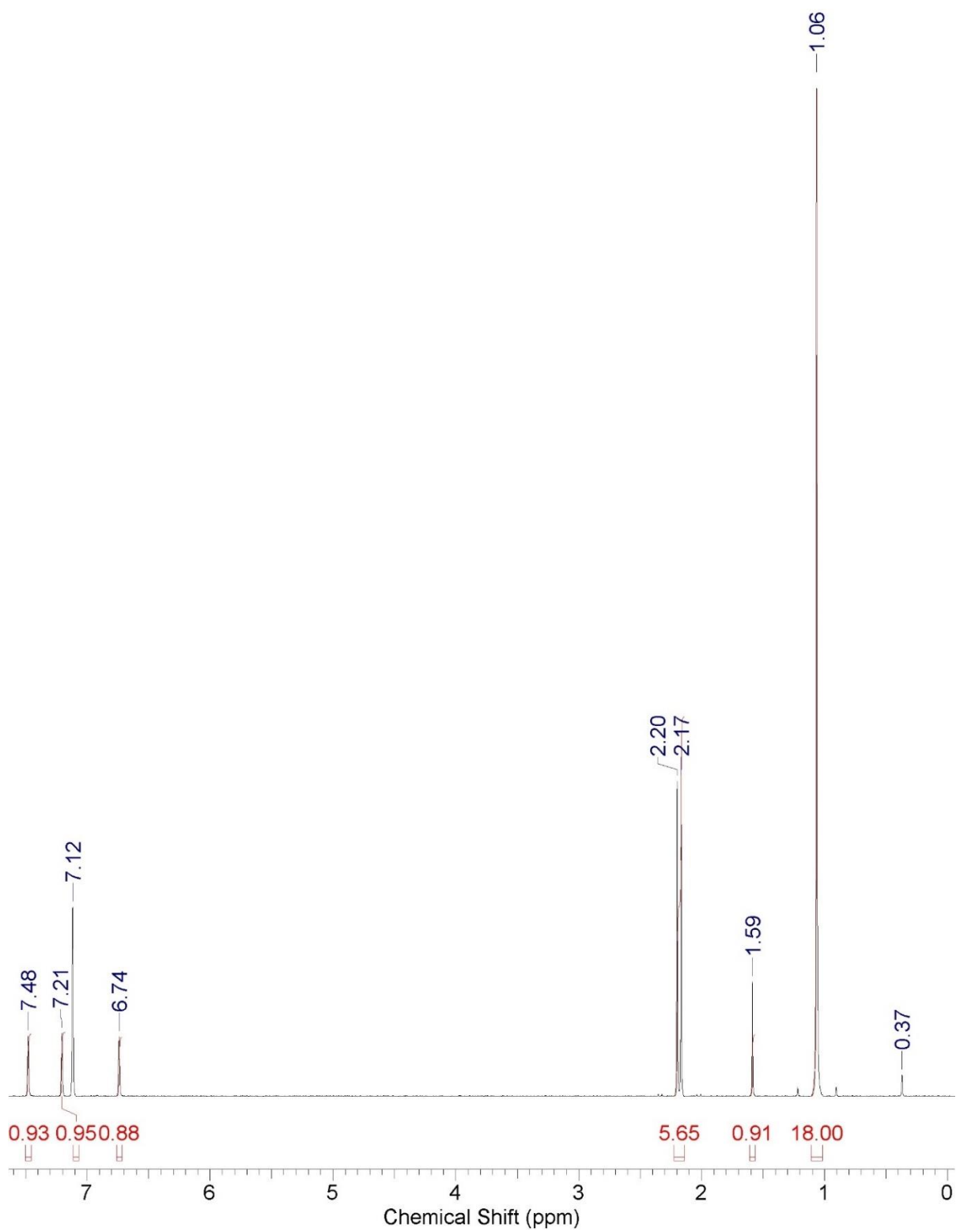
Figure C.2. ^{1}H NMR spectrum of the compound **27**.
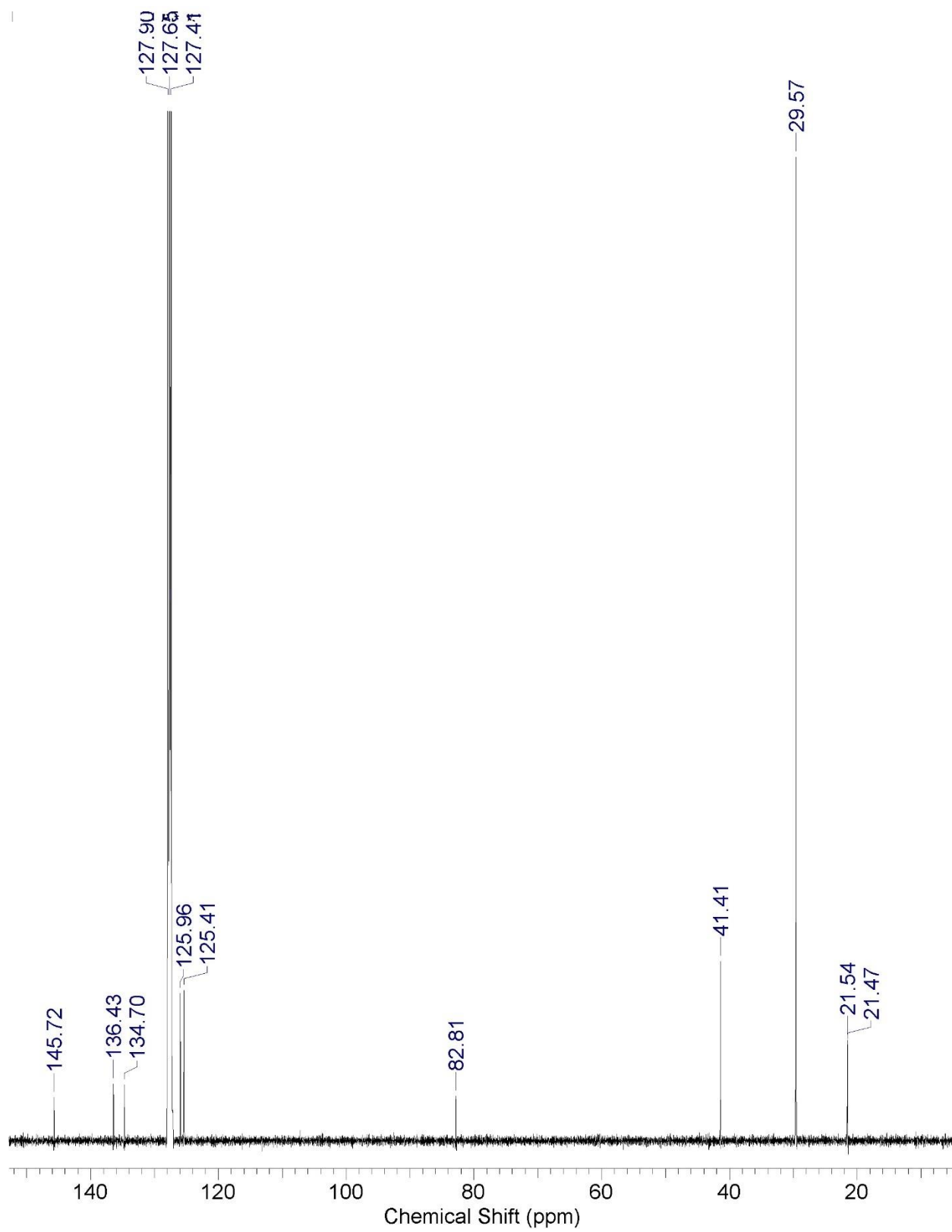
Figure C.3. ^{13}C NMR spectrum of the compound **27**.
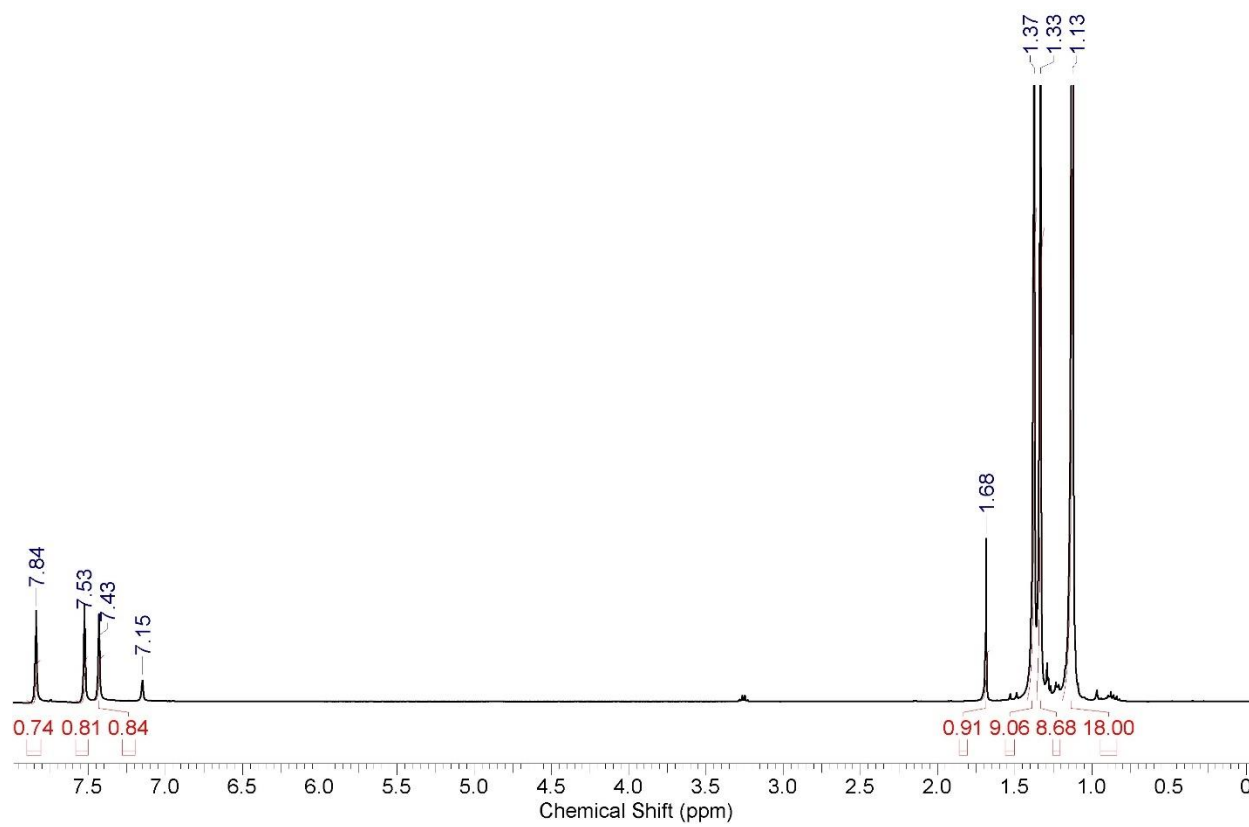
Figure C.4. ^{1}H NMR spectrum of the compound **28**.
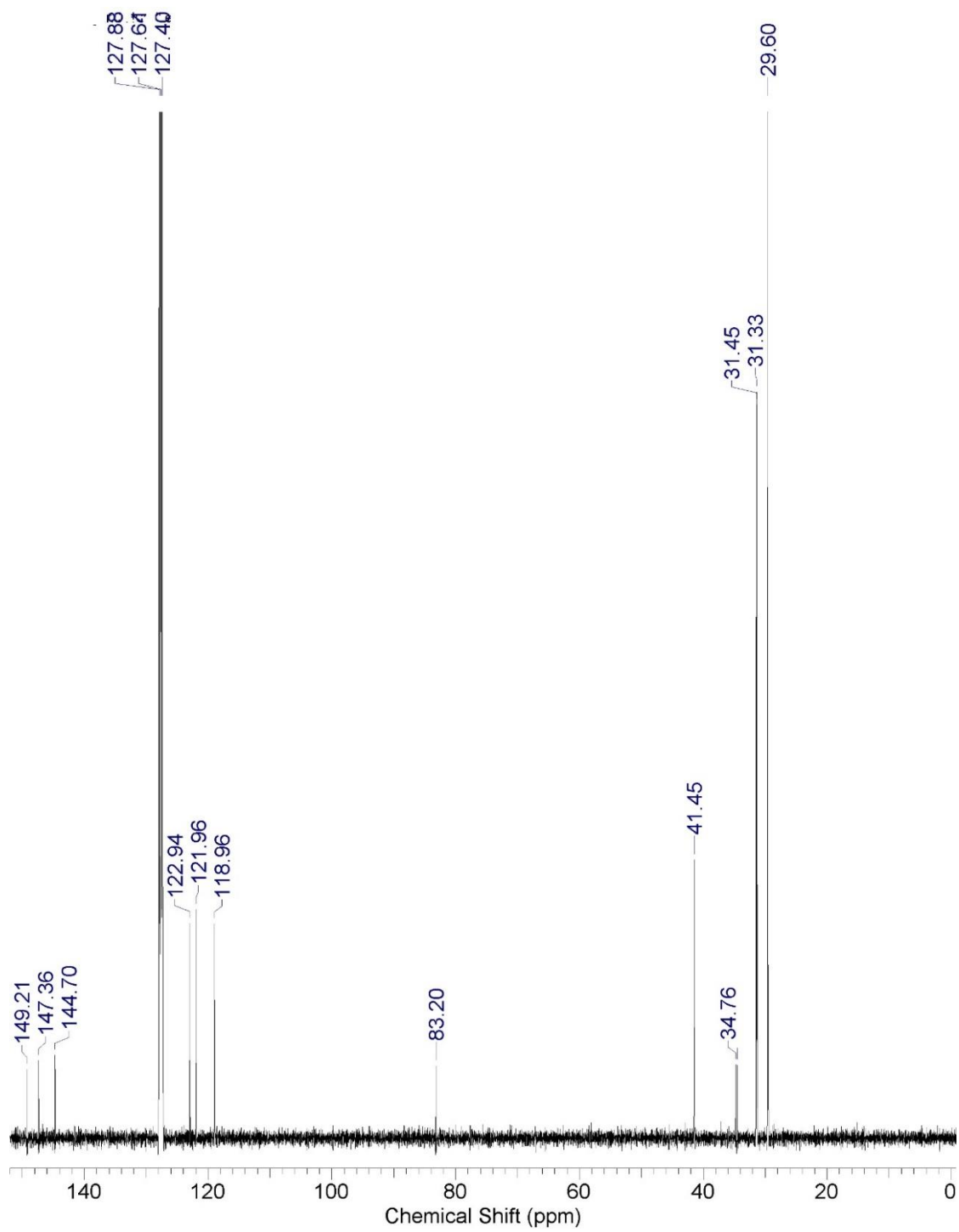
Figure C.5. ^{13}C NMR spectrum of the compound **28**.
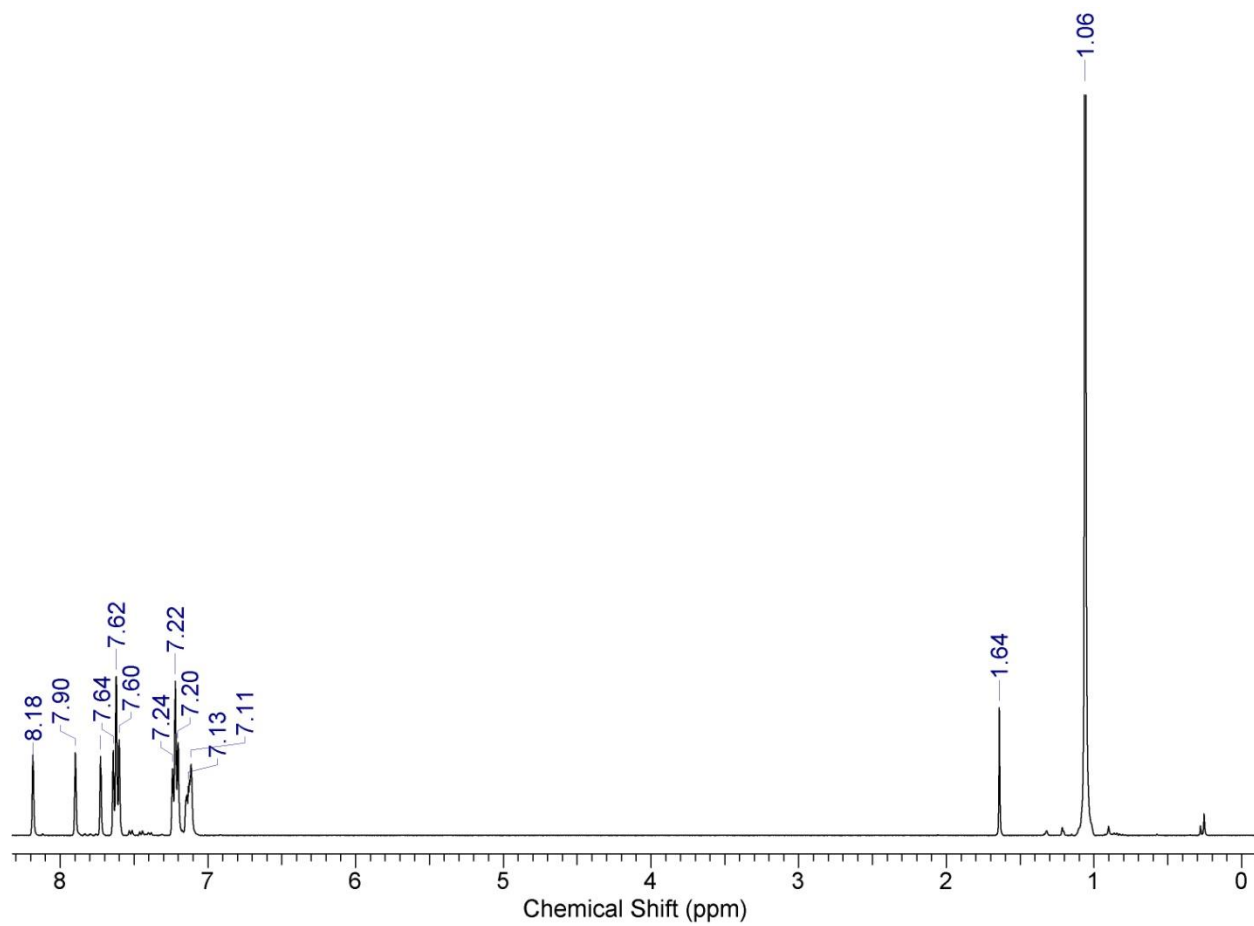
Figure C.6. ^{1}H NMR spectrum of the compound **29**.
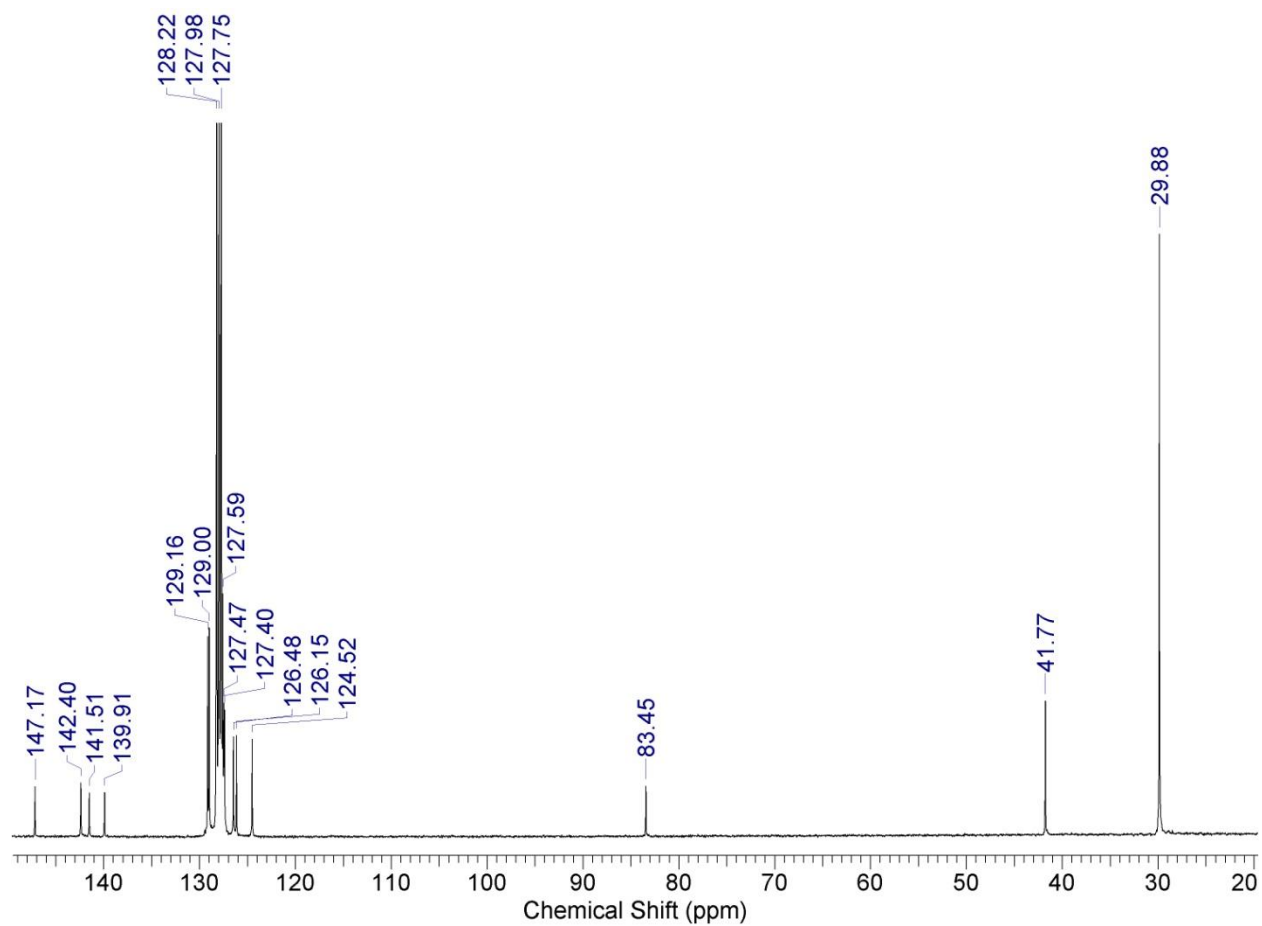
Figure C.7. ^{13}C NMR spectrum of the compound **29**.

5. IR spectra
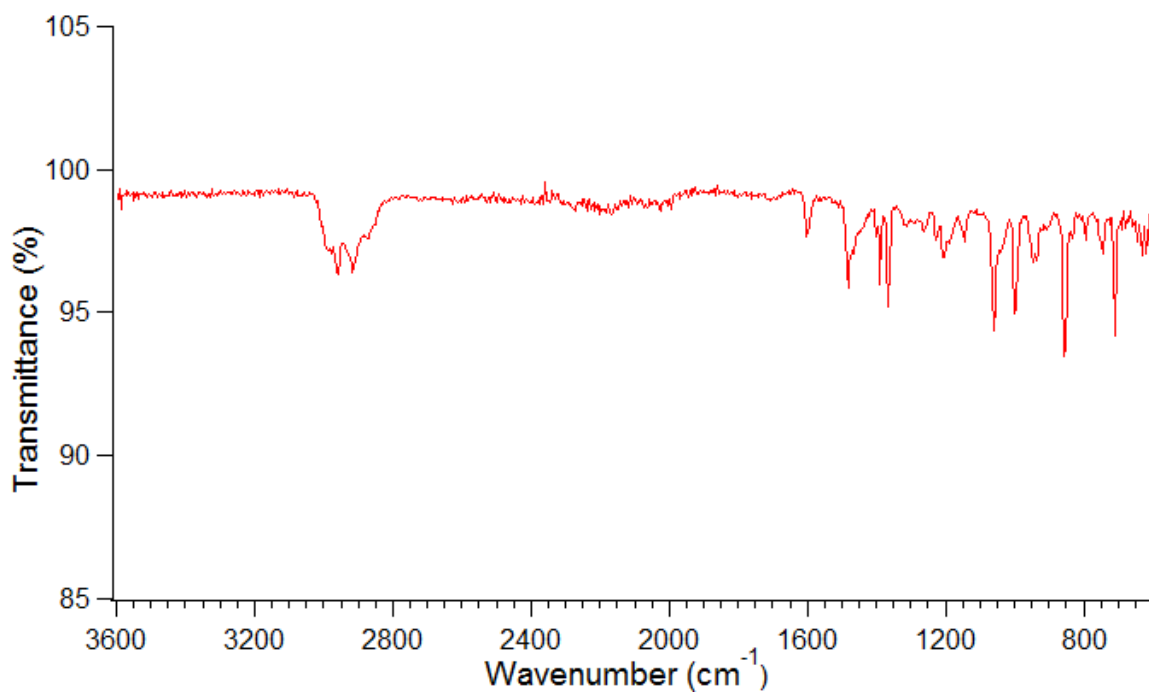
Figure C.8. IR spectra of compound **27**.
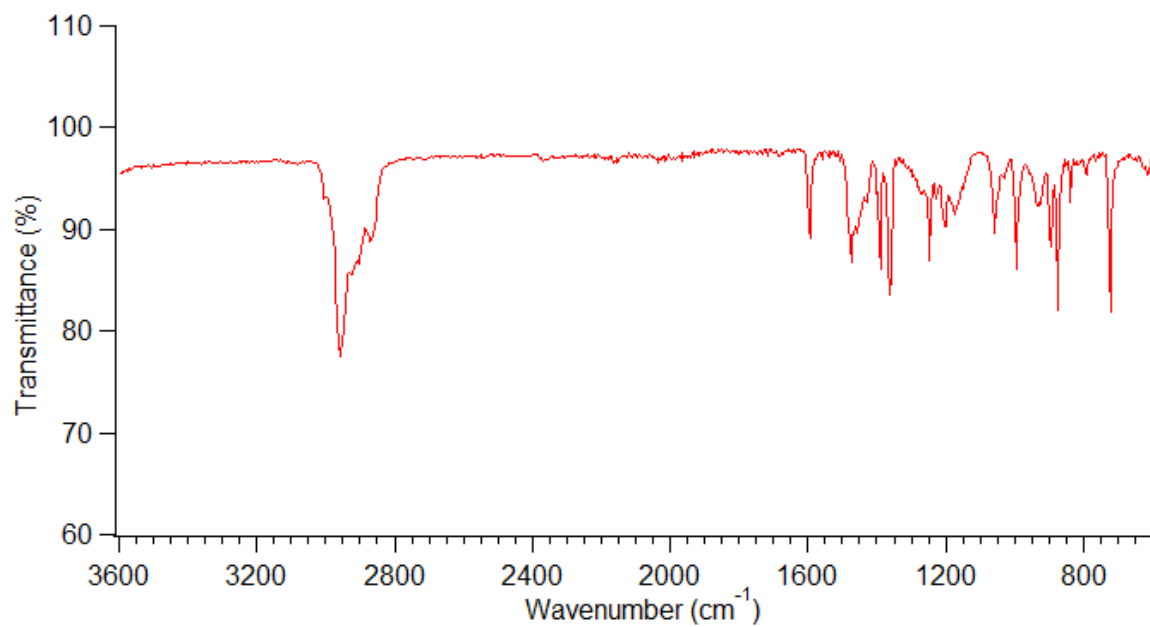
Figure C.9. IR spectra of compound **28**.
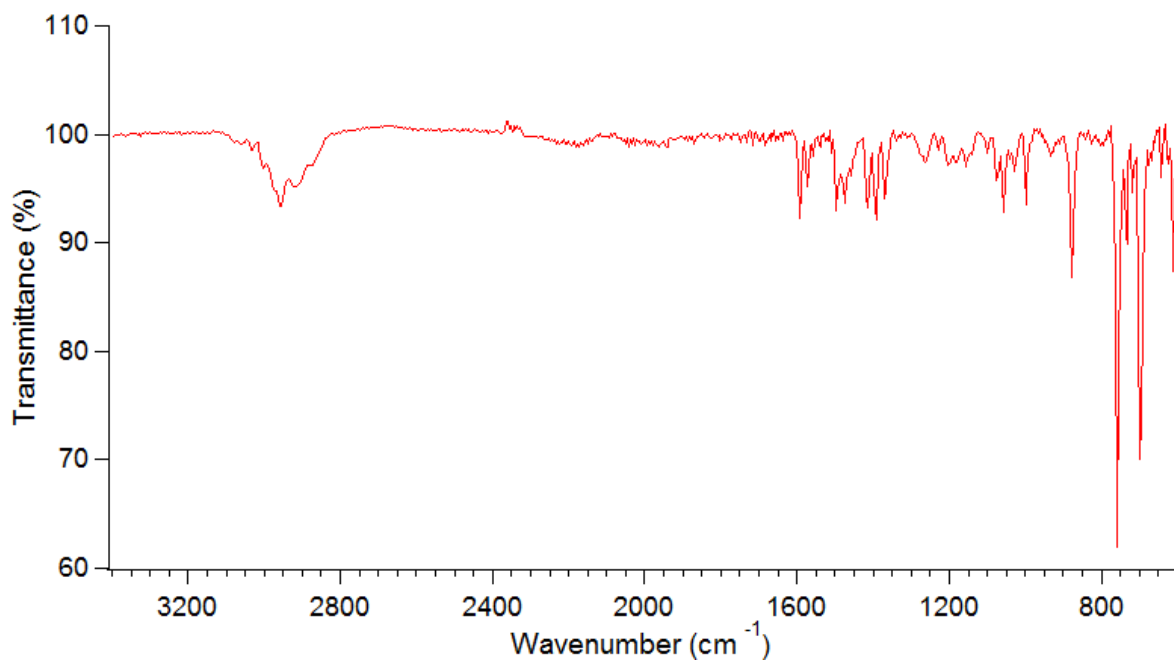
Figure C.10. IR spectra of compound **29**.
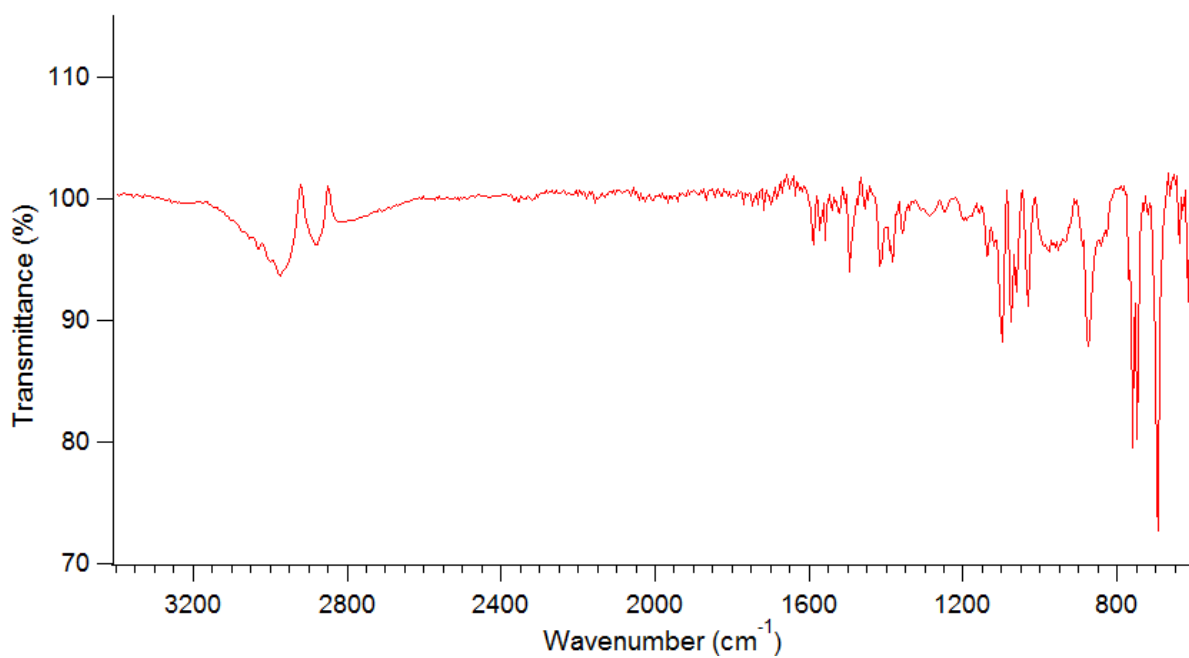
Figure C.11. IR spectra of compound **30**.
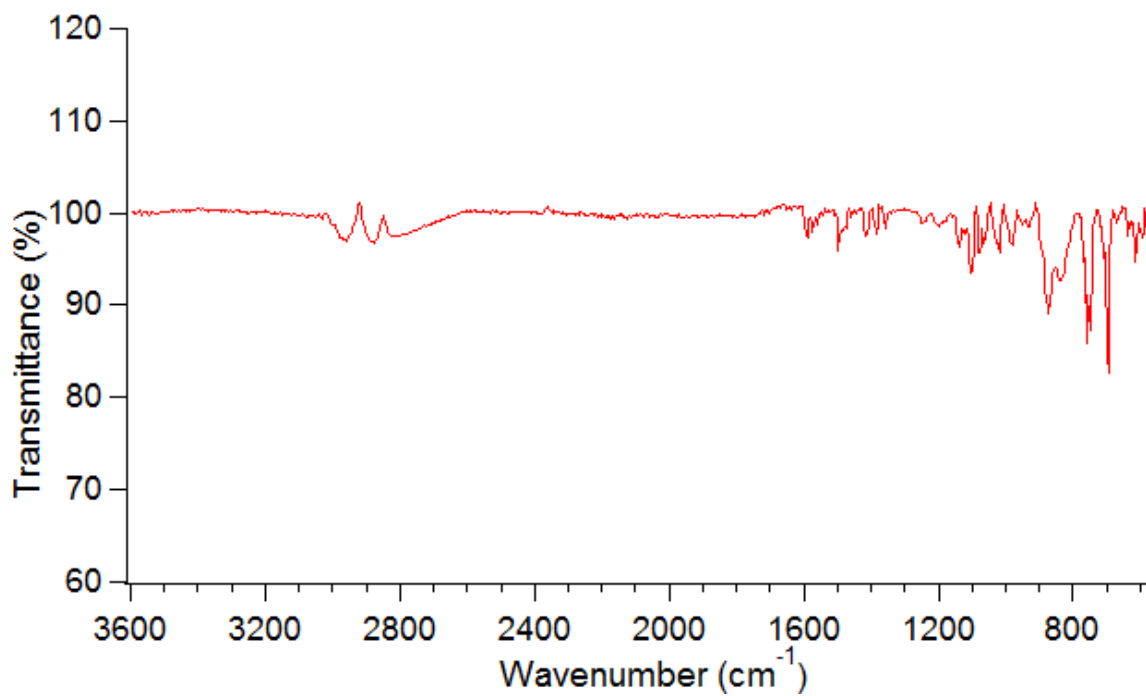
Figure C.12. IR spectra of compound **31**.
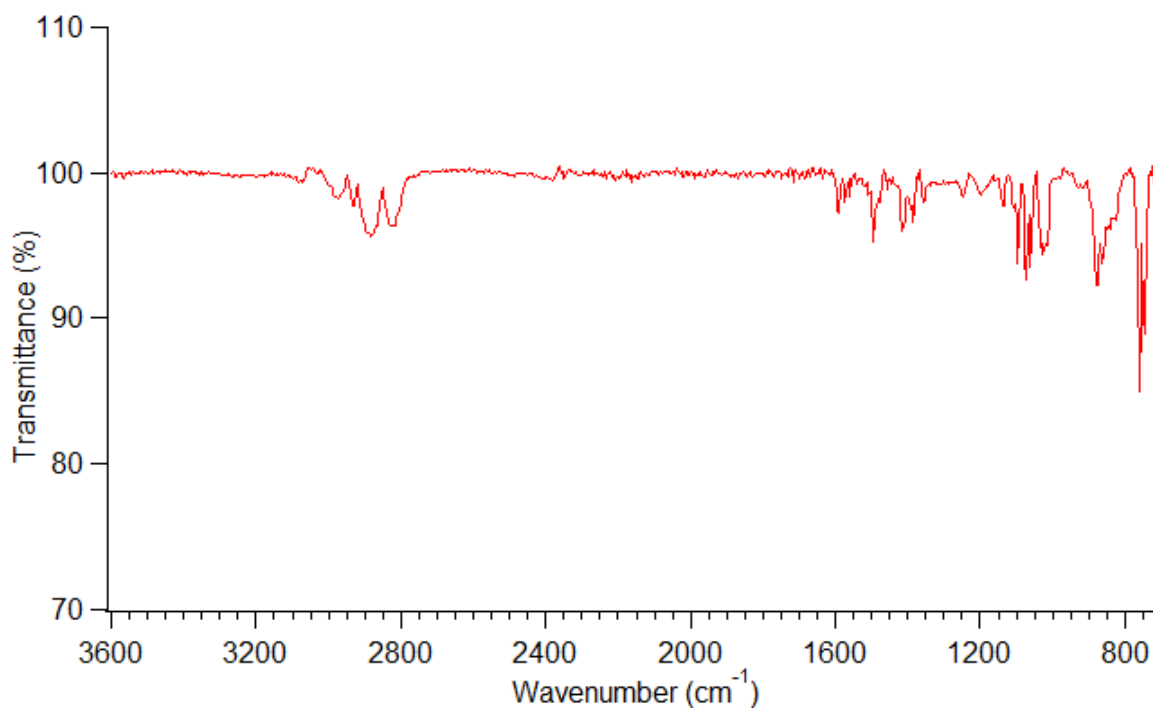
Figure C.13. IR spectra of compound $Co(OR')_2(THF)_2$ (**32**).

6. UV-Vis Spectra
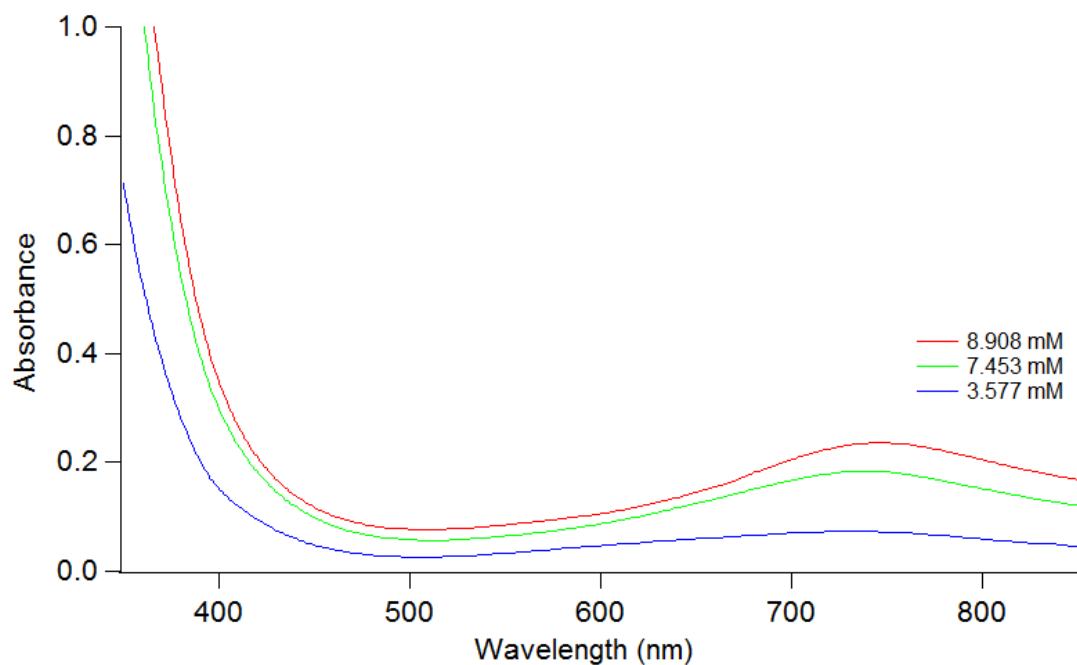
Figure C.14. UV-vis spectrum for complex $Cr(OR')_2(THF)_2$ **30** at three different concentrations. λ_{max} (ε_M): 730 (24).
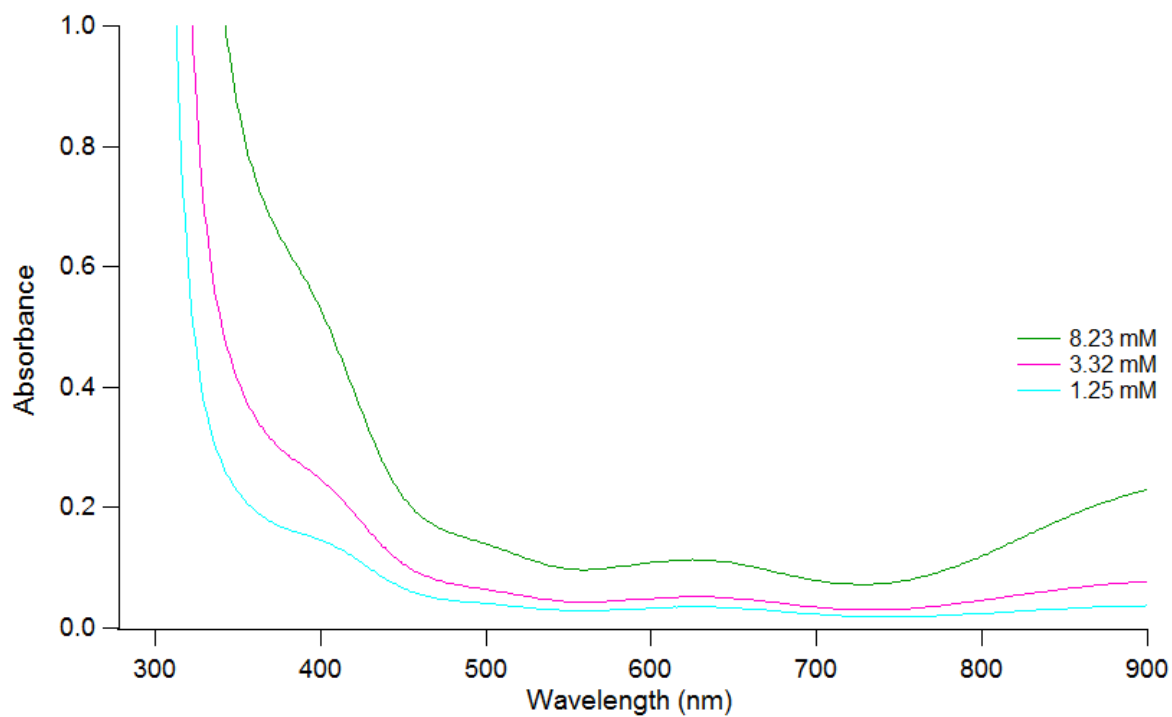
Figure C.15. UV-vis spectrum for complex $Fe(OR')_2(THF)_2$ **31** at three different concentrations. λ_{max} (ε_M): 628 (20).

APPENDIX D: SUPPLEMENTARY MATERIAL FOR CHAPTER 4

1. Evans Method and Procedure

Table D.1. Spin-only magnetic moments calculated for **33-36** using Evans method.

Complex	μ_{obs} (1) (μ_B)	μ_{obs} (2) (μ_B)	μ_{obs} (3) (μ_B)	μ_{obs} (average) (μ_B)
33	4.5	4.2	4.3	4.3$\pm$0.2
34	4.2	4.3	4.5	4.3$\pm$0.2
35	4.5	4.0	3.9	4.1$\pm$0.3
36	4.5	4.5	4.4	4.4$\pm$0.2

2.Mass Spectra
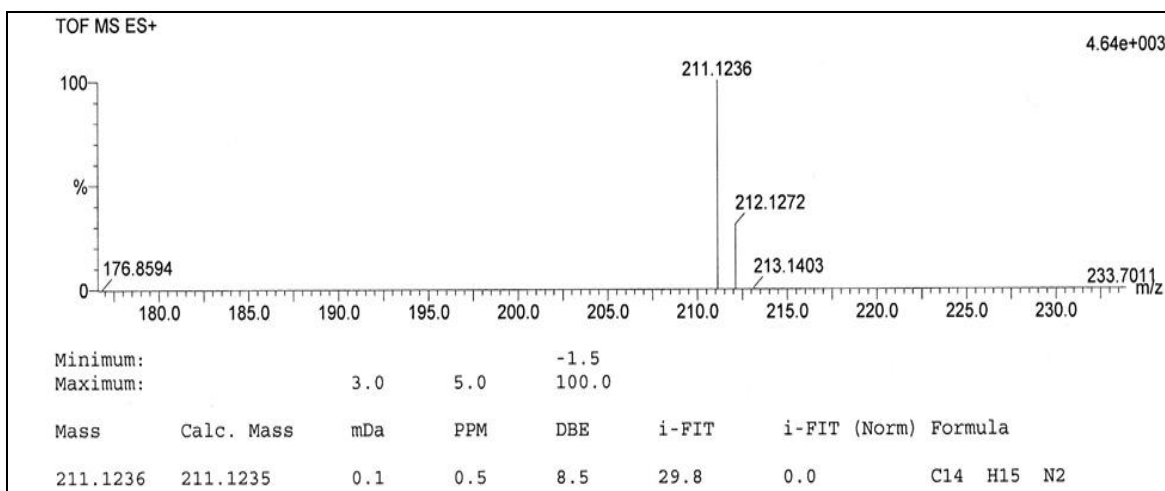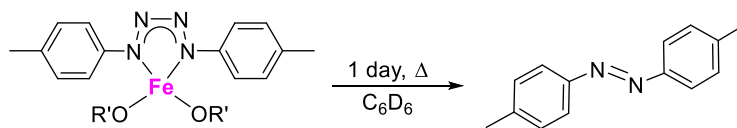
Figure D.1. Formation of (4-MeC$_6$H$_4$)N=N(4-MeC$_6$H$_4$) from complex **34**. [M+H]
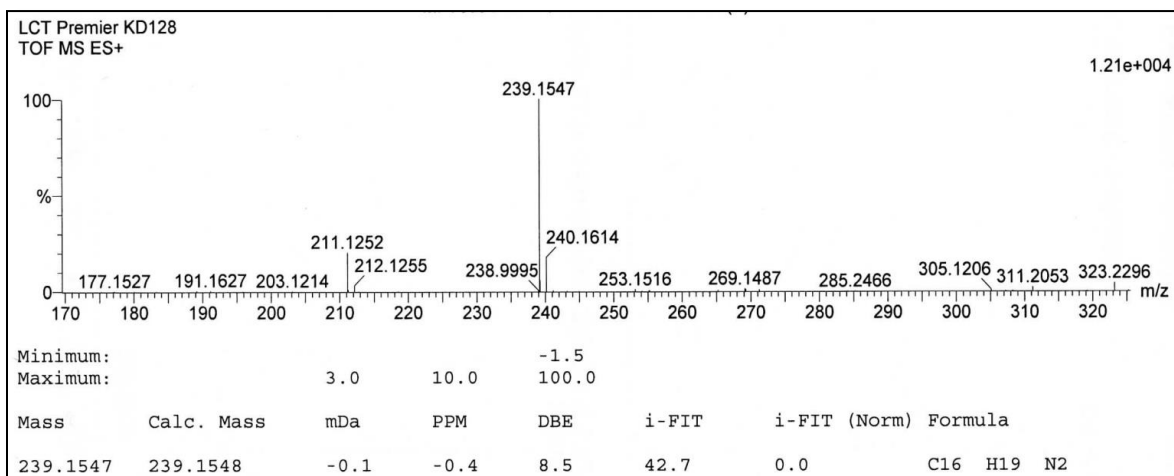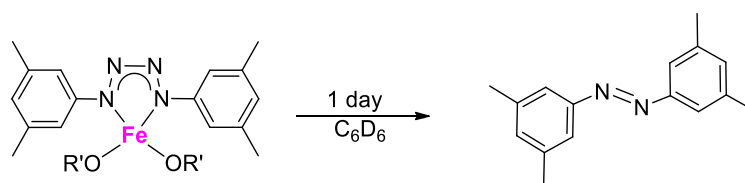
Figure D.2. Formation of $(3,5\text{-Me}_2C_6H_3)N=N(3,5\text{-Me}_2C_6H_3)$ from complex **36**. [M+H]
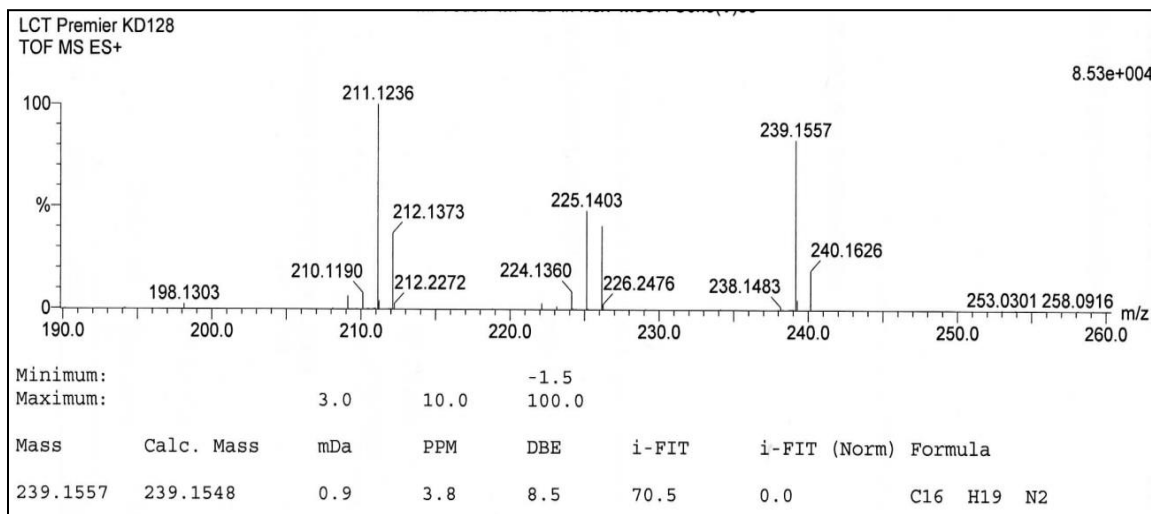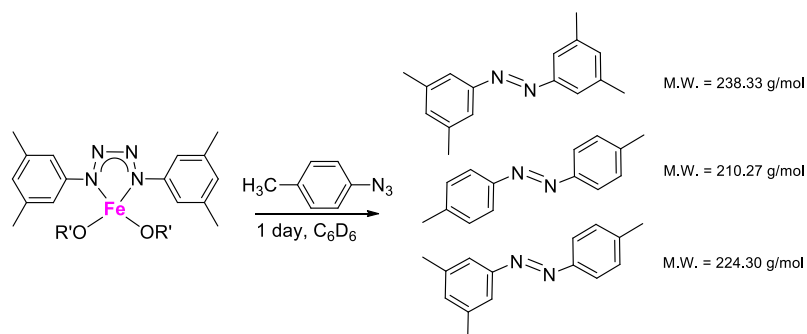
Figure D.3. Formation of the three different azoarenes from complex **36** [M+H].

3. NMR Spectra
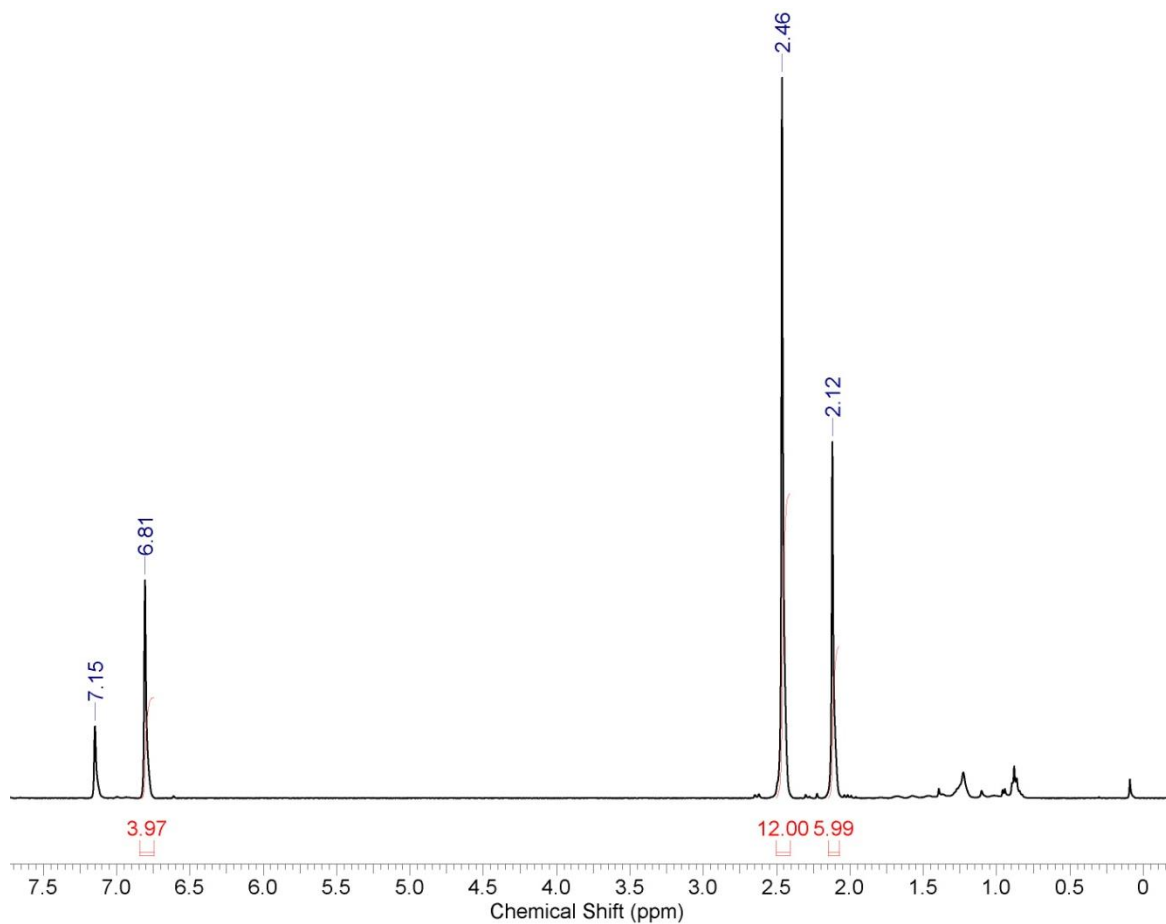
Figure D.4. ^{1}H NMR spectrum demonstrating catalytic formation of MesN=NMes in C_6D_6 by complex **31**.
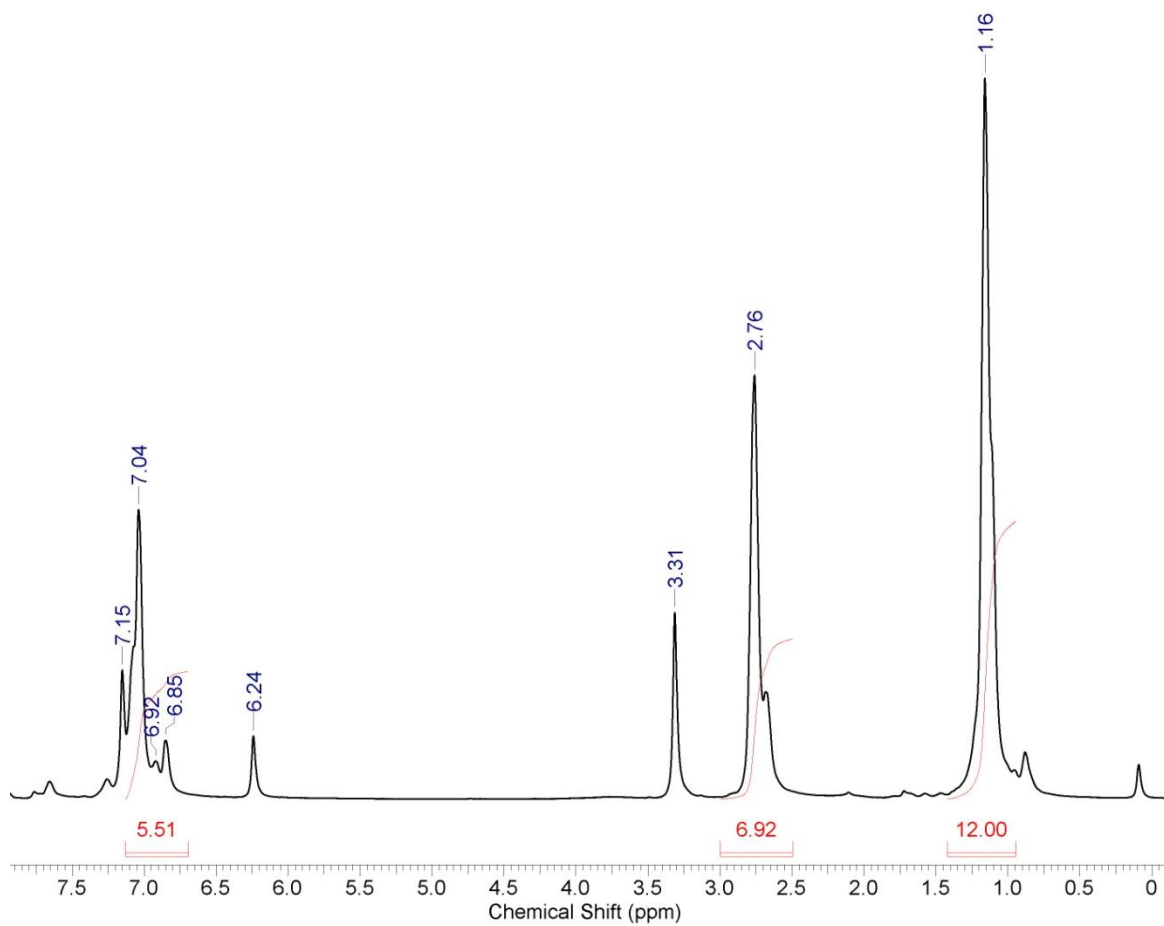
Figure D.5. ^{1}H NMR spectrum demonstrating catalytic formation of $(2,6\text{-}Et_2Ph)N=N(2,6\text{-}Et_2Ph)$ in C_6D_6 by complex **31**.
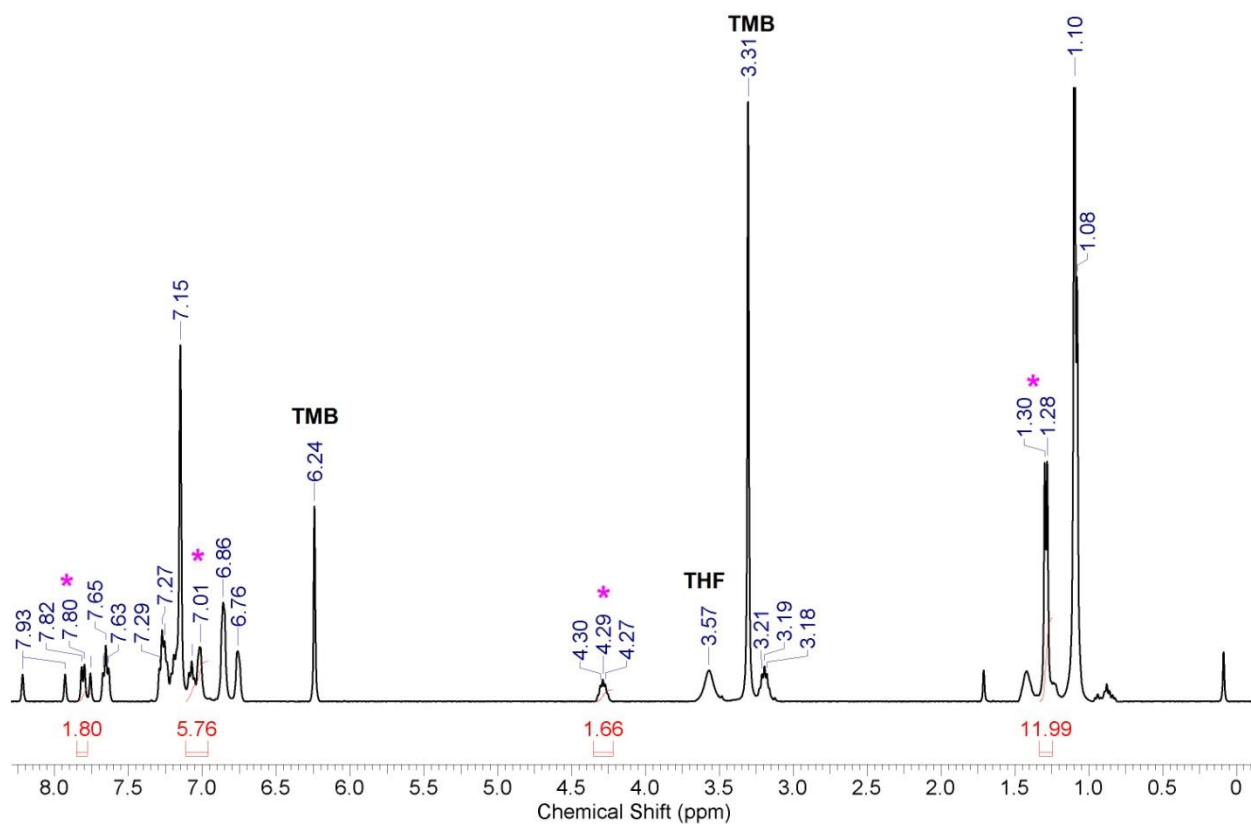
Figure D.6. ^{1}H NMR spectrum demonstrating catalytic formation of (2-$i$prC$_6$H$_4$)N=N(2-$i$prC$_6$H$_4$)in C$_6$D$_6$ by complex **31**.
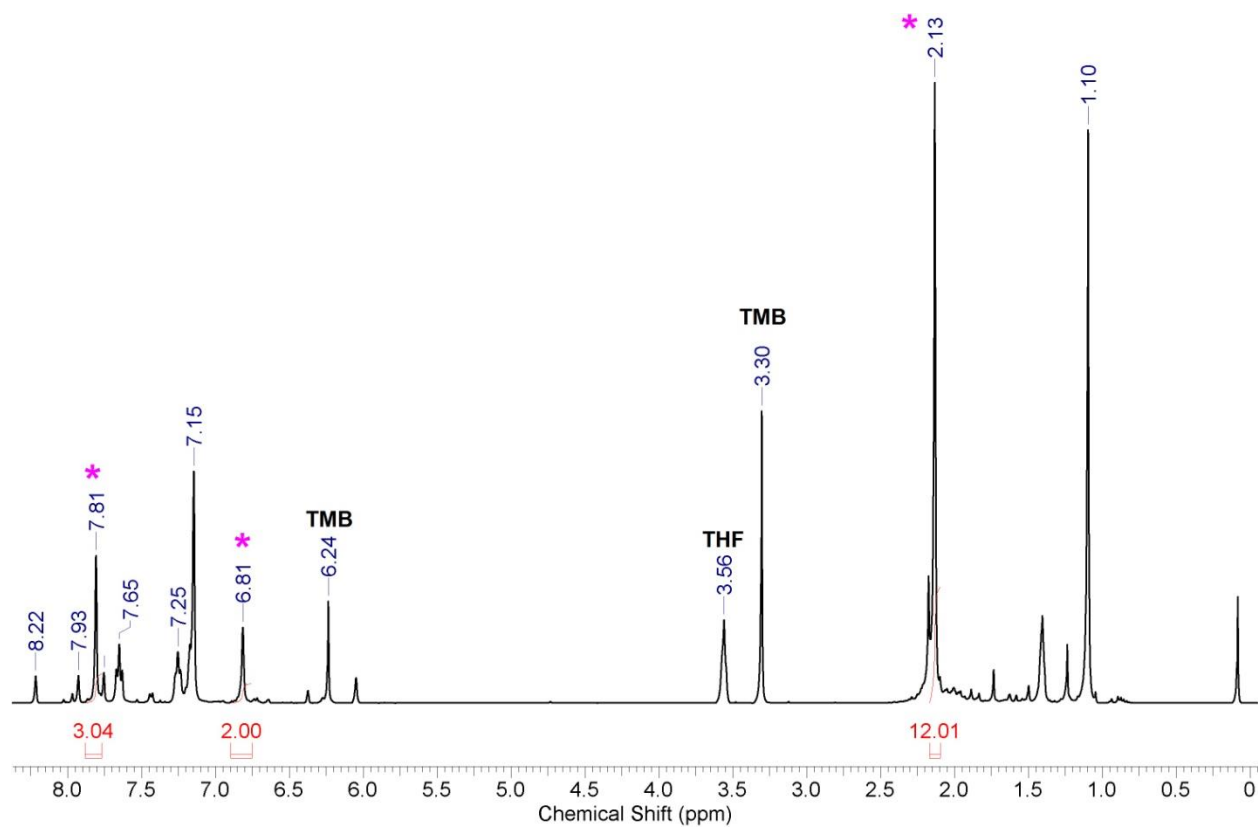
Figure D.7. ^{1}H NMR spectrum demonstrating catalytic formation of (3,5-Me$_2$C$_6$H$_3$)N=N(3,5-Me$_2$C$_6$H$_3$) in C$_6$D$_6$ by complex **31**.
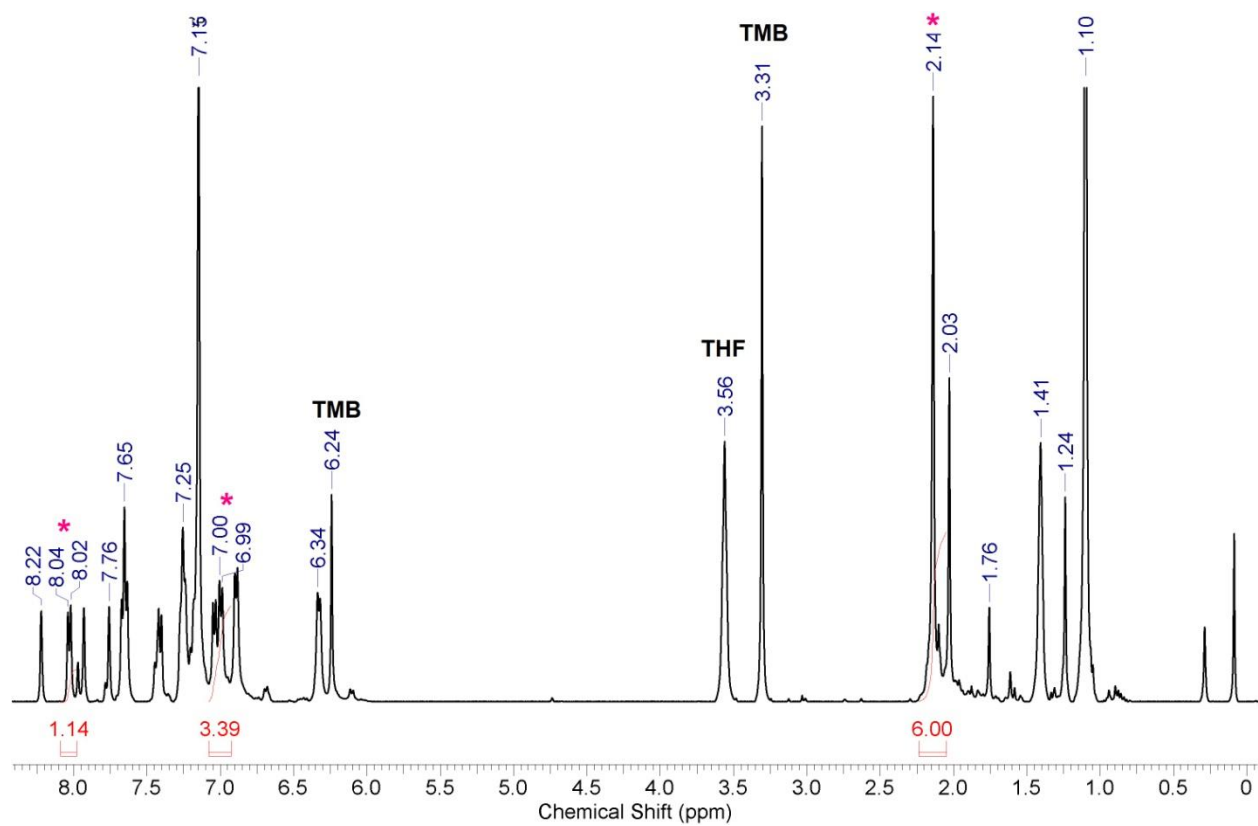
Figure D.8. ^{1}H NMR spectrum demonstrating catalytic formation of (4-CH$_3$C$_6$H$_4$)N=N(4-CH$_3$C$_6$H$_4$) in C$_6$D$_6$ by complex **31**.
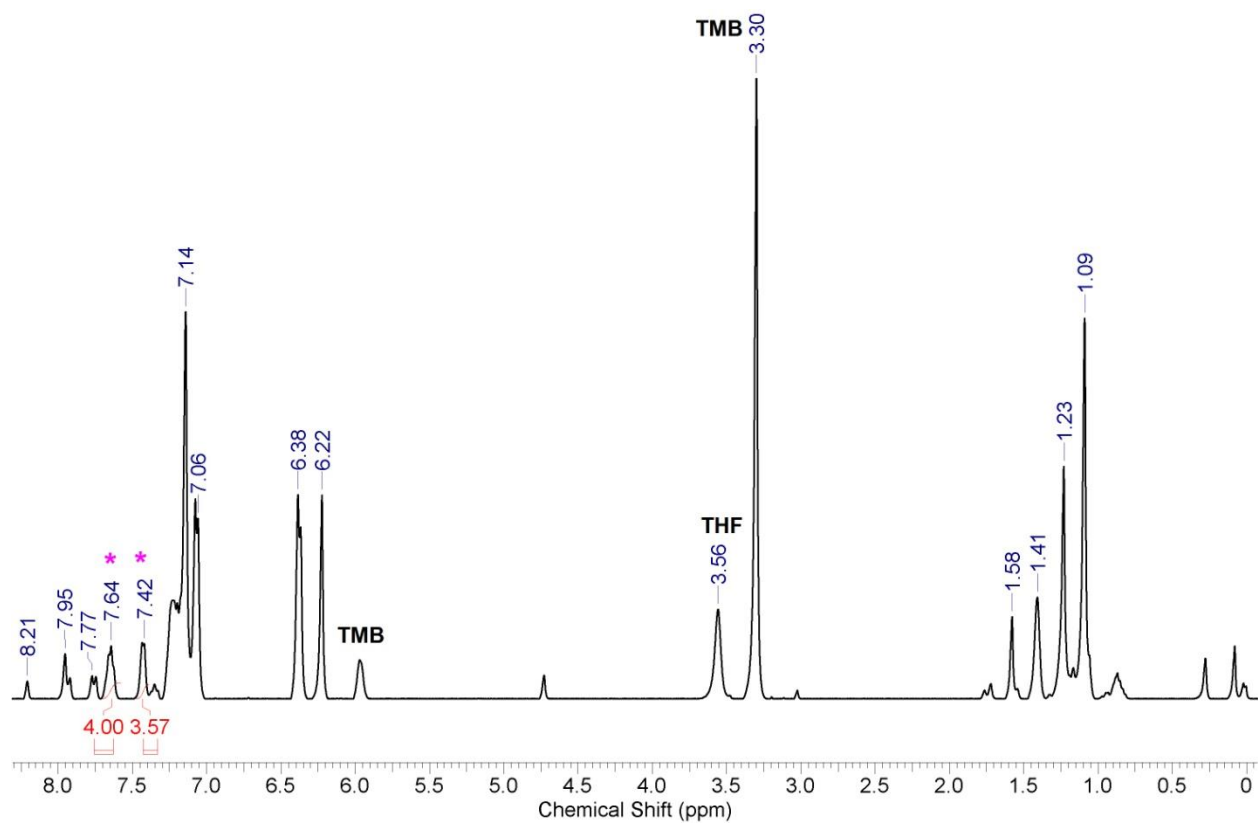
Figure D.9. ^{1}H NMR spectrum demonstrating catalytic formation of (4-CF$_3$C$_6$H$_4$)N=N(4-CF$_3$C$_6$H$_4$) in C$_6$D$_6$ by complex **31**.
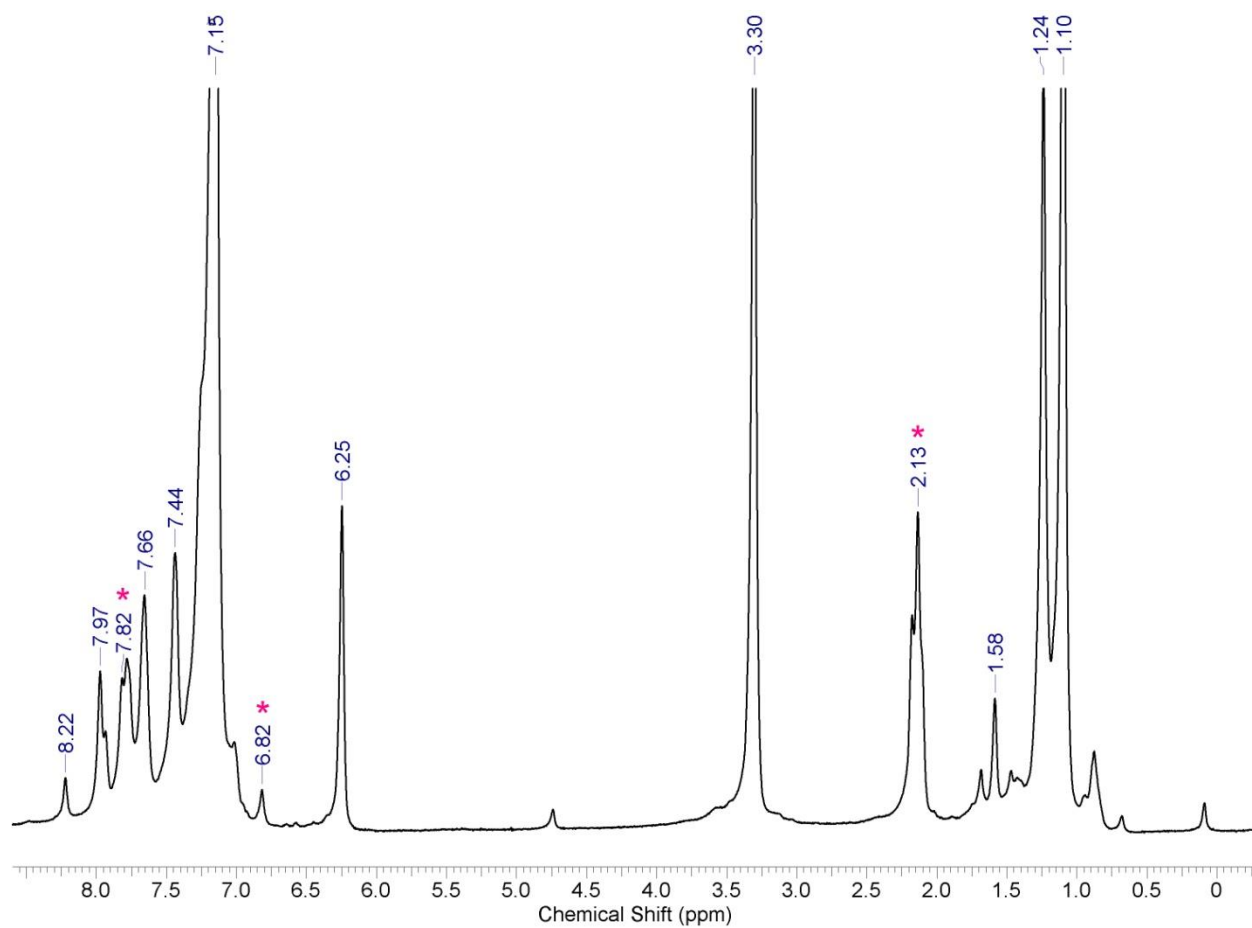
Figure D.10. ^{1}H NMR spectrum demonstrating formation of $(3,5\text{-Me}_2\text{C}_6\text{H}_3)\text{N=N}(3,5\text{-Me}_2\text{C}_6\text{H}_3)$ from complex **36** in C_6D_6.
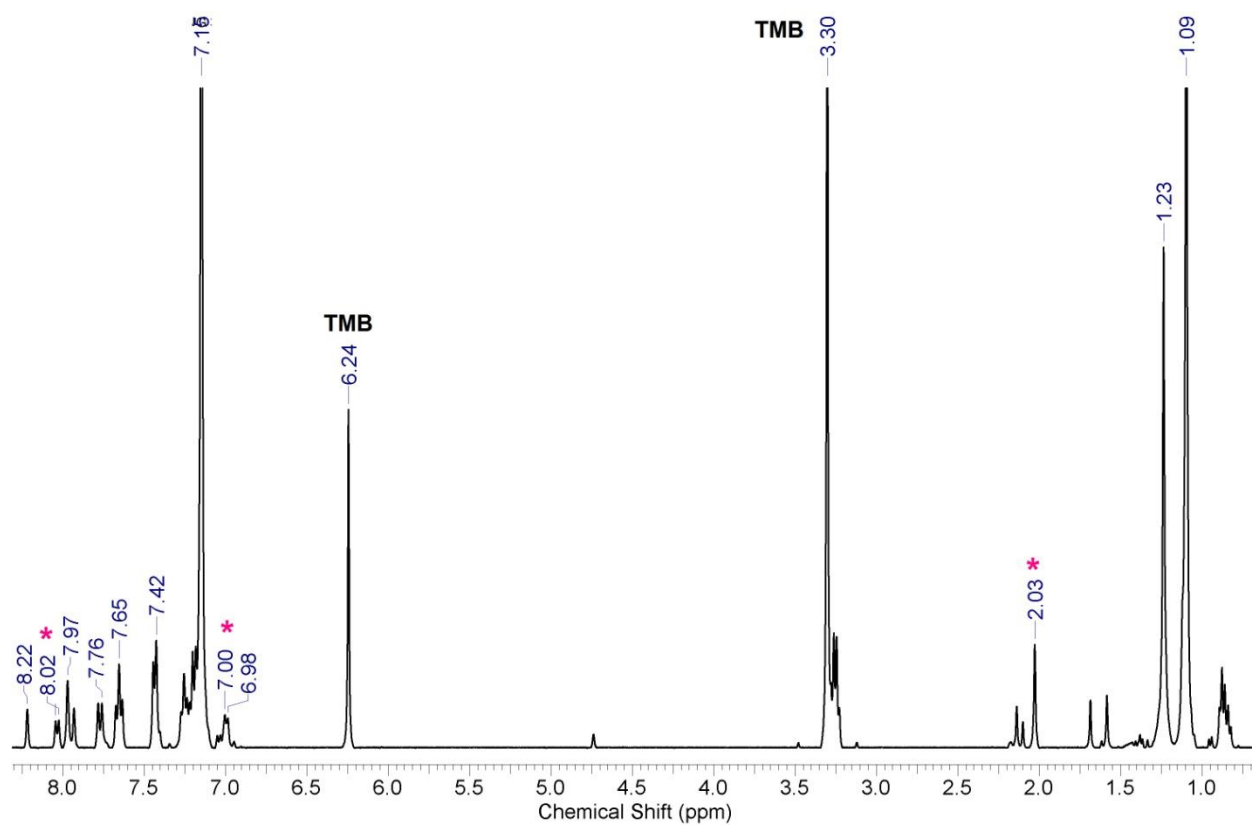
Figure D.11. ^{1}H NMR spectrum demonstrating formation of (4-MeC$_6$H$_4$)N=N(4-MeC$_6$H$_4$) from complex **34** in C$_6$D$_6$.

4. High-Frequencey EPR
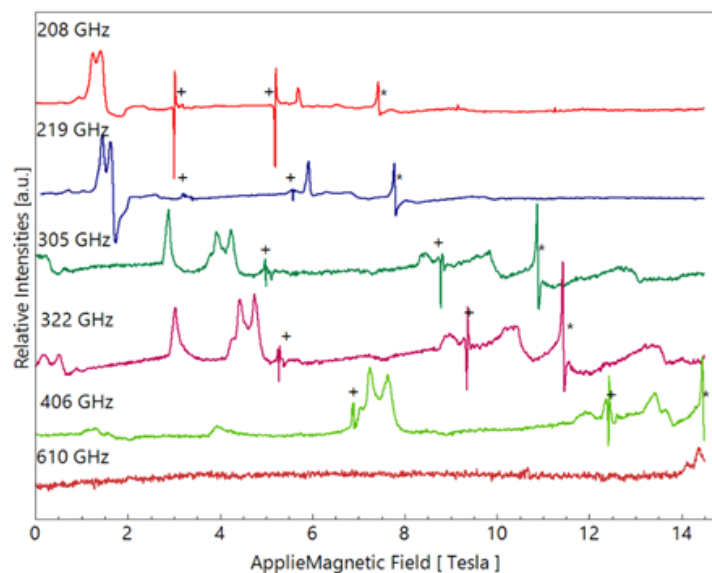
Figure D.12. Selected High-Frequency EPR spectra recorded at 5 K for a neat sample of **36**. The particular frequencies at which the spectra were recorded are indicated above each trace. The features marked by (+) are artifacts that originated from molecular oxygen adsorbed on the surface of the plastic containers. The (*) labels the EPR spectrum of a radical-based impurity that appears at $g = 2.00$.

5. IR Spectra
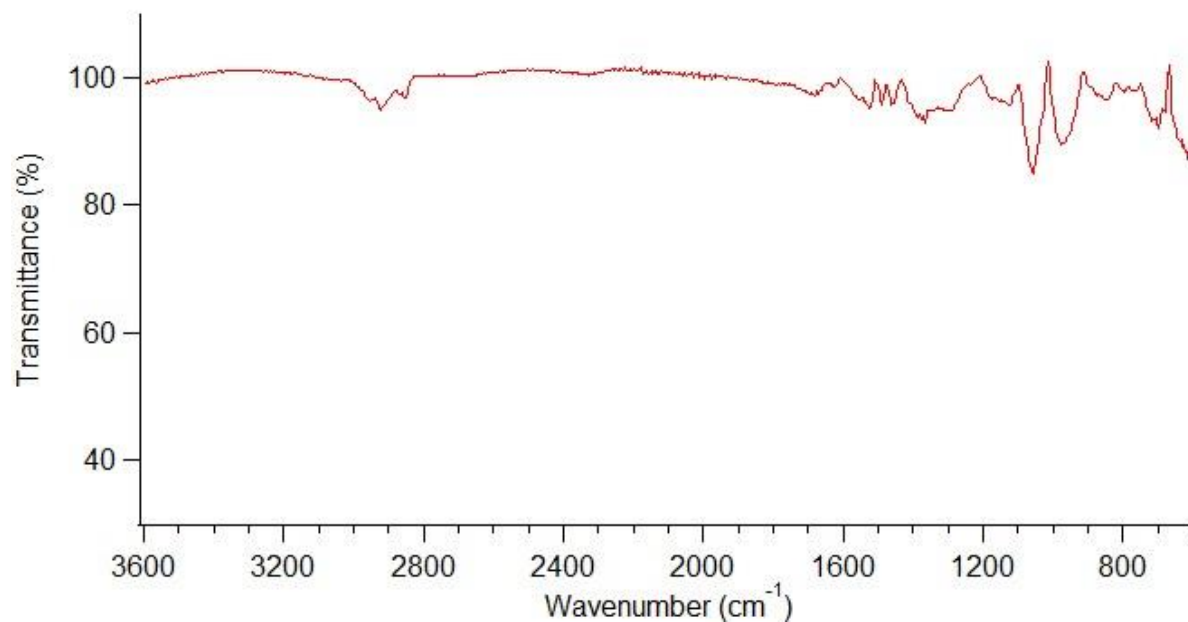
Figure D.13. IR spectra of complex **33** in the 3400-600 cm^{-1} range.
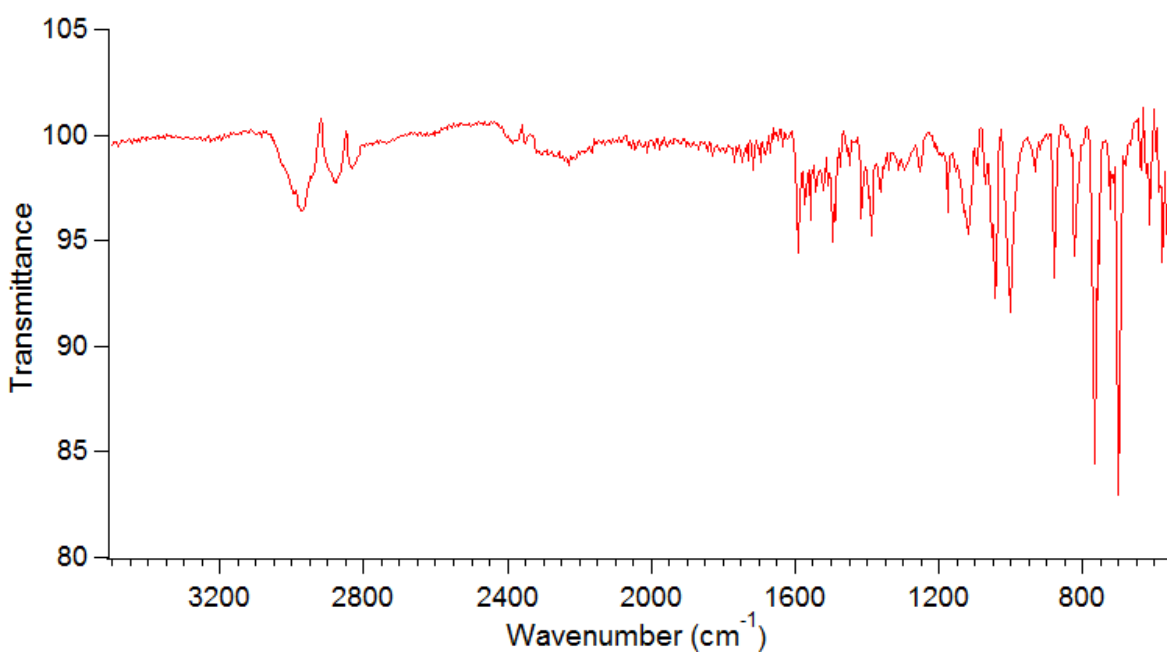
Figure D.14. IR spectra of complex **34** in the 3400-600 cm^{-1} range.
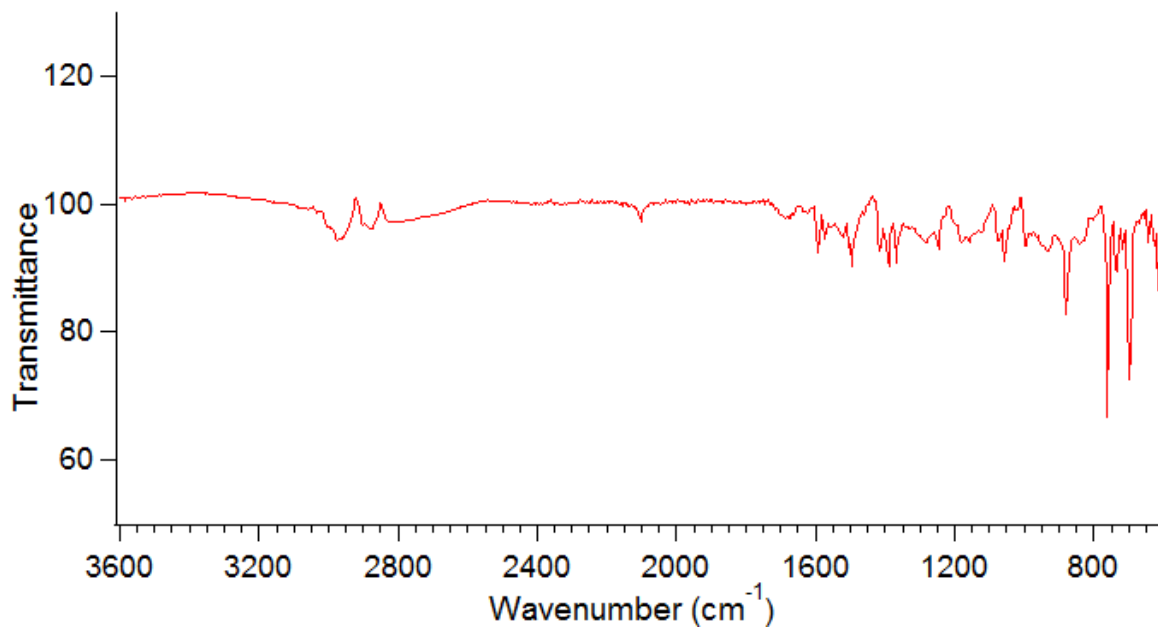
Figure D.15. IR spectra of complex **35** in the 3400-600 cm^{-1} range.
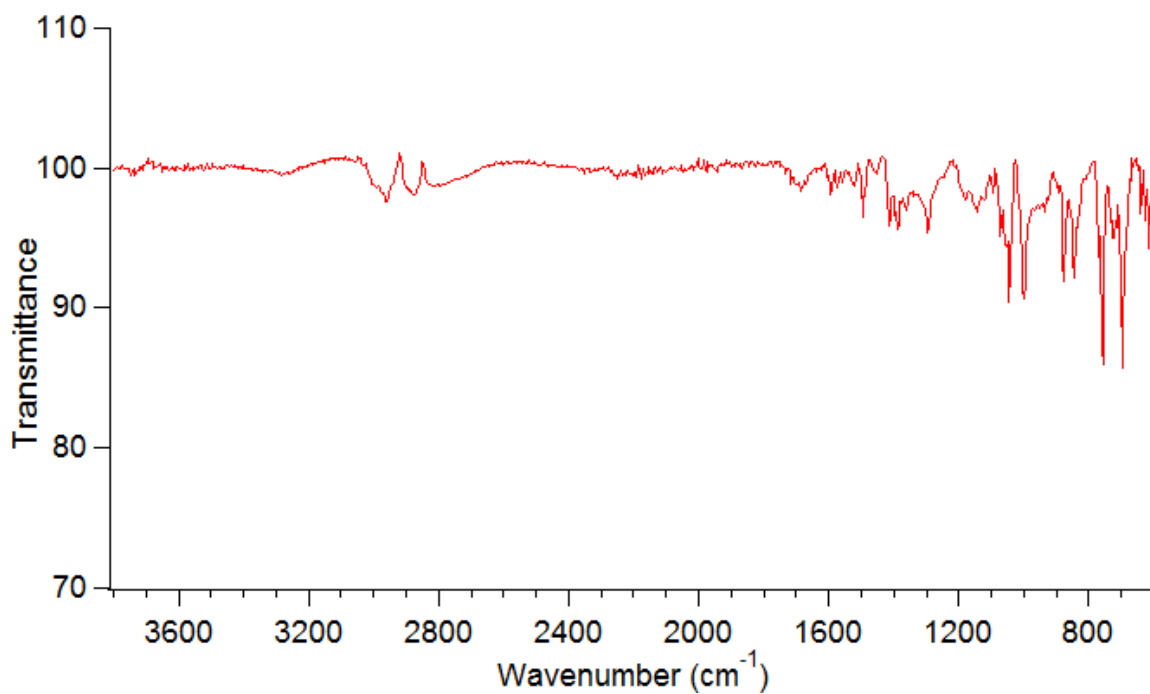
Figure D.16. IR spectra of complex **36** in the 3400-600 cm^{-1} range.

6. UV-Vis Spectra
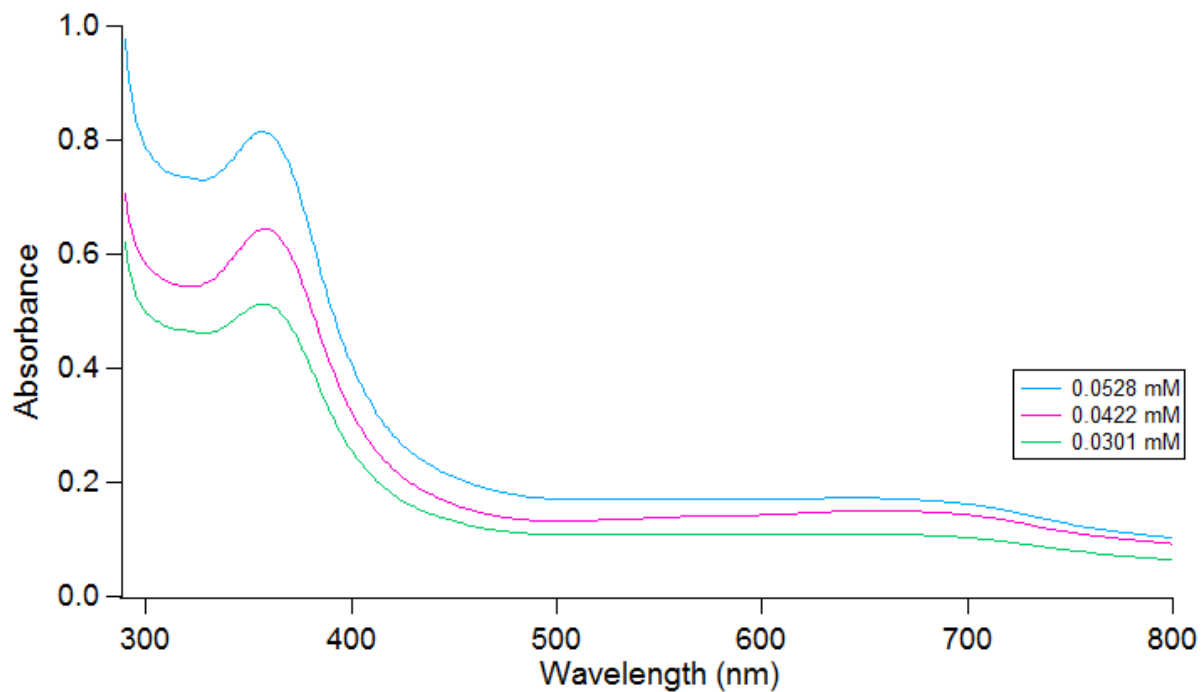
Figure D.17. UV-vis spectrum for complex **33** at three different concentrations. λ_{max} (ε_M): 358 (15909).
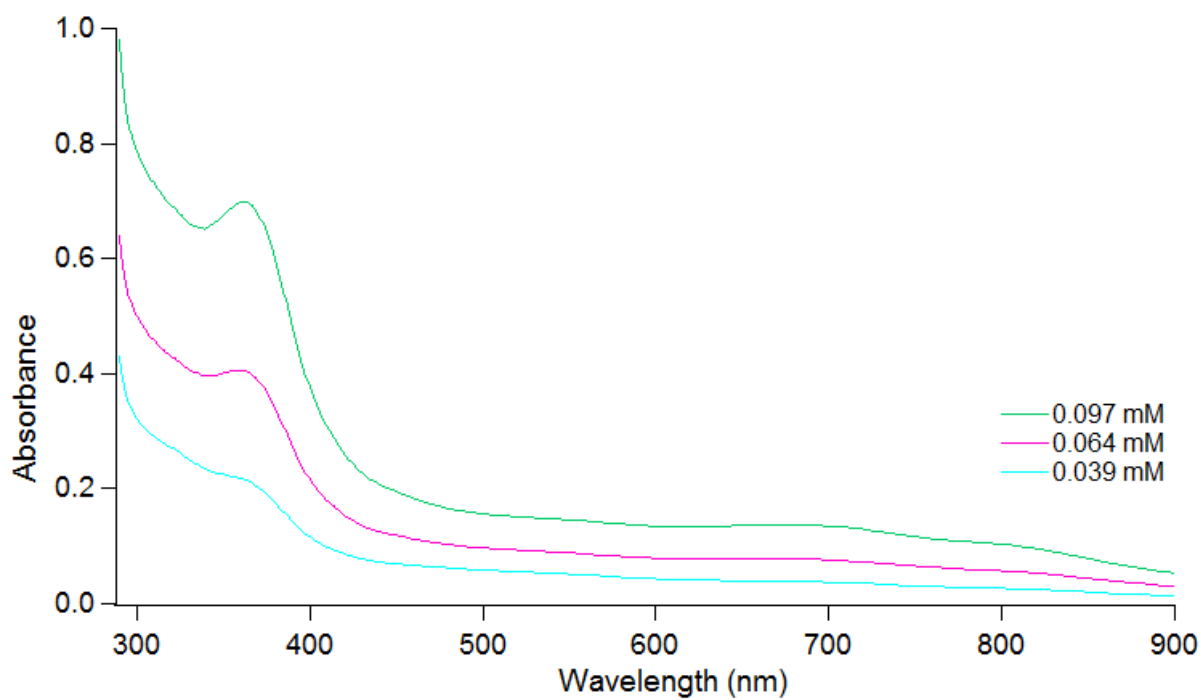
Figure D.18. UV-vis spectrum for complex **34** at three different concentrations. λ_{max} (ε_M): 363 (6352).
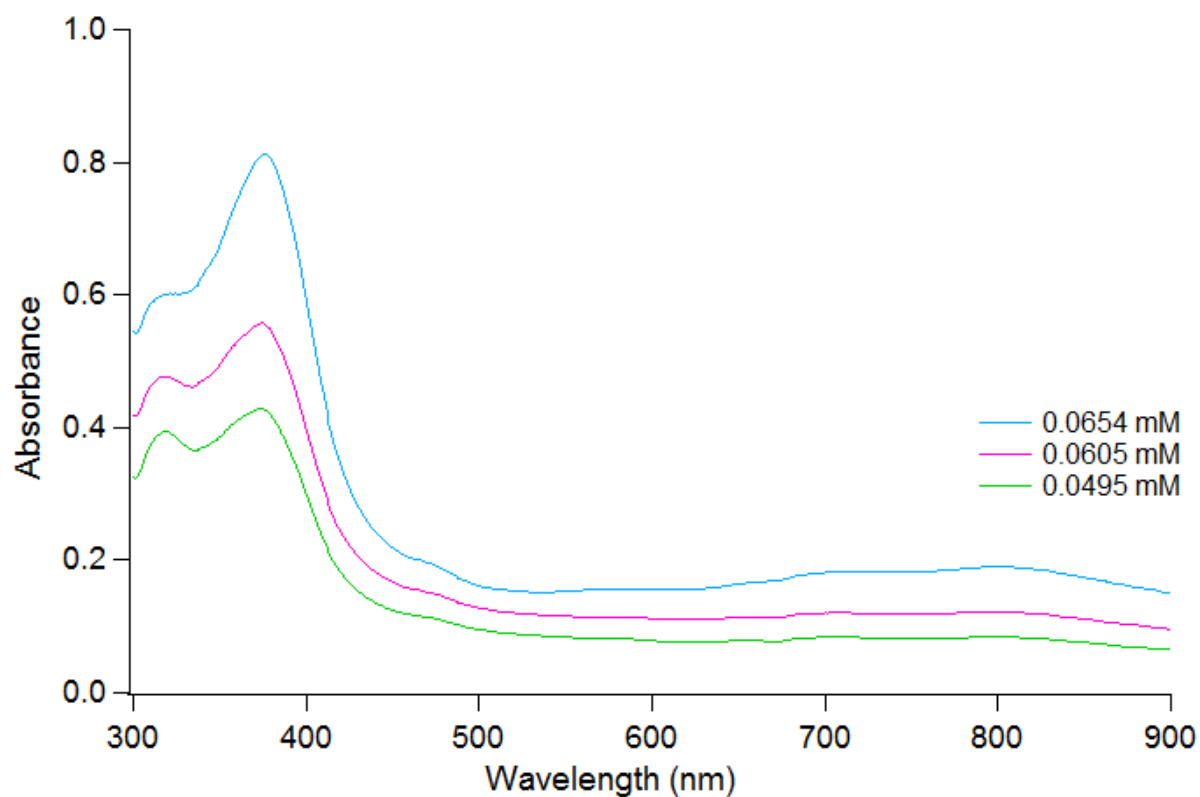
Figure D.19. UV-vis spectrum for complex 3**5** at three different concentrations. λ_{max} (ε_M): 376 (10077).
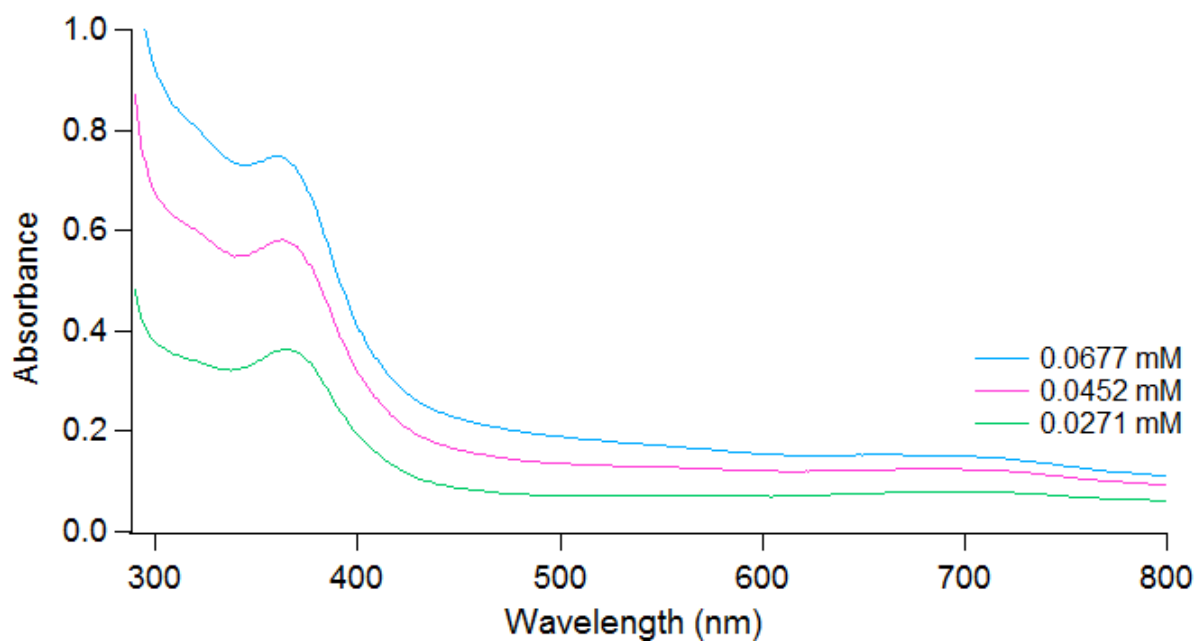
Figure D.20.UV-vis spectrum for complex **36** at three different concentrations. λ_{max} (ε_M): 363 (12426).

APPENDIX E: SUPPLEMENTARY MATERIAL FOR CHAPTER 5

1. Crystal Structure Not Shown in Chapter 5
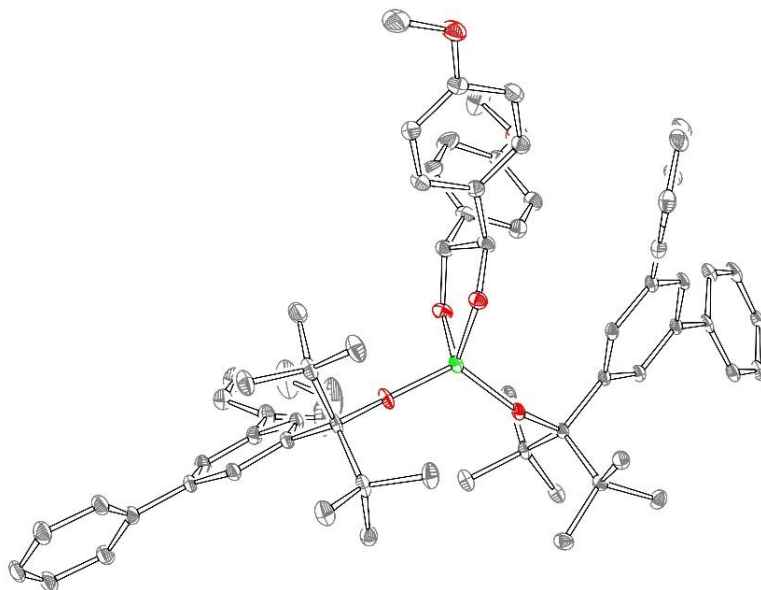
Figure E.1. X-ray structure of complex **38**.

2. Evans Method and Procedure

Table E.1. Spin-only magnetic moments calculated for **37-41** using Evans method.

Complex	μ_{obs} (1) (μ_B)	μ_{obs} (2) (μ_B)	μ_{obs} (3) (μ_B)	μ_{obs} (average) (μ_B)
37	2.2	2.4	2.6	2.4±0.3
38	2.5	2.2	2.3	2.3±0.3
39	2.8	2.3	2.4	2.5±0.3
40	2.6	2.4	2.7	2.6±0.3
41	3.8	4.0	3.5	3.8±0.4

3. NMR spectra
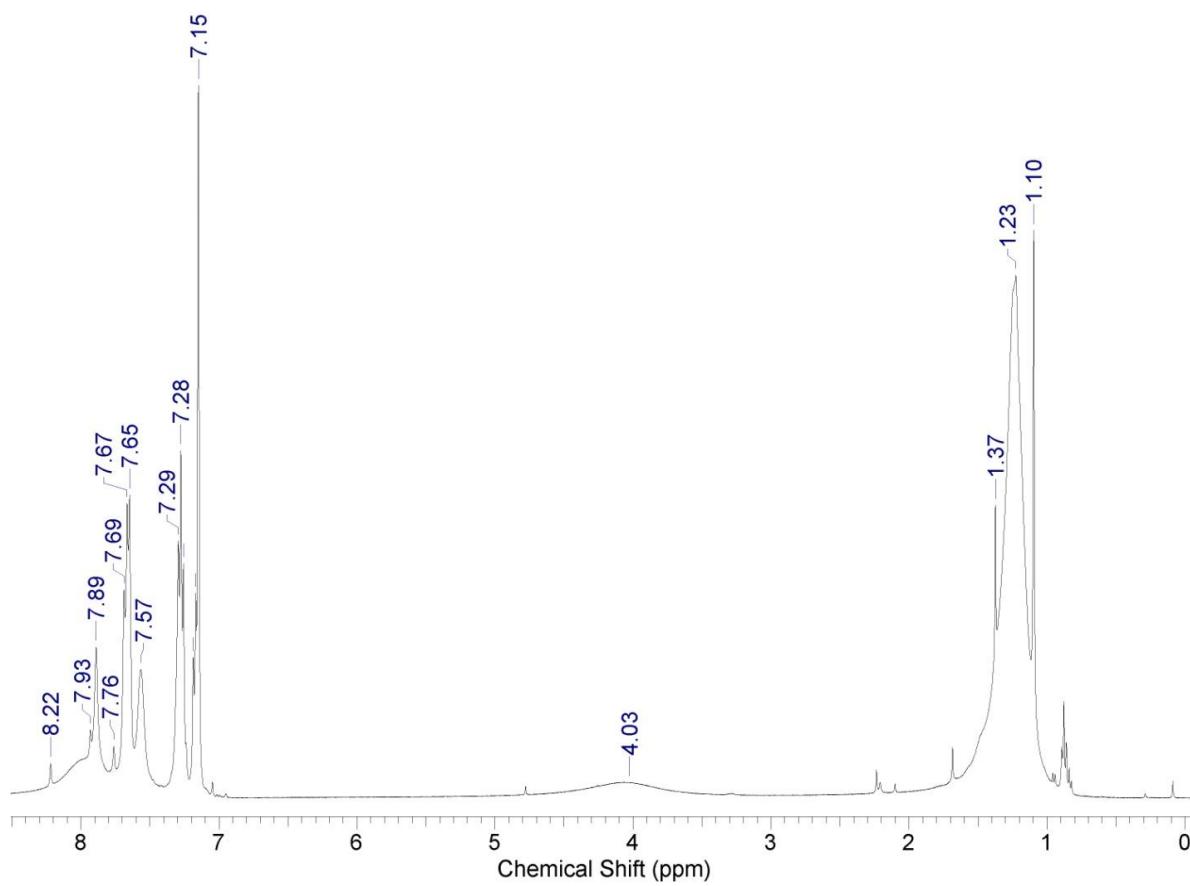
Figure E.2. ^{1}H NMR of complex **42** $Cr_2(O_2COR')_4(THF)_2$ in C_6D_6.
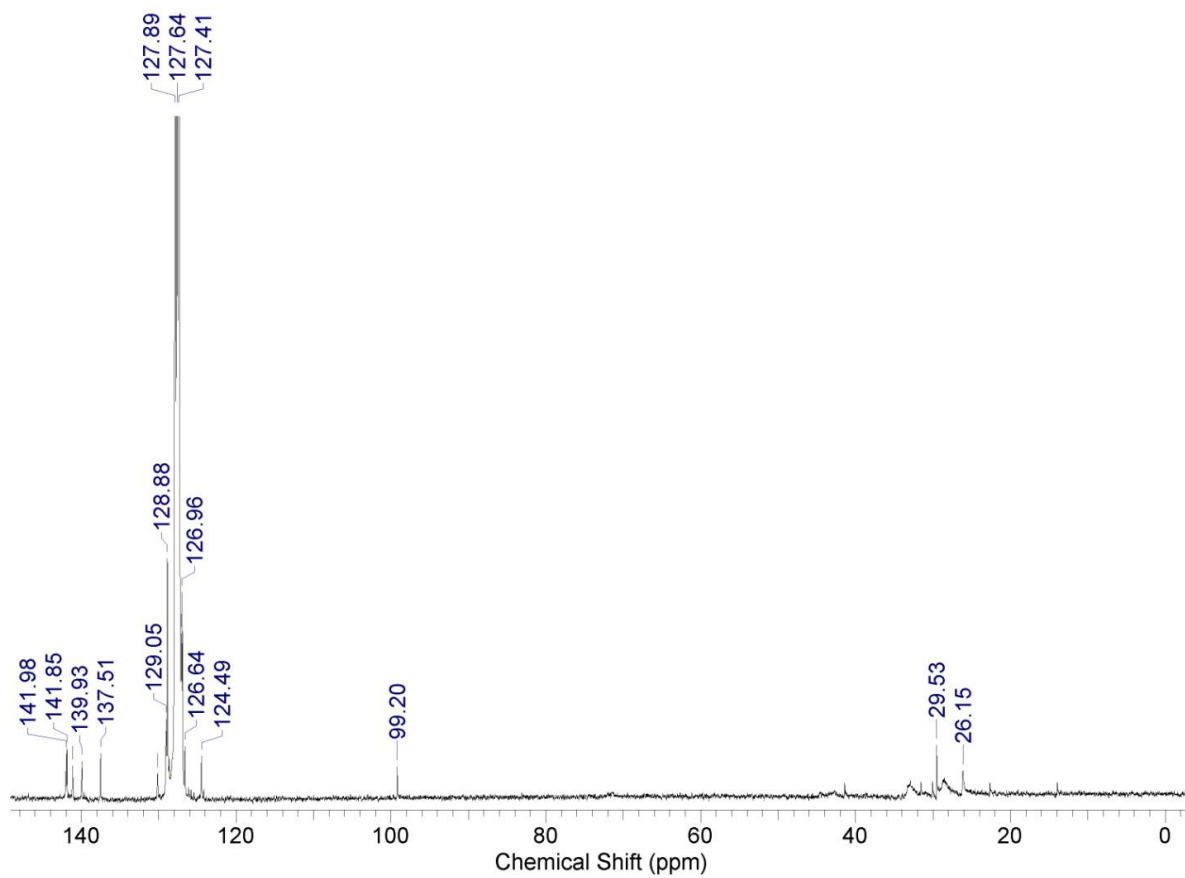
Figure E.3. ^{13}C NMR of complex **42** $Cr_2(O_2COR')_4(THF)_2$ in C_6D_6.

4. IR spectra
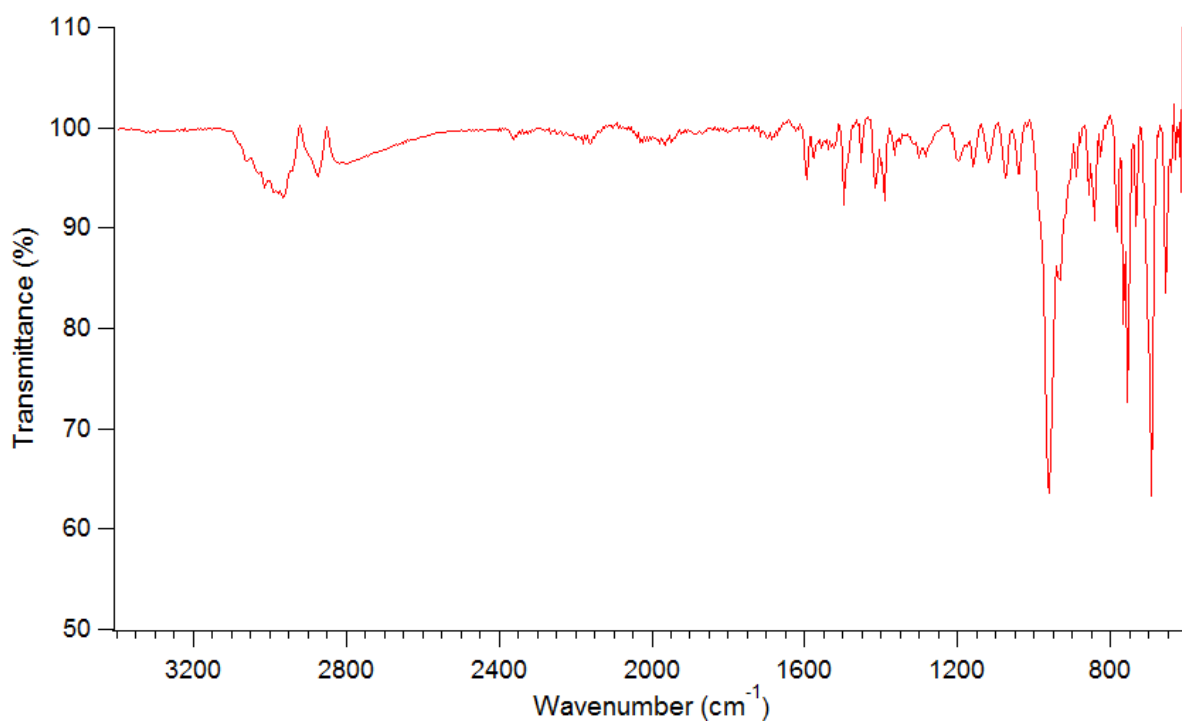
Figure E.4. IR spectra of complex **37.**
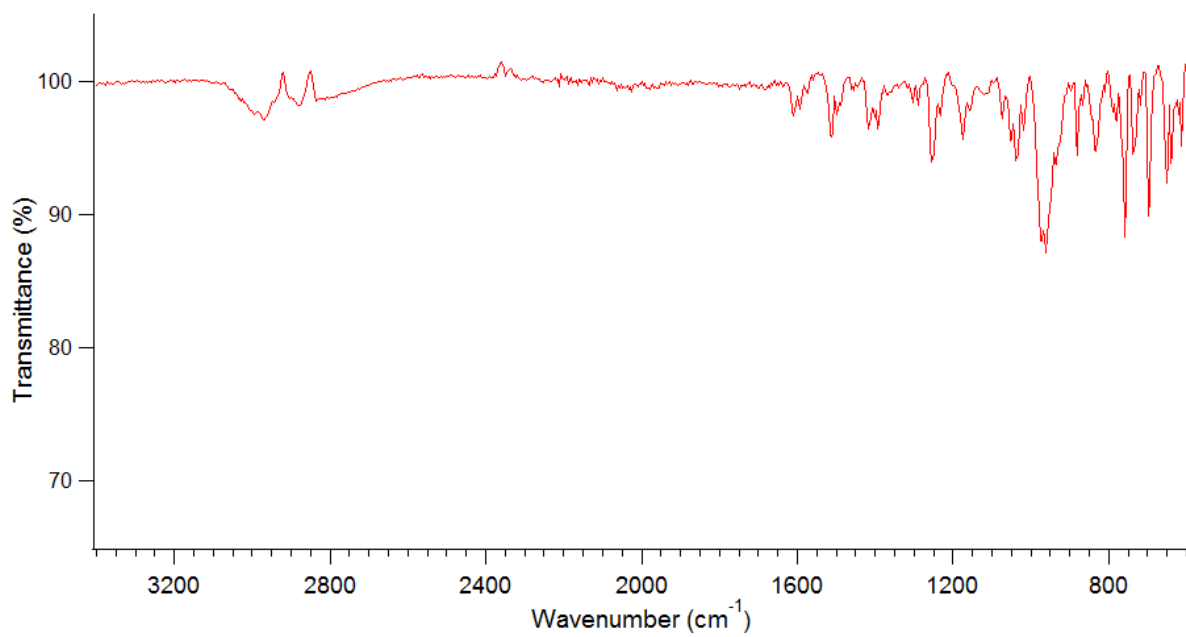
Figure E.5. IR spectra of complex **38.**
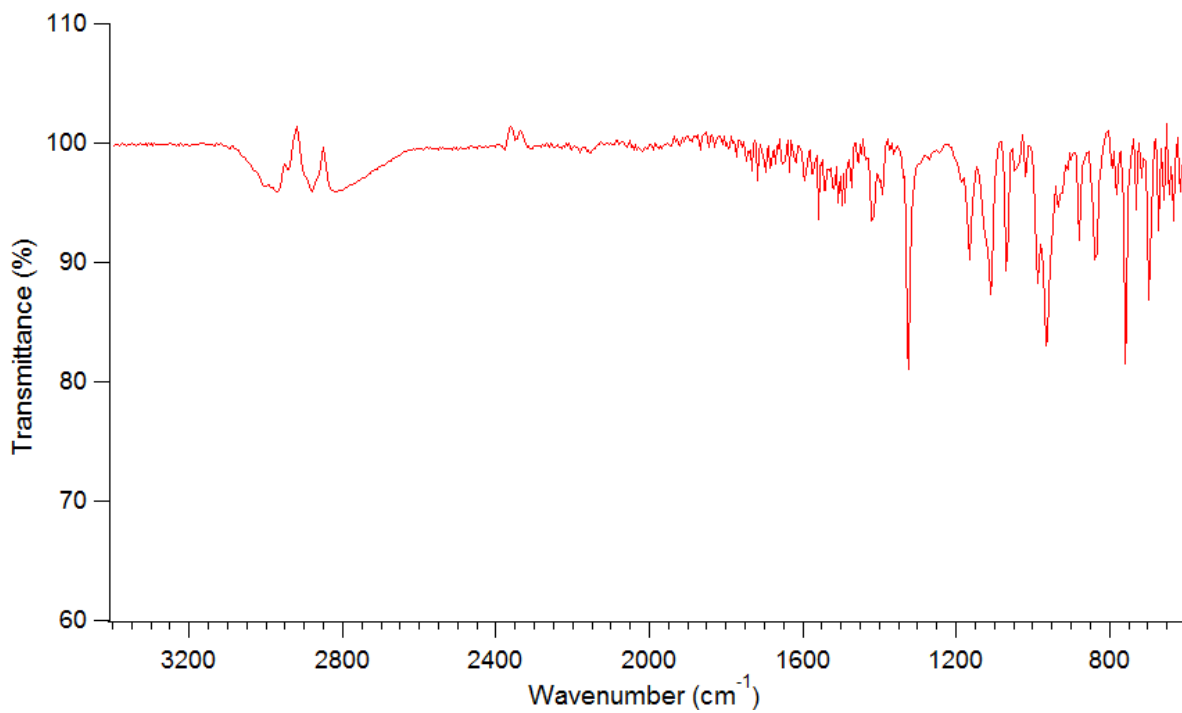
Figure E.6. IR spectra of complex **39.**
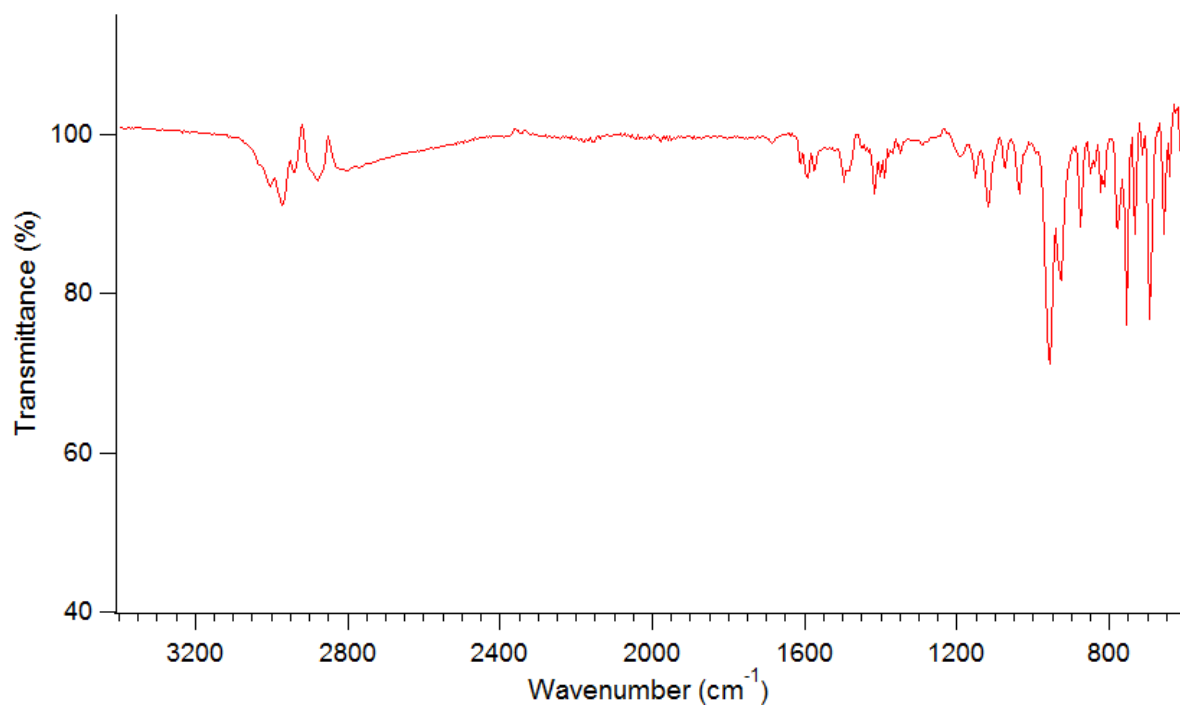
Figure E.7. IR spectra of complex **40.**
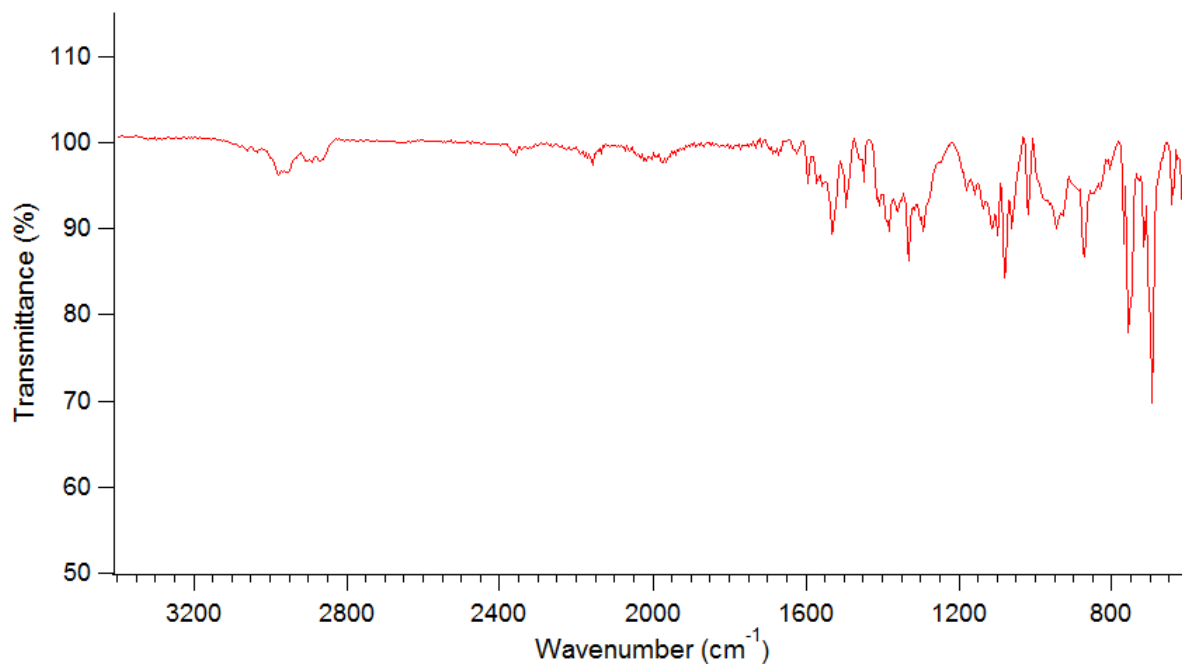
Figure E.8. IR spectra of complex **41.**
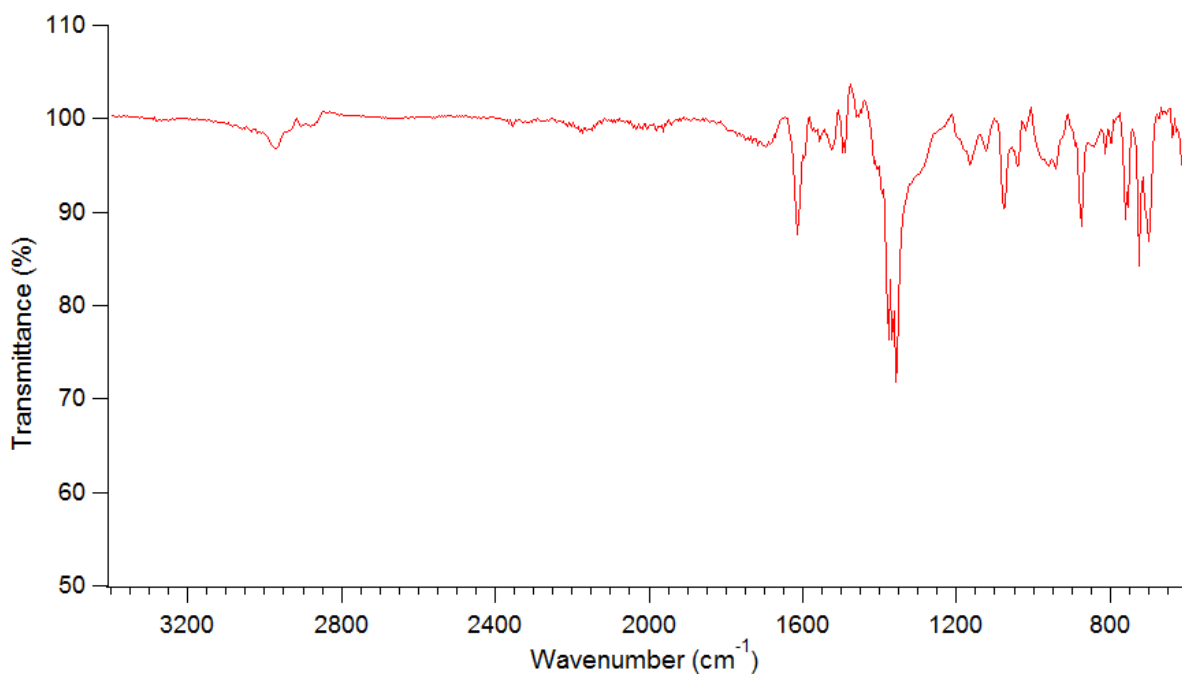
Figure E.9. IR spectra of complex **42.**

5. UV-vis spectra

The UV-vis spectra of the Cr(IV)-diolate complexes **37-39** are presented in **Figure E.X** and are compared to the corresponding spectrum of complex **41**. **Figure E.4** demonstrates that the spectra of compounds **37-39** (taken in THF) display very similar spectra featuring single band in the visible region at 615 ± 5 nm. In contrast, complex **41** has a single broad peak centered at 710 nm. We note that complex **40** (whose spectrum taken in a toluene due to its instability in THF, **Figure E.5**) demonstrates an additional spectral feature (shoulder) around 690 ppm, in addition to the expected peak at 611 nm.
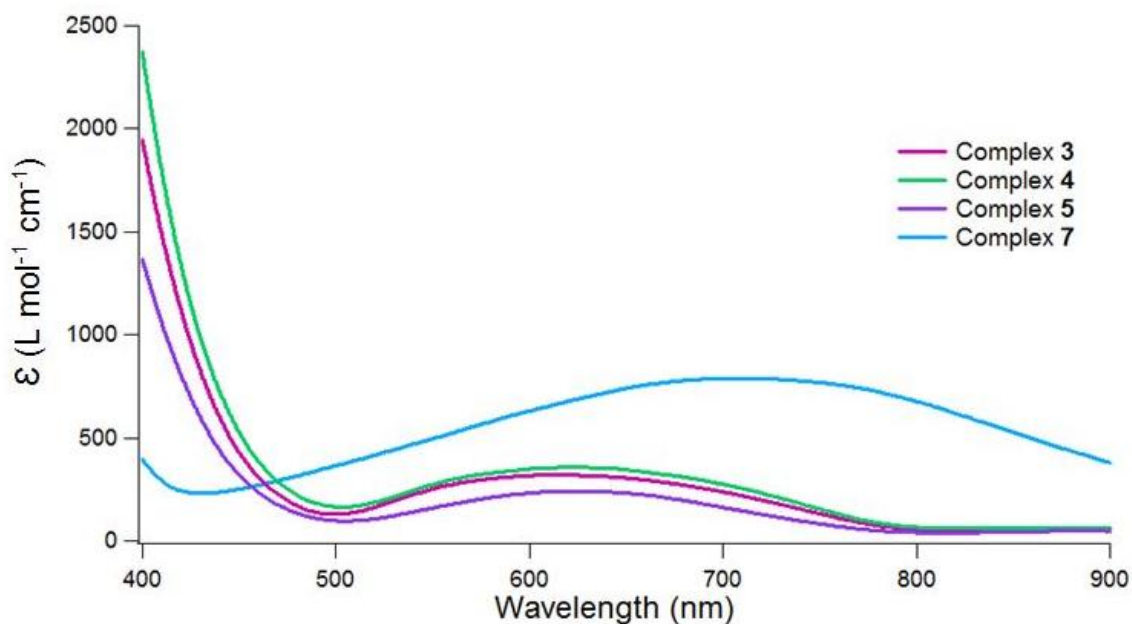
Figure E.10. The absorption spectra of complexes **38-40** and 7 in 400 – 900 nm region.
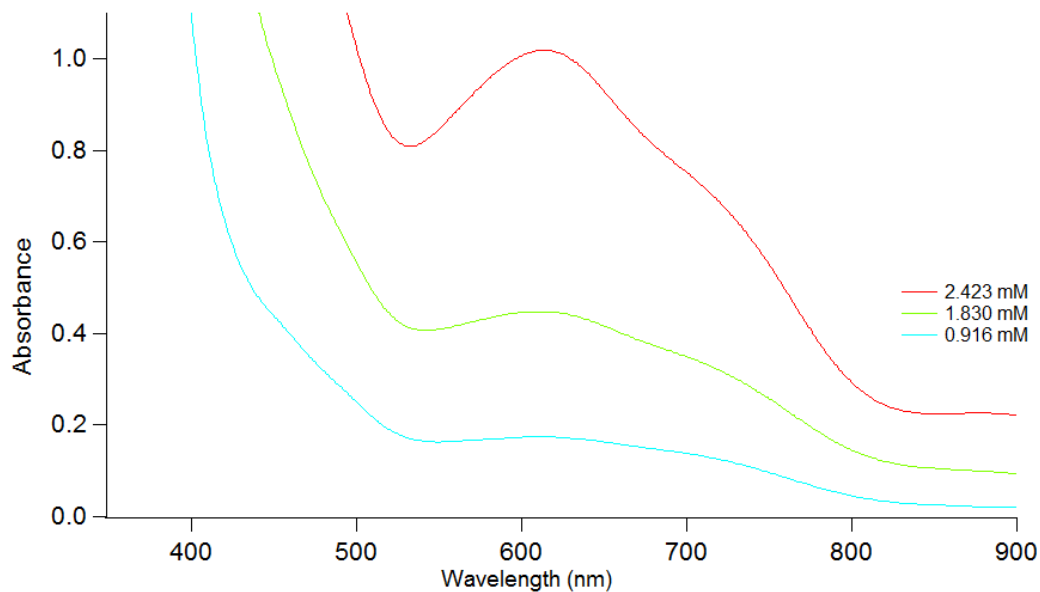
Figure E.11. UV-vis spectrum for complex **40** Cr(OR')$_2$(O$_2$C$_2$H$_2$(2,4,6-Me$_3$Ph)$_2$) at three different concentrations. λ_{max} (εM): 611 (234).
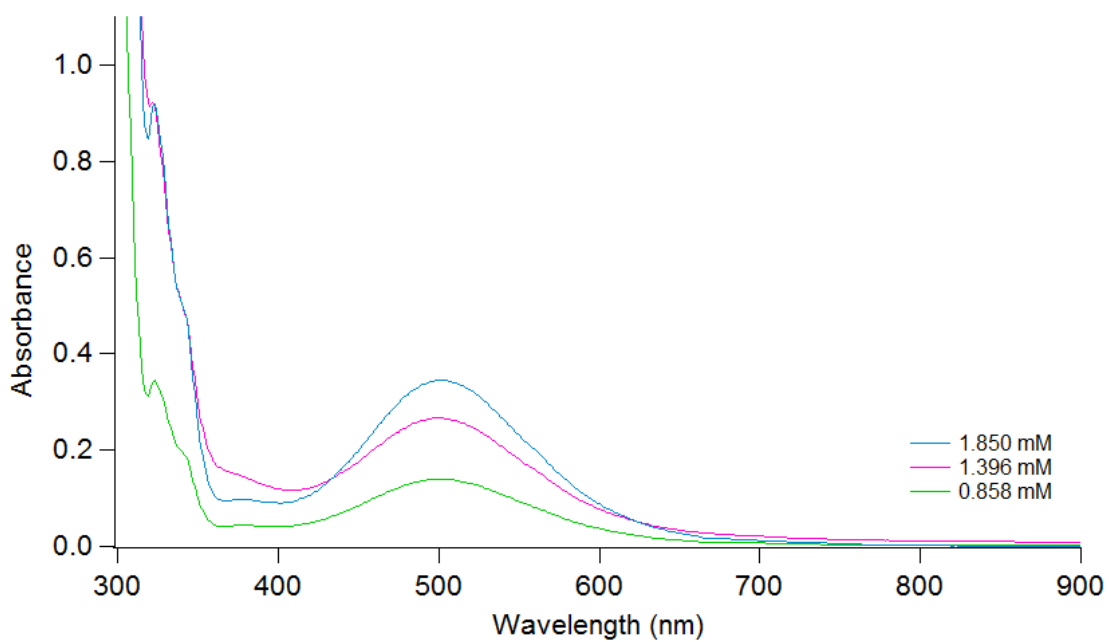
Figure E.12. UV-vis spectrum for complex **42** Cr$_2$(O$_2$COR)$_4$(THF)$_2$ at three different concentrations. λ_{max} (εM): 502(223).

6. Computational results

Figure E.13. Corresponding orbital isosurface plots (iso = 0.05 au) for triplet **22.**

APPENDIX F: SUPPLEMENTARY MATERIAL FOR CHAPTER 6

1. Evans Method and Procedure

Table F.1. Spin-only magnetic moments calculated for **43** and **44** using Evans method.

Complex	μ_{obs} (1) (μ_B)	μ_{obs} (2) (μ_B)	μ_{obs} (3) (μ_B)	μ_{obs} (average) (μ_B)
43	2.9	2.8	2.7	2.8±0.1
44	2.5	2.9	2.9	2.8±0.2

2. UV-Vis Spectra
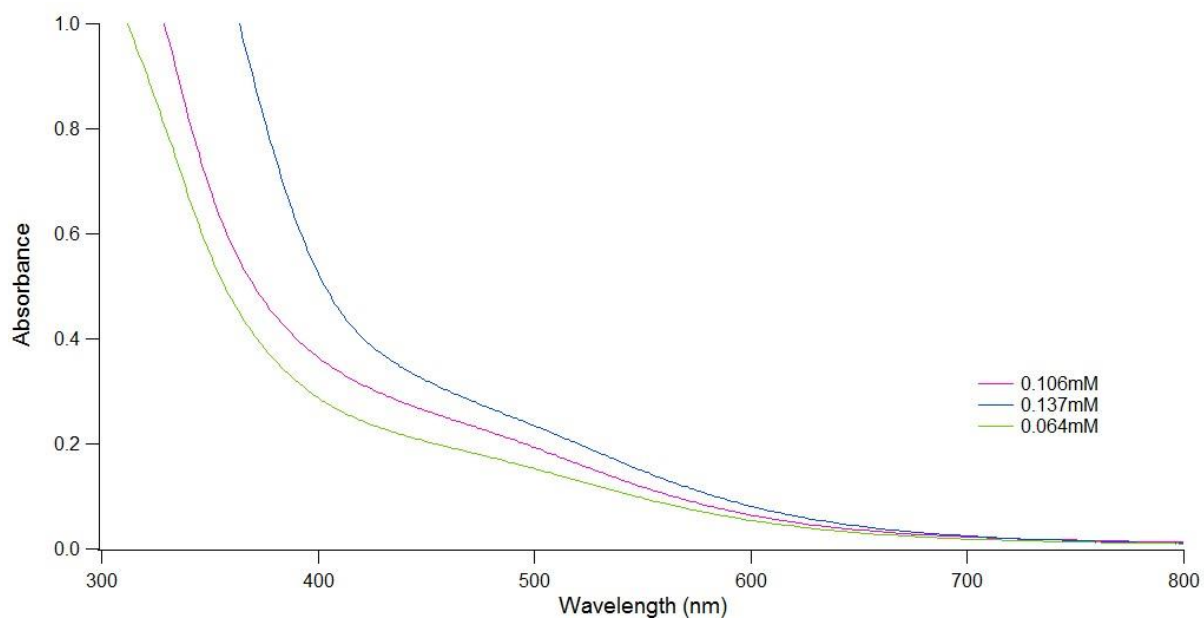
Figure F.1.: UV-vis spectrum for complex **43** ($Fe_2(O)(OR)_4(THF)_2$) at three different concentrations.
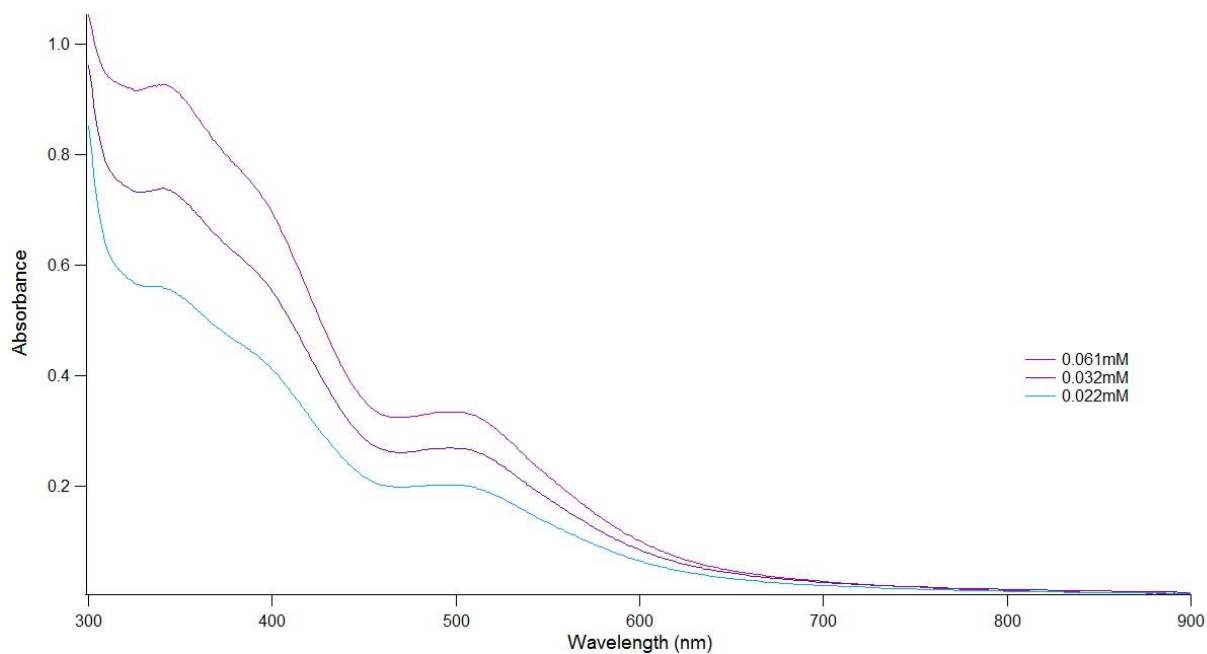
Figure F.2: UV-vis spectrum for complex **44** ($Fe_2(S)(OR)_4(THF)_2$) at three different concentrations.

REFERENCES

1. Bra¨se, S.; Banert, K. *Organic Azides Syntheses and Applications*, 1ˢᵗ ed. John Wiley & Sons Ltd., 2010.

2. Brase, S.; Gil, C.; Knepper, K.; Zimmermann, V. *Angew. Chem. Int. Ed*. **2005**, *44*, 5188-5240.

3. (a) Cundari, T. R. *J. Am. Chem. Soc*. **1992**, *114*, 7879-7888. (b) Cenini, S.; Gallo, E.; Caselli, A.; Ragaini, F.; Fantauzzi, S.; Piangiolino, C. *Coord. Chem. Rev*. **2006**, 1234-1253. (c) Eikey, R. A.; Abu-Omar, M. M. *Coord. Chem. Rev*. **2003**, *243*, 83-124. (d) Laskowski, C. A.; Miller, A. J. M.; Hillhouse, G. L.; Cundari, T. R. *J. Am. Chem. Soc*. **2011**, *133*, 771-773. (e) Toda, Y.; Hirayama, H.; Kuganathan, N.; Torrisi, A.; Sushko P. V.; Hosono, H. *Nature communications* **2013**, *4*, 2378. (f) Driver, T. G. *Org. Biomol. Chem*. **2010**, *9*, 3831-3846.

4. Intrieri, D.; Zardi, P.; Caselli, A.; Gallo, E. *Chem. Commun*. **2014**, *50*, 11440-11453.

5. (a) Williams, A.; Ibrahim, I. T. *Chem. Rev*. **1981**, *81*, 589−636. (b) Ulrich, H. *Chemistry and Technology of Carbodiimides* **2008**, 9−41; **2008**, 243−274. (c) Peng, L.; Jie-Cheng, X. Chin. *J. Chem*. **2000**, *18*, 456−466. (d) Albericio, F.; Kates, S. A. *In Solid-Phase Synthesis: A Practical Guide*; Marcel Dekker: New York, 2000; pp 275−330. (e) Albeiicio, F.; Chinchilla, R.; Dodsworth, D. J.; Najera, C. *Org. Prep. Proced. Int.* **2001**, *33*, 203−303. (f) Bauminger, S.; Wilchek, M. *Methods Enzymol.* **1980**, 70, 151− 159.

6. Louie, J. Curr. *Org. Chem*. **2005**, *9*, 605−623.

7. For selected references, see: (a) Lazar, M.; Angelici, R. J. *J. Am. Chem. Soc*. **2006**, *128*, 10613−10620. (b) Angelici, R. J. J. *Organomet. Chem.* **2008**, *693*, 847−856. (c) Ito, Y.; Hirao, T.; Saegusa, T. *J. Org. Chem.* **1975**, *40*, 2981−2982.

8. (a) Applied Homogeneous Catalysis with Organometallic Compounds, 2nd ed.; Koch, D., Naberfeld, G., Six, C., Eds.; Wiley-VCH: Weinheim, Germany, 2002; Vol. 3. (b) Birdwhistell, K. R.; Boucher, T.; Ensminger, M.; Harris, S.; Johnson, M.; Toporek, S. *Organometallics* **1993**, *12*, 1023−1025.

9. Palacios, F.; Alonso, C.; Aparicio, D.; Rubiales, G.; De Los Santos, J. M. *Tetrahedron* **2007**, *63*, 523−575.

10. Babcock, J. R.; Sita, L. R. *J. Am. Chem. Soc*. **1998**, *120*, 5585− 5586.

11. Saegusa, T.; Ito, Y.; Shimizu, T. *J. Org. Chem.* **1970**, *35*, 3995− 3996.

12. (a) Glueck, D. S.; Hollander, F. J.; Bergman, R. G. *J. Am. Chem. Soc.* **1989**, *111*, 2719−2721. (b) Glueck, D. S.; Wu, J.; Hollander, F. J.; Bergman, R. G. *J. Am. Chem. Soc.* **1991**, 113, 2041−2054.

13. Hessell, E. T.; Jones, W. D. *Organometallics* **1992**, *11*, 1496− 1505.

14. (a) Hörlin, G.; Mahr, N.; Werner, H. *Organometallics* **1993**, *12*, 1775−1779. (b) Werner, H.; Hörlin, G.; Mahr, N. *J. Organomet. Chem.* **1998**, *551*, 367−373.

15. Scepaniak, J. J.; Bontchev, R. P.; Johnson, D. L.; Smith, J. M. *Angew. Chem., Int. Ed.* **2011**, *50*, 6630−6633.

16. (a) Kim, Y.-J.; Kwak, Y.-S.; Joo, Y.-S.; Lee, S.-W. *J. Chem. Soc., Dalton Trans.* **2002**, 144−151. (b) Kim, Y.-J.; Joo, Y.-S.; Han, J.-T.; Han, W. S.; Lee, S. W. *J. Chem. Soc., Dalton Trans*. **2002**, 3611−3618.

17. (a) Mindiola, D. J.; Hillhouse, G. L. *J. Am. Chem. Soc*. **2001**, *123*, 4623−4624. (b) Mindiola, D. J.; Hillhouse, G. L. *Chem. Commun.* **2002**, *17*, 1840−1841. (c) Laskowski, C. A.; Hillhouse, G. L. *Organometallics* **2009**, *28*, 6114−6120.

18. (a) Kogut, E.; Wiencko, H. L.; Zhang, L.; Cordeau, D. E.; Warren, T. H. *J. Am. Chem. Soc.* **2005**, *127*, 11248−11249. (b) Badiei, Y. M.; Krishnaswamy, A.; Melzer, M. M.; Warren, T. H. *J. Am. Chem. Soc.* **2006**, *128*, 15056−15057. (c) Wiese, S.; Aguila, M. J. B.; Kogut, E.; Warren, T. H. *Organometallics* **2013**, *32*, 2300−2308.

19. (a) Cowley, R. E.; Ecket, N. A.; Elhaik, E.; Holland, P. L. *Chem. Commun.* **2009**, 1760−1762. (b) Cowley, R. E.; Golder, M. R.; Eckert, N. A.; Al-Afyouni, M. H.; Holland, P. L. *Organometallics* **2013**, *32*, 5289−5298.

20. Mankad, N. P.; Müller, P.; Peters, J. C. *J. Am. Chem.* Soc. **2010**, *132*, 4083−4085.

21. Zhizhko, P. A.; Zhizhin, A. A.; Belyakova, O. A.; Zubavichus, Y. V.; Kolyagin, Y. G.; Zarubin, D. N.; Ustynyuk, N. A. *Organometallics* **2013**, *32*, 3611−3617.

22. Thorman, J. L.; Guzei, I. A.; Young, V. G., Jr.; Woo, L. K. *Inorg. Chem.* **1999**, *38*, 3814−3824.

23. Heyduk, A. F.; Zarkesh, R. A.; Nguyen, A. I. *Inorg. Chem.* **2011**, *50*, 9849-9863.

24. Zhang, C.; Jiao, N. *Angew. Chem. Int. Ed.* **2010**, *49*, 6174-6177.

25. Merino, E. *Chem. Soc. Rev.* **2011**, *40*, 3835–3853.

26. (a) Ragaini, F.; Penoni, A.; Gallo, E.; Tollari, S.; Gotti, C. L.; Lapadula, M.; Mangioni, E.; Cenini, S. *Chem. Eur. J.* **2003**, *9*, 249− 259. (b) Takaoka, A.; Moret, M.-E.; Peters, J. C. *J. Am. Chem. Soc.* **2012**, *134*, 6695−6706.

27. Harrold, N. D.; Waterman, R.; Hillhouse, G. L., Cundari, T. R. *J. Am. Chem Soc.* **2009**, *131*, 12872-12873.

28. (a) Sakakura, T.; Choi, J.; Yasuda, H. *Chem. Rev.* **2007**, *107*, 2365-2387. (b) Liu, Q.; Wu, L.; Jackstell, R.; Beller, M. *Nature Communications* **2015**, 1-15.

29. (a)Yin, X.; Moss, J. R. *Coord. Chem. Rev.* **1999**, *181*, 27-59. (b) Zhang, L.; Cheng, J.; Ohishi, T.; Hou, Z. *Angew. Chem Int. Ed.* **2010**, *49*, 8670-8673. (c) Noor, A.; Qayyum, S.; Bauer, T.; Schwarz, S.; Weber, B.; Kempe, R. *Chem. Commun.* **2014**, *50*, 13127-13130. (d) Lu, C. C.; Saouma, C. T. Day, M. W. Peters, J. C. *J. Am. Chem. Soc.* **2007**, *129*, 4-5.

30. (a) Jahangiri, H.; Bennett, J.; Mahijoubi, P.; Wilson, K.; Gu, S. *Catal. Sci. Technol.* **2014**, *4*, 2210-2229. (b) Yang, J.; Ma, W.; Chen., D.; Holmen, A.; Davis, B. H. *Applied Catalysis A: General* **2014**, *470*, 250-260.

31. Olah, G. A. *Angew. Chem. Int. Ed.* **2013**, *52*, 104-107.

32. Saouma, C. T.; Lu, C.C.; Day, M. W.; Peters, J. C. *Chem. Sci.* **2013**, *4*, 4042-4051.

33. Williams, V. A.; Manke, D. R.; Wolczanski, P. T.; Cundari, T. R. *Inorg. Chim. Acta* **2011**, *369*, 203-214.

34. Zucchini, U.; Albizzati, E.; Giannini, U. *J. Organomet. Chem.* **1971**, *26*, 357.

35. (a) Offermans, W. K.; Bizzarri, C.; Leitner, W.; Muller, T. E. *Beilstein J. Org. Chem.* **2015**, *11*, 1340-1351. (b) Dibenedetto, A.; Pastore, C.; Aresta, M. *Catalysis Today* **2006**, *115*, 88-94. (c) Aresta, M.; Dibenedetto, A.; Pastore, C. *Inorg. Chem.* **2003**, *42*, 3256-3261.

36. (a) Brown, S. D.; Betley, T. A.; Peters, J. C. *J. Am. Chem. Soc.* **2003**, *125*, 322. (b) Shay, D. T.; Yap, G. P. A.; Rheingold, A. L.; Theopold, K. *Angew. Chem.* **2005**, *117*, 1532-1534.

37. (a) Wolczanski, P. T. *Polyhedron* **1995**, *14*, 3335–3362. (b) Wolczanski, P. T. *Chem. Commun.* **2009**, 740–757. (c) Power, P. P. *J. Organomet. Chem.* **2004**, *689*, 3904–3919. (d) Cantalupo, S. A.; Lum, J. S.; Buzzeo, Moore, C. DiPasquale, A. G.; Rheingold, A. L.; Doerrer, L. H. *Dalton Trans.* **2010**, *39*, 374-383. (e) Groysman, S.; Villagran, D.; Freedman, D. E.; Nocera, D. G. *Chem. Commun.* **2011**, *47*, 10242-10244. (f) Murray, D.;

Power, P.P. *J. Am. Chem. Soc.* **1984**, *106*, 7011-7-15. (g) Sigel, G. A.; Bartlett, R. A.; Decker, D.; Olmstead, M. M.; Power, P. P. *Inog. Chem.* **1987**, *26*, 1773-1780.

38. Ni, C.; Power, P. P. *Chem. Commun.* **2009**, 5543-5545.

39. Hatanaka, T.; Miyake, R.; Ishida, Y.; Kawaguchi, H. J. *Organomet. Chem.* **2011**, *696*, 4046-4050.

40. Bellow, J. A.; Fang, D.; Kovacevic, N.; Martin, P. D.; Shearer, J.; Cisneros, G. A.; Groysman, S. *Chem. Eur. J.* **2013**, *19*, 12225-12228.

41. Bellow, J. A., Yousif, M., Fang, D., Kratz, E. G., Cisneros, G. A., Groysman, S. *Inorg. Chem.* **2015**, *54*, 5624- 5633.

42. Bellow, J. A., Yousif, M., Groysman, S. *Comments Inorg. Chem.* **2015**, *36*, 92-122.

43. (a) Bellow, J. A.; Yousif, M.; Cabelof, A. C.; Lord, R. L.; Groysman, S. *Organometallics* **2015**, *34*, 2917-2923. (b) Bellow, J. A.; Martin, P. D.; Lord, R. L.; Groysman, S. *Inorg. Chem.* **2013**, *52*, 12335 -12337.

44. Cowley, R. E.; DeYonker, N. J.; Eckert, N. A.; Cundari, T. R.; DeBeer, S.; Bill, E.; Ottenwaelder, X.; Flaschenriem, C.; Holland, P. L. *Inorg. Chem.* **2010**, *49*, 6172-6187.

45. Bradley, D. C.; Hursthouse, M. B.; Newing, C. W.; Welch, A. J. *J. Chem. Soc., Chem. Commun.* **1972**, 567−568.

46. Christensen, S. H.; Holm, T.; Madsen, R. *Tetrahedron* **2014**, *70*, 1478−1483.

47. Sydora, O. L.; Kuiper, D. S.; Wolczanski, P. T.; Lobkovsky, E. B.; Dinescu, A.; Cundari, T. R. *Inorg. Chem.* **2006**, *45*, 2008−2021.

48. Murray, B. D.; Hope, H.; Power, P. P. *J. Am. Chem. Soc.* **1985**, *107*, 169−173.

49. Evans, D. F. *J. Chem. Soc.* **1959**, 2003−2005.

50. Neese, F. *J. Phys. Chem. Solids* **2004**, *65*, 781−785.

51. For a recent discussion on the electronic structure and the corresponding reactivity of metal imido complexes, see: Hennessy, E. T.; Liu, R. Y.; Iovan, D. A.; Duncan, R. A.; Betley, T. A. *Chem. Sci.* **2014**, *5*, 1526−1532.

52. A CCDC search revealed ∼130 isocyanide complexes of Cr not containing alkoxide ligands.

53. (a) Allen, J. M.; Ellis, J. E. *J. Organomet. Chem.* **2008**, *693*, 1536−1542. (b) Stevens, C. J.; Nichol, G. S.; Arnold, P. L.; Love, J. B. *Organometallics* **2013**, *32*, 6879−6882.

54. Generally, ν CN values of aryl isocyanides are only minimally affected by the electronic nature of the aryl ring. For a discussion of the comparative electronic properties of various aryl isocyanides, see: Carpenter, A. E.; Mokhtarzadeh, C. C.; Ripatti, D. S.; Havrylyuk, I.; Kamezawa, R.; Moore, C. E.; Rheingold, A. L.; Figueroa, *J. S. Inorg. Chem*. **2015**, *54*, 2936−2944.

55. For selected examples, see: (a) Schaper, F.; Wrobel, O.; Schwörer, R.; Brintzinger, H.-H. *Organometallics* **2004**, *23*, 3552− 3555. (b) Shen, J.; Yap, G. P. A.; Theopold, K. H. *J. Am. Chem. Soc.* **2014**, *136*, 3382−3384. (c) Monillas, W. H.; Yap, G. P. A.; Theopold, K. H. *Inorg. Chim. Acta* **2011**, 369, 103−119.

56. Sullivan, A. C.; Wilkinson, G.; Motevalli, M.; Hursthouse, M. B. *J. Chem. Soc., Dalton Trans.* **1988**, 53−60.

57. (a) Zhu, C.; Xu, D.; Wei, Y. *Synthesis* **2011**, 711−714. (b) Rahman, A. K. F.; Nicholas, K. M. *Tetrahedron Lett*. **2007**, *48*, 6002−6004.

58. Frisch, M. J.; Trucks, G. W.; Schlegel, H. B.; Scuseria, G. E.; et al.. Gaussian 09, Revision D.01; Gaussian, Inc., Wallingford, CT, 2009.

59. Schlegel, H. B.; McDouall, J. J. In Computational Advances in Organic Chemistry; Oegretir, C., Csizmadia, I. G., Eds.; Kluwer Academic: Amsterdam, The Netherlands, 1991.

60. Bauernschmitt, R.; Ahlrichs, R. *J. Chem. Phys.* **1996**, *104*, 9047− 9052.

61. Schlegel, H. B. *J. Comput. Chem*. **1982**, *3*, 214−218.

62. Schlegel, H. B. WIREs *Comput. Mol. Sci.* **2011**, *1*, 790−809.

63. Cramer, C. J. Essentials of Computational Chemistry: Theories and Models, 2nd ed.; Wiley: Hoboken, NJ, 2004.

64. (a) Xu, S.; Zhuang, X.; Pan, X.; Zhang, Z.; Duan, L.; Liu, Y.; Zhang, L.; Ren, X.; Ding, K. *J. Med. Chem.* **2013**, 56, 4631−4640. (b) Huang, J.; Hong, J.; Hong, S. H. *Eur. J. Org. Chem.* **2012**, 6630− 6635. (c) Barral, K.; Moorhouse, A. D.; Moses, *J. E. Org. Lett.* **2007**, *9*, 1809−1811.

65. (a) Konig, S. N.; Schadle, C.; Maichle-Mossmer, C.; Anwander, R. *Inorg. Chem*. **2014**, *53*, 4585- 4597. (b) Cai, I. C.; Lipschutz, M. I.; Tilley, T. D. *Chem. Commun.* **2014**, 50, 13062-13065. (c) Irwin, M.; Doyle, L. R.; Kramer, T.; Herchel, R.; McGrady J. E.; Goicoechea, J. M. *Inorg. Chem.* **2012**, *51*, 12301-12312. (d) Frazier, B. A.; Wolczanski, P. T.; Lobkovsky, E. P. *Inorg. Chem.* **2009**, *48*, 11576-11585. (e) Edema, J. J. H.; Gambarotta, S.; Meetsma, A.; Spek, A. L.; Smeets, W. J. J.; Chiang, M. Y. *J. Chem. Soc., Dalton Trans.* **1993**, 789-797. (f) Edema, J. J. H.; Gambarotta, S.; Meetsma, A.; Van Bolhuis, F.; Spek; A. L.; Smeets, W. J. J. *Inorg. Chem.* **1990**, *29*, 2147-2153.

66. (a) Hermes, A. R.; Morris, R. J.; Girolami, G. S. *Organometallics* **1988**, *7*, 2372-2379. (b) H. Edema, J. J. H.; Gambarotta, S.; Van Bolhuis, F.; Smeets, W. J. J.; Spek, A. L.; Chiang, M.Y. *J. Organomet. Chem.* **1990**, 389, 47-59. (c) Dillon, K. B.; Gibson, V. C.; Howard, J.

A. K.; Redshaw, C.; Sequeira, L.; Yao, J. W. *J. Organomet. Chem.* **1997**, 528, 179-183.

(d) Wang, J.; Tan, G.; An, D.; Zhu, H.; Yang, Y. *Z. Anorg. Allg. Chem.* **2011**, *637*, 1597.

(e) Danopoulos, A. A.; Yu. Monakhov, K.; Robert, V.; Braunstein, P.; Pattacini, R.; Conde-Guadaño, S.; Hanton, M.; Tooze, R. P. *Organometallics* **2013**, *32*, 1842-1850.

67. (a) Edema, J. J. H.; Gambarotta, S.; Bolhuis, F. V.; Smeets, W. J. J. ; Spek, A. L. *Inorg. Chem.* **1989**, *28*, 1407-1410. (b) Meyer, D.; Osborn; J. A.; Wesolek, M. *Polyhedron*, 1990, *9*, 1311-1315.

68. Schax, F.; Suhr, S.; Braun, B.; Bill, E.; Herwig, C.; Limberg, C. *Angew. Chem. Int. Ed.* **2015**, *54*, 1352-1356.

69. Terry, K. W.; Gantzel, P. K.; Tilley, T. D. *Inorg. Chem.,* **1993**, *32*, 5402-5404.

70. Hvoslef, J.; Hope, H.; Murray, B. D.; Power, *P. P. Chem. Commun.* **1983**, 1438.

71. (a) Broere, D. L. J.; Čorić, I.; Brosnahan, A.; Holland, P. L. *Inorg. Chem.* **2017**, *56*, 3140-3143. (b) Deschner, T.; Törnroos, K. W.; Anwander, R. *Inorg. Chem.* **2011**, 50, 7217-7228.

72. (a) Eichhofer, A.: Lan, Y.; Mereacre, V.; Bodenstein, T.; Weigened, F. *Inorg. Chem.* **2014**, *53*, 1962-1974. (b) Bryan, A. M.; Long, G. J.; Grandjean, F.; Power, P. P. *Inorg. Chem.* **2013**, *52*, 12152−12160

73. Trogler, W. C. *Acc. Chem Res*. **1990**, *23*, 426-431.

74. (a) Cowley, R. E.; Bill, E.; Neese, F. Brennessel, W. W.; Holland, P. L. *Inorg. Chem.* **2009**, *48*, 4828-4836. (b) Bellows, S. M.; Brennessel, W. W.; Holland, P. L. **2016**, *20*, 3344-3355.

75. Mock, M. T.; Popescu, C. V.; Yap, G. P. A.; Dougherty, W. G.; Riordan, C. G. *Inorg. Chem*. **2008**, *47*, 1889-1891.

76. Cramer, S. A.; Sanchez, R. H.; Brakhage, D. F.; Jenkins, D. M. *Chem. Commun.* **2014**, *50*, 1397-13970.

77. Gehrmann, T.; Lloret Fillol, J.; Wadepohl, H.; Gade, L. H. *Organometallics* **2012**, *31*, 4504–4515.

78. Vaddypally, S.; McKendry, I. G.; Tomlinson, W.; Hooper, J. P.; Zdilla, M. J. *Chem. Eur. J.* **2016**, *22*, 10548–10557.

79. Gutlich, P.; Bill, E.; Trautwein, A. X. *Mössbauer Spectroscopy and Transition Metal Chemistry* **2011**, 84-85.

80. Noodleman, L.; Baerends, E. J.; *J. Am. Chem. Soc.* **1984**, *106*, 2316-2327.

81. Vrăjmașu V.; Münck, E.; Bominaar, E. L. *Inorg. Chem.* **2003**, *42*, 5974-5988.

82. Laitar, D. S.; Mathison, C. J. N.; Davis, W. M.; Sadighi, J. P. *Inorg. Chem.* **2003**, *42*, 7354−7356.

83. (a) 'Organochromium reagents' K. Takai, K *Comprehensive Organic Synthesis,* ed. Knochel, P. Molander, G. A. Elsevier, Oxford, 2nd edn, 2014, vol. 1, pp. 159–203. (b) Chromium(II)-mediated and catalysed C–C coupling reactions Hodgson, D. M.; Comina, P. J. in Transition Metals for Fine Chemicals and Organic Synthesis, ed. Bolm, C.; Beller, M. VCH, Weinheim, 2nd edn, 2004, vol. 1, pp. 469–48.

84. (a) Suzuki, K.; Tamiya, M. 'Pinacol coupling reactions' in Comprehensive Organic Synthesis, ed. P. Knochel and G. A. Molander, Elsevier, Oxford, 2nd edn, 2014, vol. 3, pp. 563–611. (b) Y. Wakatsuki, Y.; Hou, Z. *Top. Organomet. Chem.* **1999**, *2*, 234. (c) Macedo Jr., F.; B. S. Terra, B. S. *ARKIVOC* **2012**, (i), 134.

85. For selected examples of chromium(II) complexes in reductive coupling: (a) Conant, J. B.; Cutter, H. B. *J. Am. Chem. Soc.* **1926**, *48*, 1016-1030. (b) Davis, D. D.; Bigelow, W. B. *J.*

Am. Chem. Soc. **1970**, *92*, 5127-5130. (c) Okude, Y.; Hirano, S.; Hiyama, T.; Nozaki, H. *J. Am. Chem. Soc.* **1977**, *99*, 3179-3181. (d) Svatoš A.; Boland, W. Synlett, **1998**, 549; (e) Takai, K.; Nitta, K.; Utimoto, K. *Tetrahedron Lett.* **1988**, *29*, 5263. (f) Eisch, J. J.; Shi, X.; Alila, J. R.; Thiele, S. *Chem. Ber.* **1997**, *130*, 1175. (g) Takai, K.; Morita, R.; Toratsu, C. *Angew. Chem., Int. Ed.* **2001**, *40*, 1116. (h) Takai, K.; Morita, R.; Toratsu, C. *Chirality* **2003**, *15*, 17. (i) Groth, U.; Jung, M.; Vogel, T. *Chem. Eur. J.* **2005**, *11*, 3127-3135.

86. (a) Karol, F. J.; Karapinka, G. L.; Wu, C.; Dow, A. W.; Johnson, R. N.; Carrick, W. L. *J. Polym. Sci. Part A: Polym. Chem.* **1972**, *10*, 262. (b) Ai, P.; Danopoulos, A. A.; Braunstein, P. *Organometallics* **2015**, *34*, 4109-4116. (c) Lee, D. H.; Kim, E. H.; Jeon, J. Y.; Park, S. H.; Jeong, M. S.; Kang, Y. Y.; Lee, J.; Lee, B. Y. *J. Organomet. Chem.* **2016**, 803, 13-20. (d) Zhang, J.; Qiu, P.; Liu, Z.; Liu, B.; Batrice, R. J.; Botoshansky, M.; Eisen, M.S. A*CS Catal.* **2015**, *5*, 3562.

87. (a) Berben, L. A.; Kozimor, S. A. *Inorg. Chem.* **2008**, *47*, 4639- 4647. (b) Mock, M. T.; Chen, S.; O'Hagan, M.; Rousseau, R.; Dougherty, W. G.; Kassel, W. S.; Bullock, R. M. *J. Am. Chem. Soc.* **2013**, *135*, 11493-11496.

88. For selected references on the reactivity of $CrCl_2$, see: (a) K. Kazuhiko Takai and T.-P. Loh, Chromium(II) Chloride, in Encyclopedia of Reagents for Organic Synthesis, John Wiley & Sons, New York, 2005, DOI: 10.1002/047084289X.rc166. (b) Chen, W.; Yang, Q.; Zhou, T.; Tian, Q.; Zhang, G. *Org. Lett.* **2015**, *17*, 5236-5239. (c) Steib, A. K.; Kuzmina, O. M.; Fernandez, S.; Flubacher, D.; Knochel, P. *J. Am. Chem. Soc.,* **2013**, *135*, 15346 -15349. (d) Leon, E. I.; Paz, N. R.; RiescoFagundo, C.; Suarez, E. *Tetrahedron*, **2008**, *64*, 1070. (e) Groth, U.; Jung, M.; Lang, S.; Schuppler, T. *Tetrahedron Lett.* **2009**, *50*, 152-154. (f) L. A. Wessjohann, G. Schmidt and H. S. *Schrekker, Synlett,* **2007**, 2139.

89. (a) Cotton, F. A.; DeBoer, B. G.; Laprade, M. D.; Pipal J. R.; Ucko, D. A. *J. Am. Chem. Soc.* **1970**, 92, 2926-2927. (b) Edema, J. J. H.; Gambarotta, S.; Bolhuis, F. V.; Spek*, A.L. J. Am. Chem. Soc.* **1989**, *111*, 2142-2147. (c) Sadique, A. R.; Heeg, M. J.; Winter, C. H. *J. Am. Chem. Soc.* **2003**, 125, 7774-7775. (d) Steinborn, D.; Neumann, O.; Bruhn, C.; Ruffer, T.; Boese, R.; Heinemann, F. W. *Chem. Eur. J.* **1998**, *4*, 2204. (e) Atha, P. M.; Campbell, J. C. ; Garner, C. D.; Hillier, I. H.; MacDowell, A. A. *J. Chem. Soc. Dalton Trans*.**1983**, *6*, 1085-1089. (f) Bino, A.; F. A. Cotton, F. A.; W. Kaim, W. *Inorg. Chem.* **1979**, 18, 3566-3568.

90. (a) Knochel, P.; G. A. Molander, G. A. 'Pinacol coupling reactions' K. Suzuki and M. Tamiya, in Comprehensive Organic Synthesis, ed. Elsevier, Oxford, 2nd edn, **2014**, vol. 3, pp. 563–611. (b) Wakatsuki, Y.; Hou, Z. *Top. Organomet. Chem.* **1999**, *2*, 234-.

91. Groysman, S.; Villagrán, D.; Nocera, D. G. *Inorg. Chem.* **2010**, *49*, 10759-10761.

92. Scott, T. A.; Ooro, B. A.; Collins, D. J.; Shatruk, M.; Yakovenko, A.; Dunbar, K. R.; Zhou, H. *Chem. Commun.* **2009**, 65–67.

93. O. P. Lam, O. P.; Anthon, C.; Heinemann, F. W.; O'Connor, J. M.; Meyer, K. *J. Am. Chem. Soc.* **2008**, *130*, 6567-6575.

94. Selected examples with calculations include: (a) Legzdins, P.; McNeil, W.S.; Smith, K. M.; Poli, R. *Organometallics* **1998**, *17*, 615-622. (b) Hess, J. S.; Leelasubcharoen, S.; Rheingold, A. L.; Doren, D. J.; Theopold, K. H. *J. Am. Chem. Soc*. **2002**, *124*, 2454-2455. (c) Lord, R. L.; Baik, M.-H.; *Inorg. Chem.* **2008**, *47*, 4413-4420. (d) Yang, Y.; Liu, Z.; Zhong, L.; Qiu, P.; Dong, Q.; Cheng, R.; Vanderbilt, J.; Liu, B. *Organometallics* **2011**, *30*, 5297-5302. (e) Dai, F.; Yap, G. P. A.; Theopold, K. H. *J. Am. Chem. Soc.* **2013**, *135*, 16774-16776.

95. Neese, F. *J. Chem. Phys. Solids* **2004**, *65*, 781.

96. (a) Kreisel, K. A.; Yap, G. P. A.; Theopold, K. H. *Inorg. Chem*. **2008**, *47*, 5293-5303. (b) Zhou, W.; Chiang, L.; Patrick, B. O.; Storr, T.; Smith, K. M. *Dalton Trans*. **2012**, *41*, 7920-7930. (c) Scarborough, C.C.; Sproules, S.; Doonan,C. J.; Hagen, K. S.; Weyhermüller, T.; Wieghardt, K. *Inorg. Chem.* **2012**, *51*, 6969-6982. (d) W. Zhou, A. N. Desnoyer, J. A. Bailey, B. O. Patrick and K. M. Smith, *Inorg. Chem.* **2013**, *52*, 2271-2273.

97. Adkins, H.; Cox, F. W. *J. Am. Chem. Soc.* **1938**, *60*, 1151-1159.

98. For selected examples, see: (a) Chisholm, M. H.; Cotton, F. A.; Extine, M. W.; Reichert, W. *J. Am. Chem. Soc*., **1978**, *100*, 1727–1734. (b) D. J. Darensbourg, D. J.; Sanchez, K. M.; Rheingold, A. L. *J. Am. Chem. Soc.* **1987**, *109*, 290-292. (c) Ferro, L. Hitchcock, P. B.; Coles, M. P.; Cox, H.; Fulton, J. R. *Inorg. Chem*. **2011**, *50*, 1879-1888. (d) Tam, E. C. Y.; Johnstone, N.C.; Ferro, L.; Hitchcock, P. B.; Fulton, R. *Inorg. Chem*. **2009**, *48*, 8971-8978.

99. M. H. Chisholm, M. H.; Cotton, F. A.; Extine , M. W.; Rideout, D. C. *Inorg. Chem.* **1979**, *18*, 120-125.

100. Legault, C. Y. CYLview 1.0b, Université de Sherbrooke, **2009** (http://www.cylview.org).

101. (a) Vosko, S. H.; Wilk, L.; Nusair, M.; *Can. J. Phys.* **1980**, *58*, 1200. (b) Lee, C.; Yang, W.; Parr, R. G. *Phys. Rev. B: Condens. Matter* **1988**, *37*, 785. (c) Becke, A. D. *J. Chem. Phys.* **1993**, *98*, 5648. (d) Stephens, P. J.; Devlin, F. J.; Chabalowski, C. F.; Frisch, M. J. *J. Phys. Chem.* **1994**, *98*, 11623.

102. Rappé, A. K.; Casewit, C. J.; Colwell, K. S.; Goddard III, W. A.; Skiff, W. M. *J. Am. Chem. Soc.* **1992**, *114*, 10024-10035.

103. Dapprich, S.; Komáromi, I.; Byun, K. S.; Morokuma, K.; Frisch, M. J. *J. Mol. Struct.* **1999**, 462, 1.

104. Frisch, M. J.; Trucks, G. W.; Schlegel, H. B.; Scuseria, G. E.; et al. Gaussian 09, Revision D.01, Gaussian, Inc., Wallingford, CT, 2009.

105. (a) Schlegel, H. B. *J. Comput. Chem.* **1982**, *3*, 214. (b) H. B. Schlegel, Wiley Interdiscip. Rev.: *Comput. Mol. Sci.* **2011**, *1*, 790.

106. (a) Schlegel, H. B.; McDouall, J. J. in Computational Advances in Organic Chemistry, ed. C. Oegretir and I. G. Csizmadia, Kluwer Academic, Amsterdam, The Netherlands, 1991. (b) Bauernschmitt, R.; Ahlrichs, R. *J. Chem. Phys.* **1996**, *104*, 9047.

107. Nocera, D. G. *Inorg. Chem.* **2009**, *48*, 10001-10017.

108. Coperet, C. *Chem. Rev.* **2010**, *110*, 656-680.

109. (a) Berno, P.; Floriani, C.; Chiesi-Villa, A.; Guastini, C. *J. Chem. Soc., Dalton Trans.* **1989**, 551-554. (b) Vela, J.; Stoian, S.; Flaschenriem, C. J.; Munck, E.; Holland, P. L. *J. Am. Chem. Soc.* **2004**, *126*, 4522-4523. (c) Dorfman, J. R.; Girerd, J. J.; Simhon, E. D.; Stack, T. D. P.; Holm, R. H. *Inorg.Chem.* **1984**, *23*, 4407- 4412. (d) Mukherjee, R. N.; Stack, T. D. P.; Holm, R. H. *J. Am. Chem. Soc.* **1988**, *110*, 1850-1861.

ABSTRACT

SYNTHESIS OF LOW-COORDINATE TRANSITION METAL BIS(ALKOXIDE) COMPLEXES AND THEIR REACTIVIY TOWARD SMALL MOLECULES

by

MARYAM YOUSIF

August 2017

Advisor: Dr. Stanislav Groysman

Major: Chemistry (Inorganic)

Degree: Doctor of Philosophy

This dissertation focused on the synthesis of new transition metal complexes in bis(alkoxide) ligand environments and the investigation of their reactivity in nitrene-group transfer catalysis and small molecule activation. Treatment of $Cr(N(SiMe_3)_2)_2(THF)_2$ with two equivalents of HOR (OR = OC^tBu_2Ph) led to the formation of the chromium(II) alkoxide dimer, $Cr_2(OR)_4$. Upon the reaction with bulky aryl and alkyl azides, $Cr_2(OR)_4$ led to the stable Cr(IV) mono(imido) complexes, $Cr(OR)_2(NR)$, featuring trigonal planar metal centers. In contrast, less bulky aryl azides led to the formation of chromium (VI) bis(imido) complexes $Cr(OR)_2(NR)_2$, independent of the amount of azide used. Chromium(IV) mono(imido) species $Cr(OR)_2(NR)$ is capable of nitrene transfer to isocyanides to form asymmetric carbodiimides (RNCNR'). When excess isocyanide is added to $Cr(OR)_2(NR)$, a new chromium(II) complex, $Cr(OR)_2(CNR^2)_4$, was identified by X-ray crystallography. This tetrakis(isocyanide) chromium(II) complex is also capable of forming carbodiimide when azide is introduced. Efficient catalytic formation of carbodiimides was obtained using 2.5 mol% of $Cr_2(OR)_4$ for the mixtures of bulky organoazides and isocyanides; no catalytic reactivity was observed for the non-bulky aryl azides. DFT calculations suggest that trigonal $Cr^{IV}(OR)_2(NR)$ intermediate is the key species in the reaction

mechanism as, due to it coordinative unsaturation, it allows isocyanide binding to the metal, which enables subsequent C-N bond formation.

A bulkier alkoxide ligand HOR' (R = C^{t}Bu$_2$(3,5-Ph$_2$Ph)) was synthesized by lithium-halogen exchange reaction. The protonolysis of the metal complexes, M(N(SiMe$_3$)$_2$(THF)$_x$, with HOR' enabled an easy isolation of new bis(alkoxide) precursors M(OR')$_2$(THF)$_2$ (where M = Cr, Co, Fe) featuring cis-divacant octahedral geometry. The chemistry of the iron bis(alkoxide) compound Fe(OR')$_2$(THF)$_2$ with the variety of aryl azides was investigated. Catalytic formation of various azoarenes from the corresponding azides (mesityl azide, 2,6-diethylphenylazide, azidobenzene, 4-azidotoluene, 3,5-dimethylphenylazide) using 5/10 mol% loading of Fe(OR')$_2$(THF)$_2$ was observed. Mechanistic investigation revealed that the reaction proceeds via formation of tetrazene complexes Fe(OR')$_2$ (ArNNNNAr). ^{57}Fe Mössbauer and EPR spectroscopy demonstrate a high spin iron(III) center, antiferromagnetically coupled to the tetrazene ligand radical anion. Tetrazene complexes are capable of azoarene formation, as demonstrated by NMR spectroscopy and mass spectrometry, thus confirming their role as intermediates in nitrene coupling reaction.

My next project focused on the investigation of the reactivity of Cr(OR')$_2$(THF)$_2$ with organic carbonyls and CO$_2$. Cr(OR')$_2$(THF)$_2$ catalyzes the reductive coupling of a variety of aromatic aldehydes (benzaldehyde, 4-anisaldehyde, 4-(trifluoromethyl)benzaldehyde, and 2,4,6-trimethylbenzaldehyde) to form Cr(IV) diolate complexes. In contrast, the reaction of benzophenone led to the formation of the ketone adduct Cr(OR')$_2$(OCPh$_2$). DFT calculations suggested that the reductive coupling of aldehydes proceeds via the Cr(III) bis-aldehyde intermediate. Partial radical character in the coordinated aldehydes in these species is sufficient for C-C bond formation. The calculation also suggested that that the more significant steric

demands of ketones prevented their coupling of ketone. No reductive coupling was observed with CO_2. Instead, the reaction of $Cr(OR')_2(THF)_2$ with CO_2 led to CO_2 insertion into Cr-OR' bonds to form the diamagnetic dinuclear paddlewheel complex $Cr_2(O_2COR')_4(THF)_2$.

Oxo- and sulfide-group transfer chemistry was also investigated. The reaction of $Fe(OR)_2(THF)_2$ with an oxo-transfer reagent, iodosobenzene (PhIO), forms the dinuclear μ-oxo complex $Fe_2(O)(OR)_4(THF)_2$. Similarly, the use of triphenylantimony sulfide (Ph$_3$SbS) allowed for the isolation of $Fe_2(S)(OR)_4(THF)_2$. The complexes were isolated and characterized by X-ray crystallography, IR spectroscopy, and elemental analysis. Both $Fe_2(O)(OR)_4(THF)_2$ and $Fe_2(S)(OR)_4(THF)_2$ species were found to be unreactive in the group-transfer chemistry with phosphine and olefins.

AUTOBIOGRAPHICAL STATEMENT

Maryam Yousif

Education

Ph.D., Inorganic Chemistry, Wayne State University, Detroit, MI, August 2012-June 2016, Advisor: Dr. Stanislav Groysman

B.S., Chemistry, University of Michigan, Dearborn, MI
August 2010-June 2012

Publications

1. **Yousif, M**.; Stoian, S.; Lord, R. L.; Groysman S. *Article in preparation.*

2. Reed, B. R.; **Yousif, M.;** Lord, R. L.; McKinnon, M.; Rochford, J.; Groysman, S. *Organometallics* **2017**, *36*, 582-593.

3. **Yousif, M.**; Cabelof, A. C.; Martin, P. D.; Lord, R. L.; Groysman S. *Dalton. Trans.* **2016**, *45*, 9794-9804.

4. **Yousif, M.**; Tjapkes, D. J.; Lord, R. L.; Groysman, S. *Organometallics* **2015**, *34*, 5119–5128.

5. Bellow, J. A.; **Yousif, M.**; Groysman, S. "Discrete Complexes of 3d Metals with Monodentate Bulky Alkoxide Ligands and their Reactivity in Bond Activation and Bond Formation Reactions" *Comments Inorg. Chem.* **2015**, *36*, 92-122.

6. **Yousif, M.**[¶]; Bellow, J. A.[¶]; Fang, D.; Kratz, E. G.; Cisneros, G. A.; Groysman, S. *Inorg. Chem.* **2015**, *54,* 5624- 5633. *(*[¶]*Authors have contributed equally to this work)*

7. Bellow, J. A.; **Yousif, M.**; Cabelof, A. C.; Lord, R.L.; Groysman, S. *Organometallics* **2015**, *34*, 2917-2923.

Selected Presentations

- **Yousif, M**.; Groysman, S. *"Activation of Small Molecules Using Low-Coordinate Bis(Alkoxide) Metal Complexes",* Oral Presentation, University of Michigan-Dearborn, MI, February 2016.

- **Yousif, M.;** Groysman, S. *"Reactivity of Low-Coordinate Bis(Alkoxide) Metal Complexes in C-N Bond Formation Reactions",* Oral Presentation, ACS 250th National Meeting, Boston Convention & Exhibition Center, MA, August 2015.

- **Yousif, M**.; Groysman, S. *"Reactivity of Low-Coordinate Bis(Alkoxide) Metal Complexes in C-N Bond Formation Reactions",* Oral Presentation, Michigan Catalysis Society (MCS), Wayne State University, MI, May 2015.